THERAPEUTIC NANO- AND MICROPARTICLES FOR ANGIOGENESIS DEPENDENT DISEASES

by

Ron B. Shmueli

A dissertation submitted to Johns Hopkins University in conformity with the requirements for the degree of Doctor of Philosophy

Baltimore, Maryland

March, 2015

Abstract

There are a number of diseases that are caused by, or depend on, irregular angiogenesis. In cancer, tumors require new vasculature in order to proliferate. In neovascular age-related macular degeneration (NVAMD), aberrant angiogenesis can result in leakage that damages the retina, causing progressive blindness in patients. Other ocular diseases, such as macular edema and proliferative diabetic retinopathy, also depend on diseased blood vessels, impairing the sight of many millions of people around the world. Therefore, blocking these pathologies has been, and continues to be, an important target of research and therapy.

Peptide delivery and genetic therapy are two promising strategies for the treatment of a number of diseases. Gene therapy can be used to replace lost function both in the case of inherited and acquired diseases, such as in cancer. Here, a non-viral polymeric strategy is described for the delivery of DNA. Poly(beta-amino esters) (PBAE) are a class of cationic, hydrolytically degradable polymers that can electrostatically complex with genetic material to form gene delivery nanoparticles. The modular structure of the PBAEs allows for the creation of a library of structures with varying transfection abilities. These PBAEs are used to deliver both reporter and functional genes. Polymer structures that optimally transfect cancer cell types, such as small cell lung cancer, and endothelial cell types, such as human retinal endothelial cells, are identified. The delivery of a functional gene *in vivo* shows inhibition of tumor growth in a mouse model. The delivery of reporter genes allows for the identification of PBAEs that can preferentially transfect retinal endothelial cells over retinal epithelial cells *in vitro*. Therefore, it is

shown that PBAEs can be a useful platform to deliver DNA both directly to cancer cells and to endothelial cells as a treatment for angiogenesis dependent diseases.

Peptides have a number of favorable therapeutic properties, such as high specificity. Certain serpin-derived and collagen-IV derived peptides have been shown to have potent *in vitro* and *in vivo* anti-angiogenic properties. However, peptides are often difficult to translate to the clinic due to high biological clearance and poor biodistribution. Here, the use of nanoparticle and microparticle formulations are described that can counter these limitations and extend the activity of anti-angiogenic peptides by controlled release over time. A number of poly(lactide-co-glycolide) (PLGA) based nanoparticle systems are also developed for the release and passive targeting of the collagen-IV derived peptide for cancer applications. A composite polymeric microparticle system, using PBAE and PLGA, is developed for the treatment of NVAMD. This delivery system is able to release the serpin-derived peptide and inhibit neovascularization in a clinically relevant mouse model over many months. A PLGA microparticle system is also optimized for the release of the collagen-IV derived peptides, with improved long-term efficacy observed in the clinically relevant mouse model.

Thesis Committee

Jordan J. Green (primary advisor, reader)

Associate Professor, Department of Biomedical Engineering

Johns Hopkins University School of Medicine

Kevin J. Yarema (reader)

Associate Professor, Department of Biomedical Engineering

Johns Hopkins University School of Medicine

Aleksander S. Popel

Professor, Department of Biomedical Engineering

Johns Hopkins University School of Medicine

Acknowledgements

This work would not be possible without the collaboration, support, and guidance of many, many people. I would like to thank my PI and mentor, Dr. Jordan Green. I joined his lab when it was just starting up, without any idea where things might go, but I know that I have made the right choice. He has built up a wonderful lab, doing exciting work, and, no less importantly, filled it with great people. While busy setting up the lab, and forging new collaborations, he has always been available to guide with advice, ideas, and discussions.

I would also like to thank my thesis committee members Dr. Kevin Yarema, and Dr. Aleksander Popel for their help and guidance throughout my time at Hopkins. Further, a lot of the work described here was done in collaboration with Dr. Popel and his lab. It has been a pleasure working with him and various other members in his lab including Dr. Niranjan Pandey, and Dr. Esak Lee. In fact, most of work described here has been done in collaboration with other labs, a testament both to Dr. Green's ability to form such collaborations and to the environment here at Hopkins that allows for easy connections with many great researchers. This includes working closely together with Dr. Peter Campochiaro's lab, experts in ocular diseases, as well as working on projects with the labs of Dr. Christine Hann and Dr. Elia Duh.

While I've been fortunate to work on interesting projects, I've been equally lucky to work with amazing labmates. Hello…Dr. Nupura Bhise, Dr. Joel Sunshine, Dr. Stephany Tzeng, Dr. Corey Bishop, Jayoung Kim, Kristen Kozielski, Randall Meyer, David Wilson, and Dr. Camila Zamboni. Whether or not experiments were working, I've

always looked forward to walking into lab knowing I would be able to find laughter and fun, of course in addition to their invaluable scientific and experimental knowledge and advice.

Finally, I want to thank my family, my parents Zvi and Frieda Shmueli, and my brother Dan Shmueli. I wouldn't be here, completing my doctorate at Johns Hopkins, if it wasn't for everything they have given me. I want to thank them for their constant love and support, their knowledge and advice, their humor and patience. Thank you for everything!

List of Tables

List of Figures

Table of Contents

Chapter 1

Introduction to the Thesis

1.1 Outline of the Thesis

The field of drug and gene delivery is discussed in chapters 2 and 3. **Chapter 2** focuses on drug delivery as it pertains to angiogenesis in disease. Anti-angiogenic therapies for diseases dependent on aberrant angiogenesis are discussed, with a focus on eye diseases and cancer. **Chapter 3** details electrostatic methods that can be used to enhance gene delivery in a number of applications.

The thesis is broken up into three aims. In Aim 1, a strategy for targeting and treating the vasculature, using polymeric non-viral gene delivery, is described. In this aim, a library of poly(beta-amino ester)s (PBAE) is characterized and employed to transfect both cancer (small cell lung cancer) and endothelial (human umbilical and human retinal) cells. The transfection is done with both reporter genes and then later functional genes. Aim 2 then explores another approach to anti-angiogenic therapy by the delivery of a peptide therapeutic in a biodegradable microparticle system. The focus of this aim is neovascular age-related macular degeneration (AMD), with the goal of creating a long-term treatment option. In Aim 3, additional anti-angiogenic therapies are created through the use of a different anti-angiogenic peptide and both microparticle and nanoparticle systems. A microparticle system is first developed with the goal of further improving the long-term efficacy and translatability of an ocular drug delivery system to treat

neovascular AMD as well as macular edema. Peptide encapsulation in, and presentation on, nanoparticles is the focus of the second half of Aim 3, with goal of delivering this peptide-based nanotherapeutic to treat solid tumors. *In vivo* data is presented that shows promise for future therapeutic systems.

1.2 Specific Aims of the Thesis

Aim 1: To develop a library of biodegradable poly(β-amino esters) for nanoparticle based non-viral gene delivery for angiogenesis dependent diseases

PBAEs have previously been shown to be effective at transfecting a number of cell types. Here the goal is identify specific structures that could be useful for transfecting small cell lung cancer (H446), human umbilical vein endothelial (HUVEC), and human retinal endothelial (HREC) cell lines. The first step was to synthesize and characterize both the polymers and nanoparticles, including performing gel-permeation chromatography (GPC), nuclear magnetic resonance (NMR), nanoparticle tracking analysis (NTA), dynamic light scattering (DLS). A focus of the characterization was to develop a new protocol for estimating the number of plasmid per nanoparticle (NP). This protocol is described in **chapter 4**. The number of NPs in solution was quantified by NTA. Using the assumption that all plasmid are complexed into NPs, supported by gel electrophoresis data, the number of plasmids per particle can be calculated. In collaboration with Dr. Christine Hann's lab, these PBAEs were used to target small cell lung cancer, as described in **chapter 5**. A library of PBAEs was first screened against

H446 cells. Those with highest transfection level, as measured using a luciferase assay, without causing toxicity, were selected to test in a xenograft animal model. In this model, p53 was delivered with PBAEs intratumorally and a reduction in tumor growth was observed. **Chapter** 6 describes a collaboration with Dr. Elia Duh's lab, in which PBAEs were screened on HUVECs and HRECs, as well as on RPEs. We observed that certain structures might have an ability to transfect one cell type over another. Additionally, there were PBAEs that were able to transfect all these cell types better than currently commercially available reagents, such as Lipofectamine 2000 and FuGene HD. More globally, while there was a good correlation of transfection by PBAEs between the two endothelial cell types, this correlation was much lower when comparing the endothelial and epithelial cell types. This cell type tropism can potentially be taken advantage of *in vivo* in the development of gene delivery therapies.

Aim 2: To develop poly(lactide-co-glycolide) and poly(β-amino esters) microparticles for anti-angiogenic, hydrophilic, serpin-derived peptide delivery to treat neovascular age-related macular degeneration

Dr. Aleksander Popel's lab has previously discovered and developed peptides with potent anti-angiogenic properties. These peptides have been shown to inhibit cell proliferation, adhesion, and migration, as well as reduce tumor growth *in vivo* in various mouse models. The use of these peptides to treat choroidal neovascularization (CNV) has been more recently explored. However, peptides are usually poor therapeutics due to relatively fast clearance and degradation rates. Due to the likely need for intravitreal

injections to treat CNV, reducing the number of such injections is a desired clinical goal. Therefore, **chapter 7** describes a new therapeutic consisting of a novel serpin-derived peptide encapsulated within a biodegradable microparticle was developed. The peptide used here is a negatively charged serpin-derived peptide. In the first step, this peptide is complexed with biodegradable and cationic PBAEs, then encapsulated in poly(lactide-co-glycolide) PLGA microparticles, which are also biodegradable in water. These particles were characterized using NTA, DLS, scanning electron microscopy (SEM), as well as by quantifying the release rate of the peptide *in vitro*. Subsequently, this system was tested in a laser induced CNV mouse model in collaboration with Dr. Peter Campochiaro's lab. Injections of samples and controls were done on day zero, after which choroidal neovascularization was induced over several months in replicate batches of mice. For each time point, laser-induced choroidal neovascularization began two weeks before final assay time. We evaluated whether the amount of peptide available at each time point, through release form the microparticle, could reduce the amount of CNV. We observed a statistical significant reduction over the course of 14 weeks in the mouse model.

Aim 3: To develop PLGA-based microparticles and nanoparticles for anti-angiogenic, hydrophobic, collagen-IV derived peptide delivery

Developing particle-based therapeutics that utilized biomimetic, hydrophobic, collagen-IV derived peptides was the focus in Aim 3. This peptide has a number of properties that lend it to be more translatable to the clinic. It has a monotonic response curve, has a strong anti-angiogenic effect that can block both VEGF-mediated and non-

VEGF-mediated angiogenesis, and its target is known. **Chapter 8** describes the investigation of this peptide, along with the microparticle system used to deliver this peptide. In order to optimize the release system for this peptide, PLGA with varying L:G ratio was used. Once one PLGA polymer was selected, this system was evaluated in both a laser-induced choroidal neovascularization mouse model and as a TET-Opsin genetic inducible macular edema mouse model. Promising results have been observed in terms of the particle-peptide therapeutic's ability to reduce CNV, possibly reverse CNV, and prevent leakage-induced retinal detachment. Long-term efficacy was also observed in the microparticle system in a CNV mouse model for at least four months.

In order to deliver these peptides for cancer applications, systemic administration leading to tumor targeting is required. **Chapter 9** describes the various nanoparticle (NP) formulations that were developed to encapsulate peptide, including PBAE/peptide self-assembled nanoparticles, PLGA nanospheres, PLGA nanoellipsoids, and PLGA-PEG micelles. Based on biodistribution experiments, the PLGA-PEG NPs can passively reach solid tumors in a breast cancer subcutaneous mouse model due to the biophysical properties of the nanoparticle.

Chapter 2

The Role of Angiogenesis in Disease and as a Target for Therapeutics

2.1 Introduction

Vascular perfusion is essential for adequate nutrient, waste and gas exchange for all tissues in the human body. Many diseases stem from insufficient blood perfusion, resulting in a shortage of oxygen, termed hypoxia. Angiogenesis is an important mechanism of physiological vascularization in adults, whereby new blood vessels sprout from existing ones by a coordinated interaction of endothelial cells with angiogenesis-inducing signals, like growth factors (GFs), hypoxic conditions, and extracellular matrix (ECM) components, specifically adhesion molecules [1]. Vasculogenesis is a neovascularization process that involves recruitment of circulating vascular progenitor cells, originating from the multipotent hemangioblast precursor cell residing in bone marrow or peripheral blood, instead of local endothelial cells as in case of angiogenesis [2]. Traditionally, vasculogenesis was considered to occur only during embryonic development of the circulatory system [3], and neovascularization in adults was believed to occur via angiogenesis or arteriogenesis, a process of flow-induced remodeling of pre-existing blood vessels. However recent studies have suggested that circulating endothelial

This chapter was originally published as Bhise NS, Shmueli RB, Sunshine JC, Tzeng SY, Green JJ. "Drug Delivery Strategies for Therapeutic Angiogenesis and Antiangiogenesis." Expert Opin Drug Deliv. 2011 Apr;8(4):485-504.

progenitor cells can be recruited by cytokines to induce limited vasculogenesis in ischemic areas in adults [4].

Angiogenesis is also critical in pathologic states such as psoriasis [5], atherosclerosis [6, 7], rheumatoid arthritis [8, 9], diabetes [10], cancer [11], and ocular neovascularization [12] in age-related macular degeneration (AMD) and diabetic retinopathy. Normal angiogenesis is usually focal and self-limited, whereas in pathologic processes, aberrant angiogenesis is often persistent and widespread [13].

A wide range of pro- and anti-angiogenic processes act in concert to orchestrate angiogenesis (**Figure 2.1**). Among the many GFs implicated in angiogenesis such as vascular endothelial growth factor (VEGF), platelet-derived growth factor (PDGF), epidermal growth factor (EGF) and fibroblast growth factors (FGFs) [14], VEGF has been identified as the most crucial. VEGF is relatively specific to endothelial cells, and has a non-redundant role during the "angiogenic switch" (the critical point where tumors begin to induce angiogenesis) [14, 15]. VEGF regulates several endothelial cell functions, including mitogenesis, vascular tone (inducing hypotension), and vessel permeability [16], as well as inducing the production of plasminogen activators and proteases that help to degrade the basement membrane and allow for formation of new blood vessels [17]. Hypoxia, the hypoxia inducible factor HIF-1, and other GFs and cytokines, regulate the transcription of erythropoietin and VEGF [16]. The vasoactive and angiogenic functions of VEGF are mediated primarily through VEGFR-2 [16]. VEGFR subsequently activates multiple signaling pathways (Ras/MAPK, FAK, PI3K/Akt, PLCγ) [18], which leads to

angiogensis. Additional GFs such as bFGF, PDGF, and TGFβ help to stabilize newly formed blood vessels by recruiting pericytes and smooth muscle cells [1, 19].

2.1.1 Tumor Angiogenesis and Therapy

Overexpression of oncogenes or downregulation of tumor-suppressive genes resulting in aberrant, proliferative cells is essential, but not sufficient, for the development of a lethal tumor. Tumor angiogenesis is crucial for the growth and persistence of tumors and metastases. This was first described in 1971 by Judah Folkman, who observed that tumors could only grow to 2 mm in diameter without the growth of new blood vessels [11]. Two millimeters is the distance that oxygen can diffuse through tissue [20]; tumors need blood vessels to supply the oxygen and nutrients necessary for survival and proliferation [11]. Folkman further postulated in 1971 that a "tumor-angiogenesis factor" (TAF) induces blood vessel growth and that inhibition of TAF may halt tumor progression, which he termed "antiangiogenic therapy" [11].

Compared with cancer cells, endothelial cells in malignant tumors are genetically stable, nonmalignant, and rarely drug resistant, making them a relatively stable target [21]. Destroying the tumor vasculature can also amplify a drug's antitumor effect on a per-cell basis [22]. Anti-angiogenesis can initially help to "normalize" tumor vasculature, increase tumor perfusion, and alleviate tumor hypoxia, thereby increasing the efficacy of conventional anti-cancer therapies if both anti-angiogenic and anti-cancer therapies are carefully scheduled [23]. At later time points, VEGF inhibition induces tumor hypoxia as more of the tumor vasculature is starved [24].

Many angiogenic inhibitors have been developed, and several such as bevacizumab [25], ranibizumab [26], pegaptanib [27], aflibercept [28], cetuximab [29, 30], panitumumab [31], trastuzumab [32, 33], gefitinib [34], erlotinib [35], sorafenib [36, 37], sunitinib [38, 39], temsirolimus [40], and everolimus [41] (**Table 2.1**) have passed or are close to passing FDA approval and are being utilized in therapy for various cancers and AMD. In addition, a large number of chemotherapeutics developed for cancer were later shown to have anti-angiogenic properties, especially when given often at lower doses in "metronomic chemotherapy" [42]. However, the current therapies on the market mostly target VEGF, its receptor, or the tyrosine kinases that phosphorylate its receptor. Since angiogenesis is a result of the interplay between several pro- and anti-angiogenic factors, simultaneous targeting of several pro-angiogenic signaling cascades (rather than just VEGF) should be one of the most promising anti-angiogenic approaches [15].

2.1.2 Age-related Macular Degeneration Biology and Therapy

AMD is the leading cause of blindness in the elderly and is marked by loss of central vision. It is the most common of a large number of inherited and acquired diseases, collectively called macular degeneration (MD) [43]. AMD can be further split into two main forms, exudative/wet (or choroidal neovascular) and non-exudative/dry. Wet AMD is less common but is a leading cause of blindness [44]. Dry AMD results from atrophy of retinal pigment epithelium (RPE), which leads to photoreceptor atrophy [45]. The wet form is an advanced form of AMD and is treatable with anti-angiogenic drugs. Choroidal neovascularization (CNV), the formation of new blood vessels from the choroids of the eye, leads to leakage of blood and serum, which damages the retina by stimulating

inflammation and scar formation. This damage to the retina causes central vision loss and, eventually, blindness if left untreated.

Neovascular AMD results from an interplay of genetic, metabolic, and environmental factors [46]. However, while the exact causes remain an active research area, it is known that angiogenesis and vascular imbalance play a central role in this disease, importantly involving VEGF. Many cells of the eye produce VEGF, including RPE cells, pericytes, endothelial cells, glial cells, Muller cells, and ganglion cells [47]. In addition to stimulating blood vessel growth, VEGF can also stimulate endothelial cells to produce matrix metalloproteinases (MMPs), which can degrade extracellular matrix and allow new vessels to grow into tissue [47]. It has been demonstrated that VEGF overexpression in mouse models and in human studies leads to CNV [46]. Other molecular factors are also important in AMD, including pigment epithelium-derived factor (PEDF), basic fibroblast growth factor (bFGF) and angiopoietins [47]. Stimuli due to hypoxia, ischemia, inflammation, and oxidative stress (all of which can accumulate with age) can influence the production and balance of these factors.

Recent successful treatments of AMD have been developed that target these relevant effectors, specifically treating blood vessel growth by targeting VEGF. As with cancer treatments, improved clinical results might be achieved through combination therapy that targets multiple GFs.

2.2 Drug Delivery Systems

Synthetic and biological materials have been studied in the development of safe and effective drug delivery systems. The chemical and physical properties of synthetic materials, including polymers, are often easier to control, but their biocompatibility must be carefully assessed. Biological materials already possess many desired properties but may be more difficult to modify or manufacture as well as being potentially immunogenic. Strategies under current investigation in the field of drug delivery are discussed below and summarized in **Table 2.2**, with particular focus on those that promote or suppress angiogenesis.

2.2.1 Drug-Agent Conjugates

Perhaps the simplest drug delivery system in concept is the direct conjugation of a drug to a delivery agent. Because poly(ethylene glycol) (PEG) has been shown to increase circulation time after systemic delivery, several therapeutics have been PEGylated with the goal of avoiding biological clearance mechanisms, some of which have been translated to the clinic or are in clinical trials. Also in use are antibody-drug conjugates (ADCs) for specific targeting, such as blocking angiogenesis by using cytotoxic drugs bound to antibodies against markers of tumor vasculature [48]. Adhesive peptide moieties like Arginine-Glycine-Aspartate (RGD) sequences can be used to localize a drug carrier to desired tissues [49, 50]. Because RGD sequences bind to integrins, this method has been used to target vasculature and suppress angiogenesis [51]. Other delivery conjugates bind to a therapeutic in order to increase solubility or improve biodistribution, as in the case of Abraxane™, in which the cancer drug paclitaxel is bound to albumin in order to increase its solubility and thereby reduce solvent-mediated

toxicity [52].

2.2.2 Implanted Drug-Loaded Materials

Another strategy for drug delivery is the use of implanted depots, usually made of biological or synthetic polymers that are loaded with a therapeutic. An advantage of this type of system is its suitability for localized delivery. Generally, as in the case of the GLIADEL® wafer made of poly(carboxyphenoxy propane:sebacic acid) discs loaded with bis-chloronitrosourea (BCNU) and used to treat glioblastoma multiforme (GBM) [53, 54], the depot is implanted directly at the site of the tissue to be treated. This eliminates the need for targeting mediated by specific interactions between chemical or biological moieties. Furthermore, drug-loaded depots can themselves be substrates for cell growth, as in the case of GF-loaded hydrogels [55-57]. These can be used as tissue engineering scaffolds that provide specific cues for cell survival and proliferation, wound healing, or angiogenesis [58, 59]. One concern with implantable reservoirs is the potential for local inflammation or foreign body response [60, 61]. They are also limited for use in systemic drug delivery [62, 63] unless the loaded drug can freely permeate through the matrix.

2.2.3 Micro- and Nanoparticles for Drug Delivery

An alternative to large, implanted drug reservoirs is a micro- or nanoparticulate system. In many cases, these are small enough to be injected, reducing injury due to surgical implantation. Among the frequently investigated synthetic polymers are polyesters, including poly(glycolic acid) (PGA), poly(lactic acid) (PLA), poly(ε-

caprolactone) (PCL), and derivatives or copolymers of the above, like poly(lactic-*co*-glycolic acid) (PLGA). These degrade hydrolytically under physiological conditions [64, 65] and are biocompatible *in vitro* and *in vivo* [66]. They are used in nanoparticulate delivery of proteins, small molecules, and genes [67, 68], as well as microparticulate delivery of proteins and small molecules [66, 69, 70]. In one case, VEGF and dexamethasone were released slowly from PLGA particles to encourage angiogenesis while minimizing local inflammation [71]. The drug release kinetics, degradation, biodistribution, and clearance of synthetic particles are dependent on several factors, including size, geometry, charge, surface chemistry, encapsulation procedure, and the encapsulated drug itself [72-75]. Other than direct injection, particles can also be embedded within a larger mesh, thereby providing localized delivery similar to implantable systems while also allowing for a wider biodistribution as particles are released by diffusion or degradation of the mesh [76-78]. One difficulty with particulate-based systems, however, is their tendency to be cleared relatively quickly through the liver, spleen, and kidneys in a size-dependent manner [79, 80]. Though circulation time can be lengthened (by PEGylation to form "stealth" particles [81]) and their targeting can be tailored (by changing the size or geometry of the particles and changing the surface chemistry [74, 82, 83], for many systems, an ideal *in vivo* distribution has yet to be achieved.

Amphiphilic lipids, surfactants, or block copolymers constitute another form of drug delivery. Self-assembly of amphiphiles into colloids causes micelle formation, in which a lipophilic core is isolated from the surrounding aqueous phase by an external hydrophilic shell or corona [84]. A bilayer of these molecules can form vesicles classified

as liposomes with hydrophilic moieties both at the core and in the surrounding corona, while the lipophilic moieties associate within the bilayer. The biphasic character of these molecules allows them to serve as vehicles for either hydrophilic or lipophilic drugs [85-87] and techniques can tailor the particles' size, lamellarity, fluidity, and hydrophobicity [88-91]. Liposomes were found to be effective in targeting the mononuclear phagocyte system (MPS) because they were easily captured by MPS cells and removed from circulation [92, 93]; this short lifetime in the bloodstream is a disadvantage, however, for targets beyond the MPS. Altering surface charge or size, conjugation of surface molecules like PEG, and coadministration of suppressive drugs have been shown to alleviate this problem to some degree [89, 94, 95]. Similar to the surfactant- and lipid-based micelles and liposomes are nanocapsules and polymersomes. Nanocapsules have a lipophilic interior consisting of the lipophilic block of a copolymer, which serves as a drug reservoir and is surrounded by a hydrophilic core, while polymersomes are composed of bilayers, similar to liposomes [96]. Nanocapsules and polymersomes are made of semi- or totally synthetic copolymer amphiphiles, which can be of greater molecular weight than naturally-occurring lipids [97]. These differences impart a more fluid, dynamic character to liposomes and micelles that are suitable for many biological processes [98], while nanocapsules and polymersomes often display more stability than fluidity [99], in addition to the flexibility granted by the ability to control chemical properties of the polymers [97, 98].

Cationic biomaterials, including both synthetic and biological polymers, have been used to form complexes with nucleic acids for the purpose of nanoparticulate gene delivery. Cationic moieties in polymers, including polyethyleneimine [100, 101],

chitosan [102], polyamidoamines [103], and poly(β-amino esters) [104, 105], can interact with anionic DNA, RNA, or oligonucleotides. The polycations mediate transport into cell, through degradative cellular compartments, and into the cytoplasm, nucleus, or other compartments where the cargo is active [101]. These materials have recently been studied for their potential to treat or cure many diseases, including those whose genetic basis is known but whose downstream molecular effectors are hard to target. Polymeric gene delivery has gained attention as an alternative to viral gene delivery, which suffers from limited cargo capacity, immune response, and the possibility of insertional mutagenesis [106]. Recent work on polymeric gene delivery to human endothelial cells, for example, has demonstrated virus-like efficacy along with minimal cytotoxicity [107-109]. In addition to these particles' potential to therapeutically regulate any gene of known sequence, gene delivery can also be used as a first step in cell-based drug delivery systems.

2.2.4 Cell-Based Delivery Systems

Ex vivo gene delivery can be used as a precursor to cell-based, pro-angiogenic drug delivery. In one study, human mesenchymal stem cells (hMSCs) were transfected with polymeric particles to express VEGF at high levels and subsequently seeded onto polyester scaffolds in order to promote angiogenesis *in vivo* [110]. Success in a similar system was seen with VEGF-expressing endothelial cells and adipose-derived stromal cells [111]. Cell-based systems are attractive because drug dose and release kinetics can be controlled over long periods of time of up to nearly a year [112], provided that the cell stably expresses the desired therapeutic. Other studies have used cells as a method of

delivering nanoparticles, allowing for a two-stage release of drugs or proteins [113], particles that serve as MRI contrast agents [59], or particles that enhance radiation therapy [114].

Delivery of cells can also be combined with other biomaterials such as hydrogels or other polymer capsules [110-112, 115] that encapsulate cells. In one study, Chinese hamster ovary (CHO) cells transfected with VEGF cDNA and subsequently encapsulated in alginate and poly(l-lysine) microspheres were shown to increase angiogenesis after implantation in mice [116]. Cell-based therapies, however, pose additional safety concerns, including the potential for inflammation, immune response or rejection of the graft, and unanticipated host-donor cell interactions. There are also questions of which cells to use and how to harvest enough for therapeutic purposes and dose regulation, especially for cases in which the secreted protein might have an off-target effect on the secreting cell itself [117-119].

2.2.5 Nondegradable Particles

While a great deal of research has focused on biodegradable particles, nondegradable particles are also studied for delivery of therapeutics. Mesoporous silicon microparticles can be loaded with proteins and other therapeutics, including insoluble drugs [120], and their microstructure allows surface interactions to be minimized, reducing damage to a drug during the loading process [121]. Drug delivery systems like these can be nested, such as with mesoporous microparticles that encapsulate nanoliposomes that are themselves loaded with small interfering RNA to create multistage delivery systems [122]. Another class of nondegradable particles is metal

nanoparticles, notable for their monodispersity, small sizes, and magnetic and thermal properties. Iron oxide nanoparticles have been used as MR contrast agents as they accumulate passively in tumor vasculature [123, 124] and can be encapsulated in lipids or polymeric particles[125]. They can also be conjugated to ligands like RGD that can actively target the particles to areas of high angiogenesis, such as tumors [126]. Gold nanoparticles, in part due to their relative biocompatibility, have been used as vehicles for gene or drug delivery [127, 128] and for thermal therapy [129]. While many of these particulate systems allow greater control over fabrication and processing variables, many of them are also limited by their toxicity [130, 131].

2.3 Anti-angiogenic Drug Delivery Systems

2.3.1 Anti-Cancer Drug Delivery Concepts and Systems

A key concept when considering the development of controlled release formulations for anti-angiogenic therapy is that many angiogenesis inhibitors have a biphasic dose-response curve [132]. As a result, maximum tolerated dose is not the paradigm to use for anti-angiogenic therapy [15]. As an example, a high dose regimen (120 mg/kg/day) of sunitinib leads to a compensatory increase in pro-angiogenic proteins and *reduced* survival and *increased* metastases in a mouse model, while a lower dose regimen (40-60 mg/kg/day) has the opposite, beneficial effect [133, 134]. Combinations of therapies, such as blocking the signaling of more than one GF, has also been shown to be more effective in some cases (**Figure 2.2A-B**). For example, researchers have used

simultaneous administration of antibodies against both VEGFR-2 and PlGF to suppress tumor growth as well as an anti-angiogenic antibody to enhance the efficacy of a conventional chemotherapy drug. This can be especially useful when a certain type of tumor is known to be resistant to one treatment but not another, or when treatment with a low dose of two therapies is less toxic to healthy cells than a high dose of either one the individual therapies [135]. In other cases, combination therapy is no more effective than the single therapy (**Figure 2.2C**), highlighting the importance of a systems level understanding of the effect of one pathway on another [136].

Nanoparticles can be effective in targeting tumor vasculature due to specific and non-specific biochemical and biophysical mechanisms. One of the advantages of nanoparticle-mediated delivery is due to the enhanced permeability and retention (EPR) effect (**Figure 2.1**). Nanoparticles that are ~50-200 nm have been shown to accumulate in tumors, provided they have a long circulation time, as a result of the leaky vasculature and absence of a draining lymphatic system present in the tumor bed [137-139]. Active targeting of endothelial molecules that are upregulated in response to high levels of angiogenesis can also be used for additional specificity. The size exclusion caused by leaky vasculature, as well as the increased angiogenesis at tumor sites, has been exploited to image tumor angiogenesis via metallic nanoparticles [140]. In this case, the passive targeting of nanoparticles via the EPR effect was enhanced by active targeting via α-v-β-3 integrin on the nanoparticles. Another example of an approach combining EPR with remote activation is that of metallic nanoshells, which accumulate in tumor vasculature prior to being activated externally by near-infrared light for thermal ablative therapy [129]. Other formulations include the conjugation of integrin and VEGF receptor

antagonists, which target sites of angiogenesis and also suppress signaling through receptors to inhibit vessel growth [141].

The charge of a drug or delivery vehicle affects its ability to penetrate into tissue, accumulate in desired sites, and escape rapid clearance from the bloodstream [142, 143]. Experimental anti-angiogenic therapies have included cationic liposomes, which can target neovasculature, to deliver the cancer drugs oxaliplatin [144] or paclitaxel [145], with or without pegylation to increase circulation time. Both of these exhibited not only the expected anti-tumor activity from the platinum analog drugs, but also a marked anti-angiogenic effect.

The abnormal vasculature of tumors, while potentially useful for drug delivery applications, can also be a hindrance. For example, one study found that tumor vessels composed of cells with heterogenous mutations caused preferential extravasation of 90-nm liposomes (**Figure 2.3**) [146]. This could potentially contribute to tumor recurrence from the cells in the part of the tumor mass that were not exposed to extravasating drug-loaded vehicles. Another challenge to cancer drug delivery is the increased interstitial pressure in the tumor space [147] and decreased perfusion near the center of the tumor mass [148]; as a result, most unmodified particles or other delivery agents can penetrate only a small distance. Peptide sequences that cause tumor penetration have been identified [149], and efforts are being made to use this principle to enhance the effect of peptides to tumor endothelium [150]. Also contributing to the problem of low tumor penetration is the high expression of certain collagens by tumor endothelial cells [151].

The difficulties in targeting the core of tumors further motivates the approach of targeting tumor vasculature, as it is more easily reached.

Recent studies exploring overexpressed genes [152] on tumor endothelium have shown that the collagens that may prevent tumor penetration can also be used as targets for drug delivery. For example, a di-Fab' fragment-PEG conjugate called CDP791 which targets VEGFR-2 was recently shown to prevent VEGF signaling and reduce angiogenesis in a phase II clinical trial for the treatment of non-squamous non-small-cell lung cancer [153]. A review of these delivery challenges makes it clear that simultaneous targeting of multiple barriers may improve the likelihood of success of anti-angiogenic treatments delivered to tumors.

2.3.2 AMD Drug Delivery Concepts and Systems

There are currently two anti-VEGF treatments approved in the US for AMD: pegaptanib and ranibizumab. Bevacizumab, which is approved for some cancers, is also routinely used off-label for AMD. Bevacizumab is a murine recombinant, humanized, monoclonal antibody that has been shown to bind to and inhibit all known isoforms of VEGF [46]. Ranibizumab is an antibody fragment developed from the same murine anitbody as bevacizumab, also binding to all known isoforms of VEGF [46]. The constant region was eliminated, to improve retinal penetration and reduce inflammation response. Specific amino acids were substituted to increase its binding affinity to VEGF [46]. It is administered via intravitreal injections once per month and has a half-life of three days [154]. Both have been found to work similarly well, although off-label

bevacizumab use is considerably less expensive (about $50 per dose as compared to about $2000 per dose) [155, 156].

Long-term anti-VEGF therapy can cause detrimental effects, however, and frequent intravitreal injections could damage the eye [43]. These treatments do not help all patients, as approximately 20% still lose vision over time. Newer treatments include VEGF-TRAP, a recombinant protein that targets VEGF rather than the VEGF receptor [157], and a recently completed phase III trial has found it to be comparably effective to ranibizumab.

Improving the route of drug delivery to the back of the eye is a central challenge that needs to be addressed. There are various routes of entry into the eye, including topical application, transscleral delivery, intravitreal injection, and systemic delivery. Topical application is the least invasive of these methods. However, drugs delivered topically must cross corneal epithelial layers, avoid aqueous humor clearance mechanisms, and diffuse all the way to the posterior eye [158]. Transscleral delivery is relatively less invasive and provides a more direct route to the posterior segment as compared to topical application. It still must pass a number of barriers, including tissue penetration, avoiding clearance due to circulation, and avoiding metabolic activity of these cellular barriers [159].

Intravitreal injections allow drugs or implants to be delivered directly into the vitreous. This method is also the most invasive, can cause trauma to the eye, and as a result leads to reduced patient compliance [158]. Systemic delivery has the advantage of being easier for patients than intravitreal or transscleral delivery, as well as the potential

ability to delivery higher doses. The limitations include increased risks for side effects in other tissues, as well as the difficulty of crossing the blood-retinal barrier [160]. Currently approved drugs are usually delivered via intravitreal injections, as this is the most direct route. However, depending on the delivery platform, other routes might be used. For example, a drug delivery reservoir implanted in the sclera [161] contains a controlled-release membrane fabricated from cross-linked polyethylene glycol with interconnected collagen microparticles embedded within the membrane (**Figure 2.4**). A constant and controllable release rate was obtained by tuning the membrane's chemical and physical properties.

Extending the half-life of the therapeutic is also key as it can reduce the dosage, frequency of injections, costs, and negative patient outcomes. As previously mentioned, PEGylation can increase half-life, as in the case of pegatanib, a currently approved AMD therapy. This PEGylated aptamer, made of short RNA strands with 3D conformation, binds to one specific isoform of VEGF [27].

In another strategy, an anti-angiogenic integrin antagonist, C16Y, peptide was encapsulated within PLA/PLA-PEO nanoparticles [162]. Intravitreal injections led to improved anti-angiogenic outcomes attributed to the increased half-life of the peptide in the eye. Additionally, nanoparticles were observed to penetrate the retina and localize to retinal pigment epithelial layer. The identification of a number of other anti-angiogenic peptides has also been achieved through computational and experimental methods [163]. These peptides inhibit proliferation and migration of HUVECs, as well as reduce tumor

size in *in vivo* cancer models [164]. Encapsulation of these novel agents in particles may enable combinatorial delivery, long-term activity, and enhanced efficacy.

There has been extensive work on drug depots in the context of ocular drug delivery for anti-angiogenesis. Molokhia et al. developed a capsule drug ring (CDR) that can be implanted in the peripheral lens capsule during cataract surgery [165]. This semi-permeable poly(methyl methacrylate) depot can release bevacizumab and other drugs in a continuous and controlled fashion and may allow for the replacement of intravitreal injections. This system is still being tested in animal models and there are clinical trials underway for other implantable drug delivery systems. An intravitreal polymeric non-biodegradable matrix insert system has been utilized for the delivery of fluocinolone acetonide to treat diabetic macular edema [166]. The inserts released the drug consistently for over a year in patients. Other implants degrade over time, reducing any possible future complications in the eye [167]. Systemic delivery may also be possible by temporarily easing the blood-retinal barrier [168], as shown in the delivery of RNAi to mice.

2.4 Conclusion

Angiogenesis is crucial not only to normal biology but also to many diseased states, including cancer, AMD, and ischemia. Drug delivery paradigms are being developed that combine well-studied principles of material transport and pharmacokinetics with novel biomaterials and fabrication methods. Some of these

therapeutic systems have been translated to the clinic with success. However, additional research is needed to further optimize the delivery of drugs currently available and to identify new treatment modalities.

2.5 Expert Opinion

Advanced drug delivery systems can benefit therapeutic angiogenesis and anti-angiogenesis by increasing specificity, prolonging duration, and combining multiple components together. As additional information is gleaned on a systems level view of angiogenesis, precision delivery in both time and space of multimodal agents to control angiogenesis will become increasingly important. Drug delivery systems are the enabling technologies to translate this information into new therapies.

Numerous targets have been identified for anti-angiogenic therapies, including growth factors and their receptors and ligands localized on tumor vasculature. In the case of cancer, despite the ever-increasing understanding of cancer biology and drug delivery, current therapies are still plagued by inefficiency, systemic toxicity, and tumor recurrence. Because there are so many factors that contribute to excessive tumor angiogenesis and growth, and because great flexibility is granted through drug delivery approaches, it will be advantageous to consider engineered systems and more than a single pathway to decrease angiogenesis in tumors for maximal therapeutic effect. For example, (1) the conjugation of targeting ligands to drugs can increase specificity; (2) encapsulation of multiple drug-agent conjugates in liposomes or polymer nanoparticles can protect the

drugs and facilitate extravasation from the bloodstream and into tumor tissue; (3) control of physicochemical properties can further narrow the tissues targeted by the particle and also increase efficiency; (4) the particle itself can be protected from clearance by conjugation of "stealth" molecules or secondary encapsulation in microparticles or scaffolds. Furthermore, potentially hundreds of lead drug molecules can be formulated together in different combinations into systems that control release dosages and the order of drug release. Similarly in AMD, drug delivery strategies could enable codelivery of agents for increased potency and reduce the need for repeated intravitreal injections. Such anti-angiogenic approaches for both cancer and AMD are now being explored clinically to increase both efficacy and specificity.

The goal of pro-angiogenic therapies is to successfully deliver key angiogenic factors that stimulate revascularization of an ischemic site. In the context of ischemic diseases, reperfusion improves the function of the diseased organ; whereas in the case of tissue engineered constructs and tissue implantation, revascularization enhances graft survival. A critical aspect of developing any therapeutic angiogenesis strategy is to optimize the dose, duration of expression, and timing of factor administration. According to preclinical data, in nonischemic tissues, induction angiogenesis may be required for a period of weeks or months to allow maturation of newly formed capillaries; in an ischemic environment, this period of dependence on pro-angiogenic stimulation may be longer [169]. A leading failure of many potential therapies is the limited duration of angiogenic agent expression in the targeted diseased area. Furthermore, improper targeting of angiogenic factors can have deleterious side-effects, including retinopathy and buildup of atherosclerotic plaque. To address these issues, it is critical to develop

controlled and targeted delivery strategies that can prolong the duration of factor exposure. The clinical success of a pro-angiogenic therapy may require a patient-specific tailored delivery strategy that accounts for factors such as age, level of tissue damage, route of administration, and the native in-vivo environment. Rationally designed biodegradable 3D matrices can that act as depots for growth factors and present stimuli to communicate with endogenous angiogenic cells are promising technologies. Combinatorial strategies that use such smart delivery platforms in conjunction with angiogenesis-stimulating cells and growth factors need to be further explored to expedite the successful translation of pro-angiogenic therapies. For both pro-angiogenic and anti-angiogenic approaches, the use of biomaterials to encapsulate biological molecules and cells greatly enhances efficacy and will lead to many future clinical therapies.

2.6 Acknowledgements

The authors thank the Edward N. and Della L. Thome Memorial Foundation, Bank of America N.A., Trustee, Awards Program in Age-Related Macular Degeneration Research for partial support of this work.

2.7 Tables

Table 2.1. Angiogenic Inhibitors.

Drug (Trade name)	**Target**	**Type of molecule**	**FDA approved target(s)**
Bevacizumab (Avastin®) [25]	anti-VEGF receptor	humanized mAb	mCRC, NSCLC, advanced breast cancer
Ranibizumab (Lucentis®) [26]	anti-VEGF receptor	mAb fragment	wet AMD
Pegaptanib (Macugen®) [27]	anti-VEGF receptor	pegylated anti-VEGF aptamer	wet AMD
Aflibercept (VEGF Trap) [28]	Binds/sequesters VEGF-A and PLGF	fusion protein	wet AMD
Cetuximab (Erbitux®) [29, 30]	anti-EGFR	chimeric IgG1 mAb	mCRC, head and neck cancer in KRAS-wt patients
Panitumumab (Vectibix®) [31]	anti-EGFR	fully humanized IgG2 mAb	mCRC
Trastuzumab (Herceptin®) [32, 33]	anti-HER-2	humanized IgG1 mAb	Breast cancer
Gefitinib (Iressa™) [34] and Erlotinib (Tarveca®) [35]	RTKI of EGFR	oral small molecule	NSCLC, pancreatic cancer in EGFR+ patients
Sorafenib (Nexavar®) [36, 37]	RTKI of VEGFR-1,2,3, PDGFR-ß, and Raf-1	oral small molecule	aRCC, advanced hepatocellular carcinoma
Sunitinib (Sutent®) [38, 39]	RTKI of VEGFR-1,2,3, PDGFR- ß, and RET	oral small molecule	aRCC, GIST
Temsirolimus (Torisel®) [40]	mTOR*	oral small molecule	aRCC
Everolimus (Afinitor®) [41]	mTOR*	oral small molecule	aRCC

*inhibits cell division, halts growth signaling, and reduces hypoxia inducible factor (HIF-1 and HIF-2 alpha) and VEGF expression. Abbreviations: Metastatic colorectal cancer (mCRC), Non-Small Cell Lung Cancer (NSCLC), Advanced Renal Cell Carcinoma (aRCC), Age-Related Macular Degeneration (AMD), Vascular Endothelial Growth Factor (VEGF), Epidermal Growth Factor Receptor (EGFR), Receptor Tyrosine Kinase Inhibitor (RTKI), Monoclonal antibody (mAb)

Table 2.2. Drug delivery systems and representative examples and applications thereof.

Delivery System	**Examples**	**Clinical uses / Potential applications**
Free drug	Small molecule drug against receptor tyrosine kinase [133]	Sunitinib: advanced renal cell carcinoma
	Whole antibody against VEGF [25]	Bevacizumab: Metastatic colorectal cancer (mCRC), non-small cell lung cancer (NSCLC), advanced breast cancer
	Antibody Fab' fragment against VEGF [26]	Ranibizumab: Exudative age-related macular degeneration (AMD)
	Whole protein rhPDGF [170]	Becaplermin: Pro-angiogenesis in diabetic ulcers
	Protein with VEGFR-binding domains and Fc antibody region [163]	VEGF-TRAP: Anti-angiogenesis in tumors and exudative AMD
	Protein regulating ocular blood vessel growth [171]	adPEDF: AMD
Drug-delivery agent conjugates	RGD sequences bound to drug [172]	EMD 121974 (Cilengitide): Drug targeted to vasculature for melanoma, glioblastoma, prostate cancer
	Interferon alpha bound to PEG [173-175]	Pegasys: antiviral PegIntron: antineoplastic
	Fab' fragment against VEGFR-2 conjugated to PEG [153]	CDP791: Inhibit VEGF signaling in non-squamous non-small-cell lung cancer
	Pegylated RNA aptamer targeting VEGF [27]	Pegaptanib: Exudative AMD

Implanted depots	VEGF, bFGF, or TGFβ encapsulated in collagen or gelatin hydrogels [55, 56, 58, 59]	Pro-angiogenic tissue engineering scaffolds
	Cannula depot injection of anecortave acetate [47]	Controlled release formulation of angiostatic steroid for AMD
Liposomes	Cationic liposomes containing paclitaxel or oxaliplatin [144, 145]	Targeting to tumor vasculature for cancer chemotherapy
	RGD-conjugated liposomes containing doxorubicin [50]	
Biodegradable micro- and nanoparticles	PLGA, PLA, PCL, polyanhydride, alginate, or gelatin particles [64-67]	Injectable or embedded vehicles for long-term delivery of proteins, mucleotides, or small-molecule drugs
	DNA, RNA, or oligonucleotides complexed with polycations [101]	Self-assembled nanoparticles for gene delivery
Nondegradable nanoparticles	Gold or iron-oxide nanoparticles [123-125, 127, 129]	Magnetic imaging, drug delivery, thermal therapy
	Mesoporous silicon microparticles [120, 122]	Intravenous delivery of therapeutics
Cell-based systems	VEGF-transfected CHO cells embedded in biodegradable polymer [116]	Pro-angiogenic factors secreted by cells within tissue engineering scaffolds

2.8 Figures

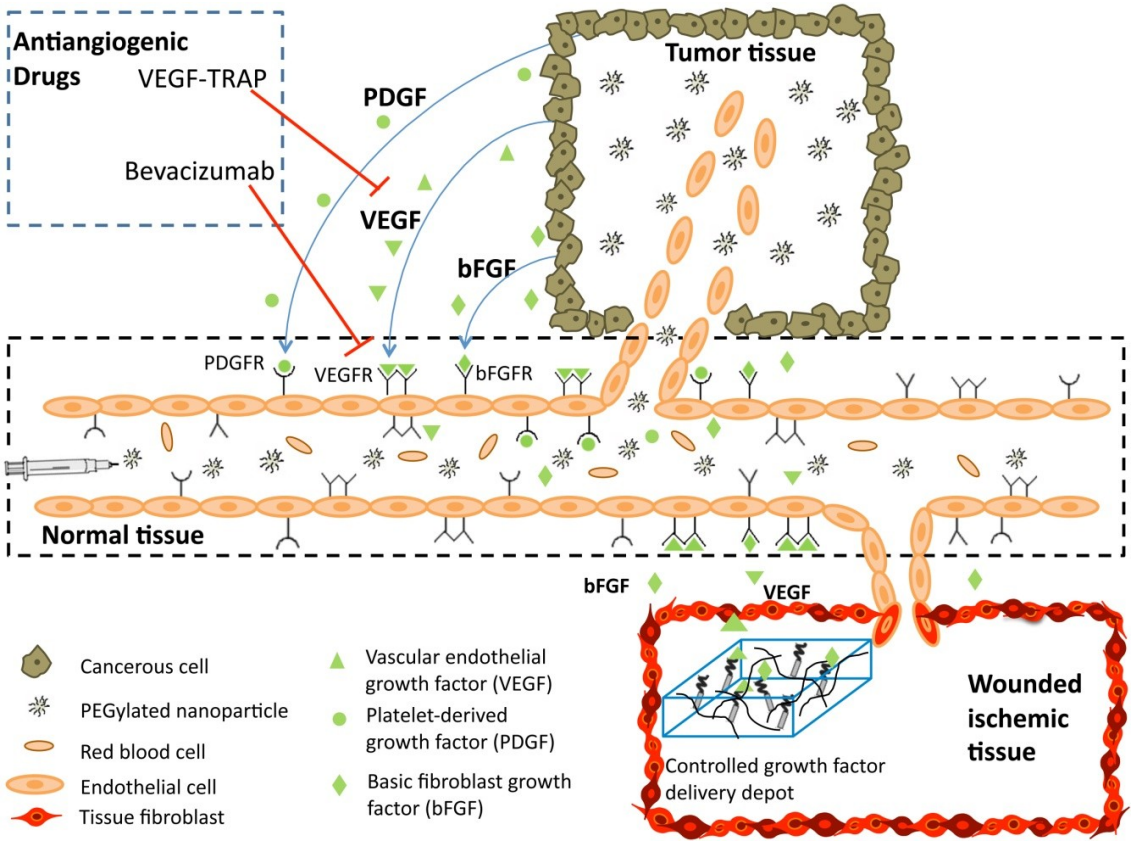

Figure 2.1. This schematic diagram depicts the angiogenic and anti-angiogenic responses at a capillary level. The cancer cells in tumor tissue secrete angiogenic growth factors that bind to their respective receptors on the endothelial cells lining the capillaries, leading to recruitment of disorganized blood vessels infiltrating into the tumor. This leaky vasculature allows entry of the systemically injected vector (eg. a PEGylated nanoparticle) into tumor tissue, while the vector cannot pass across the mature walls of normal tissue vessels. This results in passive targeting of the tumor by the enhanced permeability and retention (EPR) effect. Anti-angiogenic drugs, like VEGF-TRAP and bevacizumab, block the angiogenic effect of the growth factors. Therapeutic angiogenesis for treatment of ischemic diseases or vascularization of a tissue engineered construct is achieved by controlled local delivery of pro-angiogenic factors using a synthetic delivery scaffold (eg. fibrin hydrogel loaded with non-covalently or covalently bound growth factors).

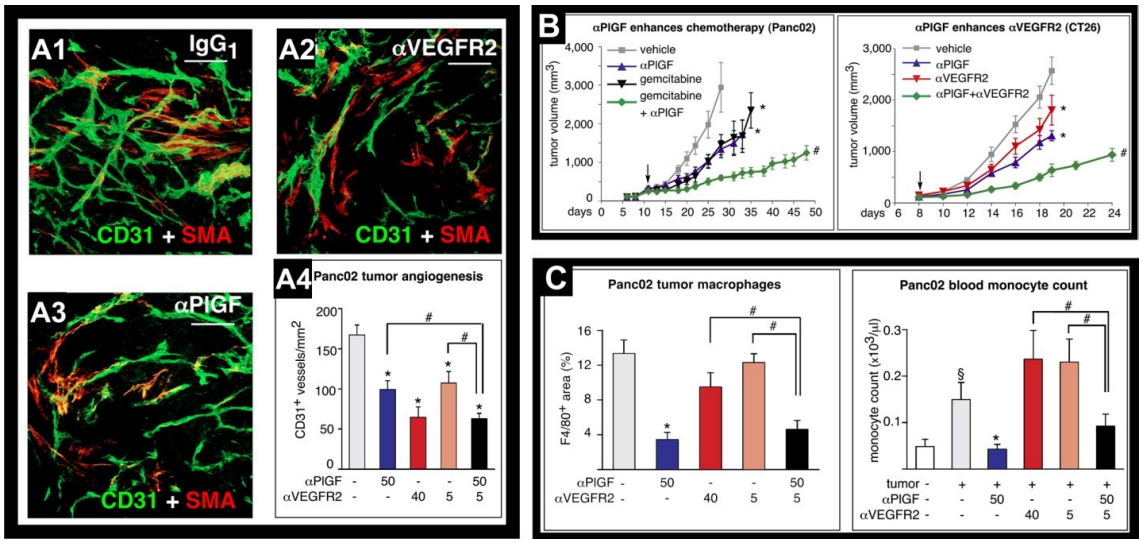

Figure 2.2. (A1-3) Antibodies against PlGF and VEGFR2 inhibit tumor angiogenesis compared to nonspecific antibody IgG_1., particularly in combination **(A4)**. PlGF antibody also enhances the effect of gemcitabine, measured by tumor volume **(B)**, and inhibits excessive recruitment of macrophages; the latter is not enhanced by coadministration of anti-VEGFR-2 **(C)**. Adapted with permission from Elsevier: Fischer et al., *Cell*, 2007 [135].

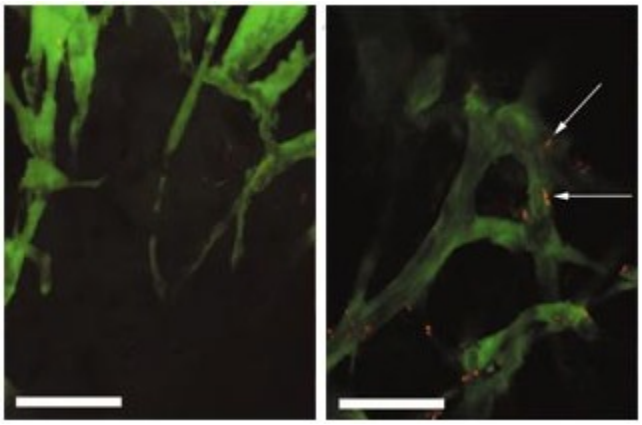

Figure 2.3. Tumor vasculature is highlighted by green fluorescence, overlaid with red-fluorescent liposomes. The two sections shown are 50 μm apart in the tumor tissue, with a large difference in liposome migration from one part of the tumor to the other. Scale

bar: 50 μm. Adapted with permission from Macmillan Publishers Ltd: Brown et al., *Nature Medicine*, 2001 [146].

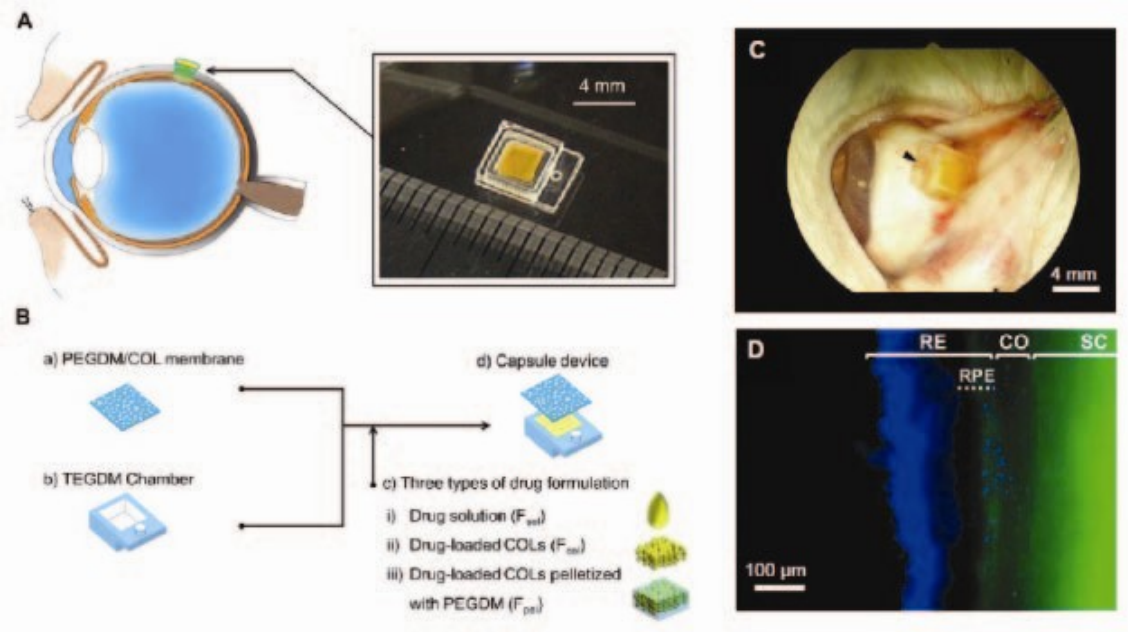

Figure 2.4. (A) Transscleral drug delivery device. **(B)** Device made with TEGDM reservoir and PEGDM/Col membrane which can be loaded with various drug solutions. **(C)** Capsule sutured onto rabbit eye sclera 3 days after implantation. Arrowhead indicates suture site. **(D)** Distribution of model drug FD40 (green) around implantation site at day 3. Cell nuclei dyed stained blue. FD40 reaches retinal pigment epithelium (RPE). Retina (RE), choroids (CO), sclera (SC). Adapted with permission from Elsevier: Kawashima et al, Biomaterials, 2010 [161].

2.9 References

1. Phelps EA, Garcia AJ. Update on therapeutic vascularization strategies. Regen Med 2009 Jan;4(1):65-80.

2. Eichmann A, Pardanaud L, Yuan L, Moyon D. Vasculogenesis and the search for the hemangioblast. J Hematoth Stem Cell 2002 Apr;11(2):207-214.

3. Risau W. Mechanisms of angiogenesis. Nature 1997 Apr 17;386(6626):671-674.

4. Glotzbach JP, Levi B, Wong VW, Longaker MT, Gurtner GC. The basic science of vascular biology: implications for the practicing surgeon. Plast Reconstr Surg 2010 Nov;126(5):1528-1538.

5. Folkman J. Angiogenesis in psoriasis: therapeutic implications. J Invest Dermatol 1972;59:40-43.

6. Moulton KS. Angiogenesis in atherosclerosis: gathering evidence beyond speculation. Curr Opin Lipidol 2006;17:548-555.

7. Moulton KS. Inhibition of plaque neovascularization reduces macrophage accumulation and progression of advanced atherosclerosis. Proc Natl Acad Sci USA 2003;100:4736-4741.

8. Paleolog EM. Angiogenesis in rheumatoid arthritis. Arthritis Res 2002;4 Suppl 3:S81-90.

9. Brown RA, Weiss JB, Tomlinson IW, Phillips P, Kumar S. Angiogenic factor from synovial fluid resembling that from tumours. Lancet 1980 Mar 29;1(8170):682-685.

10. Martin A, Komada MR, Sane DC. Abnormal angiogenesis in diabetes mellitus. Med Res Rev 2003 Mar;23(2):117-145.

11. Folkman J. Tumor angiogenesis: therapeutic implications. N Engl J Med 1971;285:1182-1186.

12. Miller JW. Vascular endothelial growth factor/vascular permeability factor is temporally and spatially correlated with ocular angiogenesis in a primate model. Am J Pathol 1994;145:574-584.

13. Folkman J. Angiogenesis: an organizing principle for drug discovery? Nat Rev Drug Discov 2007;6(4):273-286.

14. Bergers G, Benjamin LE. Tumorigenesis and the angiogenic switch. Nat Rev Cancer 2003 Jun;3(6):401-410.

15. Abdollahi A, Folkman J. Evading tumor evasion: Current concepts and perspectives of anti-angiogenic cancer therapy. Drug Resist Updat 2010 Feb-Apr;13(1-2):16-28.

16. Ferrara N. Vascular endothelial growth factor: basic science and clinical progress. Endocr Rev 2004 Aug;25(4):581-611.

17. Cross MJ, Claesson-Welsh L. FGF and VEGF function in angiogenesis: signalling pathways, biological responses and therapeutic inhibition. Trends Pharmacol Sci 2001 Apr;22(4):201-207.

18. Giles FJ. The vascular endothelial growth factor (VEGF) signaling pathway: a therapeutic target in patients with hematologic malignancies. Oncologist 2001;6 Suppl 5:32-39.

19. Hall H. Modified fibrin hydrogel matrices: both, 3D-scaffolds and local and controlled release systems to stimulate angiogenesis. Curr Pharm Des 2007;13(35):3597-3607.

20. Weinberg RA. The Biology of Cancer. New York, NY: 270 Madison Avenue, Garland Science, Taylor and Francis Group LLC, 2007.

21. Browder T, Butterfield CE, Kraling BM, Shi B, Marshall B, O'Reilly MS, et al. Antiangiogenic scheduling of chemotherapy improves efficacy against experimental drug-resistant cancer. Cancer Res 2000 Apr 1;60(7):1878-1886.

22. Wu HC, Chang DK. Peptide-mediated liposomal drug delivery system targeting tumor blood vessels in anticancer therapy. J Oncol 2010;2010:723798.

23. Jain RK. Normalization of tumor vasculature: An emerging concept in antiangiogenic therapy. Science 2005;307(5706):58-62.

24. Ng QS, Goh V, Milner J, Padhani AR, Saunders MI, Hoskin PJ. Acute tumor vascular effects following fractionated radiotherapy in human lung cancer: In vivo whole tumor assessment using volumetric perfusion computed tomography. International Journal of Radiation Oncology Biology Physics 2007;67(2):417-424.

25. Hurwitz H, Fehrenbacher L, Novotny W, Cartwright T, Hainsworth J, Heim W, et al. Bevacizumab plus irinotecan, fluorouracil, and leucovorin for metastatic colorectal cancer. N Engl J Med 2004 Jun 3;350(23):2335-2342.

26. Rosenfeld PJ, Brown DM, Heier JS, Boyer DS, Kaiser PK, Chung CY, et al. Ranibizumab for neovascular age-related macular degeneration. N Engl J Med 2006 Oct 5;355(14):1419-1431.

27. Gragoudas ES, Adamis AP, Cunningham ET, Jr., Feinsod M, Guyer DR. Pegaptanib for neovascular age-related macular degeneration. N Engl J Med 2004 Dec 30;351(27):2805-2816.

28. Dixon JA, Oliver SC, Olson JL, Mandava N. VEGF Trap-Eye for the treatment of neovascular age-related macular degeneration. Expert Opin Investig Drugs 2009 Oct;18(10):1573-1580.

29. Bonner JA, Harari PM, Giralt J, Azarnia N, Shin DM, Cohen RB, et al. Radiotherapy plus cetuximab for squamous-cell carcinoma of the head and neck. N Engl J Med 2006 Feb 9;354(6):567-578.

30. Van Cutsem E, Kohne CH, Hitre E, Zaluski J, Chang Chien CR, Makhson A, et al. Cetuximab and chemotherapy as initial treatment for metastatic colorectal cancer. N Engl J Med 2009 Apr 2;360(14):1408-1417.

31. Van Cutsem E, Peeters M, Siena S, Humblet Y, Hendlisz A, Neyns B, et al. Open-label phase III trial of panitumumab plus best supportive care compared with best supportive care alone in patients with chemotherapy-refractory metastatic colorectal cancer. J Clin Oncol 2007 May 1;25(13):1658-1664.

32. Bang YJ, Van Cutsem E, Feyereislova A, Chung HC, Shen L, Sawaki A, et al. Trastuzumab in combination with chemotherapy versus chemotherapy alone for treatment of HER2-positive advanced gastric or gastro-oesophageal junction cancer (ToGA): a phase 3, open-label, randomised controlled trial. Lancet 2010 Aug 28;376(9742):687-697.

33. Slamon DJ, Leyland-Jones B, Shak S, Fuchs H, Paton V, Bajamonde A, et al. Use of chemotherapy plus a monoclonal antibody against HER2 for metastatic breast cancer that overexpresses HER2. N Engl J Med 2001 Mar 15;344(11):783-792.

34. Mok TS, Wu YL, Thongprasert S, Yang CH, Chu DT, Saijo N, et al. Gefitinib or carboplatin-paclitaxel in pulmonary adenocarcinoma. N Engl J Med 2009 Sep 3;361(10):947-957.

35. Cappuzzo F, Ciuleanu T, Stelmakh L, Cicenas S, Szczesna A, Juhasz E, et al. Erlotinib as maintenance treatment in advanced non-small-cell lung cancer: a multicentre, randomised, placebo-controlled phase 3 study. Lancet Oncol 2010 Jun;11(6):521-529.

36. Llovet JM, Ricci S, Mazzaferro V, Hilgard P, Gane E, Blanc JF, et al. Sorafenib in advanced hepatocellular carcinoma. N Engl J Med 2008 Jul 24;359(4):378-390.

37. Escudier B, Eisen T, Stadler WM, Szczylik C, Oudard S, Siebels M, et al. Sorafenib in advanced clear-cell renal-cell carcinoma. N Engl J Med 2007 Jan 11;356(2):125-134.

38. Motzer RJ, Hutson TE, Tomczak P, Michaelson MD, Bukowski RM, Rixe O, et al. Sunitinib versus interferon alfa in metastatic renal-cell carcinoma. N Engl J Med 2007 Jan 11;356(2):115-124.

39. Demetri GD, van Oosterom AT, Garrett CR, Blackstein ME, Shah MH, Verweij J, et al. Efficacy and safety of sunitinib in patients with advanced gastrointestinal stromal tumour after failure of imatinib: a randomised controlled trial. Lancet 2006 Oct 14;368(9544):1329-1338.

40. Hudes G, Carducci M, Tomczak P, Dutcher J, Figlin R, Kapoor A, et al. Temsirolimus, interferon alfa, or both for advanced renal-cell carcinoma. N Engl J Med 2007 May 31;356(22):2271-2281.

41. Motzer RJ, Escudier B, Oudard S, Hutson TE, Porta C, Bracarda S, et al. Efficacy of everolimus in advanced renal cell carcinoma: a double-blind, randomised, placebo-controlled phase III trial. Lancet 2008 Aug 9;372(9637):449-456.

42. Kerbel RS, Kamen BA. The anti-angiogenic basis of metronomic chemotherapy. Nat Rev Cancer 2004 Jun;4(6):423-436.

43. Chakravarthy U, Evans J, Rosenfeld PJ. Age related macular degeneration. BMJ 2010;340:c981.

44. Nguyen QD, Shah SM, Browning DJ, Hudson H, Sonkin P, Hariprasad SM, et al. A phase I study of intravitreal vascular endothelial growth factor trap-eye in patients with neovascular age-related macular degeneration. Ophthalmology 2009 Nov;116(11):2141-2148 e2141.

45. Ambati J, Ambati BK, Yoo SH, Ianchulev S, Adamis AP. Age-related macular degeneration: etiology, pathogenesis, and therapeutic strategies. Surv Ophthalmol 2003 May-Jun;48(3):257-293.

46. Bressler SB. Introduction: Understanding the role of angiogenesis and antiangiogenic agents in age-related macular degeneration. Ophthalmology 2009 Oct;116(10 Suppl):S1-7.

47. Lu M, Adamis AP. Molecular biology of choroidal neovascularization. Ophthalmol Clin North Am 2006 Sep;19(3):323-334.

48. Gerber HP, Senter PD, Grewal IS. Antibody drug-conjugates targeting the tumor vasculature: Current and future developments. MAbs 2009;1(3):247-253.

49. Temming K, Schiffelers RM, Molema G, Kok RJ. RGD-based strategies for selective delivery of therapeutics and imaging agents to the tumour vasculature. Drug Resist Updat 2005;8(6):381-402. Epub 2005 Nov 2023.

50. Murphy EA, Majeti BK, Barnes LA, Makale M, Weis SM, Lutu-Fuga K, et al. Nanoparticle-mediated drug delivery to tumor vasculature suppresses metastasis. Proc Natl Acad Sci U S A 2008;105(27):9343-9348. Epub 2008 Jul 9347.

51. Mitra A, Mulholland J, Nan A, McNeill E, Ghandehari H, Line BR. Targeting tumor angiogenic vasculature using polymer-RGD conjugates. J Control Release 2005;102(1):191-201.

52. Green MR, Manikhas GM, Orlov S, Afanasyev B, Makhson AM, Bhar P, et al. Abraxane®, a novel Cremophor®-free, albumin-bound particle form of paclitaxel for the treatment of advanced non-small-cell lung cancer. Annals of Oncology 2006;17(8):1263-1268.

53. Brem H, Mahaley MS, Vick NA, Black KL, Schold SC, Burger PC, et al. Interstitial chemotherapy with drug polymer implants for the treatment of recurrent gliomas. Journal of Neurosurgery 1991;74(3):441-446.

54. Perry J, Chambers A, Spithoff K, Laperriere N. Gliadel wafers in the treatment of malignant glioma: a systematic review. Curr Oncol 2007;14(5):189-194.

55. Benoit DSW, Nuttelman CR, Collins SD, Anseth KS. Synthesis and characterization of a fluvastatin-releasing hydrogel delivery system to modulate hMSC differentiation and function for bone regeneration. Biomaterials 2006;27(36):6102-6110.

56. Tabata Y, Miyao M, Ozeki M, Ikada Y. Controlled release of vascular endothelial growth factor by use of collagen hydrogels. Journal of Biomaterials Science, Polymer Edition 2000;11:915-930.

57. Lutolf MP, Lauer-Fields JL, Schmoekel HG, Metters AT, Weber FE, Fields GB, et al. Synthetic matrix metalloproteinase-sensitive hydrogels for the conduction of tissue regeneration: engineering cell-invasion characteristics. Proc Natl Acad Sci U S A 2003;100(9):5413-5418. Epub 2003 Apr 5419.

58. Yasuhiko T. Current status of regenerative medical therapy based on drug delivery technology. Reproductive biomedicine online 2008;16(1):70-80.

59. Hoare TR, Kohane DS. Hydrogels in drug delivery: Progress and challenges. Polymer 2008;49(8):1993-2007.

60. Williams DF. Tissue-biomaterial interactions. Journal of Materials Science 1987;22(10):3421-3445.

61. Anderson JM, Rodriguez A, Chang DT. Foreign body reaction to biomaterials. Seminars in Immunology 2008;20(2):86-100.

62. Willerth SM, Sakiyama-Elbert SE. Approaches to neural tissue engineering using scaffolds for drug delivery. Advanced Drug Delivery Reviews 2007;59(4-5):325-338.

63. Saltzman WM, Olbricht WL. Building drug delivery into tissue engineering. Nat Rev Drug Discov 2002;1(3):177-186.

64. Schakenraad JM, Hardonk MJ, Feijen J, Molenaar I, Nieuwenhuis P. Enzymatic activity toward poly(L-lactic acid) implants. Journal of Biomedical Materials Research 1990;24(5):529-545.

65. Spenlehauer G, Vert M, Benoit JP, Boddaert A. In vitro and In vivo degradation of poly(D,L lactide/glycolide) type microspheres made by solvent evaporation method. Biomaterials 1989;10(8):557-563.

66. Anderson JM, Shive MS. Biodegradation and biocompatibility of PLA and PLGA microspheres. Advanced Drug Delivery Reviews 1997;28(1):5-24.

67. Panyam J, Labhasetwar V. Biodegradable nanoparticles for drug and gene delivery to cells and tissue. Advanced Drug Delivery Reviews 2003;55(3):329-347.

68. Faraji AH, Wipf P. Nanoparticles in cellular drug delivery. Bioorganic & Medicinal Chemistry 2009;17(8):2950-2962.

69. Freiberg S, Zhu XX. Polymer microspheres for controlled drug release. International Journal of Pharmaceutics 2004;282(1-2):1-18.

70. Varde NK, Pack DW. Microspheres for controlled release drug delivery. Expert Opinion on Biological Therapy 2004;4(1):35-51.

71. Patil SD, Papadmitrakopoulos F, Burgess DJ. Concurrent delivery of dexamethasone and VEGF for localized inflammation control and angiogenesis. Journal of Controlled Release 2007;117(1):68-79.

72. Visscher GE, Pearson JE, Fong JW, Argentieri GJ, Robison RL, Maulding HV. Effect of particle size on the in vitro and in vivo degradation rates of poly(DL-lactide-co-glycolide) microcapsules. Journal of Biomedical Materials Research 1988;22(8):733-746.

73. Grizzi I, Garreau H, Li S, Vert M. Hydrolytic degradation of devices based on poly(-lactic acid) size-dependence. Biomaterials 1995;16(4):305-311.

74. Bertram JP, Jay SM, Hynes SR, Robinson R, Criscione JM, Lavik EB. Functionalized poly(lactic-co-glycolic acid) enhances drug delivery and provides chemical moieties for surface engineering while preserving biocompatibility. Acta Biomaterialia 2009;5(8):2860-2871.

75. Blanco MD, Alonso MJ. Development and characterization of protein-loaded poly(lactide-co-glycolide) nanospheres. European Journal of Pharmaceutics and Biopharmaceutics 1997;43(3):287-294.

76. Qi H, Hu P, Xu J, Wang A. Encapsulation of Drug Reservoirs in Fibers by Emulsion Electrospinning: Morphology Characterization and Preliminary Release Assessment. Biomacromolecules 2006;7(8):2327-2330.

77. Holland TA, Tabata Y, Mikos AG. In vitro release of transforming growth factor-[beta]1 from gelatin microparticles encapsulated in biodegradable, injectable oligo(poly(ethylene glycol) fumarate) hydrogels. Journal of Controlled Release 2003;91(3):299-313.

78. Tzeng SY, Lavik EB. Photopolymerizable nanoarray hydrogels deliver CNTF and promote differentiation of neural stem cells. Soft Matter 2010;6(10):2208-2215.

79. Dobrovolskaia MA, Aggarwal P, Hall JB, McNeil SE. Preclinical Studies To Understand Nanoparticle Interaction with the Immune System and Its Potential Effects on Nanoparticle Biodistribution. Molecular Pharmaceutics 2008;5(4):487-495.

80. Li S-D, Huang L. Pharmacokinetics and Biodistribution of Nanoparticles. Molecular Pharmaceutics 2008;5(4):496-504.

81. Owens Iii DE, Peppas NA. Opsonization, biodistribution, and pharmacokinetics of polymeric nanoparticles. International Journal of Pharmaceutics 2006;307(1):93-102.

82. Bertram JP, Williams CA, Robinson R, Segal SS, Flynn NT, Lavik EB. Intravenous Hemostat: Nanotechnology to Halt Bleeding. Science Translational Medicine 2009 December 16, 2009;1(11):11ra22.

83. Shmueli RB, Anderson DG, Green JJ. Electrostatic surface modifications to improve gene delivery. Expert Opin Drug Deliv 2010 2010;7(4):535-550.

84. Jones M, Leroux J. Polymeric micelles - a new generation of colloidal drug carriers. Eur J Pharm Biopharm 1999 Sep;48(2):101-111.

85. Gulati M, Grover M, Singh S, Singh M. Lipophilic drug derivatives in liposomes. International Journal of Pharmaceutics 1998;165(2):129-168.

86. Fresta M, Puglisi G, Panico AM, Marco SD, Mazzone G. Cdp-Choline Entrapment and Release from Multilamellar and Reverse-Phase Evaporation Liposomes. Drug Development and Industrial Pharmacy 1993;19(5):559-585.

87. Vadiei K, Lopez-Berestein G, Perez-Soler R, Luke DR. In vitro evaluation of liposomal cyclosporine. International Journal of Pharmaceutics 1989;57(2):133-138.

88. Damen J, Regts J, Scherphof G. Transfer and exchange of phospholipid between small unilamellar liposomes and rat plasma high density lipoproteins. Dependence on cholesterol content and phospholipid composition. Biochim Biophys Acta 1981;665(3):538-545.

89. Chonn A, Semple SC, Cullis PR. Association of blood proteins with large unilamellar liposomes in vivo. Relation to circulation lifetimes. J Biol Chem 1992;267(26):18759-18765.

90. Senior J, Gregoriadis G. Is half-life of circulating liposomes determined by changes in their permeability? FEBS Letters 1982;145(1):109-114.

91. Juliano RL, Stamp D. The effect of particle size and charge on the clearance rates of liposomes and liposome encapsulated drugs. Biochemical and Biophysical Research Communications 1975;63(3):651-658.

92. Scherphof GL, Dijkstra J, Spanjer HH, Derksen JT, Roerdink FH. Uptake and intracellular processing of targeted and nontargeted liposomes by rat Kupffer cells in vivo and in vitro. Ann N Y Acad Sci 1985;446:368-384.

93. Alving CR, Steck EA, Chapman WL, Jr., Waits VB, Hendricks LD, Swartz GM, Jr., et al. Therapy of leishmaniasis: superior efficacies of liposome-encapsulated drugs. Proc Natl Acad Sci U S A 1978;75(6):2959-2963.

94. Harashima H, Sakata K, Funato K, Kiwada H. Enhanced hepatic uptake of liposomes through complement activation depending on the size of liposomes. Pharm Res 1994;11(3):402-406.

95. Senior JH. Fate and behavior of liposomes in vivo: a review of controlling factors. Crit Rev Ther Drug Carrier Syst 1987;3(2):123-193.

96. Soppimath KS, Aminabhavi TM, Kulkarni AR, Rudzinski WE. Biodegradable polymeric nanoparticles as drug delivery devices. Journal of Controlled Release 2001 Jan 29;70(1-2):1-20.

97. Discher DE, Ahmed F. Polymersomes. Annual Review of Biomedical Engineering 2006;8:323-341.

98. Letchford K, Burt H. A review of the formation and classification of amphiphilic block copolymer nanoparticulate structures: micelles, nanospheres, nanocapsules and polymersomes. Eur J Pharm Biopharm 2007 Mar;65(3):259-269.

99. Luo LB, Eisenberg A. Thermodynamic size control of block copolymer vesicles in solution. Langmuir 2001 Oct 30;17(22):6804-6811.

100. Fischer D, Bieber T, Li Y, Elsasser HP, Kissel T. A novel non-viral vector for DNA delivery based on low molecular weight, branched polyethylenimine: effect of molecular weight on transfection efficiency and cytotoxicity. Pharm Res 1999;16(8):1273-1279.

101. Putnam D. Polymers for gene delivery across length scales. Nat Mater 2006;5(6):439-451.

102. Leong KW, Mao HQ, Truong-Le VL, Roy K, Walsh SM, August JT. DNA-polycation nanospheres as non-viral gene delivery vehicles. Journal of Controlled Release 1998;53(1-3):183-193.

103. Haensler J, Szoka FC. Polyamidoamine cascade polymers mediate efficient transfection of cells in culture. Bioconjugate Chemistry 1993;4(5):372-379.

104. Green JJ, Langer R, Anderson DG. A Combinatorial Polymer Library Approach Yields Insight into Nonviral Gene Delivery. Acc Chem Res 2008 May 29.

105. Bhise NS, Gray RS, Sunshine JC, Htet S, Ewald AJ, Green JJ. The relationship between terminal functionalization and molecular weight of a gene delivery polymer and transfection efficacy in mammary epithelial 2-D cultures and 3-D organotypic cultures. Biomaterials 2010 Nov;31(31):8088-8096.

106. Thomas CE, Ehrhardt A, Kay MA. Progress and problems with the use of viral vectors for gene therapy. Nat Rev Genet 2003;4(5):346-358.

107. Green JJ, Shi J, Chiu E, Leshchiner ES, Langer R, Anderson DG. Biodegradable polymeric vectors for gene delivery to human endothelial cells. Bioconjugate Chemistry 2006;17:1162-1169.

108. Green JJ, Zugates GT, Tedford NC, Huang Y, Griffith LG, Lauffenburger DA, et al. Combinatorial modification of degradable polymers enables transfection of human cells comparable to adenovirus. Advanced Materials 2007;19(19):2836-2842.

109. Sunshine J, Green JJ, Mahon K, Yang F, Eltoukhy A, Nguyen DN, et al. Small molecule end group of linear polymer determine cell-type gene delivery efficacy. Advanced Materials 2009;21(48):4947-4951.

110. Yang F, Cho SW, Son SM, Bogatyrev SR, Singh D, Green JJ, et al. Genetic engineering of human stem cells for enhanced angiogenesis using biodegradable polymeric nanoparticles. Proc Natl Acad Sci U S A 2009;107(8):3317-3322.

111. Karoubi G, Ormiston ML, Stewart DJ, Courtman DW. Single-cell hydrogel encapsulation for enhanced survival of human marrow stromal cells. Biomaterials 2009;30(29):5445-5455.

112. Orive G, De Castro M, Kong H-J, Hernández RM, Ponce S, Mooney DJ, et al. Bioactive cell-hydrogel microcapsules for cell-based drug delivery. Journal of Controlled Release 2009;135(3):203-210.

113. Roger M, Clavreul A, Venier-Julienne M-C, Passirani C, Sindji L, Schiller P, et al. Mesenchymal stem cells as cellular vehicles for delivery of nanoparticles to brain tumors. Biomaterials 2010;31(32):8393-8401.

114. Devika BC, Michael D, James S, Christine A, David AJ. Cellular uptake and transport of gold nanoparticles incorporated in a liposomal carrier. Nanomedicine 2010 Feb;6(1):161-169.

115. Hernández RM, Orive G, Murua A, Pedraz JL. Microcapsules and microcarriers for in situ cell delivery. Advanced Drug Delivery Reviews 2010;62(7-8):711-730.

116. Soker S, Machado M, Atala A. Systems for therapeutic angiogenesis in tissue engineering. World Journal of Urology 2000;18(1):10-18.

117. Han Bae Y, Mikos AG. Cells for drug delivery platforms. Adv Drug Deliv Rev 2000;42(1-2):1-2.

118. Tresco PA, Biran R, Noble MD. Cellular transplants as sources for therapeutic agents. Adv Drug Deliv Rev 2000;42(1-2):3-27.

119. Sheyn D, Mizrahi O, Benjamin S, Gazit Z, Pelled G, Gazit D. Genetically modified cells in regenerative medicine and tissue engineering. Advanced Drug Delivery Reviews 2010;62(7-8):683-698.

120. Lu J, Liong M, Zink JI, Tamanoi F. Mesoporous silica nanoparticles as a delivery system for hydrophobic anticancer drugs. Small 2007;3(8):1341-1346.

121. Salonen J, Kaukonen AM, Hirvonen J, Lehto VP. Mesoporous silicon in drug delivery applications. J Pharm Sci 2008;97(2):632-653.

122. Tanaka T, Mangala LS, Vivas-Mejia PE, Nieves-Alicea R, Mann AP, Mora E, et al. Sustained small interfering RNA delivery by mesoporous silicon particles. Cancer Research 2010;70(9):3687-3696.

123. Weissleder R, Elizondo G, Wittenberg J, Rabito CA, Bengele HH, Josephson L. Ultrasmall superparamagnetic iron oxide: characterization of a new class of contrast agents for MR imaging. Radiology 1990;175(2):489-493.

124. Lee H, Lee E, Kim DK, Jang NK, Jeong YY, Jon S. Antibiofouling Polymer-Coated Superparamagnetic Iron Oxide Nanoparticles as Potential Magnetic Resonance Contrast Agents for in Vivo Cancer Imaging. Journal of the American Chemical Society 2006;128(22):7383-7389.

125. De Cuyper M, Joniau M. Magnetoliposomes. Formation and structural characterization. Eur Biophys J 1988;15(5):311-319.

126. Zhang C, Jugold M, Woenne EC, Lammers T, Morgenstern B, Mueller MM, et al. Specific targeting of tumor angiogenesis by RGD-conjugated ultrasmall superparamagnetic iron oxide particles using a clinical 1.5-T magnetic resonance scanner. Cancer Res 2007;67(4):1555-1562.

127. Kawano T, Yamagata M, Takahashi H, Niidome Y, Yamada S, Katayama Y, et al. Stabilizing of plasmid DNA in vivo by PEG-modified cationic gold nanoparticles and the gene expression assisted with electrical pulses. J Control Release 2006;111(3):382-389. Epub 2006 Feb 2017.

128. Lee J-S, Green JJ, Love KT, Sunshine J, Langer R, Anderson DG. Gold, Poly(B-amino ester) Nanoparticles for Small Interfering RNA Delivery. Nano Letters 2009;9(6):2402-2406.

129. Hirsch LR, Stafford RJ, Bankson JA, Sershen SR, Rivera B, Price RE, et al. Nanoshell-mediated near-infrared thermal therapy of tumors under magnetic resonance guidance. Proc Natl Acad Sci U S A 2003;100(23):13549-13554. Epub 12003 Nov 13543.

130. Nel A, Xia T, Madler L, Li N. Toxic potential of materials at the nanolevel. Science 2006;311(5761):622-627.

131. Di Pasqua AJ, Sharma KK, Shi Y-L, Toms BB, Ouellette W, Dabrowiak JC, et al. Cytotoxicity of mesoporous silica nanomaterials. Journal of Inorganic Biochemistry 2008;102(7):1416-1423.

132. Folkman J. Angiogenesis. Annu Rev Med 2006;57:1-18.

133. Ebos JML, Lee CR, Christensen JG, Mutsaers AJ, Kerbel RS. Multiple circulating proangiogenic factors induced by sunitinib malate are tumor-independent and correlate with antitumor efficacy. Proceedings of the National Academy of Sciences of the United States of America 2007;104(43):17069-17074.

134. Ebos JML, Lee CR, Cruz-Munoz W, Bjarnason GA, Christensen JG, Kerbel RS. Accelerated Metastasis after Short-Term Treatment with a Potent Inhibitor of Tumor Angiogenesis. Cancer Cell 2009;15(3):232-239.

135. Fischer C, Jonckx B, Mazzone M, Zacchigna S, Loges S, Pattarini L, et al. Anti-PlGF inhibits growth of VEGF(R)-inhibitor-resistant tumors without affecting healthy vessels. Cell 2007 Nov 2;131(3):463-475.

136. Mac Gabhann F, Qutub AA, Annex BH, Popel AS. Systems biology of pro-angiogenic therapies targeting the VEGF system. Wiley Interdiscip Rev Syst Biol Med 2010 Nov-Dec;2(6):694-707.

137. Tang C, Russell PJ, Martiniello-Wilks R, Rasko JE, Khatri A. Concise Review: Nanoparticles and Cellular Carriers-Allies in Cancer Imaging and Cellular Gene Therapy? Stem Cells 2010 Jul 13;28(9):1686-1702.

138. Phillips MA, Gran ML, Peppas NA. Targeted Nanodelivery of Drugs and Diagnostics. Nano Today 2010 Apr 1;5(2):143-159.

139. Greish K. Enhanced permeability and retention of macromolecular drugs in solid tumors: a royal gate for targeted anticancer nanomedicines. J Drug Target 2007 Aug-Sep;15(7-8):457-464.

140. Sipkins DA, Cheresh DA, Kazemi MR, Nevin LM, Bednarski MD, Li KCP. Detection of tumor angiogenesis in vivo by [alpha]v[beta]3-targeted magnetic resonance imaging. Nat Med 1998;4(5):623-626.

141. Li L, Wartchow CA, Danthi SN, Shen Z, Dechene N, Pease J, et al. A novel antiangiogenesis therapy using an integrin antagonist or anti-Flk-1 antibody coated 90Y-labeled nanoparticles. Int J Radiat Oncol Biol Phys 2004 Mar 15;58(4):1215-1227.

142. Dellian M, Yuan F, Trubetskoy VS, Torchilin VP, Jain RK. Vascular permeability in a human tumour xenograft: molecular charge dependence. Br J Cancer 2000;82(9):1513-1518.

143. Juliano RL, Stamp D. The effect of particle size and charge on the clearance rates of liposomes and liposome encapsulated drugs. Biochem Biophys Res Commun 1975 Apr 7;63(3):651-658.

144. Abu-Lila A, Suzuki T, Doi Y, Ishida T, Kiwada H. Oxaliplatin targeting to angiogenic vessels by PEGylated cationic liposomes suppresses the angiogenesis in a dorsal air sac mouse model. J Control Release 2009 Feb 20;134(1):18-25.

145. Kunstfeld R, Wickenhauser G, Michaelis U, Teifel M, Umek W, Naujoks K, et al. Paclitaxel Encapsulated in Cationic Liposomes Diminishes Tumor Angiogenesis and Melanoma Growth in a [ldquo]Humanized[rdquo] SCID Mouse Model. J Investig Dermatol 2003;120(3):476-482.

146. Brown EB, Campbell RB, Tsuzuki Y, Xu L, Carmeliet P, Fukumura D, et al. In vivo measurement of gene expression, angiogenesis and physiological function in tumors using multiphoton laser scanning microscopy. Nat Med 2001 Jul;7(7):864-868.

147. Jain RK. Transport of molecules, particles, and cells in solid tumors. Annu Rev Biomed Eng 1999;1:241-263.

148. Endrich B, Reinhold HS, Gross JF, Intaglietta M. Tissue perfusion inhomogeneity during early tumor growth in rats. J Natl Cancer Inst 1979 Feb;62(2):387-395.

149. Teesalu T, Sugahara KN, Kotamraju VR, Ruoslahti E. C-end rule peptides mediate neuropilin-1-dependent cell, vascular, and tissue penetration. Proc Natl Acad Sci U S A 2009 Sep 22;106(38):16157-16162.

150. Porkka K, Laakkonen P, Hoffman JA, Bernasconi M, Ruoslahti E. A fragment of the HMGN2 protein homes to the nuclei of tumor cells and tumor endothelial cells in vivo. Proc Natl Acad Sci U S A 2002 May 28;99(11):7444-7449.

151. Nanda A, Carson-Walter EB, Seaman S, Barber TD, Stampfl J, Singh S, et al. TEM8 interacts with the cleaved C5 domain of collagen alpha 3(VI). Cancer Res 2004 Feb 1;64(3):817-820.

152. Carson-Walter EB, Watkins DN, Nanda A, Vogelstein B, Kinzler KW, St Croix B. Cell surface tumor endothelial markers are conserved in mice and humans. Cancer Res 2001 Sep 15;61(18):6649-6655.

153. Pasut G, Veronese FM. PEG conjugates in clinical development or use as anticancer agents: an overview. Adv Drug Deliv Rev 2009 Nov 12;61(13):1177-1188.

154. Mordenti J, Cuthbertson RA, Ferrara N, Thomsen K, Berleau L, Licko V, et al. Comparisons of the intraocular tissue distribution, pharmacokinetics, and safety of 125I-labeled full-length and Fab antibodies in rhesus monkeys following intravitreal administration. Toxicol Pathol 1999 Sep-Oct;27(5):536-544.

155. Schmucker C, Ehlken C, Hansen LL, Antes G, Agostini HT, Lelgemann M. Intravitreal bevacizumab (Avastin) vs. ranibizumab (Lucentis) for the treatment of age-related macular degeneration: a systematic review. Curr Opin Ophthalmol 2010 May;21(3):218-226.

156. Subramanian ML, Abedi G, Ness S, Ahmed E, Fenberg M, Daly MK, et al. Bevacizumab vs ranibizumab for age-related macular degeneration: 1-year outcomes of a prospective, double-masked randomised clinical trial. Eye (Lond) 2010 Nov;24(11):1708-1715.

157. Holash J, Davis S, Papadopoulos N, Croll SD, Ho L, Russell M, et al. VEGF-Trap: a VEGF blocker with potent antitumor effects. Proc Natl Acad Sci U S A 2002 Aug 20;99(17):11393-11398.

158. Del Amo EM, Urtti A. Current and future ophthalmic drug delivery systems. A shift to the posterior segment. Drug Discov Today 2008 Feb;13(3-4):135-143.

159. Kim SH, Lutz RJ, Wang NS, Robinson MR. Transport barriers in transscleral drug delivery for retinal diseases. Ophthalmic Res 2007;39(5):244-254.

160. Gaudana R, Ananthula HK, Parenky A, Mitra AK. Ocular drug delivery. AAPS J 2010 Sep;12(3):348-360.

161. Kawashima T, Nagai N, Kaji H, Kumasaka N, Onami H, Ishikawa Y, et al. A scalable controlled-release device for transscleral drug delivery to the retina. Biomaterials 2010 Nov 26.

162. Kim H, Csaky KG. Nanoparticle-integrin antagonist C16Y peptide treatment of choroidal neovascularization in rats. J Control Release 2010 Mar 3;142(2):286-293.

163. Karagiannis ED, Popel AS. A systematic methodology for proteome-wide identification of peptides inhibiting the proliferation and migration of endothelial cells. Proc Natl Acad Sci U S A 2008 Sep 16;105(37):13775-13780.

164. Koskimaki JE, Karagiannis ED, Rosca EV, Vesuna F, Winnard PT, Jr., Raman V, et al. Peptides derived from type IV collagen, CXC chemokines, and thrombospondin-1 domain-containing proteins inhibit neovascularization and suppress tumor growth in MDA-MB-231 breast cancer xenografts. Neoplasia 2009 Dec;11(12):1285-1291.

165. Molokhia SA, Sant H, Simonis J, Bishop CJ, Burr RM, Gale BK, et al. The capsule drug device: novel approach for drug delivery to the eye. Vision Res 2010 Mar 31;50(7):680-685.

166. Campochiaro PA, Hafiz G, Shah SM, Bloom S, Brown DM, Busquets M, et al. Sustained ocular delivery of fluocinolone acetonide by an intravitreal insert. Ophthalmology 2010 Jul;117(7):1393-1399 e1393.

167. Yasukawa T, Ogura Y. Medical devices for the treatment of eye diseases. Handb Exp Pharmacol 2010(197):469-489.

168. Campbell M, Nguyen AT, Kiang AS, Tam LC, Gobbo OL, Kerskens C, et al. An experimental platform for systemic drug delivery to the retina. Proc Natl Acad Sci U S A 2009 Oct 20;106(42):17817-17822.

169. Gupta R, Tongers J, Losordo DW. Human studies of angiogenic gene therapy. Circ Res 2009 Oct 9;105(8):724-736.

170. Papanas N, Maltezos E. Benefit-Risk Assessment of Becaplermin in the Treatment of Diabetic Foot Ulcers. Drug Safety 2010 Jun 1;33(6):455-461.

171. Rasmussen H, Chu KW, Campochiaro P, Gehlbach PL, Haller JA, Handa JT, et al. Clinical protocol. An open-label, phase I, single administration, dose-escalation study of ADGVPEDF.11D (ADPEDF) in neovascular age-related macular degeneration (AMD). Hum Gene Ther 2001 Nov 1;12(16):2029-2032.

172. Dechantsreiter MA, Planker E, Matha B, Lohof E, Holzemann G, Jonczyk A, et al. N-Methylated Cyclic RGD Peptides as Highly Active and Selective alpha-v-beta-3 Integrin Antagonists. Journal of Medicinal Chemistry 1999;42(16):3033-3040.

173. Reddy KR, Wright TL, Pockros PJ, Shiffman M, Everson G, Reindollar R, et al. Efficacy and safety of pegylated (40-kd) interferon alpha-2a compared with interferon alpha-2a in noncirrhotic patients with chronic hepatitis C. Hepatology 2001;33(2):433-438.

174. Bukowski RM, Tendler C, Cutler D, Rose E, Laughlin MM, Statkevich P. Treating cancer with PEG Intron: pharmacokinetic profile and dosing guidelines for an improved interferon-alpha-2b formulation. Cancer 2002;95(2):389-396.

175. Lindsay KL, Trepo C, Heintges T, Shiffman ML, Gordon SC, Hoefs JC, et al. A randomized, double-blind trial comparing pegylated interferon alfa-2b to interferon alfa-2b as initial treatment for chronic hepatitis C. Hepatology 2001;34(2):395-403.

Chapter 3

Electrostatic Surface Modifications to Improve Gene Delivery

3.1 Introduction

Biomaterials have been developed for use in many fields including tissue engineering and drug delivery. There are many types of biomaterials, including macromolecules, synthetic polymers, and lipid systems [1, 2]. Biomaterials have been designed to respond to and interact with biological systems in a variety of ways. For example, in tissue engineering, which includes the regeneration and replacement of damaged and diseased tissues, biomaterials support a specific function of the target tissue. In drug delivery, biomaterials need to have the required encapsulation and release profiles necessary to treat the particular disease with a particular drug. A hydrophobic biomaterial may be preferred for delivery of a small molecule hydrophobic drug for cancer therapy, whereas a hydrophilic cationic biomaterial may be preferred for gene delivery. Gene delivery is particularly challenging as the drug cargos (nucleic acids) are large, highly charged, and degradable. Fortunately, the charged, polyvalent nature of nucleic acids enables various strategies for forming electrostatically associated coatings, complexes, and films. This review highlights how biomaterials can be used for particle-based and surface-based gene delivery and how electrostatic coatings can further enhance efficacy.

This chapter was originally published as Shmueli RB, Anderson DG, Green JJ. "Electrostatic Surface Modifications to Improve Gene Delivery." Expert Opin Drug Deliv. 2010 Apr;7(4):535-50.

3.2 Biomaterials

Synthetic polymers are a popular biomaterial choice for drug and gene delivery. The ability to control the properties of synthetic polymers facilitates rational design. For example, polymers that contain positive charges are made so that they can electrostatically bind to negatively charged nucleic acids such as DNA molecules. These materials can be used directly to encapsulate cargos or as coatings for particles and devices. Examples of some of the commonly used biomaterials investigated for gene delivery are shown in **Figure 3.1**. Polyethylenimine (PEI) [3] is a polymer that is composed of multiple units of ethylenimine in both linear and branched arrangements. The branched PEI polymer contains primary, secondary and tertiary amines at a ratio of 1:2:1, while the linear polymer is composed of all secondary amines except for primary amines at the end groups. These amines are responsible for the positive charges that are necessary to bind to DNA. PEI is an off-the-shelf polymer for gene delivery that can condense DNA into nano-sized complexes and facilitate some amount of *in vitro* and *in vivo* gene transfer [4]. Further modifications to PEI have been made to increase its performance at various points of the gene delivery process [5-7]. Polyamidoamine (PAMAM) [8] is a dendrimer system composed of amidoamine bonds. The dendrimer is built by adding esters and amines to different core molecules that have amine functionalities.

Many types of degradable biomaterials have been created including hydrolytically degradable esters such as polylactic acid (PLA) [9, 10], polyglycolic acid (PGA) and co-polymers [11], polycaprolactone (PCL) [12], and others [13]. The physical properties of

the materials tune its degradation and rates of drug release. Poly(beta-amino ester)s (PBAE) [14-16] are a class of polymers that are both positively charged and hydrolytically degradable. They are synthesized from the conjugate addition of amine to diacrylates. The type of monomer diacrylates and amines can be varied to achieve different polymer properties. Poly(ester-anhydrides) [17] are often used to form microparticles that can encapsulate drugs or genetic material and degrade through surface erosion rather than the bulk erosion exhibited by PLA/PGA microspheres. Lipid based systems such as 1,2-Dioleyl-3-triethylammoniumpropane (DOTAP) can also form liposomes or lipoplexes that encapsulate drugs or nucleic acids [18]. The cationic head, linker region and hydrophobic tails can be modified to alter delivery properties.

Natural polymer based systems have also been studied as they are often biocompatible and degradable [19]. For example, poly-L-Lysine (PLL) [20] is a linear polymer made from the amino acid lysine and it is a highly positively charged macromolecule due to the basic primary amine at the end of the lysine residue. Other natural-based biomaterials include sugars such as chitosan [21, 22], dextran [23], and cyclodextrins [24]. Combining natural polymers with synthetic polymers can improve drug delivery or tissue engineering functionality.

3.3 Nucleic Acid Delivery

A particularly promising, but challenging drug delivery cargo are nucleic acids such as DNA and various types of RNA including antisense RNA, siRNA, isRNA, and

miRNA [25, 26]. Genetic material is relatively large compared to most therapeutics. This makes it more difficult to transport within the body, into a cell, within a cell and into the nucleus. Viral vectors such as adenovirus [27] or lentivirus [28] have been developed for therapeutic gene delivery as they have evolved to do this very efficiently. However, there are continuing safety concerns with their use such as the potential for tumor induction [29] and the generation of immune responses [30]. Once the nucleic acid-containing particle is formed, it must remain stable and enable internalization within target cells. Common pathways for nano-formulations to enter the cell are via clathrin and caveolae-mediated endocytosis [31]. If the DNA/delivery particle is too large it will not be able to enter the cell. As the cell surface is negatively charged, particles need to be neutral or positively charged in order to promote cell interactions and efficient internalization.

For intracellular delivery, internalization is necessary, but not sufficient. There must also be efficient escape from the endosomal compartment to the cytoplasm to be active in the cell [32]. One proposed mechanism by which many of the polymer systems facilitate endosomal escape is through a proton-sponge mechanism. In this model, the basic nature of the polymer buffers the hydrogen ions pumped into the vesicle by the cell. To maintain electroneutrality, chloride ions flux into the endosome as well, creating osmotic pressure. The cell continues to attempt to acidify the vesicle until the vesicle finally ruptures due to the swelling of the endosome with water, releasing the particle [33]. Additional endosome escape mechanisms include the use of viral-based proteins that puncture the lipid bilayer, allowing particle escape.

Once in the cytoplasm, the encapsulated cargo must then be released from the particle in an efficient manner [34]. The delivery system needs to reach a balance between binding and dissociation with DNA. The system needs to bind tightly enough for particle formation, but must be able to unpack to release the DNA when in the cytoplasm or nucleoplasm. One method is for the release of DNA to be triggered by a stimuli that is present inside the cell, but not outside, such as a reducing environment.

An additional requirement for DNA delivery is transport of the DNA into the nucleus following cargo release [35]. It has been reported that the ability of DNA to cross the nuclear pore complex can be enhanced by binding nuclear localization sequence (NLS)-signal peptides to the DNA that allow the DNA to be picked up by the nucleoporin active transport system [36]. Gene expression can occur transiently from an episomal plasmid or targeted integration can be designed [37]. Although longer acting, integration of the exogenous DNA carries the risk of insertional mutagenesis and cancer cell generation.

The delivery of genes holds potential to treat both genetic diseases and acquired diseases such as cancer. While significant progress has been made in the field, non-viral biomaterial-mediated gene delivery is still much less effective than viral gene delivery [38]. New biomaterials continue to be developed to enhance efficacy and safety [39, 40]. Recent approaches to finding new synthetic polymers for gene delivery include polymer library approaches. High-throughput synthesis and screening techniques were used to search over two thousand different polymer structures for gene delivery [16]. Lead

structures, poly(beta-amino ester)s, are biodegradable and rival adenovirus for gene transfer to human primary cells *in vitro* [41].

3.4 Coated Particles for Delivery

3.4.1 Nanoparticles

Nanoparticles are particles with length scales from 1-1000 nm. They can be "hard" nanoparticles primarily composed of gold [42-44], silver [45], or other inorganic materials [46-48] or they could be "soft" nanoparticles such as polyplexes [49, 50], liposomes [51], lipidoids [52], or other organic molecules. Beyond spheres, they can also be crafted into various shapes such as crystals or prisms [53]. Novel processing methods can enable printing of nanoparticles into more complex shapes such as cylinders, "hex nuts," or toroids [54]. New kinds of therapies are being packaged into these nanoparticles [55]. The use of nanoparticle systems can allow for improved drug targeting, specific intracellular delivery, and potentially more control over delivery profiles.

Targeting is especially important in cancer drug delivery since the therapeutic is often intentionally cytotoxic. Targeting of cancer cells with nanoparticles is often done by targeting specific cancer cell surface receptors. Specific interactions can be achieved by modifying the delivery vehicle with specific peptides, proteins, or antibodies that bind to the surface receptors [56]. More recently, some groups have used aptamers, which are RNA and DNA molecules with the ability to bind to specific targets with high affinity

[57]. Cancer gene therapy can also obtain additional specificity by delivering genes that only a cancer cell would be able to efficiently transcribe via transcriptional targeting [58].

3.4.2 Microparticles

While microparticles have been typically used as drug reservoirs for controlled release of drugs, peptides, and proteins [59], they can also be used for intracellular delivery. Although most cells cannot take-up microparticles, immune cells such as macrophages can internalize them. Thus, the size of a particle can also affect targeting and a microparticle system can specifically deliver drugs or genes to cells of the immune system. Delivering antigen-coding genes can be useful for vaccine purposes. Cationic PLGA particles have been shown to significantly increase *in vivo* antibody responses to create better vaccine systems [60]. Positively charged surfactant molecules were added to PLGA during the microparticle fabrication process, resulting in positively charged PLGA particles. The positively charged surface allowed for adsorption of DNA molecules onto the particle surface. In this case, DNA plasmids that code for HIV proteins were used in order to improve vaccination response. Poly(beta-amino ester)s can also be blended with PLGA microparticles to provide pH triggered release and enhanced efficacy [61]. Singh et al., review microparticle systems used for vaccine applications [62].

3.4.3 Types of Coatings

Various particulate formulations have been used to deliver drugs, whether that cargo is small molecules, protein, sugars, or genetic material [63-66]. The surfaces of these particles have been modified in various ways to improve delivery. Covalent modifications, such as PEGylation and polysaccharide coats, have been used to improve

particle stability in serum *in vitro* and *in vivo* [67, 68]. These alterations reduce the interactions of the particles with the various serum proteins that can cause aggregation or degradation of the particles. Enhanced stability can also be achieved used electrostatic coatings. For example, Trubetskoy et al. showed that polyacrylic acid can be used to coat polyethylenimine/DNA or cationic lipid/DNA complexes and thereby prevent serum inhibition of the complexes [69]. The polyacrylic acid provides electrostatic shielding from the serum proteins, increasing *in vivo* gene delivery following systemic injection, and reducing toxicity.

Virus particles have also been coated with polymers to improve their *in vivo* stability. Adenovirus has been coated with polymers that protect the viral particles from interaction with specific blood components and reduces interaction with the immune system [70]. A hydrophilic polymer, N-(2-hydroxypropyl) methacrylamide (HPMA)-based copolymer, was functionalized in order to bind to the viral surface. The binding included both covalent and electrostatic interactions to further increase the coating stability. The polymer also contained reducible disulfide bonds that would allow the coating to be degraded so that transfection can still occur. Additional modifications have included specific receptor targeting elements [71]. In another electrostatic coating approach, PEI was used to modify the surface of baculoviral vectors [72]. These coating modifications can therefore allow viral gene delivery to overcome some of the limitations mentioned earlier in the review.

Targeted delivery to cells has been achieved by functionalizing the surfaces of particles so that they can interact more favorably with specific cells. These targeting

molecules can be covalently bound to the particles [73] or can be coated to the particles via electrostatic interactions [74]. These targeting molecules are often proteins or protein fragments that bind to a specific cell receptor, such as transferrin, epidermal growth factor (EGF), and Arginine-Glycine-Aspartic Acid (RGD) domains [73, 75-77]. In the case of gene delivery, one problem with covalent modification with targeting ligands is that this changes the functionality of polymer moieties and efficacy can decrease [76, 77]. A coating approach avoids this potential issue. A schematic for multilayer electrostatically coated particles is depicted in **Figure 3.2**.

In one example of an electrostatic coating approach, positively charged poly(beta-amino ester)/DNA nanoparticles were coated with negatively charged peptides [74]. Peptides were chosen such that they contained a stretch of anionic amino acids (Glutamic Acid residues), a linker (Glycine residues), and a ligand (Arginine-Glycine-Aspartic Acid). Addition of the peptide coating was found to neutralize the particle charge and promote gene delivery to human umbilical vein endothelial cells. Interestingly, it was only when the surface charge was neutralized, and the non-specific delivery of the nanoparticles reduced, that the presence of the ligand impacted gene delivery. However, once neutralized, nanoparticles coated with polyglutamic acid-polyglycine-RGD peptides had up to an order of magnitude higher gene delivery efficacy than the same particles coated with the scrambled sequence polyglutamic acid-polyglycine-RDG peptides [74]. Thus, the sequence of the ligand and the overall charge of the particle were important for intracellular deliver of the particles.

As a complementary strategy, negatively charged particles can be coated with cationic polymers to improve their delivery properties. For example, Lee et al. [78]

showed that gold nanoparticles thiolated with siRNA could subsequently be coated with PBAEs to achieve significantly enhanced cytoplasmic delivery of the siRNA. In this work (depicted in **Figure 3.3**), gold-siRNA nanoparticles were unable to mediate gene silencing alone, but when coated with polymer, silencing increased to >95% using the same dose of gold-siRNA nanoparticles. Interestingly, small structural differences to the PBAEs used as coatings, dramatically changed the silencing behavior of the gold-siRNA particles. The most effective polymers were those that had terminal tertiary amine groups. In other work Fuller et al. [79] showed that PEI could be used as a cationic polymer to coat negatively charged fluorescent silica particles to enable enhanced intracellular delivery and endosomal escape. This system enabled the combination of both imaging and gene delivery within the same nanoparticles.

In vivo, it has also been shown that tissue targeting can be tuned via electrostatic coating [80]. In this study, cationic polymer/DNA nanoparticles were coated with anionic peptides and following tail-vein injection, gene delivery was directed away from the lungs and to the spleen and bone marrow or alternatively to liver cells depending on the coating amount and type. Following systemic administration, cationic particles can potentially aggregate with blood constituents that embolize in the vascular beds of the lung [69, 81, 82]. These coatings were shown to prevent aggregation with erythrocytes and prevent lethality following injection as compared to uncoated polymeric particles.

Thus the effectiveness of charged nanoparticles, either cationic or anionic, can be greatly improved by single coats of an oppositely charged biomaterial that incorporates new functionality to the nanoparticle. This functionality could consist of improved serum

resistance, cell or tissue targeting, efficient internalization, endosomal escape, controlled release, and reduced toxicity.

3.4.4 Multilayer Particle Coating

Multiple electrostatic layers can be deposited on a particle using a layer-by-layer (LbL) approach (**Figure 3.2**). For this method, successive and alternating anionic and cationic layers are added to a particle core [83, 84]. After each layer is added, centrifugation allows for isolation of the particles so that further layers can be added. In some formulations, DNA is added as one of the anionic layers [85]. Using this approach, the layers were observed to disassemble inside the cell, where the DNA molecules then have access to the nucleus. In another system, DNA was added first as an internal layer adsorbed to a core. After multilayers were formed with spermidine and DNA coats, the core substrate was subsequently dissolved away so that the DNA becomes an internal encapsulated layer within a capsule [86]. In other work, DNA has also been encapsulated within chondroitin sulfate/poly(-L-arginine) LbL particles [87]. DNA was first added to the core particle and then alternating layers of chondroitin sulfate and poly(-L-arginine) polyelectrolytes were added subsequently to create a core/shell structure. The core was then dissolved so that only the DNA was left encapsulated and free inside the polyelectrolyte shell. Many of these systems are on the micrometer scale, which can reduce the ability of cells to take up the particles. Reducing the size of these LbL particles would therefore improve delivery of DNA. One such example uses liposomes as the substrate onto which polyelectrolyte layers, such as DNA, can be added [88]. Additionally, polyplexes have been used as a substrate onto which further layers are

added electrostatically [89]. In this case, the extra PEI layer increased transfection activity further, presumably because the increased amount of PEI enabled greater endosomal escape. A negatively charged poly(acrylic acid) layer was added in between the PEI layers in order to construct the multilayer particle. Examples of multilayer coatings are summarized in Table 3.2.

3.5 Multilayer Coated Non-Particulate Substrates for Delivery

In addition to particles, other surfaces can also be coated for controlled release and drug delivery. The sequential addition of positively and negatively charged polyelectrolytes to form a multilayered structure is a general approach that can be applied to diverse fields including optics, separations, and drug delivery [90]. Many different materials can be incorporated into these multilayers. These multilayers can then also be used as substrates themselves onto which cells can adhere. Surface mediated gene delivery can be useful as a mechanism for efficient gene transfer and as an enabling technology for tissue engineering [91]. Growing transfected cells on a surface can enable the release of soluble drugs, such as proteins, and has other potential advantages over particulate systems. One such advantage is spatial control of release of the therapeutic molecule. Surface-mediated delivery also allows for more efficient delivery since there is a much higher local concentration of drug available to the cells. The reverse system has also been developed where a live cell can serve as the substrate for multilayer coating [92, 93].

Multilayer electrostatic coatings have been used by researchers to tune the release of various biomolecules from substrates. One common method of fabricating such multilayer surfaces is an electrostatic-based layer-by-layer approach as shown in **Figure 3.4**. The first step is to coat a charged substrate with a layer of oppositely charged polyelectrolytes. The substrate can range from an inorganic material of any shape to biological tissue surfaces [94, 95]. The substrate is then washed to remove excess polyelectrolytes. Another layer of polyelectrolytes is added next which has an opposite charge to that of the first layer. Once again the surface is washed to remove the excess. This process cycle can then be repeated until the desired multilayer structure is achieved. Many different polyelectrolytes can be used, which gives flexibility and control over the type of surface and release characteristics that can be attained. Table 3.2 summarizes some of the multilayer structures discussed in this section.

3.5.1 Controlled Delivery via Multilayer Structures

Drug release from the multilayered surfaces has been achieved via different mechanisms. Polyelectrolyte layers that are hydrolytically degradable allow for controlled release in aqueous environments, such as in the body [96]. Therapeutic polysaccharides, such as heparin, have been used for negatively charged layers, along with poly(beta-amino esters) as positively charged layers. PBAE hydrolysis rate is dependent on the pH of the solution and this controls the degradation of PBAE based multilayers. With this system, drugs are released more slowly at lower pH solutions as expected. Other hydrolytically degradable polymers can be used in similar systems. Wood et al. showed that rather than relying on hydrolytic degradation, these multilayer

films can have triggered release based on an applied voltage [97]. The key development was using Prussian Blue, a non-toxic FDA-approved material, to assemble the films. Electric current can similarly tune release of encapsulated insulin from hydrogen-bonded gels composed of poly(ethyloxazoline) and poly(acrylic acid) multilayers [98].

Multilayer structures that exhibit pH dependent swelling have also been designed [99]. PH-dependent swelling was achieved by using a combination of polyelectrolyte layers, one of which contains pH responsive functional groups, and the other which has hydrophobic domains. The swelling behavior allows for encapsulation of various drug delivery cargos and release that is highly tuned to environmental stimuli. Polypeptides can also be used to construct similar multilayer films, including those with pH responsive triggered release [100]. Loading of the layers with a drug is a function of solution pH and by varying the polypeptide polyelectrolyte layer composition, one can tune pH triggered response of the multilayer.

These methods can be extended for the controlled release of multiple drugs from one film [101, 102]. In one example, a hydrolytically degradable layer is used to control the overall release profile of a therapeutic polysaccharide and small hydrophobic molecule. In this case, one of the drugs (the polysaccharide) also serves a structural role as a polyelectrolyte that composes the multilayer. The other drug is encapsulated in polymeric micelles that are incorporated within the multilayer. The two delivered drugs can act synergistically to improve therapeutic activity [102]. This approach could be extended for multi-stage gene delivery. For multi-drug release, it is important to control interlayer diffusion. One such strategy is to add covalently cross-linked barriers between

the two main polyelectrolyte layers [101]. The cross-linked barriers are also polyelectrolyte layers as well so that they can be seamlessly added during multilayer fabrication. Researchers found that one bilayer of cross-linked barrier is sufficient to block interlayer diffusion. However, the base layers underneath the barrier influence how well the barrier blocked diffusion.

A spray method can be used instead of the dip method to apply each polyelectrolyte layer in order to decrease processing time. Spraying can also be used to introduce asymmetry into multilayers which can be useful for drug delivery and other applications such as purification or biocatalytic membranes [103]. The spraying method is based on electrospinning technology, which involves the use of an applied voltage between the polyelectrolyte solution and surface to create a micrometer or nanometer sized fiber deposited onto the surface.

3.5.2 Delivery of DNA via Multilayer Structures

These multilayer structures can be useful for gene delivery in particular, where DNA acts as both one of the negatively charged polyelectrolyte structural layers and the drug of interest. For example Zhang et al. showed release of functional DNA from multilayered films [104]. In this study, the addition of an extra gene delivery agent (Lipofectamine) was required to permit intracellular delivery of the released DNA into mammalian cells, but this work demonstrated that the multilayer could serve as a DNA transfection reservoir. Building on this result Jewell et al. showed that PBAE/DNA multilayers could degrade into PBAE/DNA associated complexes that enable gene delivery at areas physically close to the multilayer coatings [105]. **Figure 3.5**

demonstrates how this system can enable spatial control of gene expression through quartz slides that were coated with PBAE polymer and enhanced green fluorescent protein (EGFP) DNA. Gene expression is high in areas adjacent to the slide surface, but low in areas further away. In principle, the breakdown products of the multilayer films themselves could serve as *in situ* gene delivery agents. Combinations of multiple biomaterials, each with specific intracellular gene delivery function (DNA condensation, endosomal escape, nuclear import, etc.), may prove to be the most effective.

DNA and PEI have been used to create multilayer structures using an electrospun polymeric mesh as a substrate [106]. Cells were cultured on these multilayered meshes and transfection was observed. Such a system can be useful for drug delivery and tissue engineering applications. Using a bioreducible polyelectrolyte provides another method for controlled delivery [107]. Disulfide bonds within a poly(amido amine) polymer enable degradation in the presence of a reducing environment. Alternating layers of the cationic polymer and plasmid DNA were deposited on a stainless steel mesh, which is a similar system to a stent. Increased and longer lasting transfection was observed as compared to the non-reducible controls. The release and gene expression of this system over 12 days is shown in **Figure 3.6**. The authors hypothesized that the plasma membrane might provide a reducing environment, so that polymer degradation can take place upon interaction with the cell surface. Significant gene expression was achieved in both fibroblasts (NIH-3T3) and smooth muscle cells (SMC).

Another method of delivery is the incorporation of pre-formed DNA nanoparticles embedded into a layer-by-layer structure [108]. In one study, poly(L-lysine) and

hyaluronic acid were used as the positively and negatively charged polyelectrolyte layers, respectively. Plasmid DNA was complexed with various formulations of PLL and cyclodextrin. This combination approach, a multilayer structure embedded with DNA complexes, allows for both tunable release of the complexes and improved protection/uptake of the pre-formed nanoparticles.

3.6 Conclusion

Electrostatic coatings are useful to modify the surfaces of particles and substrates for gene delivery. In the case of particles, these coatings can improve multiple steps of delivery including improved serum resistance, cell targeting, cellular uptake, endosomal escape, controlled release, and reduced toxicity. In the case of substrates, these electrostatic modifications can enable spatial and temporal control of release. These methods can also be used to facilitate triggered release either from environmental cues (pH) or an external source (electric field). Electrostatically adsorbed multilayers permit the creation of more complicated structures such as hollow capsules and surfaces that can release multiple therapeutic components over differing time scales. As these coatings and films can be constructed using a wide array of biomaterials and gentle processing conditions, they can have widespread applications to drug delivery and tissue engineering.

3.7 Expert Opinion

Physical and chemical properties of particles and substrates can be controlled through the modification of their surfaces with polyelectrolytes. These modifications are especially promising to the fields of drug and gene delivery. A major strength of this approach is its suitability for a wide range of biomaterials including peptides, sugars, polymers, and nucleic acids. Indeed, any macromolecule with a multivalent charge is amenable to this technology.

In some applications, coated nanoparticles were utilized for enhanced intracellular delivery. Specific intracellular delivery bottlenecks improved through electrostatic biomaterial coatings include cell targeting, cellular uptake, and endosomal escape. This work can be extended to include coatings with moieties for active transport through the cell, nuclear uptake, and other intracellular functions. Multilayered particles could be constructed that contain specialized biomaterials for each layer rather than the same two alternating layers throughout the coating. These customized layers could enable enhanced intracellular delivery or more precise multidrug release.

One natural extension of this work, and something that is already appearing in the literature [109, 110], is the use of nucleic acids other than DNA. Small interfering RNA (siRNA), immunostimulatory RNA (isRNA), micro RNA (miRNA), small activating RNA (saRNA), and antigene RNA (agRNA) are all examples of nucleic acids that would be very promising for both encapsulated cargos and coatings for particles and surfaces. There are many applications of this technology including cancer therapy [56] and targeting [111]. In addition, these materials can be used for immunotherapy and as vaccines, enabling controlled delivery of the immune stimulating molecules [112, 113].

In another application, multiple combinations of nucleic acids within the same particle may be especially interesting in creating new tools for efficient non-viral reprogramming of differentiated cells to induced pluripotent stem cells [114].

Encapsulation of cells within polyelectrolytes may enable protection and control of the cells. For example, a cell could be engineered to have a particular affinity for another cell or biomacromolecule through its electrostatic coatings. Such cells could potentially enable increased cell-cell interactions in the formation of engineered tissues, novel mechanisms for the recognition of pathogens, or aid in wound healing. In the case of stem cell engineering, such an approach may enable the controlled differentiation and/or reprogramming of the encapsulated cells within the multilayer coating. This approach could be useful for tissue engineering and regenerative medicine.

Multilayer films could also be designed not just for how they behave as films, but also how their breakdown products behave. For example, polyelectrolyte layers of the film could be therapeutics themselves or be prodrugs that degrade into therapeutic molecules. They could also form *in situ* particles or structures that then have functionality even after the multilayer degrades (such as self-assembly into targeted nanoparticles). These coatings and films could also be used to coat virtually any device including stents and stent-like devices.

These biomaterials and approaches can also be utilized to combine drug delivery with imaging to create new theranostics and multifunctional nanomedicines [115]. With such a system, one could visualize the spatial and temporal delivery of the therapeutic agent. It could also be used to better tune ligand coatings or stimuli responsive coatings

for improved *in vivo* function. Putting these two elements together, a triggered diagnostic signal and drug release profile could be engineered to occur in the presence of a target compound or environment.

Although this technology is promising and there are many interesting applications, challenges remain before there can be broad clinical application. Ensuring safety is critical and may be a challenge as the fields of gene therapy and nanotechnology have already had their share of safety-related setbacks. One way that electrostatically coated nanoparticles can improve safety is through specific targeting. By targeting certain tissues or aberrant cells (cancer) with increased specificity compared to uncoated non-viral particles or to viral particles, off-target serious adverse events can be reduced. Proper coatings can also facilitate long circulation times and increased efficacy with a lower dose of active drug, further increasing safety. Biodegradable and biocompatible materials, like many of the polymeric materials discussed, are key to minimizing toxicity. In the case of gene therapy clinical trials, it is important that the DNA itself is also designed with safety in mind so that it is maximally effective and minimally immunogenic. One way to achieve this is by the elimination of toll-like receptor signaling CpG motifs in the DNA vector backbone or through utilization of a minicircle DNA vector free of bacterial backbone elements. Choosing the appropriate biomaterials, animal models, and manufacturing procedures will all be crucial as well. Nonetheless, given the versatile and powerful approach of electrostatic coatings and multilayers, including increasing spatial and temporal precision, many new therapeutics and diagnostics based on this technology will likely appear in the future.

3.8 Acknowledgements

The authors thank the TEDCO MSCRF (2009-MSCRFE-0098-00) and the NIH (EB000244 and CA132091) for support.

3.9 Tables

Table 3.1. Electrostatic surface modifications of particle systems for gene delivery.

Base Material	Modification	Drug	Zeta-potential (mV)	Size (nm)	Application	Cell Viability (relative to	Activity (relative to control)	Notes	Ref.
PLGA	CTAB	pDNA-HIV p55	+36±6	1540±200	Balb/c mice		~ ≥ x100 (PLGA, DNA)	Improved serum antibody and CTL response	60
bPEI	Chondroitin Sulfate	pDNA-Luc	-29.2±0.2	77.0±3.2	B16-F10 cells *in vitro* (Opti-MEM)	~ x5 (pDNA/PEI)	~ x1 (bPEI)	Reduces RBC agglutination	68
bPEI	Poly(acrylic acid)	pDNA-Luc	(approx. neutral)	~ 500	A549 cells *in vitro* (100% serum)		~ x100 - x1000 (bPEI)	Increased *in vivo* transfection and reduced *in vivo* toxicity	69
Baculovirus (BV)	PEI	pDNA-Luc	~ +30	~ 350	Human U87 and HepG2 cells	~ 95% up to MOI of 100	up to ~ x1000 (uncoated BV) in serum	Increased *in vivo* transfection as well	72
PBAE	E12-RGD peptide	pDNA-GFP	~ -5	~ 200	HUVEC *in vitro* (12% serum)	~ 80-100%	~ x3 (PBAE/E12-RDG); ~ x50 (bPEI); ~ x1 (Lipo2000)	Targeted delivery at specific material ratios	74
Gold nanoparticle	PBAE	siRNA	~ +13	~ 100	Luc modified HeLa cells *in vitro* (10% serum)	~ 85-100%	~ x6 (Lipo2000); ~ x20 (AuNP)	Greater than 95% knockdown	78
Core-shell fluorescent silica nanoparticles	PEI	pDNA-Luc	+31.22±2.68	117±1.1	COS-7 *in vitro* (Opti-MEM)	~ 100%	~ x1 (PEI/DNA)	Particles can be used for imaging and delivery	79
PBAE	Poly(glutamic acid)	pDNA-Luc	~ -10	~ 200	Swiss Webster mice	No lethality (mice died with uncoated)	~ x10 Liver (PBAE); ~ x30 - 40 (spleen, marrow)	Varying coating affects tissue specificity	80

CTAB = Cetyltrimethylammonium bromide; CTL = Cytotoxic T lymphocyte; MOI = Multiplicity of infection (number of viral particles per cell); pDNA-GFP = GFP coding plasmid; pDNA-Luc = Luciferase coding plasmid.

Table 3.2. Multilayered particles and films.

Core Substrate	Anionic Layers	Cationic Layers	No. Layers (Range used in papers)	Zeta-potential (mV)	Layer thickness (nm)	Application	Notes	Ref
Silica particles (~3 μm)	DXS, pDNA-GFP	PAH, PRM	7-12			HEK 293T cells (5% FBS)	Increased cellular uptake with cationic outer layer	85
Liposome (~100 nm)	DSX, DNA	Chitosan	1-4	~ -90	order of a few nm		Increased liposome stability	88
PEI/DNA polyplex (~100 nm)	PAA	PEI	4 (including interior PEI/DNA polyplex)	+15.1±6.9 (Quaternary complex)	order of a few nm	NIH-3T3 cells	Quaternary complexes showed improved transfection with no change in toxicity	89
E. coli cells	Alginate, Hyaluronic Acid, DNA (ODN)	Chitosan	4-7	~ -30 (anionic layers); ~ +30 (cationic layers)	~ 24 - 60 (per 2 bilayers)		Cells maintain viability, ability to divide	93
316L Stainless steel intravascular stent	pDNA-GFP, SPS	PBAE, lPEI	8 bilayers PBAE/pDNA + 10 bilayers lPEI/SPS core		~ 120 total	COS-7 cells	Uniform coating did not crack, peel or delaminate under mechanical stress; Successful transfection of cells	94
Silicon, Zinc Selenide substrate	DXS, Heparin, SPS, PAA	PBAE, lPEI, PAH	up to 40 bilayers PBAE/DXS or PBAE/Heparin + up to 10 bilayers PAH/PAA + 10 bilayers lPEI/SPS core		~ 100 (20 bilayers PBAE/DXS + 10 lPEI/SPS		Better controlled release by including covalently crosslinking layers that prevent interlayer diffusion	101
PLA electrospun fibers (~1-10 μm diameter)	pDNA-Luc	PEI	1-3 bilayers		order of a few nm	COS-7 cells	Allows for gene delivery for tissue engineering applications	106
Stainless steel mesh	pDNA	RHB	15 bilayers		~ 70	NIH-3T3 and SMC cells	Use of bioredicble polycations increases and prolongs transfection activity	107
ITO glass and silicon substrate	RNA	PABA	4-8 bilayers		~ 10 per bilayer		Potential for electrochemical control of RNA release	108

DXS = dextran sulfate; ODN = oligonucleotide; PAA = poly(acrylic acid); PABA = Poly(anilineboronic acid); PAH = poly(allylamine hydrochloride); PRM = protamine sulfate; RHB = reducible hyperbranched poly(amido amine); SPS = poly(sodium styrene sulfonate)

3.10 Figures

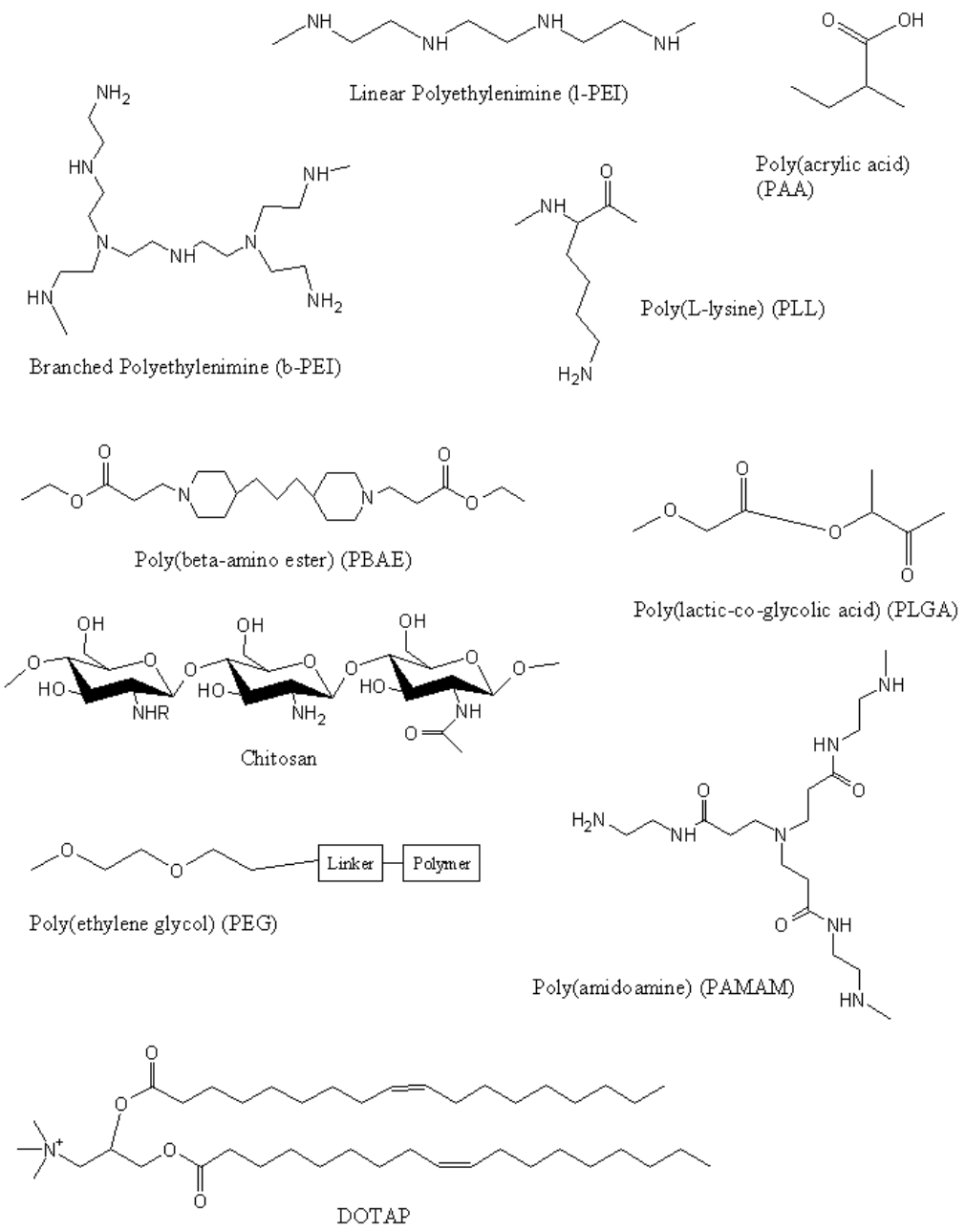

Figure 3.1. Biomaterials used to form particles and coatings for gene delivery.

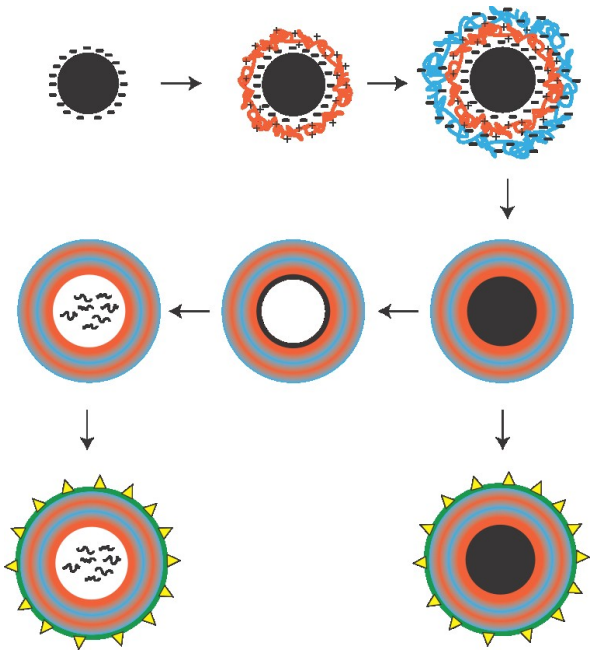

Figure 3.2. Fabrication of a multilayer particle. Synthesis begins with a charged colloidal substrate. Oppositely charged polyelectrolytes are added in solution in a cyclic fashion. After the addition of each polyelectrolyte there is a wash and centrifugation step. As a final step, targeting ligands can be electrostatically added (yellow triangles). The colloidal substrate can be left encapsulated for delivery or can be chemically degraded and removed to form a hollow core.

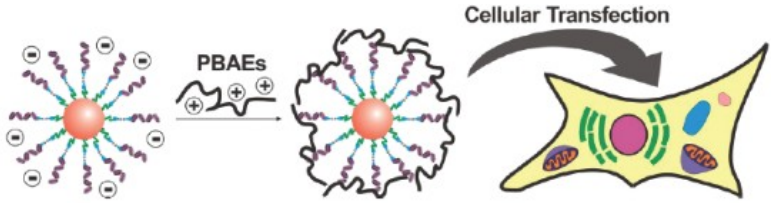

Figure 3.3. SiRNA modified gold-nanoparticles (orange sphere) are electrostatically coated with cationic polymers (PBAEs) to enhance cell transfection. Reproduced with permission from Nano Letters. Copyright ACS 2009 [78].

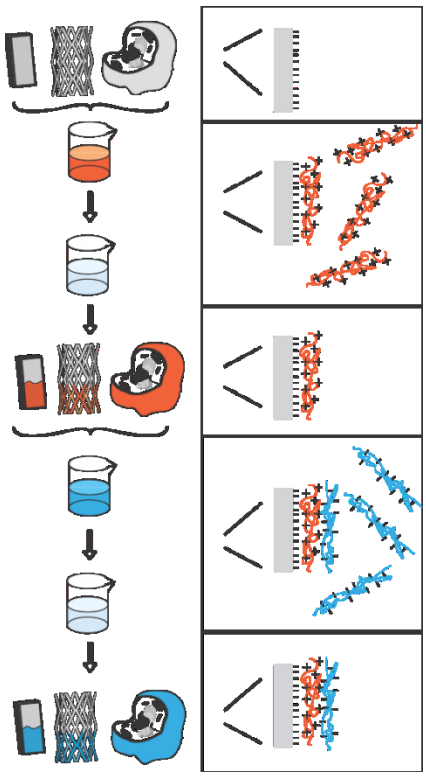

Figure 3.4. Multilayered coatings can be added to structures such as glass slides, stents, and organic tissues. In each case, an oppositely charged polyelectrolyte is added to a charged surface followed by a wash step to remove excess polyelectrolyte. The next layer of oppositely charged polyelectrolytes can then be added and this cycle can be repeated as needed.

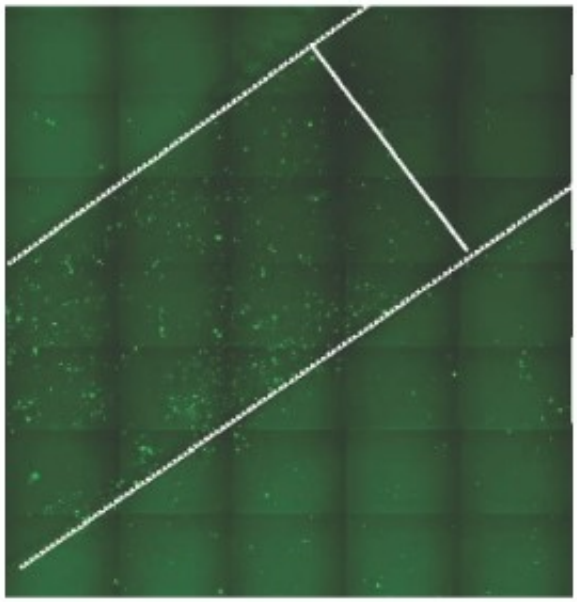

Figure 3.5. Fluorescence microscopy image showing localized transfection of COS-7 cells. The white lines show the approximate boundary between targeted and non-targeted delivery areas. The targeted areas are the quartz substrate functionalized with multilayered films of a PBAE polymer (seen in **Figure 3.1**) and pEGFP. Reproduced with permission from Journal of Controlled Release. Copyright Elsevier 2005 [105].

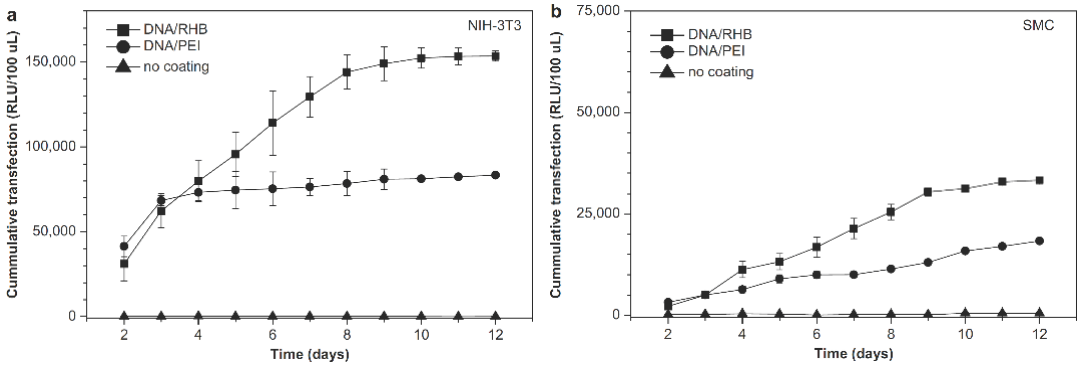

Figure 3.6. Cumulative transfection of NIH-3T3 **(a)** and SMC **(b)** cells with SEAP-DNA (secreted alkaline phosphatase based luminescence). Three surfaces were used: stainless steel mesh coated with DNA/reducible polymer multilayer (■), DNA/PEI multilayer (●), and control non-coated mesh (▲). Reproduced with permission from Biomaterials. Copyright Elsevier 2009 [107].

3.11 References

1. Langer R, Tirrell DA. Designing materials for biology and medicine. Nature 2004;428(6982):487-92.

2. Hubbell J. Bioactive biomaterials. Curr Opin Biotechnol 1999;10(2):123-9.

3. Godbey WT, Barry MA, Saggau P, et al. Poly(ethylenimine)-mediated transfection: a new paradigm for gene delivery. J Biomed Mater Res 2000;51(3):321-8.

4. Boussif O, Lezoualc'h F, Zanta MA, et al. A versatile vector for gene and oligonucleotide transfer into cells in culture and in vivo: polyethylenimine. Proc Natl Acad Sci U S A 1995;92(16):7297-301.

5. Thomas M, Klibanov AM. Enhancing polyethylenimine's delivery of plasmid DNA into mammalian cells. Proc Natl Acad Sci U S A 2002;99(23):14640-5.

6. Thomas M, Lu JJ, Ge Q, et al. Full deacylation of polyethylenimine dramatically boosts its gene delivery efficiency and specificity to mouse lung. Proc Natl Acad Sci U S A 2005;102(16):5679-84.

7. Thomas M, Ge Q, Lu JJ, et al. Cross-linked small polyethylenimines: While still nontoxic, deliver DNA efficiently to mammalian cells in vitro and in vivo. Pharm Res 2005;22(3):373-80.

8. Tang MX, Redemann CT, Szoka FC, Jr. In vitro gene delivery by degraded polyamidoamine dendrimers. Bioconjug Chem 1996;7(6):703-14.

9. Luo D, Woodrow-Mumford K, Belcheva N, et al. Controlled DNA delivery systems. Pharm Res 1999;16(8):1300-8.

10. Zeisser-Labouebe M, Lange N, Gurny R, et al. Hypericin-loaded nanoparticles for the photodynamic treatment of ovarian cancer. Int J Pharm 2006;326(1-2):174-81.

11. Panyam J, Labhasetwar V. Biodegradable nanoparticles for drug and gene delivery to cells and tissue. Adv Drug Deliv Rev 2003;55(3):329-47.

12. Shuai XT, Merdan T, Unger F, et al. Novel biodegradable ternary copolymers hy-PEI-g-PCL-b-PEG: Synthesis, characterization, and potential as efficient nonviral gene delivery vectors. Macromolecules 2003;36(15):5751-9.

13. Wang C, Ge Q, Ting D, et al. Molecularly engineered poly(ortho ester) microspheres for enhanced delivery of DNA vaccines. Nat Mater 2004;3(3):190-6.

14. Lynn DM, Langer R. Degradable poly(beta-amino esters): Synthesis, characterization, and self-assembly with plasmid DNA. J Am Chem Soc 2000;122:10761-8.

15. Anderson DG, Lynn DM, Langer R. Semi-automated synthesis and screening of a large library of degradable cationic polymers for gene delivery. Angew Chem Int Ed Engl 2003;42:3153-8.

16. Green JJ, Langer R, Anderson DG. A combinatorial polymer library approach yields insight into nonviral gene delivery. Acc Chem Res 2008;41(6):749-59.

17. Pfeifer BA, Burdick JA, Langer R. Formulation and surface modification of poly(ester-anhydride) micro- and nanospheres. Biomaterials 2005;26(2):117-24.

18. Zhang S, Zhao B, Jiang H, et al. Cationic lipids and polymers mediated vectors for delivery of siRNA. J Control Release 2007;123(1):1-10.

19. Numata K, Subramanian B, Currie HA, et al. Bioengineered silk protein-based gene delivery systems. Biomaterials 2009;30(29):5775-84.

20. Lollo CP, Banaszczyk MG, Mullen PM, et al. Poly-L-lysine-based gene delivery systems. Synthesis, purification, and application. Methods Mol Med 2002;69:1-13.

21. Borchard G, Bivas-Benita M. Gene delivery using chitosan and chitosan derivatives. In: Amiji MM, ed. New York: CRC Press 2005:301-10.

22. Wang C, Ye S, Dai L, et al. Enzymatic desorption of layer-by-layer assembled multilayer films and effects on the release of encapsulated indomethacin microcrystals. Carbohydr Res 2007;342(15):2237-43.

23. Chen FM, Wu ZF, Sun HH, et al. Release of bioactive BMP from dextran-derived microspheres: a novel delivery concept. Int J Pharm 2006;307(1):23-32.

24. Davis ME, Brewster ME. Cyclodextrin-based pharmaceutics: past, present and future. Nat Rev Drug Discov 2004;3(12):1023-35.

25. Medina-Kauwe LK, Xie J, Hamm-Alvarez S. Intracellular trafficking of nonviral vectors. Gene Ther 2005;12(24):1734-51.

26. Nguyen DN, Chen SC, Lu J, et al. Drug delivery-mediated control of RNA immunostimulation. Mol Ther 2009;17(9):1555-62.

27. Cao H, Koehler DR, Hu J. Adenoviral vectors for gene replacement therapy. Viral Immunol 2004;17(3):327-33.

28. Manjunath N, Wu H, Subramanya S, et al. Lentiviral delivery of short hairpin RNAs. Adv Drug Deliv Rev 2009;61(9):732-45.

29. Check E. Gene therapy put on hold as third child develops cancer. Nature 2005;433(7026):561-.

30. Thomas CE, Ehrhardt A, Kay MA. Progress and problems with the use of viral vectors for gene therapy. Nat Rev Genet 2003;4(5):346-58.

31. Rejman J, Bragonzi A, Conese M. Role of clathrin- and caveolae-mediated endocytosis in gene transfer mediated by lipo- and polyplexes. Mol Ther 2005;12(3):468-74.

32. Yang S, May S. Release of cationic polymer-DNA complexes from the endosome: A theoretical investigation of the proton sponge hypothesis. J Chem Phys 2008;129(18):185105.

33. Sonawane ND, Szoka FC, Verkman AS. Chloride accumulation and swelling in endosomes enhances DNA transfer by polyamine-DNA polyplexes. J Biol Chem 2003;278(45):44826-31.

34. Schaffer DV, Fidelman NA, Dan N, et al. Vector unpacking as a potential barrier for receptor-mediated polyplex gene delivery. Biotechnol Bioeng 2000;67(5):598-606.

35. van der Aa MA, Mastrobattista E, Oosting RS, et al. The nuclear pore complex: the gateway to successful nonviral gene delivery. Pharm Res 2006;23(3):447-59.

36. Zanta MA, Belguise-Valladier P, Behr JP. Gene delivery: A single nuclear localization signal peptide is sufficient to carry DNA to the cell nucleus. Proc Natl Acad Sci U S A 1999;96(1):91-6.

37. Ehrhardt A, Xu H, Huang Z, et al. A direct comparison of two nonviral gene therapy vectors for somatic integration: in vivo evaluation of the bacteriophage integrase phiC31 and the Sleeping Beauty transposase. Mol Ther 2005;11(5):695-706.

38. Park TG, Jeong JH, Kim SW. Current status of polymeric gene delivery systems. Adv Drug Delivery Rev 2006;58(4):467-86.

39. Putnam D. Polymers for gene delivery across length scales. Nat Mater 2006;5(6):439-51.

*** Excellent review of polymeric gene delivery**

40. Luten J, van Nostrum CF, De Smedt SC, et al. Biodegradable polymers as non-viral carriers for plasmid DNA delivery. J Control Release 2008;126(2):97-110.

41. Green JJ, Zugates GT, Tedford NC, et al. Combinatorial modification of degradable polymers enables transfection of human cells comparable to adenovirus. Adv Mater 2007;19(19):2836-42.

42. Hill HD, Millstone JE, Banholzer MJ, et al. The role radius of curvature plays in thiolated oligonucleotide loading on gold nanoparticles. ACS Nano 2009;3(2):418-24.

43. Thomas M, Klibanov AM. Conjugation to gold nanoparticles enhances polyethylenimine's transfer of plasmid DNA into mammalian cells. Proc Natl Acad Sci U S A 2003;100(16):9138-43.

44. Dhar S, Daniel WL, Giljohann DA, et al. Polyvalent oligonucleotide gold nanoparticle conjugates as delivery vehicles for platinum(IV) warheads. J Am Chem Soc 2009;131(41):14652-3.

45. Lee JS, Lytton-Jean AK, Hurst SJ, et al. Silver nanoparticle-oligonucleotide conjugates based on DNA with triple cyclic disulfide moieties. Nano Lett 2007;7(7):2112-5.

46. Akerman ME, Chan WC, Laakkonen P, et al. Nanocrystal targeting in vivo. Proc Natl Acad Sci U S A 2002;99(20):12617-21.

47. Derfus AM, Chen AA, Min DH, et al. Targeted quantum dot conjugates for siRNA delivery. Bioconjug Chem 2007;18(5):1391-6.

48. Chowdhury EH, Akaike T. Bio-functional inorganic materials: an attractive branch of gene-based nano-medicine delivery for 21st century. Curr Gene Ther 2005;5(6):669-76.

49. Wagner E. Strategies to improve DNA polyplexes for in vivo gene transfer: Will "artificial viruses" be the answer? Pharm Res 2004;21(1):8-14.

50. Gebhart CL, Kabanov AV. Evaluation of polyplexes as gene transfer agents. J Control Release 2001;73(2-3):401-16.

51. Pedroso de Lima MC, Simoes S, Pires P, et al. Cationic lipid-DNA complexes in gene delivery: from biophysics to biological applications. Adv Drug Delivery Rev 2001;47(2-3):277-94.

52. Akinc A, Zumbuehl A, Goldberg M, et al. A combinatorial library of lipid-like materials for delivery of RNAi therapeutics. Nat Biotechnol 2008;26(5):561-9.

53. Millstone JE, Hurst SJ, Metraux GS, et al. Colloidal gold and silver triangular nanoprisms. Small 2009;5(6):646-64.

54. Gratton SE, Williams SS, Napier ME, et al. The pursuit of a scalable nanofabrication platform for use in material and life science applications. Acc Chem Res 2008;41(12):1685-95.

**** Top-down fabrication for patterning nanoparticles with a wide array of features and morphologies**

55. Farokhzad OC, Langer R. Impact of nanotechnology on drug delivery. ACS Nano 2009;3(1):16-20.

56. Brannon-Peppas L, Blanchette JO. Nanoparticle and targeted systems for cancer therapy. Adv Drug Deliv Rev 2004;56(11):1649-59.

57. Farokhzad OC, Karp JM, Langer R. Nanoparticle-aptamer bioconjugates for cancer targeting. Expert Opin Drug Deliv 2006;3(3):311-24.

58. Huang YH, Zugates GT, Peng W, et al. Nanoparticle-delivered suicide gene therapy effectively reduces ovarian tumor burden in mice. Cancer Res 2009;69(15):6184-91.

59. Jain RA. The manufacturing techniques of various drug loaded biodegradable poly(lactide-co-glycolide) (PLGA) devices. Biomaterials 2000;21(23):2475-90.

60. Singh M, Briones M, Ott G, et al. Cationic microparticles: A potent delivery system for DNA vaccines. Proc Natl Acad Sci U S A 2000;97(2):811-6.

*** Electrostatic coatings of microparticles to create genetic vaccines**

61. Little SR, Lynn DM, Ge Q, et al. Poly-beta amino ester-containing microparticles enhance the activity of nonviral genetic vaccines. Proc Natl Acad Sci U S A 2004;101(26):9534-9.

62. Singh M, Chakrapani A, O'Hagan D. Nanoparticles and microparticles as vaccine-delivery systems. Expert Rev Vaccines 2007;6(5):797-808.

63. Kidane A, Bhatt PP. Recent advances in small molecule drug delivery. Curr Opin Chem Biol 2005;9(4):347-51.

64. Malik DK, Baboota S, Ahuja A, et al. Recent advances in protein and peptide drug delivery systems. Curr Drug Deliv 2007;4(2):141-51.

65. Bae KH, Moon CW, Lee Y, et al. Intracellular delivery of heparin complexed with chitosan-g-poly(ethylene glycol) for inducing apoptosis. Pharm Res 2009;26(1):93-100.

66. Thomas M, Klibanov AM. Non-viral gene therapy: polycation-mediated DNA delivery. Appl Microbiol Biotechnol 2003;62(1):27-34.

67. Caliceti P, Veronese FM. Pharmacokinetic and biodistribution properties of poly(ethylene glycol)-protein conjugates. Adv Drug Deliv Rev 2003;55(10):1261-77.

68. Kurosaki T, Kitahara T, Kawakami S, et al. The development of a gene vector electrostatically assembled with a polysaccharide capsule. Biomaterials 2009;30(26):4427-34.

69. Trubetskoy VS, Wong SC, Subbotin V, et al. Recharging cationic DNA complexes with highly charged polyanions for in vitro and in vivo gene delivery. Gene Ther 2003;10:261-71.

*** Anionic coating of cationic particles increases gene delivery efficacy in vivo**

70. Subr V, Kostka L, Selby-Milic T, et al. Coating of adenovirus type 5 with polymers containing quaternary amines prevents binding to blood components. J Control Release 2009;135(2):152-8.

71. Fisher KD, Stallwood Y, Green NK, et al. Polymer-coated adenovirus permits efficient retargeting and evades neutralising antibodies. Gene Ther 2001;8(5):341-8.

72. Yang Y, Lo SL, Yang J, et al. Polyethylenimine coating to produce serum-resistant baculoviral vectors for in vivo gene delivery. Biomaterials 2009;30(29):5767-74.

73. Ogris M, Walker G, Blessing T, et al. Tumor-targeted gene therapy: strategies for the preparation of ligand-polyethylene glycol-polyethylenimine/DNA complexes. J Controlled Release 2003;91(1-2):173-81.

*** Parallel strategies for shielding and targeting electrostatic polymer/DNA particles**

74. Green JJ, Chiu E, Leshchiner ES, et al. Electrostatic ligand coatings of nanoparticles enable ligand-specific gene delivery to human primary cells. Nano Lett 2007;7(4):874-9.

*** Anionic coating of cationic particles increases gene delivery specificity**

75. Kunath K, Merdan T, Hegener O, et al. Integrin targeting using RGD-PEI conjugates for in vitro gene transfer. J Gene Med 2003;5:588-99.

76. Suh W, Han SO, Yu L, et al. An angiogenic, endothelial-cell-targeted polymeric gene carrier. Mol Ther 2002;6:664-72.

77. Kursa M, Walker GF, Roessler V, et al. Novel shielded transferrin-polyethylene glycol-polyethylenimine/DNA complexes for systemic tumor-targeted gene transfer. Bioconjug Chem 2003;14:222-31.

78. Lee JS, Green JJ, Love KT, et al. Gold, poly(beta-amino ester) nanoparticles for small interfering RNA delivery. Nano Lett 2009;9(6):2402-6.

**** Cationic electrostatic coating of gold/siRNA hybrid nanoparticles**

79. Fuller JE, Zugates GT, Ferreira LS, et al. Intracellular delivery of core-shell fluorescent silica nanoparticles. Biomaterials 2008;29(10):1526-32.

80. Harris TJ, Green JJ, Fung PW, et al. Tissue-specific gene delivery via nanoparticle coating. Biomaterials 2009.

81. Dash PR, Read ML, Barrett LB, et al. Factors affecting blood clearance and in vivo distribution of polyelectrolyte complexes for gene delivery. Gene Ther 1999;6(4):643-50.

82. Zou SM, Erbacher P, Remy JS, et al. Systemic linear polyethylenimine (L-PEI)-mediated gene delivery in the mouse. J Gene Med 2000;2(2):128-34.

83. Peyratout CS, Dahne L. Tailor-made polyelectrolyte microcapsules: from multilayers to smart containers. Angew Chem Int Ed Engl 2004;43(29):3762-83.

84. De Geest BG, Sanders NN, Sukhorukov GB, et al. Release mechanisms for polyelectrolyte capsules. Chem Soc Rev 2007;36(4):636-49.

85. Reibetanz U, Claus C, Typlt E, et al. Defoliation and plasmid delivery with layer-by-layer coated colloids. Macromol Biosci 2006;6(2):153-60.

86. Schuler C, Caruso F. Decomposable hollow biopolymer-based capsules. Biomacromolecules 2001;2(3):921-6.

87. Shchukin DG, Patel AA, Sukhorukov GB, et al. Nanoassembly of biodegradable microcapsules for DNA encasing. J Am Chem Soc 2004;126(11):3374-5.

88. Fukui Y, Fujimoto K. The Preparation of Sugar Polymer-Coated Nanocapsules by the Layer-by-Layer Deposition on the Liposome. Langmuir 2009;25(17):10020-5.

89. Saul JM, Wang CHK, Ng CP, et al. Multilayer nanocomplexes of polymer and DNA exhibit enhanced gene delivery. Advanced Materials 2008;20(1):19-+.

90. Decher G. Fuzzy nanoassemblies: Toward layered polymeric multicomposites. Science 1997;277(5330):1232-7.

**** Classic account of multilayer assembly**

91. Shen H, Tan J, Saltzman WM. Surface-mediated gene transfer from nanocomposites of controlled texture. Nat Mater 2004;3(8):569-74.

92. Diaspro A, Silvano D, Krol S, et al. Single living cell encapsulation in nano-organized polyelectrolyte shells. Langmuir 2002;18(13):5047-50.

*** Use of a living cell as the "core" coated by multilayer films**

93. Hillberg AL, Tabrizian M. Biorecognition through layer-by-layer polyelectrolyte assembly: in-situ hybridization on living cells. Biomacromolecules 2006;7(10):2742-50.

94. Jewell CM, Zhang J, Fredin NJ, et al. Release of plasmid DNA from intravascular stents coated with ultrathin multilayered polyelectrolyte films. Biomacromolecules 2006;7(9):2483-91.

*** Coated stents for gene delivery**

95. Elbert DL, Herbert CB, Hubbell JA. Thin polymer layers formed by polyelectrolyte multilayer techniques on biological surfaces. Langmuir 1999;15(16):5355-62.

96. Wood KC, Boedicker JQ, Lynn DM, et al. Tunable drug release from hydrolytically degradable layer-by-layer thin films. Langmuir 2005;21(4):1603-9.

97. Wood KC, Zacharia NS, Schmidt DJ, et al. Electroactive controlled release thin films. Proc Natl Acad Sci U S A 2008;105(7):2280-5.

*** Triggered release from multilayer films**

98. Kwon IC, Bae YH, Kim SW. Electrically erodible polymer gel for controlled release of drugs. Nature 1991;354(6351):291-3.

99. Hiller J, Rubner MF. Reversible molecular memory and pH-switchable swelling transitions in polyelectrolyte multilayers. Macromolecules 2003;36(11):4078-83.

100. Jiang B, Li B. Tunable drug loading and release from polypeptide multilayer nanofilms. Int J Nanomedicine 2009;4:37-53.

101. Wood KC, Chuang HF, Batten RD, et al. Controlling interlayer diffusion to achieve sustained, multiagent delivery from layer-by-layer thin films. Proc Natl Acad Sci U S A 2006;103(27):10207-12.

102. Kim BS, Smith RC, Poon Z, et al. MAD (Multiagent Delivery) Nanolayer: Delivering Multiple Therapeutics from Hierarchically Assembled Surface Coatings (dagger). Langmuir 2009.

103. Krogman KC, Lowery JL, Zacharia NS, et al. Spraying asymmetry into functional membranes layer-by-layer. Nat Mater 2009;8(6):512-8.

104. Zhang J, Chua LS, Lynn DM. Multilayered thin films that sustain the release of functional DNA under physiological conditions. Langmuir 2004;20(19):8015-21.

105. Jewell CM, Zhang J, Fredin NJ, et al. Multilayered polyelectrolyte films promote the direct and localized delivery of DNA to cells. J Control Release 2005;106(1-2):214-23.

106. Sakai S, Yamada Y, Yamaguchi T, et al. Surface immobilization of poly(ethyleneimine) and plasmid DNA on electrospun poly(L-lactic acid) fibrous mats using a layer-by-layer approach for gene delivery. J Biomed Mater Res A 2009;88(2):281-7.

107. Blacklock J, You YZ, Zhou QH, et al. Gene delivery in vitro and in vivo from bioreducible multilayered polyelectrolyte films of plasmid DNA. Biomaterials 2009;30(5):939-50.

108. Zhang X, Sharma KK, Boeglin M, et al. Transfection ability and intracellular DNA pathway of nanostructured gene-delivery systems. Nano Lett 2008;8(8):2432-6.

109. Recksiedler CL, Deore BA, Freund MS. A novel layer-by-layer approach for the fabrication of conducting polymer/RNA multilayer films for controlled release. Langmuir 2006;22(6):2811-5.

110. Zhao X, Pan F, Holt CM, et al. Controlled delivery of antisense oligonucleotides: a brief review of current strategies. Expert Opin Drug Deliv 2009;6(7):673-86.

111. Nasongkla N, Bey E, Ren J, et al. Multifunctional polymeric micelles as cancer-targeted, MRI-ultrasensitive drug delivery systems. Nano Lett 2006;6(11):2427-30.

112. Nguyen DN, Green JJ, Chan JM, et al. Polymeric Materials for Gene Delivery and DNA Vaccination. Adv Mater 2009;21(8):847-67.

113. Nordly P, Madsen HB, Nielsen HM, et al. Status and future prospects of lipid-based particulate delivery systems as vaccine adjuvants and their combination with immunostimulators. Expert Opin Drug Deliv 2009;6(7):657-72.

114. Yu J, Hu K, Smuga-Otto K, et al. Human induced pluripotent stem cells free of vector and transgene sequences. Science 2009;324(5928):797-801.

115. Khemtong C, Kessinger CW, Gao J. Polymeric nanomedicine for cancer MR imaging and drug delivery. Chem Commun (Camb) 2009(24):3497-510.

Chapter 4

Methods and Characterization of Polymeric Gene Delivery Nanoparticles

4.1 Introduction

Gene delivery is attractive both to treat genetic diseases [1] and as a technology for regenerative medicine [2]. For successful clinical translation of a cell-based gene therapy approach [3], it is important to address two key challenges: 1) to develop safe and effective gene delivery vectors [4] and 2) to find a replenishable and genetically matched source of cells [5, 6]. Non-viral gene delivery is a safer alternative to viral vectors [7-10]. Cationic polymers condense DNA via electrostatic interaction with the negatively charged DNA backbone to form self-assembled complexes on the order of ~100 nm and are commonly termed polyplexes or polymeric nanoparticles. Polyethylenimine (PEI) is a widely-used off-the-shelf cationic polymer that forms polymeric nanoparticles with DNA and is non-degradable [11]. Poly(beta-amino ester)s (PBAEs) are a newer class of cationic polymers that similarly form polymeric nanoparticles, but are hydrolytically degradable [12]. End-modification of PBAEs has shown improved gene delivery efficacy in certain cell types [13-15].

Parts of this chapter were originally published as Bhise NS, Shmueli RB, Gonzalez J, Green JJ. "A Novel Assay for Quantifying the Number of Plasmids Encapsulated by Polymer Nanoparticles." Small. 2012 Feb 6;8(3):367-73. This chapter also includes excerpts from Shmueli RB, Bhise NS, Green JJ. "Evaluation of Polymeric Gene Delivery Nanoparticles by Nanoparticle Tracking Analysis and High-throughput Flow Cytometry." J Vis Exp. 2013 Mar 1;(73);e50176.

Recently, human fibroblasts have been successfully reprogrammed to induced pluripotent stem cells (iPSCs) [16] that offer potential applications in regenerative medicine as a replenishable source of autologous stem cells [16-18]. Many reprogramming studies utilize viral vectors that have higher efficiency but are unsafe for clinical applications, while non-viral methods, such as nanoparticle-based methods, have reported low reprogramming efficiency [6]. Reprogramming requires transfection of a combination of plasmids that encode reprogramming factors [6, 19]. Since the number of plasmids complexed per particle affects transfection efficiency, a quantitative determination of this number would benefit the development of nanoparticle-based gene delivery strategies, especially for co-delivery of multiple plasmids to the same target as required in factor-based reprogramming.

Few studies have investigated the composition of gene delivery nanoparticles in terms of the number of plasmids associated with a single nanoparticle, and the assays used have had significant drawbacks that affect the estimation [20-23]. In the present study, we developed a novel assay to easily quantify the number of plasmids within polymeric nanoparticles in physiologically relevant aqueous conditions using a nanoparticle tracking analysis technique. We investigated PEI and six formulations of PBAEs optimized for gene delivery to human primary fibroblasts (IMR90). We studied how small modifications, including to the polymer structure and polymer to DNA weight ratio, affect the composition of the nanoparticles in terms of plasmids associated per particle and its implications in co-transfection of multiple plasmids to the same cells. Particles effective at transfecting primary human fibroblasts had 30-120 plasmids per particle, depending on polymer structure. Nanoparticles that contain a high level of

plasmids per particle (120 vs. 30) proved promising for coexpression. This quantitative understanding has implications for co-delivery of therapeutic genes and for stem cell reprogramming using nanoparticles.

4.2 Materials and Methods

4.2.1 Polymer synthesis and nanoparticle formation

Details of the polymer synthesis and nanoparticle formation method have been previously described [13]. Briefly, diacrylate terminated base polymers (BxSx) were first synthesized at 90˚C by conjugate addition of acrylate and amine monomers for 24 hours. As a second step, the base polymers were end-capped with amine containing small molecules at room temperature in DMSO to form amine terminated end-capped PBAE versions (BxSxEx). To form nanoparticles, PBAE stock solutions of 100 mg/mL in DMSO and EGFP-N1 DNA stock of 1 mg/mL in deionized (DI) water were both diluted separately in 25 mM, pH 5 sodium acetate (NaAc) solution at concentrations required to achieve polymer to DNA weight ratios (wt/wt) of 40, 60 and 100 and mixed vigorously at a 1:1 ratio, with final concentrations at 0.006 or 0.06 mg DNA/mL. The nanoparticles were formed through self-assembly during a 10-minute incubation. PEI-based nanoparticles at a 2 wt/wt ratio were prepared similarly, but using a 150 mM, pH 5.5 sodium chloride solution.

4.2.2 Cell Transfection

IMR90s maintained in Eagle's Minimum Essential Medium supplemented with 10% FBS were plated at a density of $1.8x10^5$ cells per well and transfected at 6 µg DNA/100 µl particles per well in a 6-well plate. After incubating the cells with nanoparticles for 4 hours, the media was aspirated and replaced with fresh media and the fluorescence expression was analyzed using microscopy after 48 hours. See supplementary methods for a step-by-step protocol.

4.2.3 Nanoparticle characterization by NTA and TEM

A Nanosight LM10 equipped with a sensitive CCD camera was used for characterizing the nanoparticles by NTA. Two hundred microliters of diluted nanoparticle solution was loaded into the sample chamber using a 1 mL syringe, the chamber connected to a 405 nm laser source was placed on the Nanosight microscope stage, and a 60 s movie containing the Brownian motion tracking of the scattering centroids (particles) was recorded using the NTA software (Version 2.0). The movie was processed using the manufacturer recommended auto settings with manual adjustment of the gain, blur and brightness as recommended. The particle solution was diluted in DI water to adjust the sample concentration to 10^7-10^9 particles/mL. For TEM studies, nanoparticles were formed by complexing with EGFP-DNA as described earlier and 10 µL of these particles was placed on a formvar/carbon coated copper grid (FCF400-Cu, Electron Microscopy Sciences). The nanoparticles were dried for 2 hours and then imaged in a Philips/FEI BioTwin CM120 Transmission Electron Microscope at the JHU-SOM Microscope Facility. The images were processed using ImageJ software. See supplementary methods for a step-by-step protocol.

4.2.4 Plasmid per particle distribution calculations

The known total plasmid concentration was multiplied by the volume fraction of each 1 nm-spaced particle-size class to get the number of plasmids in each 1 nm-spaced particle-size class. This plasmid number was divided by the number of particles in that particle-size class to get the number of plasmids per particle for each particle-size class. The particle per plasmid distribution was determined for all replicates, the replicates were averaged and the average was rounded off to the nearest whole number to plot a graph of number of plasmids per particle (at each 1-nm spaced particle class) against the concentration of particles that contain that given number of plasmids. Both the mode and mean of the distribution were calculated, where the peak of the distribution represents the mode plasmid per particle number for each formulation. The mean of 1 nm distribution matched the mean obtained from overall average calculations.

4.3 Results and Discussion

The structures of the polymers used in this study are shown in **Figure 4.1.** We focused on six end-capped PBAE formulations: B4S4E7, with base polymer synthesized at a 1.2:1 monomer ratio and formulated at 40 weight polymer to weight DNA (wt/wt), B4S4E7 (1.2:1, 60 wt/wt), B5S3E7 (1.05:1, 60 wt/wt), B5S3E7 (1.05:1, 100 wt/wt), B4S5E7 (1.2:1, 100 wt/wt), and B5S5E1 (1.2:1, 100 wt/wt). The nanoparticles were formed by complexing polymers with enhanced green fluorescent (EGFP-N1) plasmid DNA in 25 mM, pH 5 sodium acetate (NaAc) solution. The 25 kDa branched PEI-based

control nanoparticles were prepared in 150 mM, pH 5.5 sodium chloride (NaCl) solution at 2 wt/wt ratio (N/P ratio of 16).

The nanoparticles were used for transfecting human fetal fibroblasts (IMR90) with EGFP and DsRed plasmids. The cells were transfected in three different conditions, a) transfection with complexes containing both EGFP and DsRed plasmids for 4 hours, b) transfection with exclusively EGFP containing complexes for 2 hours, followed by transfection with the same dose of exclusively DsRed containing complexes for 2 hours after media change and c) transfection with exclusively EGFP containing complexes for 4 hours, followed by transfection with the same dose of exclusively DsRed containing complexes for 4 hours after a gap of 24 hours.

The nanoparticles were analyzed by nanoparticle tracking analysis (NTA) using a Nanosight LM10 that tracks the random Brownian motion of individual nanoparticles suspended in an aqueous solution. The particle characterization performed using NTA was confirmed by dynamic light scattering (DLS) using Malvern Zetasizer NanoZS. Unlike the intensity-based distribution of particle size given by DLS, NTA gives a direct number-averaged distribution of the particle hydrodynamic diameter by tracking individual particles in real-time as light scattering centroids using a sensitive CCD camera. The number mean particle size (diameter in nanometers) and absolute particle concentration (number of particles/mL) were determined using NTA.

All polymers used in this study formed monodisperse particle size distributions as verified by a unimodal distribution by NTA (**Figure 4.2A**). Transmission Electron Microscopy (TEM) was also performed with dried nanoparticles and gave comparable

sizes to the hydrated nanoparticles (**Figure 4.2B**). The samples were analyzed by gel electrophoresis to evaluate whether 100% of plasmid was complexed into particles at the wt/wt ratios used for NTA measurements. Each lane in the gel contained nanoparticles formulated at a particular wt/wt and the first lane contained a control sample of free DNA by itself (**Figure 4.S1**). The gel electrophoresis results validate that free DNA is not present in these samples and all plasmid for these formulations is complexed within nanoparticles. The known mass (calculated from concentration and total volume) and molecular weight of the EGFP-N1 plasmid (4.7 kilobase pairs, kbp) used for particle formulation was used to calculate the number of plasmids/mL. As all of the DNA was complexed within nanoparticles and all the nanoparticles were monodisperse, the ratio of plasmids/mL to particles/mL (concentration measured using NTA) determines the average number of plasmids per particle. The analysis was performed for PEI and the six different PBAE formulations to study the effect of varying polymer structure and wt/wt ratio on the number of plasmids associated per nanoparticle.

NTA tracks individual nanoparticles so that number fractions can be directly calculated. The nanoparticle sizes were binned rounding to the nearest nanometer, and the following equations were used to determine average nanoparticle size (**Table 4.1**). The number mean diameter, $\overline{d}$, reported by NTA is determined using eq.1. The mean volume based-diameter, $\left(\overline{d^3}\right)^{1/3}$, was calculated using eq.2 and used to estimate the average theoretical maximum number of plasmids per particle. This average quantity gives the average volume of a particle randomly selected (or taken up by the cell) from the population of particles.

$$\bar{d} = \frac{\sum_i n_i d_i}{\sum_i n_i} \qquad (1)$$

$$\left(\overline{d^3}\right)^{1/3} = \left[\frac{\sum_i n_i d_i^3}{\sum_i n_i}\right]^{1/3} \qquad (2)$$

$\bar{d}$ = Number - weighted Mean Diameter

$\left(\overline{d^3}\right)^{1/3}$ = Mean Volume - based Diameter

Single condensed plasmid size was estimated from literature data to determine the average plasmid volume. Dividing the average particle volume by the volume of a condensed plasmid determines the average theoretical maximum number of plasmids per particle. Based on branched 25 kDa PEI saturated DNA condensate sizes and cationic thiol-detergent compacted single plasmid DNA dimensions reported in previous publications, the diameter used for a single condensed 5 kbp plasmid DNA can range from 20-40 nm [24, 25]. The choice of a plasmid size from within this range can dramatically affect the theoretical maximum calculation. Therefore, a likely minimum condensed plasmid size was calculated using the result that the distance between DNA helices in DNA condensates is 2.7 nm [26]. This value has been reported to range from 2.4-2.8 nm [27, 28], but this variation has a smaller effect on the calculations than varying the plasmid diameter. Assuming a cylindrical shape, the volume of a minimum condensed plasmid can then be calculated to be 9140 nm^3 (= π*(2.7/2 nm)^2*(0.34 nm/base pair)*(4.7 kbp), where 0.34 nm equals the length of a DNA rod per base pair [29] and each plasmid contains 4.7 kbp). A volume of 9140 nm^3 corresponds to an equivalent spherical diameter of 25.9 nm. In general, the actual number of plasmids per particle for any sized particle is less than the theoretical maximum. This may be due to

nanoparticle volume taken up by extra polymer that is not tightly associated to condensed DNA as well as a possible range in the degree of plasmid condensation.

Another important point is that there is a distribution of plasmid/particle numbers, reflecting the distribution of particle sizes observed within a population. Therefore, there will be particles with plasmid/particle numbers both greater than and less than the average numbers. An example of the profiles can be seen in **Figure 4.2C**, as well as in supplemental **Figure 4.S2**, which together show the plasmid per particle distribution data for all formulations as determined by calculating the number of plasmids per particle for each 1 nm increment (see methods).

Table 4.2 shows the particle per plasmid quantification. Each nanoparticle condition was fabricated and analyzed in at least duplicate independent batches and each of these replicates included a minimum of 500 completed tracks by NTA to ensure good statistics for the number of particles and their size. The 25 kDa branched PEI-based nanoparticles had 90±10 plasmids per particle on average as calculated by NTA with an average theoretical maximum estimate of 267 plasmids per particle. The average plasmids per particle counts, calculated by NTA, for the six PBAE formulations ranged from 30±2 to 120±20 and the average theoretical maximum average estimates ranged from 80 to 195. Similar to PEI-based nanoparticles, B4S4E7 nanoparticles at 60 wt/wt had 110±10 plasmids per particle and at 40 wt/wt, 120±20 plasmids per particle as calculated by NTA. Changing the polymer to DNA weight ratio, from 40 to 60 wt/wt for B4S4E7-based nanoparticles and 60 to 100 wt/wt for B5S3E7-based nanoparticles did not significantly change the number of plasmids associated per particle. Interestingly,

B4S4E7 nanoparticles, which are highly effective at transfecting IMR90 cells, have the highest plasmid per particle counts in the PBAE-DNA nanoparticles tested. This indicates that, in addition to polymer structure, plasmid per particle count maybe an important parameter to determine the transfection efficacy of PBAE-based nanoparticles for a specific cell type. A study conducted by Ogris et al. correlated DNA/PEI (with or without transferrin ligand) complex size with transfection efficiency [30]. Greater average intensity of green fluorescent protein (GFP) expression per cell was found following transfection with larger sized particles compared to smaller sized particles. This may be due in part to the larger particles containing more plasmids per particle than the smaller particles.

The three B4-based nanoparticles have similar plasmids per particle counts (90-120) and the three B5-based nanoparticles have similar plasmids per particle counts (30-45). Intriguingly, the B4-based nanoparticles have approximately 3-fold the DNA carrying capacity per particle even though the structure of B4 and B5 differ by only a single carbon to the repeating backbone and both B4-based and B5-based nanoparticles have similar ~100 nm particle size as measured by NTA analysis. This finding highlights how the number of plasmids/particle is an important parameter for consideration in nanoparticle design and characterization and it can be tuned through changes to biomaterial structure.

A critical barrier to the generation of induced pluripotent stem cells and to achieving high reprogramming efficiency with non-viral vectors is the low probability of uptake and expression of multiple plasmids (carrying multiple reprogramming factors) by

the same cell. Accordingly, co-transfection experiments using EGFP and DsRed plasmids were conducted in IMR90s to gain insight into the process of delivering multiple plasmid types intracellularly using nanoparticles. Similar co-delivery is seen with PBAE-based nanoparticles as with Lipofectamine 2000, a leading commercially available transfection agent, but with higher cell viability for the PBAE-based nanoparticles. Gene expression following co-delivery with nanoparticles containing multiple plasmids differs from delivery of the same genes in the same type of nanoparticles when formulated and administered separately. **Figure 4.3** shows that if the two plasmids are mixed together before nanoparticle self-assembly to form co-delivery particles, more cells coexpress the two plasmids together (orange-yellow cells) than when the two plasmids are formulated and delivered separately with the same type of nanoparticles on two different days (green and red cells, **Figure 4.3A**). When the nanoparticles are formulated separately and administered together on the same day, the trend of reduced co-delivery also holds (**Figure 4.3B**).

In the case of nanoparticles that contain both GFP and DsRed plasmids, most of the cells exhibit coexpression (yellow/orange cells). When the same type of nanoparticles are used on the same day at the same dose, but containing exclusively GFP and then exclusively DsRed, very few cells exhibit coexpression (yellow/orange cells) and instead individual plasmid expression is strongly seen as either EGFP (green cells) or DsRed (red cells). Cells also do not exhibit coexpression (yellow/orange cells) of the GFP and DsRed plasmids in the separate particles when they are administered 24 hours apart. Thus, for certain applications, co-delivery within the same nanoparticles is critical to ensure coexpression. Schwake et al. presented a stochastic model of transfection to predict co-

transfection ratio and plasmid expression level distribution in Lipofectamine and PEI complexes [31]. They studied co-transfection of pre-mixed plasmids encoding yellow fluorescent protein (YFP) and cyan fluorescent protein (CFP) and post-mixed plasmids (complexes contains either CFP or YFP plasmid) and observed that the co-transfection ratio was higher (21.9%) in pre-mixed than in post-mixed complexes (12.9%), which could also be predicted by their mathematical model [31]. This observation is consistent with our observations in the co-transfection experiments in IMR90 cells. Choosing nanoparticles that contain a high level of plasmids per particle (120 vs. 30) may be a promising strategy to maximize coexpression. Flow cytometry analysis of the co-transfected cells (same day, same particle) showed that B4S4E7-based nanoparticles achieved coexpression in 15.8±0.5% of live cells, whereas B5S3E7-based nanoparticles achieved coexpression in 3.3±1% of live cells (**Figure 4.S3**).

Previous studies on the number of plasmids contained within gene delivery nanoparticles have been limited [20-23]. In studies using cryo-TEM, X-ray scattering, and DLS to evaluate lipopolyamine-DNA complexes, up to 7 plasmids (6.4 kbp) per ~50 nm lipoplex particle and 13 plasmids (3.7 kbp) per 50-100 nm lipoplex particle were calculated [21, 23]. In making these calculations, the particles were assumed as monodisperse spheres although size showed irregularities. Based on the periodicity of ordered microdomains of the particles, half the TEM volume of the ~50 nm spheres was assumed to be occupied by DNA and the number of plasmids was calculated by dividing this volume by the density of DNA as 1.66 g/cm^3. In this manner, as the length of DNA was shortened, the number of plasmids per particle was calculated to increase linearly up to 55 plasmids per lipoplex particle when the DNA was 0.9 kbp in size.[24] This study,

which analyzed lipoplexes and did not include polymeric nanoparticles, is dependent on the observation of ordered microdomain structure and did not look at the effect of varying biomaterial structure on nanoparticle composition and properties.

In an alternative strategy, Ho et al. reported the use of quantum dot (QD) labeling combined with regular TEM for estimation of plasmids per particle in chitosan-based nanoparticles [20]. The number of quantum dots per polyplex nanoparticle can be determined by the ratio of fluorescence signal from a single polyplex compared to a single QD and by counting the electron-dense regions of QDs within a polyplex in a TEM image. Estimating 0-3 QD per plasmid, ~30 plasmids per particle were calculated for a ~60 nm particle [20]. While this QD technique works very well as a novel tool to evaluate intracellular stability and DNA unpacking, it has limitations in easily estimating plasmids per particle as the DNA must be first labeled and this may change its self-assembly properties with certain materials, unlabeled DNA that may be encapsulated is not directly detected, counting QDs per particle by TEM becomes more difficult as the number of plasmids increases due to potentially overlapping plasmids and QDs in the 2D image, and other simplifying assumptions.

A third approach at measuring plasmids per particle was developed by Collins et al. who studied $(Lys)_{16}$ containing peptide/DNA complexes and quantified the number of plasmids per particle in physiologically relevant aqueous solution [22]. However, the technique used, Flow Particle Image Analysis, is only amenable to sizing larger, micron-sized particles. A polylysine-based Polymol peptide was found to form ~1 μm particles that contained an estimated 70,000 6.0 kbp plasmids per particle. These microparticles

are approximately 10-fold larger than the nanoparticles used in the current study, and hence, their volume is ~10^3-fold greater.

For all formulations described in this manuscript, calculated plasmid per particle counts were lower than the estimated theoretical maximum value, but of the same order of magnitude. The calculated values determined from this novel NTA method are similar in some ways to the numbers previously reported in literature including an average of 30 plasmids per particle for chitosan-DNA nanoparticles [20] and 13 plasmids per particle for lipopolyamine-DNA lipoplex nanoparticles [21]. These are both close to the low range of the PBAE nanoparticles described. However, we also show that other PBAE nanoparticles as well as PEI nanoparticles can have a much higher DNA carrying capacity of ~100 plasmids per particle. This higher DNA loading may be especially important for the co-delivery of genetic therapeutics for the treatment of diseases such as cancer or as an enabling tool for stem cell reprogramming.

Although TEM is routinely used for nanoparticle characterization, and can be used to estimate particle concentration, there are drawbacks of using this method. They include errors introduced by processing effects such as dehydration and aggregation of "soft" self-assembled particles that are typically hydrated in their native state, limited sample size per image for sufficient statistics, consumption of the sample by the assay, and relatively high cost and time consumed for sample collection and analysis. DLS is unable to measure particle concentration and reports size that is biased towards larger particles. Thus, a new technique is required. Here, we show that NTA is a technique that

is able to meet this need. In addition to its utility at measuring number-averaged size and concentration of nanoparticles, the assay is also quick and non-destructive of the sample.

In comparison to viruses, which are natural nanoparticles, the polymeric nanoparticles are found to contain up to 100-fold more copies of their delivery genome than viruses contain. For example, while adenovirus particles and the polymer-based nanoparticles evaluated here both contain double stranded DNA, are both ~100 nm in size, and have been shown to have comparable efficacy *in vitro* to certain human cells [32], this work shows that each synthetic nanoparticle is dramatically less efficient in delivery. Future work is needed to improve the efficiency of synthetic nanoparticles for non-viral gene delivery.

In conclusion, a quick, easy and robust assay for quantifying the number of plasmids per nanoparticle in physiologically relevant aqueous solution was developed. PBAE-based and PEI-based polymeric nanoparticles were analyzed by varying their polymer structure and polymer to DNA weight ratio. The plasmids per particle values ranged from 30 to 120 plasmids per particle and depended on polymer structure. More plasmids per particle led to higher co-expression following gene delivery. To our knowledge, this is the first study to report characterization of polymeric nanoparticles in terms of plasmids per particle in aqueous conditions. Characterization of polymeric nanoparticles in terms of the number of plasmids per particle can allow for improved design to non-virally co-deliver multiple plasmids to the same target, a requirement for certain gene therapies and for factor-based stem cell reprogramming.

4.4 Acknowledgements

The authors thank the TEDCO MSCRF (2009-MSCRFE-0098-00) and NIH R21CA152473 for support. Corey Bishop and Stephany Tzeng are thanked for technical assistance in acquiring the TEM images.

4.5 Tables

Table 4.1. Nanoparticle size averages of the seven formulations. Z-average determined by dynamic light scattering (DLS), with all other sizing determined by nanoparticle tracking analysis (NTA). Error reported is standard error of the mean.

Polymer	Molecular Weight (Da)	wt/ wt	Number-weighted mean particle diameter (nm)	Mean volume based-diameter (nm)	Z-average particle diameter (nm)
B4S4E7	28590	40	120±10	130±10	291±9
B4S4E7	28590	60	130±10	150±10	379±9
B4S5E7	11072	60	110±10	130±10	106±9
B5S3E7	4632	60	114±3	124±4	110±10
B5S3E7	4632	100	101±2	112±4	120±10
B5S5E1	2873	100	106±1	115±1	113±5
PEI 25kDa	25000	2	150±10	170±10	317±2

Table 4.2. The average number of plasmids per nanoparticle for the seven nanoparticle formulations as determined by nanoparticle tracking analysis (NTA).

Polymer	wt/wt	Mode plasmid/ particle	Average plasmid/ particle	Standard Error	Number of Tracks	Average theoretical max plasmid/particle	Average kbp/particle	Average theoretical max kbp/particle
B4S4E7	40	57	120	20	>500	127	564	597
B4S4E7	60	63	110	10	>500	195	517	917
B4S5E7	60	29	90	30	>500	119	423	559
B5S3E7	60	23	45	9	>500	110	212	517
B5S3E7	100	17	30	2	>500	80	141	376
B5S5E1	100	23	35	2	>500	86	165	404
PEI 25kDa	2	49	90	10	>500	267	423	1255

4.6 Figures

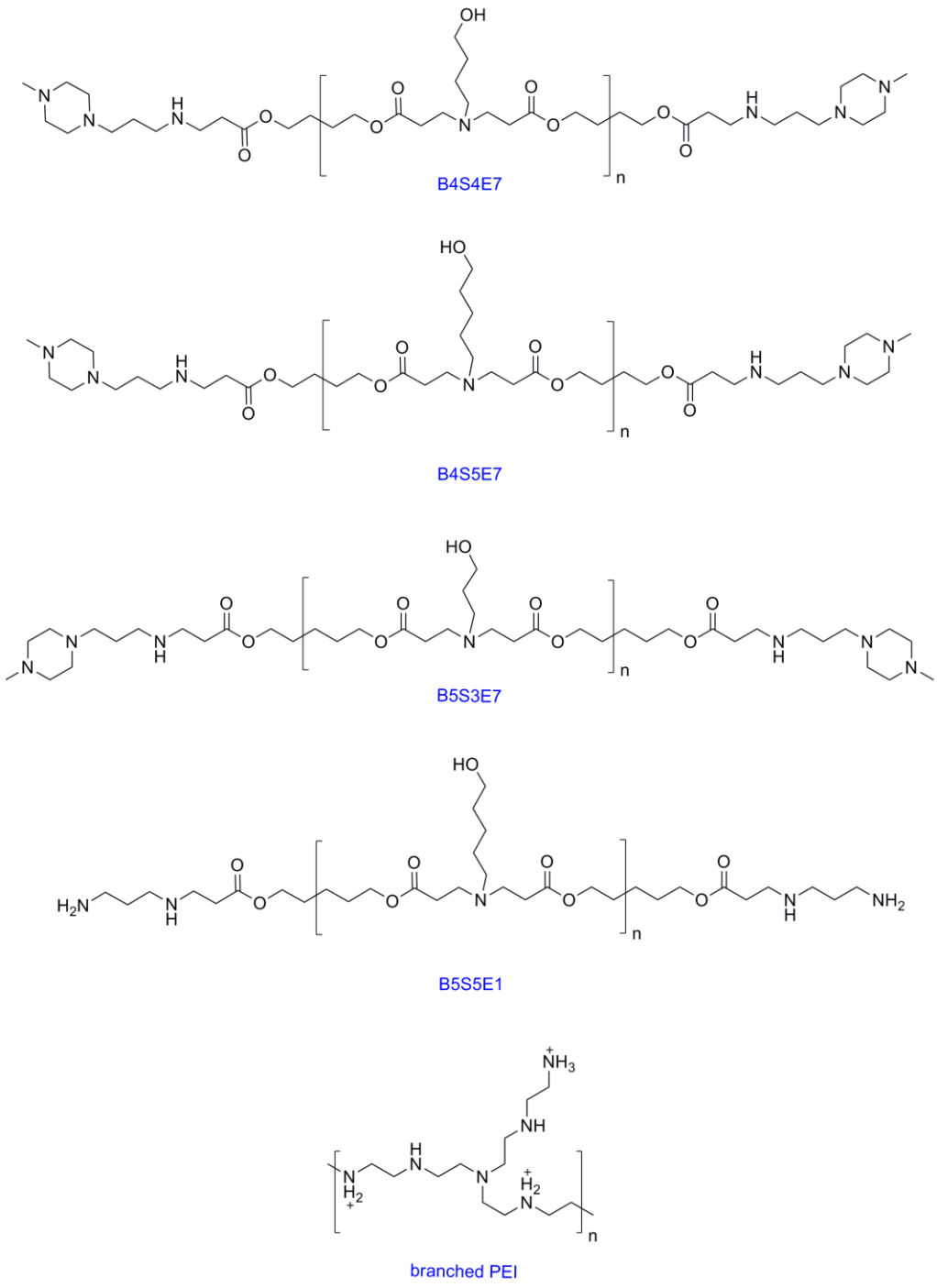

Figure 4.1. The chemical structures of the PBAEs and PEI used in this study.

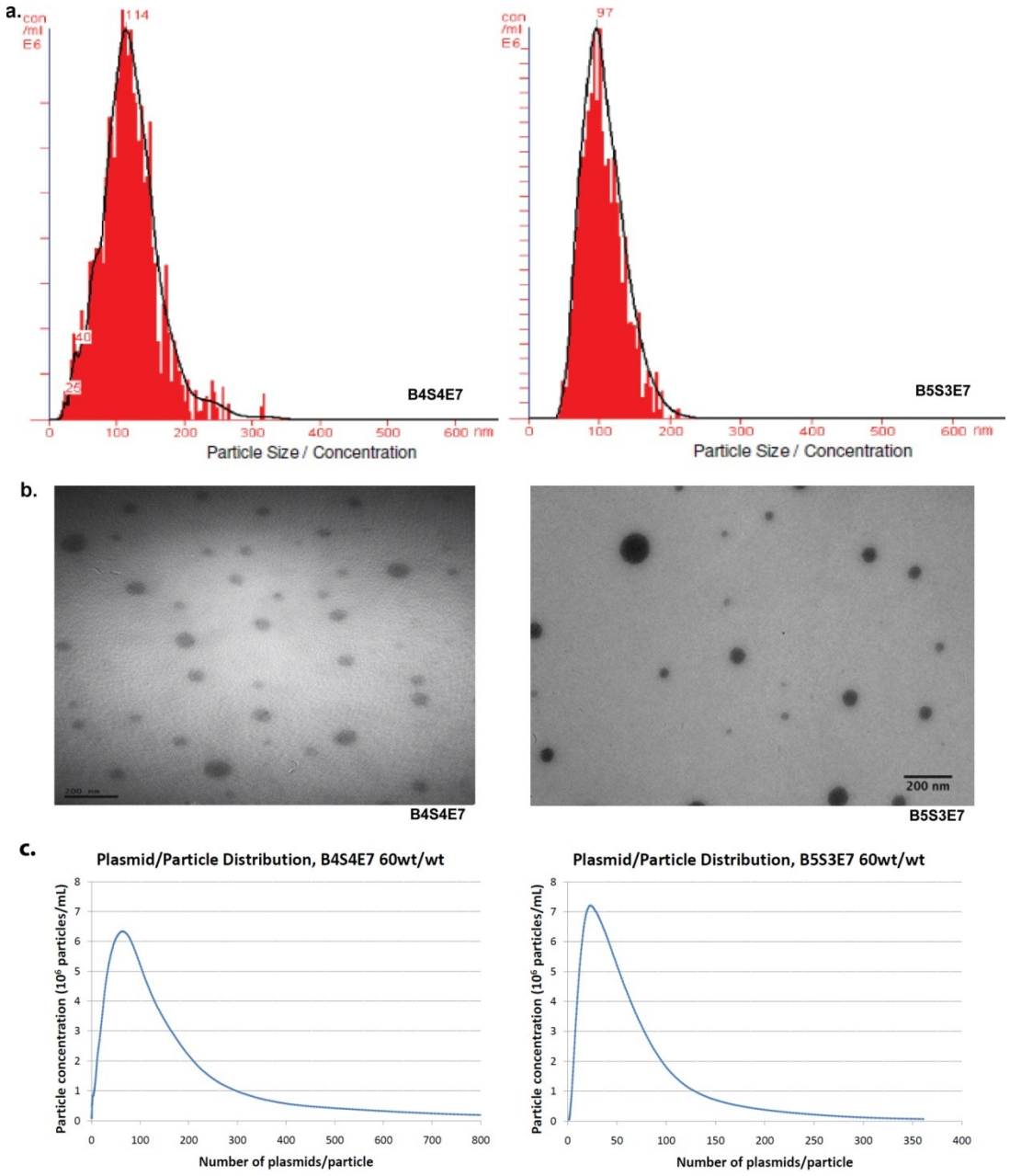

Figure 4.2. Size distribution and plasmid per particle distribution data of PBAE (B4S4E7 and B5S3E7, both 60wt/wt) based nanoparticles. **(a)** particle size from nanoparticle tracking analysis **(b)** particle size from transmission electron microscopy **(c)** plasmid per particle distribution from nanoparticle tracking analysis.

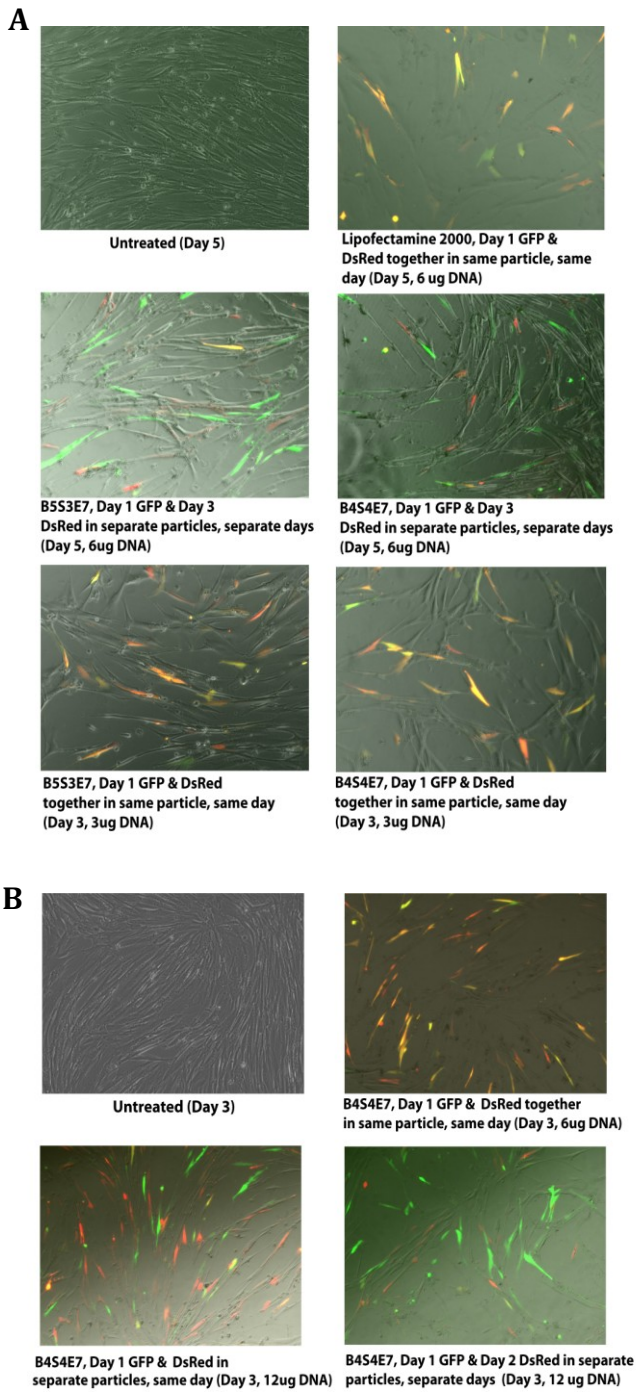

Figure 4.3. Co-transfection data in IMR90 human fibroblasts. B4S4E7 and B5S3E7-based nanoparticles were used to deliver EGFP and DsRed plasmids within the same particles on the same day as well as **(a)** within separate particles on separate days and **(b)** within separate particles on the same day. Lipofectamine 2000 was used as a positive control.

4.7 Supplementary Methods

1.) Cell Seeding.

1.1) Do not allow cells to grow to overconfluency. Use early passage cells when transfecting primary cells.

1.2) Twenty-four hours prior to transfection, trypsinize the cells, count the cells using a hemocytometer, and dilute the cell suspension with media to achieve the desired cell density (cells/volume). Seed cells into clear tissue culture-treated flat-bottom 96-well plates using a reservoir and multichannel pipettes. The chosen density should give 70-80% confluency on the day of transfection. For example, as displayed in **Table 4.SM1**, cells were diluted to 25 to 50 cells/μL for the transfection data shown here.

2.) Cell Transfection.

2.1.) Dilution of polymer and DNA stocks. Thaw polymer and DNA stock solutions at room temperature (RT). Dilute polymer stock solution and DNA stock solution, separately in clear 96-well plates using a twelve-channel pipette, with the appropriate solvent to concentrations required to obtain the desired polymer weight to DNA weight ratios (wt/wt). In this case, the chosen solvent is 25 mM sodium acetate buffer (pH=5.2).

2.1.1.) DNA dilution. Typically, DNA stored at 1 mg/mL is diluted in sodium acetate buffer to a concentration of 0.03 to 0.06 mg/mL in a clear non-tissue culture-treated 96-well plate (one well for a single formulation). **Table 4.SM2** shows the typical DNA dilution protocol for a single formulation used to transfect four replicate wells in a 96-well plate seeded with cells from Step 1.

2.1.2.) Polymer dilution. The 100 mg/mL polymer/DMSO solution is diluted in sodium acetate buffer according to the concentration required to obtain the desired polymer to DNA wt/wt ratio. The range of wt/wt ratios typically used for gene delivery with poly(beta-amino ester)s (PBAEs) is 20 to 100. PBAE polymers are first diluted to 10 mg/mL, followed by the dilution protocol as shown in **Table 4.SM3**. The polymer dilutions can be performed in a clear non-tissue culture-treated 96-well plate that matches the sample orientation of the DNA dilution plate.

2.2.) Nanoparticle formation. Add the PBAE solution to an equal volume of the plasmid DNA solution using a twelve-channel pipette and mix vigorously. Let the mixture incubate at RT for 10 minutes to allow self-assembly.

2.3.) Nanoparticle transfection. Following self-assembly, 20 μL nanoparticles are added per well to the culture medium dropwise using the twelve-channel pipette. Replicate wells are left untreated or are transfected with commercially available reagents as

controls. The transfected cells are incubated at 37˚C for two to four hours and then the wells are replaced with fresh media (100 μL/well).The choice of incubation time will depend on the cell line, culture conditions, and transfection system. The difference in transfection efficiency and cell toxicity as a result of varying incubation period will be quantified by the analysis protocol described in Step 3.

3.) Analysis of Transfection Efficiency and Cell Toxicity.

Transfection efficiency is analyzed visually with a fluorescence microscope and quantified using a flow cytometer forty-eight hours post-transfection. Cell toxicity is analyzed visually with a fluorescence microscope and quantified using the CellTiter 96® AQueous One assay twenty-four hours post-transfection.

3.1.) Fluorescence microscopy. Visually analyze the wells for the expression of the transfected reporter gene (for example, EGFP or DsRed) using the appropriate fluorescence channel. Acquire images for each well, choosing fields of view that appropriately represent the transfection efficiency for the particular formulations (**Figure 4.SM1**). Make a note of any cell toxicity observed visually.

3.2.) Flow Cytometry.

3.2.1.) Use multichannel pipettes to prepare the 96-well plate for flow cytometry. Wash with PBS, trypsinize with 30 μL/well of trypsin/EDTA, neutralize with 170 μL FACS buffer (PBS + 2%FBS), pipette up and down in each well, including around edges, and transfer the entire 200-μL volume of each well into corresponding wells in a round-bottom or V-bottom 96-well plate.

3.2.2.) Centrifuge the plate at 130g for 5 min at 4°C.

3.2.3.) Remove 170 μL media from each well and pipette to resuspend cells while avoiding bubbles. To use a viability stain like propidium iodide (PI), add 10 μL of FACS buffer+PI (50:1 FACS buffer:PI dilution; PI stock concentration 1 mg/mL) to each well. Immediately place on ice and cover from light.

3.2.4.) Start the C6 Accuri flow cytometer, the HyperCyt® 96-well attachment, and the HyperView® software. Use HyperView® Design and Protocol tabs to choose the appropriate plate type, plate layout, and other settings such as shake/sip/rinse/shake time. For the above protocol, the following parameters were used, a pre-plate prime for one minute, and a pre-plate shake for 30 seconds at 2400rpm. Sip time was set for 15 seconds at 15 rpm, a probe rinse every well for 2 seconds, and an interwell shake every 12 wells for 12 seconds at 2400 rpm. The interwell shake is important to keep the cells dispersed in the media, as well as for improved ability to process the data by including timed breaks between groups of wells (in this case 12 seconds).

3.2.5.) Use HyperView® Well Identification tab to process the data and separate into the appropriate well (**Figure 4.SM2**). In order to identify the individual wells, it can help to use the software's noise filter, as well as including a base even filter under the advanced settings.

3.2.6.) Quantify percentage of positively transfected live cells by appropriate gating to separate different populations (**Figure 4.SM3**).First view the flow data on a FSC vs.SSC scatter plot in order to separate cells from debris (**Figure 4.SM3A**). If propidium iodide (PI) was used, gate the individual cell population and view that data on a FSC vs. FL3plot in order to separate live cells from dead cells and gate the live cells. In order to quantify the number of transfected cells, view the live cell population on the appropriate channels, for example, GFP can be seen in FL1. Using the untreated population, gate the untreated cells in order to identify the background signal (**Figure 4.SM3B**).The positively transfected cells can then be isolated using this gate and by viewing the transfected populations using both scatter and contour plots (**Figure 4.SM3C** and **4.SM3D**). There may be a continuum of positively transfected cells, as different cells will be transfected to different degrees of fluorescence.

3.3.) CellTiter 96® AQueous One assay

3.3.1.) Transfect another plate in exactly the same manner for cell toxicity measurements.

3.3.2.) Premix 1 mL of the CellTiter 96® AQueous One assay solution with 10mL fresh media. Remove media from cells and use a multichannel pipette to add 110 uL of the premixed solution+media per well.

3.3.3.) Measure the absorbance at 490 nm every one hour interval from 1 to 4 hours until the absorbance from the well with untreated condition is in the linear range of the assay. Include four control wells with only solution+media for a background absorbance reading.

3.3.4.) Average the absorbance values from the four replicate wells per condition and subtract the average background absorbance from each average. Normalize the corrected average for each treated condition to the corrected average of the untreated condition to determine the percent cell viability.

4.) Nanoparticle sizing with NTA and plasmid per particle calculations.

4.1.) Prime the fluidics system of the Nanosight NS500 by running the diluent pump forward at approximately 1/5th the max speed and the sample pump backward at approximately 1/10th the max speed. Continue until the fluidics system is flushed with diluent.

4.2.) Prepare the nanoparticles to be analyzed. In the case of PBAEs, separately dilute the stock plasmid DNA (1 mg/mL) and stock PBAE (100 mg/mL) in sodium acetate buffer (25 mM, pH 5) in eppendorf tubes.

4.3.) Dilute the plasmid DNA concentration to 0.06 mg/mL. Polymer concentration can vary depending on the required weight-weight ratio of polymer to DNA (for example, for 60 wt/wt particles, polymer is diluted to 3.6 mg/mL).

4.4.) Add the polymer solution to an equal volume of the plasmid DNA solution and mix vigorously. Incubate the mixture at room temperature for 10 minutes to allow self-assembly.

4.5.) Dilute the nanoparticle solution 100-fold into PBS in order for the nanoparticle concentration to be in the appropriate range for NTA and to obtain a final volume of at least 500 μL.

4.6.) Load the sample into the Nanosight by placing the loading tube into the sample eppendorf tube (**Figure 4.SM4A**). Make sure not to introduce air bubbles.

4.7.) In capture mode, increase the camera level until particles can be seen. Adjust the focus so that the particles look smooth (**Figure 4.SM4A** and **4.SM4B**).

4.8.) While in standard mode, adjust the camera level past the point that all particles can be seen on screen. Then decrease the camera level to the lowest level such that the particles can all still be observed. If an intermediate camera level is needed, go into advanced mode and modify the camera shutter and gain to the appropriate levels.

4.9.) Visually check to make sure there are between 20 – 100 particles on the screen. An ideal number for nanoparticle tracking is approximately 50 particles. If there are too many or too few, flush the NS500, adjust the dilution into PBS, and re-load the sample.

4.10.) Adjust the capture duration according to the standard mode table. Typically 30 – 60 seconds is an appropriate capture length (**Figure 4.SM4B**).

4.11.) To load the next sample, flush the system, then re-load the new sample.

4.12.) Once videos are captured, proceed to the processing stage by opening a video file.

4.13.) There are a number of parameters that can be tuned in order to best process a video (**Figure 4.SM4C**). The goal is to select parameters that best capture each particle on the screen, as indicated by a red cross mark on the screen over each particle (**Figure 4.SM5**).

4.14.) Increase the screen gain to better see the particles. Under the standard or advanced mode, select the auto adjust for the parameters by clicking the appropriate boxes. In the case that the auto settings do not adequately select particles, unclick the box and manually set the parameters (**Figure 4.SM4C**).

4.15.) Once all the particles are picked on screen, click the process button of the software to process the video file (**Figure 4.SM4C**). This provides the particle size distribution, size averages, as well as particle concentration.

4.16.) In order to make certain that the particle concentration is accurate, change the PBS dilution, such as by increasing dilution by 2x, and repeat the above procedure. Measuring multiple dilutions of the same sample is recommended to ensure that the concentration measurement of the sample is accurate. A good range for measurement is 10^7-10^9 particles/mL.

4.17) Verify that all plasmids are incorporated into nanoparticles by running gel electrophoresis of the nanoparticles and evaluating whether any free DNA is present. If not all plasmids are encapsulated, use standard techniques to measure DNA absorbance in order to quantify total encapsulated plasmids.

4.18.) To calculate the average number of plasmids per particle, divide the total encapsulated plasmid concentration by the NTA measured particle concentration. In order to estimate the plasmid per particle sample distribution, first use the NTA particle size histogram to calculate the volume fraction of each 1-nm bin of particle. Multiply this volume fraction distribution by the total plasmid amount to obtain the number of plasmids in each bin. Divide these numbers by the number of particles in each bin to obtain the number of plasmids-per-particle for each particle size.

4.7.1 Supplementary Methods (SM) Tables

Table 4.SM1. Typical cell plating protocol for a 96-well plate format.

Wells/Plate	Volume/Well (μL)	Cells/Well
96	100	2,500 to 5,000

Table 4.SM2. Typical DNA dilution protocol for a 96-well plate format.

Wells /Plate	Volume/ Well (μL)	Particle Volume/ Well (μL)	DNA/Well (μg)	DNA (μg/ μL)	DNA stock (μL)	NaAc (μL)
96	100	20	0.6 to 1.2	0.03 to 0.06	3.0to 6.0	47 to 44

Table 4.SM3. Typical polymer dilution protocol for a 96-well plate format.

Polymer: DNA (wt/wt)	Particle Volume/ Well (µL)	# Replicate Wells	DNA/ Well (µg)	Polymer/ Well (µg)	Polymer/ DMSO stock (µL)	NaAc (µL)
20	20	4	0.6 to 1.2	12 to 24	1.2 to 2.4	55
40	20	4	0.6 to 1.2	24 to 48	2.4 to 4.8	55
60	20	4	0.6 to 1.2	36 to 72	3.6 to 7.2	50
100	20	4	0.6 to 1.2	60 to 120	6.0 to 12	50

4.7.2 Supplementary Methods (SM) Figures

Figure 4.SM1. Single color channel fluorescence imaging of HRECs transfected with PBAE. **(Left)** GFP fluorescence, colored green; **(Middle)** Brightfield image; **(Right)** Composite image.

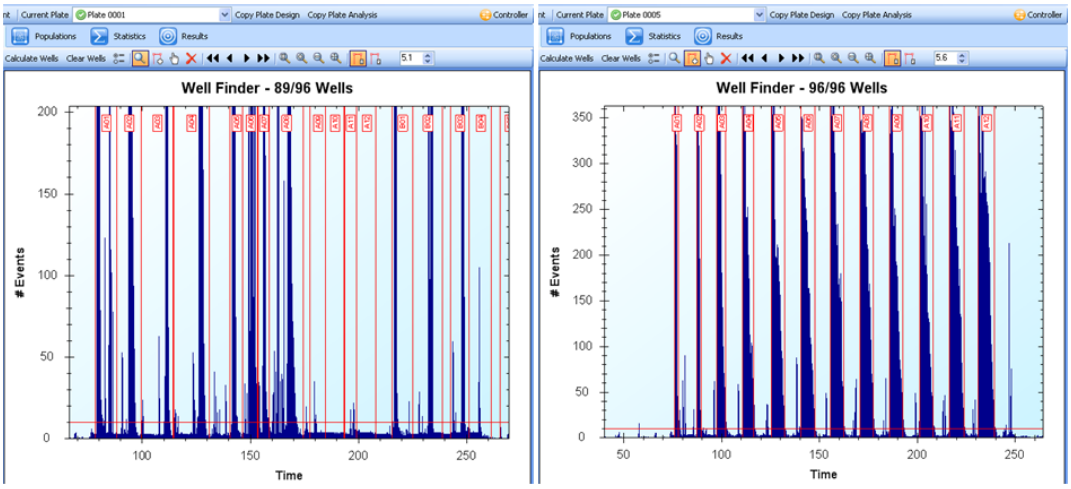

Figure 4.SM2. Hypercyt software well identification step after data collected. **(Left)** Example of problematic data due to low counts or issue with the fluidics; **(Right)** Example of clean data, with easily identified wells.

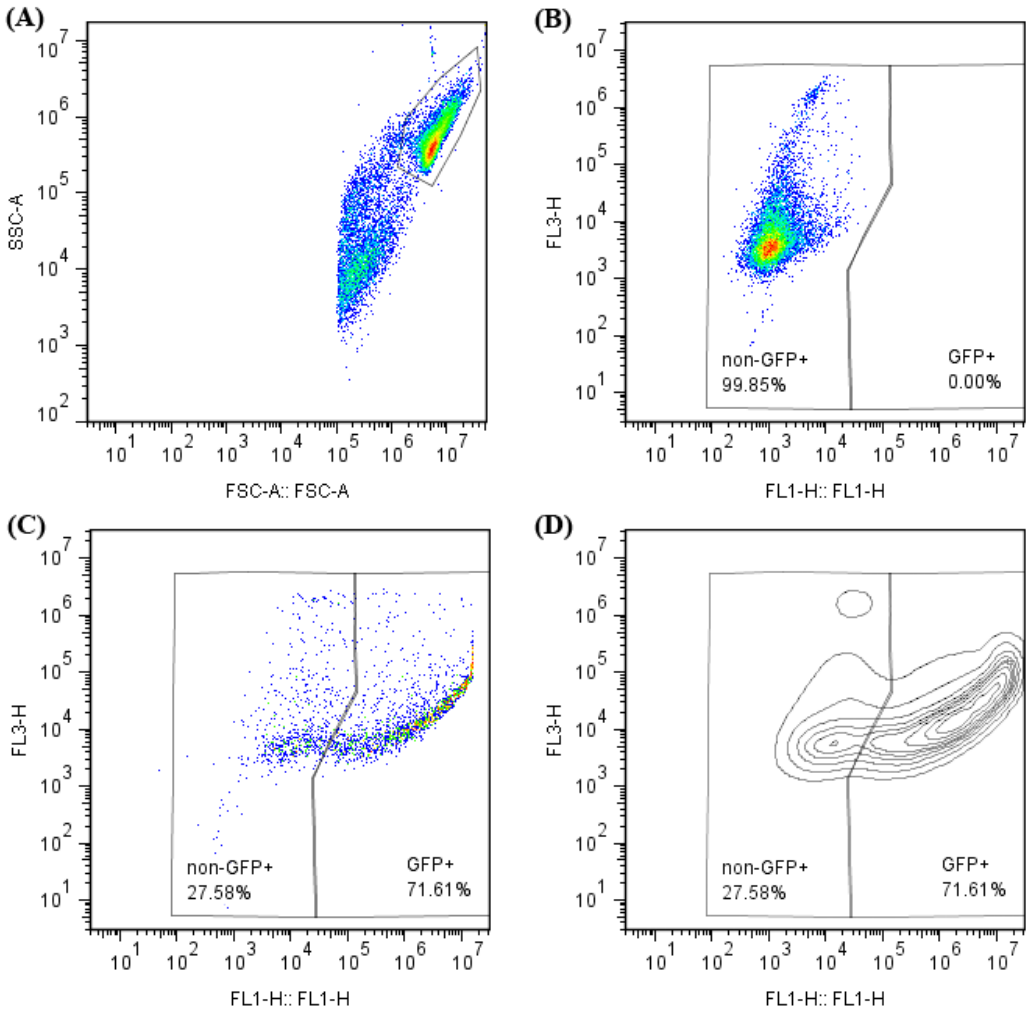

Figure 4.SM3. FlowJo gating for cells transfected with EGFP plasmid. **(A)** FSC vs. SSC for untreated cells; **(B)** FL1 vs. FL3 for untreated cells; **(C, D)** FL1 vs. FL3 for cells transfected with PBAE. Both pseudo-color density **(C)** and **(D)** contour plots are useful to determine the location to draw gates.

Figure 4.SM4. Screenshot of parts of the Nanosight nanoparticle tracking analysis software, version 2.2. **(A)** The fluidics control; **(B)** Capture mode, used to capture video of the nanoparticles; **(C)** Processing mode available after opening a previously captured video. Red boxes highlight functions discussed in the protocol.

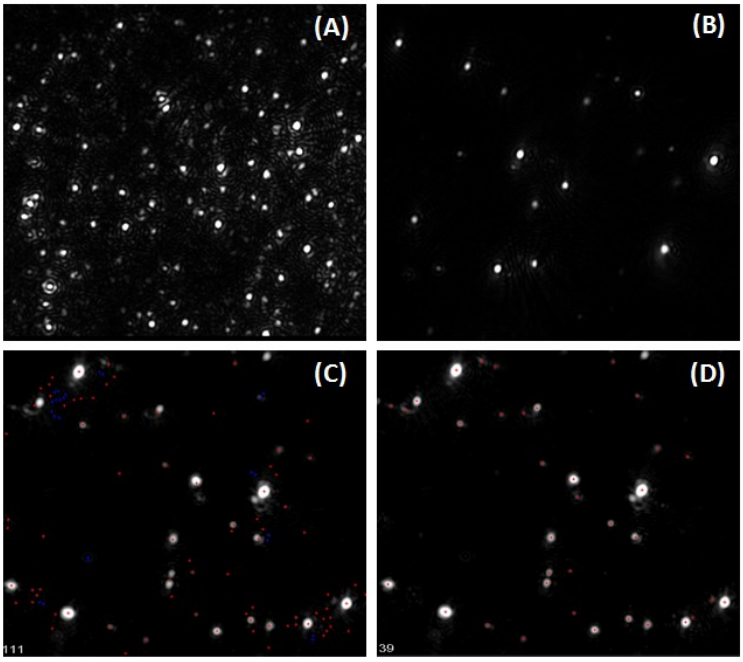

Figure 4.SM5. Example of Nanosight video capture and analysis. Screenshots of sample before video capture for sample that is not diluted enough **(A)**, and with appropriate dilution **(B)**; Screenshots of analysis mode with particle detection threshold set too low **(C)** and set appropriately **(D)**, with red cross hairs identifying all particles appropriately.

4.8 Supplementary Figures

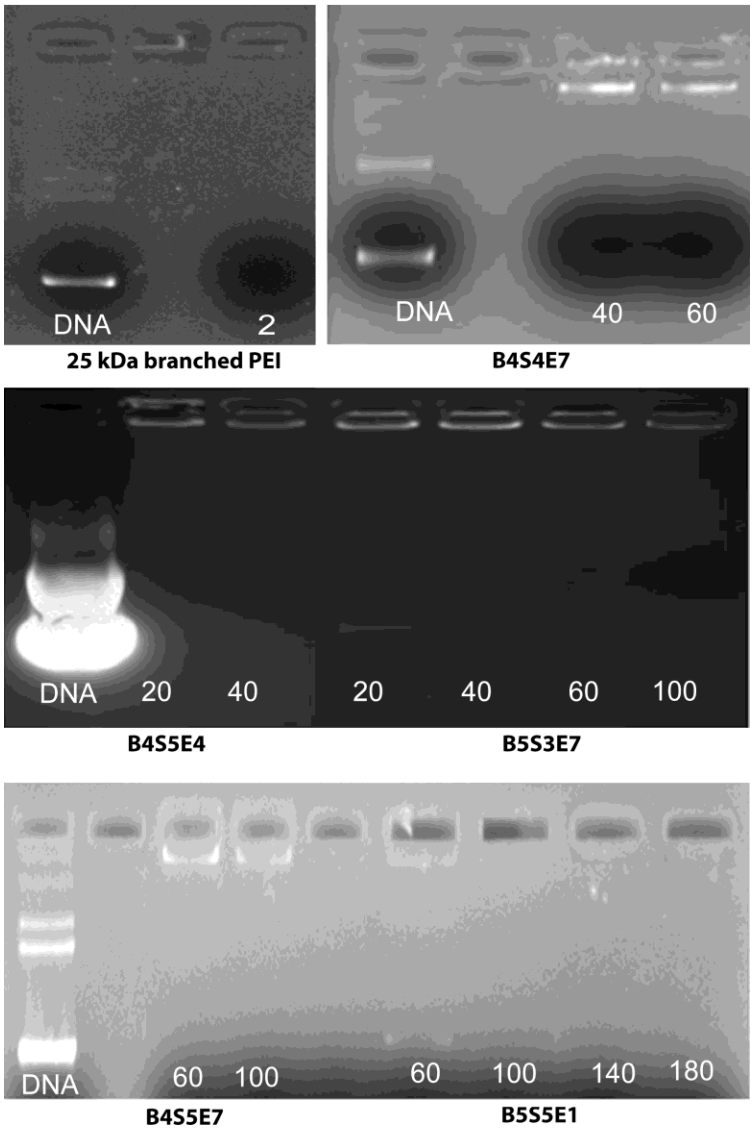

Figure 4.S1. Gel electrophoresis data of the six PBAE-based nanoparticle formulations at different polymer to DNA weight ratios (wt/wt – 20,40,60,100,140,180) and PEI-based nanoparticles control at 2 wt/wt prepared by complexing polymer with EGFP plasmid.

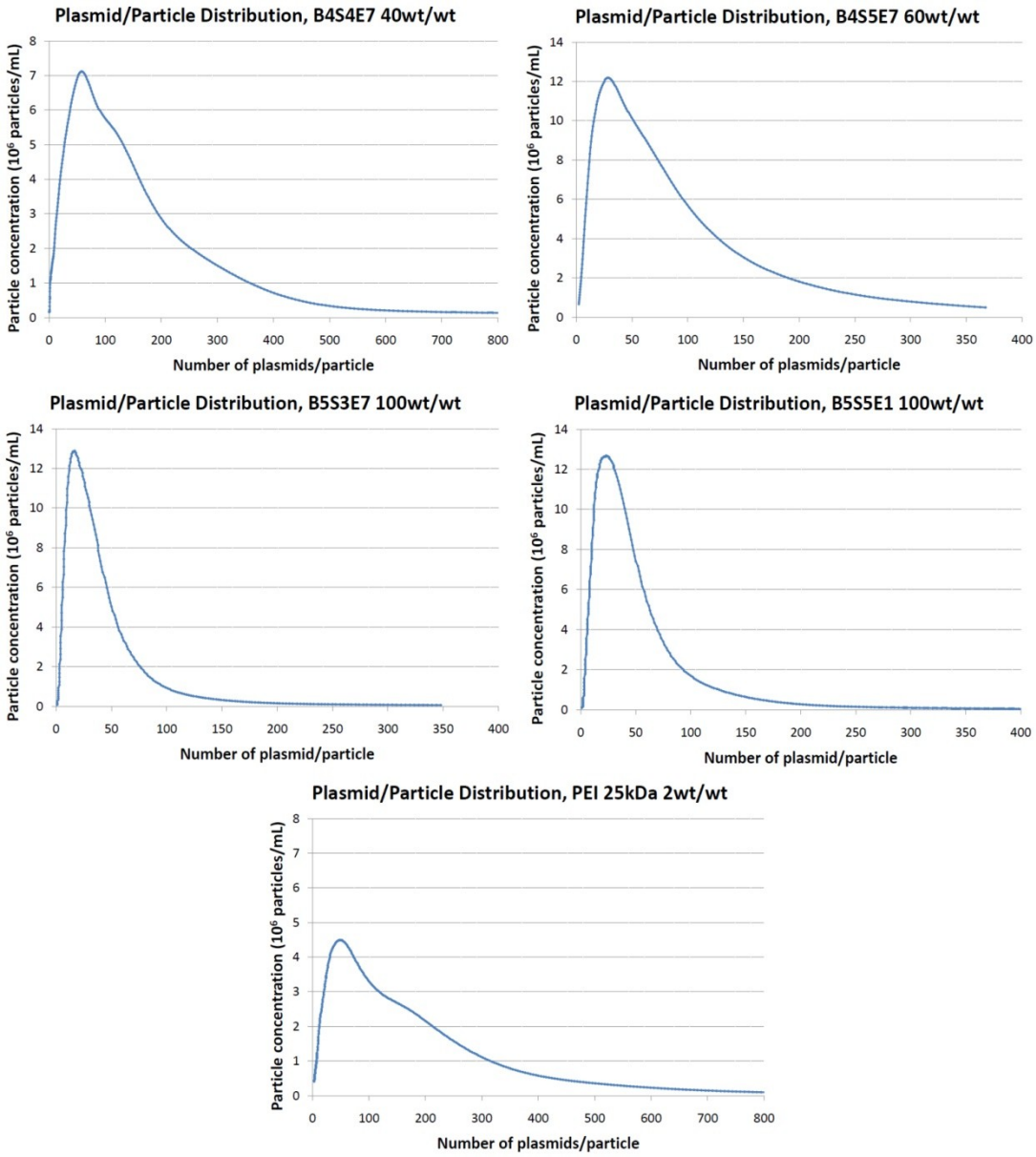

Figure 4.S2. Plasmid per particle distributions from nanoparticle tracking analysis. Figure shows the plasmid per particle distribution data for the rest of the formulations as determined by calculating the number of plasmids per particle for each 1 nm increment of particle size. The peak of the distribution represents the mode plasmid per particle number for each formulation. The mean of 1 nm distribution was also determined and found to be equal to the mean obtained from overall average calculations. For all formulations, the mode was lower than the mean indicating that a few particles may contain a lot of the plasmids and other particles contain fewer plasmids.

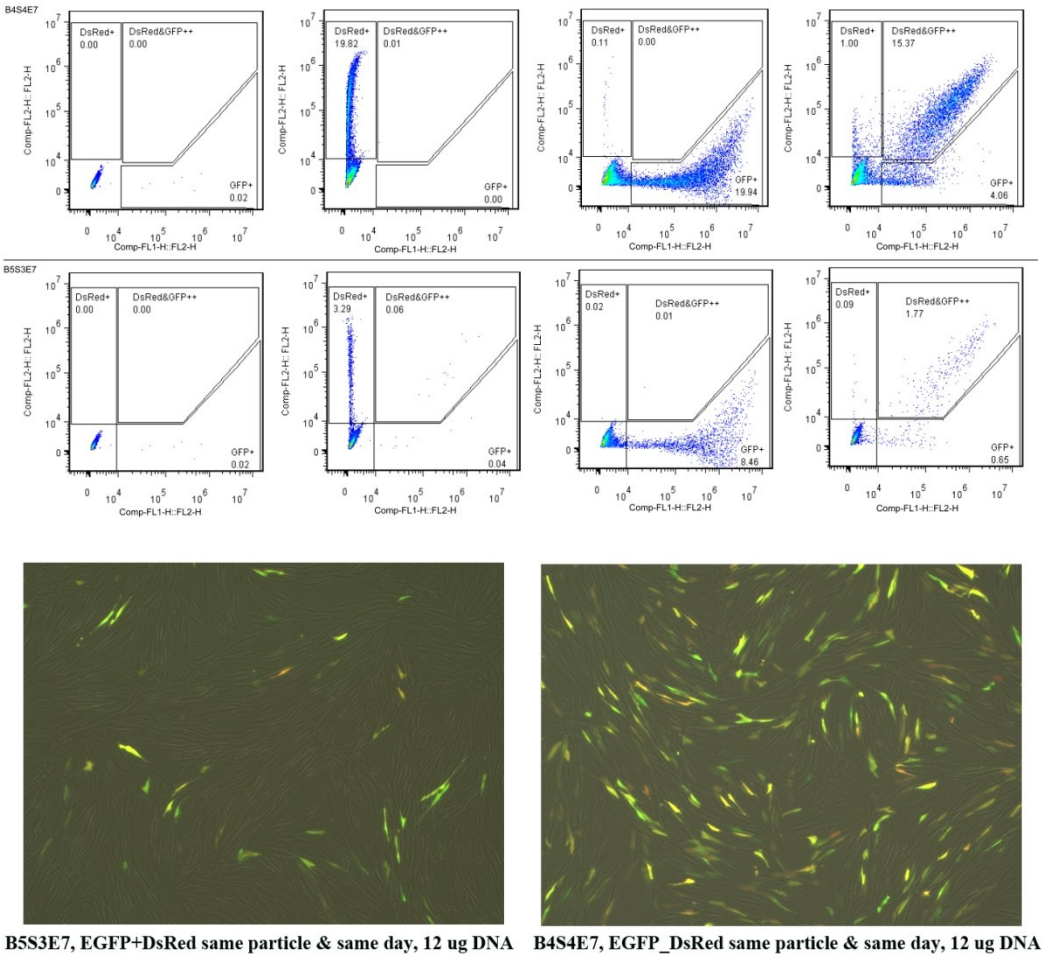

Figure 4.S3. Flow cytometry (FC) and fluorescence microscopy (FM) images of IMR90 cells co-transfected with DsRed and EGFP plasmids using B5S3E7 (FC-bottom panel, FM-left image) and B4S4E7 (FC-top panel, FM-right image) based nanoparticles. 15.8±0.5% cells were co-transfected by B4S4E7 based nanoparticles as compared to 3.3±0.5% co-transfected by B5S3E7 based nanoparticles. The polymer B4S4E7 with a high plasmid/particle count (~120) is more effective at co-transfection than B5S3E7 with a low plasmid/particle count (~30).

4.9 References

1. Putnam D. Polymers for gene delivery across length scales. Nat Mater 2006 Jun;5(6):439-451.

2. Sheyn D, Mizrahi O, Benjamin S, Gazit Z, Pelled G, Gazit D. Genetically modified cells in regenerative medicine and tissue engineering. Adv Drug Deliv Rev 2010 Jun 15;62(7-8):683-698.

3. Angoulvant D, Fazel S, Weisel RD, Lai TY, Fedak PW, Chen L, et al. Cell-based gene therapy modifies matrix remodeling after a myocardial infarction in tissue inhibitor of matrix metalloproteinase-3-deficient mice. J Thorac Cardiovasc Surg 2009 Feb;137(2):471-480.

4. Sunshine JC, Bishop CJ, Green JJ. Advances in polymeric and inorganic vectors for nonviral nucleic acid delivery. Therapeutic Delivery 2011;2(4):493-521.

5. Mercola M, Ruiz-Lozano P, Schneider MD. Cardiac muscle regeneration: lessons from development. Gene Dev 2011 Feb 15;25(4):299-309.

6. Yu J. Human induced pluripotent stem cells free of vector and transgene sequences (vol 324, pg 797, 2009). Science 2009 Jun 5;324(5932):1266-1266.

7. Verma IM, Somia N. Gene therapy -- promises, problems and prospects. Nature 1997 Sep 18;389(6648):239-242.

8. Hollon T. Researchers and regulators reflect on first gene therapy death. Am J Ophthalmol 2000 May;129(5):701.

9. Check E. Gene therapy put on hold as third child develops cancer. Nature 2005 FEB 10;433(7026):561-561.

10. Cavazzana-Calvo M, Thrasher A, Mavilio F. The future of gene therapy. Nature 2004 Feb 26;427(6977):779-781.

11. Boussif O, Lezoualc'h F, Zanta MA, Mergny MD, Scherman D, Demeneix B, et al. A versatile vector for gene and oligonucleotide transfer into cells in culture and in vivo: polyethylenimine. Proc Natl Acad Sci 1995 Aug 1;92(16):7297-7301.

12. Lynn DM, Langer R. Degradable poly(beta-amino esters): Synthesis, characterization, and self-assembly with plasmid DNA. J Am Chem Soc 2000 Nov 8;122(44):10761-10768.

13. Bhise NS, Gray RS, Sunshine JC, Htet S, Ewald AJ, Green JJ. The relationship between terminal functionalization and molecular weight of a gene delivery polymer and

transfection efficacy in mammary epithelial 2-D cultures and 3-D organotypic cultures. Biomaterials 2010 Nov;31(31):8088-8096.

14. Tzeng SY, Guerrero-Cazares H, Martinez EE, Sunshine JC, Quinones-Hinojosa A, Green JJ. Non-viral gene delivery nanoparticles based on Poly(beta-amino esters) for treatment of glioblastoma. Biomaterials 2011 Apr 30.

15. Sunshine J, Green JJ, Mahon K, Yang F, Eltoukhy A, Nguyen DN, et al. Small molecule end group of linear polymer determine cell-type gene delivery efficacy. Adv Mater 2009;21(48):4947-4951.

16. Yu JY, Vodyanik MA, Smuga-Otto K, Antosiewicz-Bourget J, Frane JL, Tian S, et al. Induced pluripotent stem cell lines derived from human somatic cells. Science 2007 Dec 21;318(5858):1917-1920.

17. Takahashi K, Tanabe K, Ohnuki M, Narita M, Ichisaka T, Tomoda K, et al. Induction of pluripotent stem cells from adult human fibroblasts by defined factors. Cell 2007 Nov 30;131(5):861-872.

18. Park IH, Zhao R, West JA, Yabuuchi A, Huo H, Ince TA, et al. Reprogramming of human somatic cells to pluripotency with defined factors. Nature 2008 Jan 10;451(7175):141-146.

19. Yusa K, Rad R, Takeda J, Bradley A. Generation of transgene-free induced pluripotent mouse stem cells by the piggyBac transposon. Nat Methods 2009 May;6(5):363-369.

20. Ho YP, Chen HH, Leong KW, Wang TH. Evaluating the intracellular stability and unpacking of DNA nanocomplexes by quantum dots-FRET. J Control Release 2006 Nov;116(1):83-89.

21. Kreiss P, Cameron B, Rangara R, Mailhe P, Aguerre-Charriol O, Airiau M, et al. Plasmid DNA size does not affect the physicochemical properties of lipoplexes but modulates gene transfer efficiency. Nucleic Acids Res 1999 Oct 1;27(19):3792-3798.

22. Collins L, Kaszuba M, Fabre JW. Imaging in solution of (Lys)(16)-containing bifunctional synthetic peptide/DNA nanoparticles for gene delivery. Biochim Biophys Acta 2004 Apr 7;1672(1):12-20.

23. Pitard B, Aguerre O, Airiau M, Lachages AM, Boukhnikachvili T, Byk G, et al. Virus-sized self-assembling lamellar complexes between plasmid DNA and cationic micelles promote gene transfer. Proceedings of the National Academy of Sciences of the United States of America 1997 Dec 23;94(26):14412-14417.

24. Dunlap DD, Maggi A, Soria MR, Monaco L. Nanoscopic structure of DNA condensed for gene delivery. Nucleic Acids Res 1997 Aug 1;25(15):3095-3101.

25. Dauty E, Behr JP, Remy JS. Development of plasmid and oligonucleotide nanometric particles. Gene Ther 2002 Jun;9(11):743-748.

26. Arscott PG, Li AZ, Bloomfield VA. Condensation of DNA by trivalent cations. 1. Effects of DNA length and topology on the size and shape of condensed particles. Biopolymers 1990;30(5-6):619-630.

27. Blessing T, Remy JS, Behr JP. Template oligomerization of DNA-Bound cations produces calibrated nanometric particles. J Am Chem Soc 1998 Aug 26;120(33):8519-8520.

28. DeRouchey J, Netz RR, Radler JO. Structural investigations of DNA-polycation complexes. European Physical Journal E 2005 Jan;16(1):17-28.

29. Watson JD, Crick FH. Molecular structure of nucleic acids; a structure for deoxyribose nucleic acid. Nature 1953 Apr 25;171(4356):737-738.

30. Ogris M, Steinlein P, Kursa M, Mechtler K, Kircheis R, Wagner E. The size of DNA/transferrin-PEI complexes is an important factor for gene expression in cultured cells. Gene Ther 1998 Oct;5(10):1425-1433.

31. Schwake G, Youssef S, Kuhr JT, Gude S, David MP, Mendoza E, et al. Predictive modeling of non-viral gene transfer. Biotechnol Bioeng Mar 1;105(4):805-813.

32. Green JJ, Zugates GT, Tedford NC, Huang Y, Griffith LG, Lauffenburger DA, et al. Combinatorial modification of degradable polymers enables transfection of human cells comparable to adenovirus. Adv Mater 2007;19(19):2836-2842.

Chapter 5

Poly(beta-aminoester) Nanoparticle Delivery of p53 has Activity Against Small Cell Lung Cancer *In Vitro* and *In Vivo*

5.1 Introduction

Small cell lung cancer (SCLC) represents 15% of all lung cancer cases and has one of the highest case-fatality rates of all cancers with nearly as many deaths as diagnoses per year. In 2011 over 25,000 deaths were attributable to this disease in the US alone [1]. The median survival of patients diagnosed with SCLC is less than 1 year. This statistic has not changed significantly over the past 3 decades despite over 52 randomized phase 3 clinical trials evaluating numerous cytotoxic chemotherapies [2]. The combination of etoposide and cisplatin has been the standard first-line therapy for SCLC since the 1980s. In 2003 topotecan became the only drug approved for treatment of patients with relapsed SCLC. New therapeutic approaches are needed to improve long-term survival in this disease.

SCLC exhibits certain recurrent genetic alterations most notably inactivation of the tumor suppressor genes, *TP53* and *RB*. *TP53* encodes a transcription factor whose targets regulate cell cycle progression, senescence, DNA repair and apoptosis [3, 4]. *TP53* mutations are the most common genetic alteration in human cancer, occurring in

This chapter was originally published as Kamat CD, Shmueli RB, Connis N, Rudin CM, Green JJ, Hann CL. "Poly(β-amino ester) nanoparticle delivery of TP53 has activity against small cell lung cancer in vitro and in vivo." Mol Cancer Ther. 2013 Apr;12(4):405-15.

over 50% of cases [5, 6]. Wild-type (WT) p53 activity can also be abrogated by endogenous MDM2 or viral proteins; the human papilloma virus E6 protein, SV-40 large T antigen and adenovirus E1B-55kDa proteins can bind and attenuate p53 activity resulting in cellular transformation [7-9]. In transgenic mouse models disruption of*TP53* results in increased susceptibility to tumor development, most notably lymphomas and sarcomas. Restoration of p53 in these models results in potent antitumor activity in a cell-type specific manner; *TP53* re-expression induces apoptosis in autochthonous lymphomas but senescence in sarcoma and hepatocellular carcinoma models [10, 11].

In SCLC, *TP53* alterations are prevalent; among 67 independent SCLC cell lines and 231 primary SCLC tumors *TP53* was mutated in 90% and 74% of cases respectively [12]. Support for the critical role of *TP53* in SCLC pathogenesis also derives from transgenic mouse models, in which Cre-mediated loss of *TP53* and *RB* results in murine SCLC which shares histopathologic features of human SCLC including neural cell adhesion molecule (NCAM; CD56) expression, and elaboration of neuroendocrine (NE) markers such as synaptophysin and chromogranin [13]. In this genetic background, AdenoCre placed under the control of the NE cell-specific calcitonin/calcitonin-gene related peptide (CGRP) promoter, but not a Clara-cell specific promoter, resulted in murine SCLC, implicating pulmonary NE cells as the putative cell of origin for SCLC [14]. *In vitro*, Adachi et al, has demonstrated that expression of WT p53 in a p53-null SCLC cell line results in apoptosis [15]. As loss of *TP53* appears to be critical in SCLC development, restoration of functional p53 may have therapeutic efficacy.

Adenovirus is the one of the most widely studied gene therapy vectors; in non-small cell lung cancer (NSCLC), adenoviral-mediated *TP53* (Ad.p53) delivery has been evaluated in several early-phase clinical trials [16, 17]. Intratumoral (IT) delivery of Ad.p53 in combination with chemotherapy was found to be safe and histological examination of tumor tissue revealed apoptosis in Ad.p53 treated samples [16]. A phase II study, however, failed to show increased response or local benefit of combined Ad.p53 and chemotherapy over chemotherapy alone [17]. Adenoviral gene therapy has also been evaluated preclinically in SCLC models. Adenoviral delivery of a siRNA targeting the hepatocyte growth factor receptor, c-Met, in the H446 SCLC cell line resulted in decreased proliferation *in vitro* and tumor growth inhibition (TGI) *in vivo* [18]. Similarly, adenoviral delivery of fragile histidine triad complex, a putative tumor suppressor gene often mutated in SCLC, induced apoptosis in multiple SCLC cell lines [19].

The use of viral vectors has been limited by safety concerns including insertional mutagenesis and toxicity as well as limited cargo capacity and manufacturing challenges [20, 21]. Many patients have pre-existing humoral immunity to adenovirus, or rapidly develop neutralizing antibodies, limiting the potential of adenoviral therapies. Alternative approaches to gene delivery, using non-viral biomaterials such as inorganic nanoparticles, cationic lipids, liposomes, polymers, and peptides, have been limited by low efficicency, resulting in limited efficacy [22-24].

We have developed highly effective biomaterials for non-viral gene delivery to hard-to-transfect cells [23, 25-28]. These poly(□-amino ester) (PBAE) polymers are biodegradable due to ester linkages throughout the polymer backbone which allows for

lower toxicity and release of DNA intracellularly. Through their secondary and tertiary amines, these polymers are also able to buffer the endosome, which facilitates endosomal escape [29, 30]. Additionally, subtle changes to PBAE structure can improve specificity of transfection and these polymers have been adapted for gene delivery to various cell types including HUVECs, human retinal endothelial cells and human mesenchymal stem cells as well as glioblastoma multiforme, ovarian, prostate and pancreatic cell lines [25, 27, 31-33].

In this study, we sought to develop non-viral nanoparticles which could deliver therapeutic genes with high efficiency to SCLC cells. We synthesized an array of PBAEs using combinatorial chemistry [34] and found several polymers with transfection efficiencies comparable to commercially available agents in SCLC cell lines. These polymers may be generally useful as efficient gene-delivery vectors. As a proof of principle for this approach, we used two PBAE polymers to assess the activity of WT *TP53* delivery to the p53-mutant H446 SCLC cell line *in vitro* and *in vivo*.

5.2 Materials and Methods

5.2.1 Plasmids, Chemicals and Reagents

Unless otherwise stated, all reagents were purchased from Sigma Chemical Company (St. Louis, MO USA) or Fisher Scientific (Pittsburgh, PA USA) in the highest available purity. The CMV-GFP (EGFPN1) and CMV-LUC plasmids were purchased from Elim Biopharm (Palo Alto, CA). p53-CMV-GFP plasmid (Addgene, San Diego,

CA) contained CMV-promoter regulating the fusion of two gene segments: WT p53 and EGFPN1 backbone.

5.2.2 Monomers Reagents

Monomers used for polymer synthesis were the following: from Acros Organics [1-(3-aminopropyl)pyrrolidine (E8)], Alfa Aesar [1,4-butanediol diacrylate (B4), 1-(3-aminopropyl)-4-methylpiperazine (E7)], Fluka [2-(3-aminopropylamino)ethanol (E6), 3-amino-1-propanol (S3), 4-amino-1-butanol (S4), 5-amino-1-pentanol (S5)], Monomer-Polymer and Dajac Laboratories [1,3-propanediol diacrylate (B3), 1,5-pentanediol diacrylate (B5)], Sigma-Aldrich [1,3-butanediol diacrylate (B3m)], and TCI America [1,3-diaminopentane (E3), 2-methyl-1,5-diaminopentane (E4), (PEO)4-bis-amine (E5)] and as previously described [34].

5.2.3 Preparation of Cy5 labeled dsRED DNA

pDsRed-Max-N1 DNA (Promega, Madison, WI) was labeled with Cy5 fluorophore using the Label IT Cy 5 Tracker kit (Mirus, Madison, WI) as per manufacturer's protocol and stored at -20°C in light protective conditions.

5.2.4 Cell lines

All cell lines were obtained from American Type Culture Collection (ATCC) and grown in complete RPMI [RPMI 1640 (Quality Biologicals, Gaithersburg, MD) supplemented with 10% fetal bovine serum, L-glutamine, pen/strep, sodium pyruvate, HEPES, and sodium bicarbonate] per ATCC recommendations.

5.2.5 Synthesis of poly(β-amino esters) (PBAEs)

The PBAEs were synthesized in a two-step reaction procedure (**Figure 5.1**). In the first step, the base polymers were synthesized by mixing diacrylates (B) with amino alcohols (S) at a molar ratio of 1.1:1 or 1.2:1. The reaction was performed in glass scintillating vials with teflon stir bars at 90^{o}C for 24 hours. The base polymer was then dissolved in anhydrous dimethyl sulfoxide (DMSO) to 167 mg/mL. In the second step of the reaction, 480 μL of the base polymer solution is mixed with 320 μL of 0.5 M end-capping amine (E) in 1.5 mL eppendorf tubes and allowed to react in a shaker for 24 hours. Polymers were then divided into smaller volumes and stored at frozen and with desiccant until needed. These polymers were characterized with gel permeation chromatography and proton nuclear magnetic resonance as previously described [34]. Select polymers, including polymers used *in vivo*, were made in larger quantities and further purified. In this case, after the base polymer reaction step, the polymers are dissolved in tetrahydrofuran (THF), instead of DMSO, and then end-capped as above, but with end-capped monomers also diluted in THF. Once the reaction is complete, the polymer is mixed with 4x the volume of ethyl ether. These mixtures were vortexed vigorously and then centrifuged at 4 krpm for 5 minutes, after which the supernatant containing unreacted monomer and organic solvents was removed. This process was then repeated a second time and the purified polymers dried under vacuum for 2 days. The polymers were then dissolved in anhydrous dimethyl sulfoxide and kept frozen with desiccant as described above.

5.2.6 Nanoparticle Preparation

For each transfection, PBAE:DNA nanoparticles were prepared by separately dissolving PBAE polymer and DNA in 25 mM sodium acetate (pH 5.0). The polymer and DNA solutions were mixed in equal volumes, gently pipetted and incubated for 10 min at RT. A range of w/w ratios were evaluated for the high-throughput screen and are described in the *High-throughput screening of PBAE polymer library* section found in the Supplemental Data. For all other experiments, PBAE:DNA ratios of 75 w/w and 30 w/w ratios were for *in vitro* and *in vivo* studies, respectively. Polymer and DNA stocks were stored at -20°C and thawed on ice before mixing and treating the cells. For Cy5-DsRed experiments, 0.1ug of Cy 5 labeled DsRED was included in the DNA mixtures and PBAE:DNA nanoparticles were prepared as described above.

5.2.7 Nanoparticle characterization

Plasmid DNA and PBAEs were separately diluted in 25 mM sodium acetate buffer to 0.06 mg/mL and either 1.8, 3.6, or 4.5 mg/mL, respectively (corresponding to PBAE:DNA weight/weight, wt/wt, ratios of 30, 60, or 90). Equal volumes of the DNA and PBAE solutions were mixed and incubated for 10 minutes at room temperature. The resulting solution of nanoparticles was then used either for sizing or DNA complexation studies. In the case of sizing, the samples were further diluted in PBS and loaded into a Nanosight NS500 nanoparticle tracking analysis (NTA) instrument. The solutions were diluted anywhere from 50x to 200x, so that the nanoparticle concentrations were appropriate for NTA analysis [35]. NTA videos were captured for 60 seconds and analyzed using the NTA software, version 2.1. To further examine the ability of the polymers to bind to the DNA, the nanoparticle solutions were run on a gel using

electrophoresis and compared to naked DNA. A 1% agarose gel with 0.1 μL/mL ethidium bromide was made. The naked DNA solution was mixed with a 30% glycerol loading buffer with bromophenol blue dye, while the nanoparticle solutions were mixed with the loading buffer without the dye to prevent interference between the dye and PBAE-DNA interaction. The gel was run for 30 min at 100V and imaged using the UVP BioDoc-It Imaging Center.

5.2.8 Transfection protocol

Adherent cells: H446 cells were seeded at low density and allowed to adhere overnight. PBAE:DNA nanoparticles were added to cells followed by gentle shaking. After 4 hours, the media was replaced with fresh media and the cells were incubated at 37°C for 44 h.

Suspension cells (H146, H187): Cells were seeded in complete RPMI overnight then incubated with PBAE/DNA nanoparticles for 4 h with gentle shaking. After 4 h, cells were centrifuged at low speed for 2 min, fresh media was added and the cells further incubated at 37°C for next 44 hours.

5.2.9 Fluorescence microscopy

GFP positive cells were analyzed using a Motic AE31 inverted microscope using a FITC 480nm filter. Cy5 labeled cells were visualized and analyzed using a Zeiss Axio Observer microscope fitted with a Cy5 specific filter (emission wavelength of 690nm).

5.2.10 Flow cytometry

GFP fluorescence was used to indicate successful transfection, propidium iodide (PI) was used for dead cell discrimination, and Cy5 fluorescence to indicate successful nanoparticle association using a FACSCalibur flow cytometer (BD Biosciences, Rockville, MD). Briefly, adherent cells were trypsinized, centrifuged and resuspended in 500 μL of fresh media and analyzed by flow cytometry. A total of 10,000 cells were acquired per analysis. All analyses were run with triplicate samples. Data analysis was performed using BD CellQuest Pro software (BD Biosciences).

5.2.11 Western blot

Whole cell extracts were prepared using RIPA buffer containing protease and phosphatase inhibitors and clarified by low-speed centrifugation. The protein extracts were quantitated by BCA assay, resolved by SDS-PAGE on 4-12% Bis-Tris gels and transferred to PVDF membranes. Membranes were blotted with a 1:500 dilution of primary antibodies to p53 (Santa Cruz Biotechnologies), p21 (Calbiochem), anti-GFP (Abcam) and actin (Santa Cruz) and detected using HRP-conjugated secondary antibodies and visualized by ECL per protocol (Pierce).

5.2.12 Cell cycle analysis

Cells were prepared at 48 and 72 hrs post-treatment for cell cycle analysis following a standard PI staining protocol and analyzed by flow cytometry using a FACSCalibur flow cytometer and CellQuest Pro software. Each assay was run in triplicate and all data is presented as the mean +/- SEM.

5.2.13 Annexin V staining

To determine early apoptotic events, cells were assessed for Annexin V positivity. Cells were plated and transfected as described above. At the indicated time after transfection cells were detached from the tissue culture plates using Accutase (Sigma), stained with Annexin V Cy5 (BD Biosciences) per manufacturer's directions and analyzed on a FACSCalibur flow cytometer. Cisplatin (10uM) treated cells were used as a positive control. Each assay was run in triplicate and all data is represented as the mean +/- SEM.

5.2.14 Fluorescence-activated cell sorting (FACS)

Cells were sorted using a using a FACS Aria II (BD Biosciences) into GFP-positive and GFP-negative populations 18 hrs post-transfection. Untreated cells passed through the sorting machine were used as an additional control. Post-sort analysis was completed within 2 hrs of collection, cells were replated in complete RPMI and assessed at 48 and 72hrs post-transfection.

5.2.15 *In vivo* experiments

Three-to-four week old athymic female nude mice were injected subcutaneously with $1.5x10^6$ H446 cells suspended in PBS and mixed 1:1 in matrigel (BD Biosciences). Once tumor volumes reached 200 mm^3, the mice were randomized [N=3-4] into three groups: 1) Untreated, 2) 457:CMV-LUC, 3) 457:CMV-p53-LUC. The PBAE:DNA nanoparticles were prepared at 30 w/w; 50 μg of DNA was used per IT injection and the mice were treated twice a week for 3 weeks. Tumor measurements, using a digital caliper, and weights were collected twice a week. Tumor volume was calculated as follows: tumor volume (mm^3) = [length (mm) x width $(mm)^2$]/2. Toxicity was monitored by

weight loss and animal activity following ACUC protocols. Tumor growth curves are presented as mean +/- SEM. The area under curve (AUC) was calculated using GraphPad Prism estimating total AUC from day 1 to day 18 for respective treatment groups. The percentage inhibition in tumor growth was compared among all the treatment groups over the total time course of the study. Statistical significance was then determined by two-way ANOVA followed by Bonferroni post-hoc test. (* $p \leq 0.001$ CMV-p53-LUC vs. CMV-LUC; $^{\#}$ $p \leq 0.01$ CMV-p53-LUC vs. untreated). All animal experiments were performed following JHU Animal Care and Use Committee regulations.

5.3 Results

We generated a polymer array of 30 structurally distinct PBAEs and over 120 nanoparticle formulations (**Figure 5.1**). This array contained base polymers composed of four backbone monomers that differed by single carbons between the acrylate groups (B3, B3m, B4, and B5 corresponded to 3 carbons, 3 carbons + 1 methyl group, 4 carbons, and 5 carbons respectively) and three side chain monomers (S3, S4, and S5 that differed by having 3, 4, and 5 carbons respectively between amine and alcohol groups). These base polymers were terminated with one of six amine-containing small molecule end-groups. Structures were validated by GPC and NMR [34]. We performed a high-throughput luciferase-based screen of the PBAE array to identify leading polymers optimized for efficient transfection of SCLC cells. Gene delivery of exogenous luciferase plasmid resulted in luminescence that was quantified and normalized to untreated cells (**Figure 5.S1**). The leading candidate polymers, such as 456 (**Figure 5.1**), were able to transfect

H446 cells several orders of magnitude better than other nanoparticle formulations, and resulted in transfection efficiencies as high or higher than both positive controls, FuGENE HD and Lipofectamine 2000. The size of the leading PBAE/DNA nanoparticles was examined using nanoparticle tracking analysis [35] and quantified by nanoparticle number-average size (**Figure 5.2A**). DNA encapsulation and binding by the leading polymers was determined by gel electrophoresis, demonstrating that at the optimized PBAE:DNA weight:weight ratios used in our study, the DNA is completely complexed by the polymers (**Figure 5.2B**). In general, the nanoparticle diameters range from 100-200 nm, with the range for the leading polymers, a more narrow 100-150 nm. It has been previously reported that within this range, the size of the particle does not correlate strongly with transfection efficacy [29].

The extensive luciferase-based screen identified PBAEs that could induce high levels of expression, but to identify those PBAEs which could transfect the highest percentage of cells, we used a GFP-based analysis. We selected 32 of the top candidates from the initial screen and quantitated the transfection efficiency by fluorescence microscopy and flow cytometry (**Figure 5.3A-B**). Two of the top polymers, 456 and 457, exhibited transfection efficiencies of approximately 40%, comparable to the commercially available transfection agent, Fugene-HD (**Figure 5.3C**, grey bars). The majority of the polymers also induced higher level GFP expression, quantitated by geometric mean fluorescence, compared with Fugene HD (**Figure 5.3C**, black bars). We adapted our transfection protocol for suspension cells and found that 456 polymers could transfect H146 and H187 SCLC cell lines with effieciencies of 33 ±3% and 22±2%, respectively (**Figure 5.3D-F**). As suspension cells are notoriously difficult to transfect,

we found these results encouraging. We further assessed the ability of 456 polymers to transfect non-transformed cell lines. The transfection efficiency of our nanopartcles in the WI-38 and IMR-90 human lung fibroblast lines was 13% and 11%, respectively; therefore, the 456 polymers appeared to be fairly selective for SCLC over non-transformed cells (**Figure 5.S2**). To determine whether the transfection efficiency was limited by poor nanoparticle association and uptake by SCLC cells, we transfected H446 cells with PBAEs complexed with a Cy5-labeled plasmid. We observed that >95% of cells were Cy5-positive (**Figure 5.S3**) suggesting that events downstream of nanoparticle uptake such as intracellular trafficking, endosomal release or nuclear uptake and processing may be additional determinants of PBAE transfection.

We next evaluated the ability of the 456 polymer to deliver functional p53. Transfection of H446 cells with 456:CMV-p53-GFP, but not 456:CMV-GFP, induced morphologic changes and punctate GFP localization (**Figure 5.4A**). At 48 hrs post-transfection, 22% of cells transfected with 456:CMV-p53-GFP were strongly GFP-positive, compared to 41% of those transfected with 456:CMV-GFP (**Figure 5.4B-C**). p53-GFP expression was seen as early as 2 hrs and peaked at 18-24 hrs post-transfection (**Figure 5.4D**). Consistent with functional p53 activity, we observed p21 induction at 18-24 hrs, a significant increase of Annexin V positive cells at 48 hrs and cellular accumulation in sub-G1 at 72 hrs post-transfection with 456:CMV-p53-GFP (**Figure 5.4D-F**). To ascertain the effect of WT p53 restoration in more homogeneous populations, we sorted H446 cells transfected with either 456:CMV-GFP or 456:CMV-p53-GFP into GFP-positive and GFP-negative populations (**Figure 5.5A**). Post-sort (20 hrs post-transfection) flow cytometry confirmed that the sorted cells were relatively homogeneous

(>80%) and GFP expression was maintained over 72 hrs (**Figure 5.5B**). At 48 and 72 hrs, we observed robust p53-GFP expression and p21 induction in GFP-positive cells transfected with 456:CMV-p53-GFP (population 4), but in none of the other sorted populations (**Figure 5.5C**). Cell cycle analysis also revealed > 40% of the population 4 cells had accumulated in sub-G1 at 48 and 72 hrs, consistent with functional p53 activity (**Figure 5.5D-E**).

Successful nanoparticle delivery of WT p53 would be expected to result in cell cycle arrest, induction of apoptosis and inhibition of tumor progression *in vivo*. To determine whether PBAE-mediated p53 delivery had antitumor activity *in vivo*, we administered nanoparticles carrying CMV-p53-LUC intratumorally (IT) into subcutaneous H446 xenografts. For this proof of principal analysis, we selected another leading PBAE polymer from our *in vitro* studies, 457, as this polymer appeared to better target subcutaneous tumors in pilot *in vivo* experiments (data not shown). Nude mice bearing H446 xenografts received twice weekly IT injections of 457:CMV-p53-LUC, 457:CMV-LUC, or neither nanoparticle formulation, and the tumors were serially measured (**Figure 5.6**). We observed > 50% tumor growth inhibition with IT injection of 457:CMV-p53-LUC relative to either 457:CMV-LUC or no treatment control ($p \leq 0.01$ for comparison to either control). Thus, when effectively delivered to tumors, PBAE-mediated nanoparticle delivery and exogenous expression of WT p53 can inhibit tumor growth of human SCLC xenografts.

5.4 Discussion

Here we report on a non-viral, biodegradable PBAE nanoparticle that self-assembles with DNA and can deliver WT *TP53* to SCLC cells. Using a luciferase-based high throughput screening approach, we were able to identify PBAE polymers that could transfect SCLC lines at efficiencies comparable to commercially available transfection reagents. We showed that the 456 polymer could deliver functional p53 to SCLC cell lines resulting in p21 expression, induction of apoptosis and accumulation in sub-G1. Finally, we demonstrated that IT delivery of 457:CMV-p53-LUC significantly suppressed tumor growth while injection of the polymer with CMV-LUC had no effect. Thus, when effectively delivered, exogenously expressed WT p53 suppresses tumor growth of H446 xenografts.

Loss of p53 tumor-suppressor activity is a critical event in cancer development across multiple tumor types. In transgenic SCLC models, *TP53* loss is required for tumor development [13, 36]. Re-expression of WT p53 has potent efficacy in established p53-null lymphomas, sarcomas and hepatocellular carcinomas [10, 11, 37]. Nanoparticle delivery of *TP53* using (D,L-lactide-co-glycolide) (PLGA) polymers caused growth inhibition in p53-null PC-3 prostate cancer xenografts [38].

In addition to p53 deletion or inactivation, some p53 mutations result in dominant negative (DN) or gain-of-function activities. The ability of WT p53 to overcome a gain-of-function p53 mutation is unclear. In spontaneous p53-mutant lymphoma and sarcoma models, WT p53 restoration resulted in tumor growth arrest but not tumor regression [39]. In these experiments, p53 was restored to endogenous levels, and the authors suggested that the ability of p53 to overcome a DN p53 mutant may be dose-dependent. As an

alternative approach, small molecules that can restore mutant p53 to its WT conformation have been explored. One such molecule, PRIMA-1 (p53-dependent reactivation of massive apoptosis), is able to restore the transcriptional activity of mutant p53 and has efficacy in several preclinical cancers models including SCLC [40]. A primary limitation is the requirement for mutant p53; PRIMA-1 would not be effective in tumors harboring a null mutant or that are driven by overexpression of p53 binding proteins such as MDM2. The H446 SCLC cell line harbors a G154V alteration in the DNA binding domain of *TP53* and expresses high basal levels of the mutant protein. We demonstrated that CMV-driven expression of p53 was effective in this p53-mutant cell line; our cell sorting experiments show that H446 cells that expressed high-level exogenous WT p53 had robust p21 induction and accumulated in sub-G1.

This study demonstrates that PBAE-mediated gene transfection is feasible both *in vitro* and, importantly, in tumor-bearing animals. Further, this work shows that this approach can be used to restore activity of a silenced or absent tumor suppressor, resulting in specific inhibition of tumor growth. This same approach could be used to restore multiple silenced genes or to deliver other therapeutic agents. These polymers are amenable to a variety of modifications that may improve their efficiency in targeted delivery of an anti-cancer payload.

A better understanding of the limitations on DNA delivery is required to improve the utility of this non-viral gene transfer system. While nearly 100% of the cells take up the particles, about 40% of the cells successfully expressed the target protein in our initial experiments. This indicates that events downstream may be limiting transfection

efficiency PBAEs are able to successfully escape endosomes [41], thus cytosolic transport and nuclear import are possible barriers and are the subject of active investigation[23]. Delivery of therapeutic agents that are not reliant on 100% transfection, that can induce a bystander effect, may be well-suited for this system. For example, nanoparticle delivery of the tumor necrosis factor-related apoptosis-inducing ligand (TRAIL) induces apoptosis and tumor regression in the A549 NSCLC cell line [42]. TRAIL-induced death, however, is reliant on host factors, including the presence of TRAIL receptors, DR4 or DR5, and caspase 8. Agents such as mitomycin C, doxorubicin, etoposide and epigenetic modulators are able to sensitize cells to TRAIL by upregulating of DR4/5 or caspase 8 [43-45]. Another approach, gene-directed enzyme prodrug therapy (GDEPT), is based on cell-specific delivery of an enzyme which can covert a systemically administered prodrug into a toxin. While the direct effects are cell-specific, this system could be adapted to induce a bystander effect by selecting a drug whose metabolite can traverse gap junctions.

Our *in vivo* data demonstrate that if effectively delivered to tumors, PBAE nanoparticles can successfully transfect SCLC xenografts and inhibit tumor growth. Our work is further supported by Huang et al. demonstrating that PBAE nanoparticles can deliver diptheria toxin and induce tumor regression when delivered locally in an ovarian cancer xenograft model [46]. Systemic delivery and *in vivo* stability are major challenges in the clinical development of these nanoparticles. PBAE particles are readily amenable to approaches to add electrostatic coatings to improve these properties [42, 47, 48]. In SCLC, cell-surface expression of CD56 is nearly universal and can be targeted effectively by antibodies. A mantaysinoid-conjugated anti-CD56 antibody is being

evaluated clinically in SCLC and other tumors [49, 50]. Coatings which incorporate NCAM-binding moieties may enhance SCLC specificity and improve *in vivo* stability of PBAE particles.

Therapeutic gene delivery has held great promise for decades but has been limited by the lack of stable, safe delivery vehicles. Here we report the first demonstration to our knowledge of effective non-viral polymeric delivery of therapeutic genes in SCLC *in vivo*. The ability to deliver high level gene expression utilizing a non-toxic biodegradable nanoparticle has multiple advantages over viral-based delivery systems, including flexibility in cargo capacity, ability to deliver mixed nucleic acids targets, lack of insertional mutagenesis and minimal immunogenicity. PBAEs fulfill all of these criteria and, with optimization of DNA delivery and systemic stability, may ultimately provide a powerful platform for therapeutic restoration of gene expression.

5.5 Acknowledgments

The authors would like to thank Gary L. Gallia, MD, PhD, Timothy Burns, MD, PhD and John Poirier, PhD for scientific discussions and manuscript review. This research was supported by Barbara's Fund at the Community Foundation for the National Capital Region (CLH), the Cigarette Restitution Fund (CLH), and NIH (R21CA152473) (JJG).

5.6 Figures

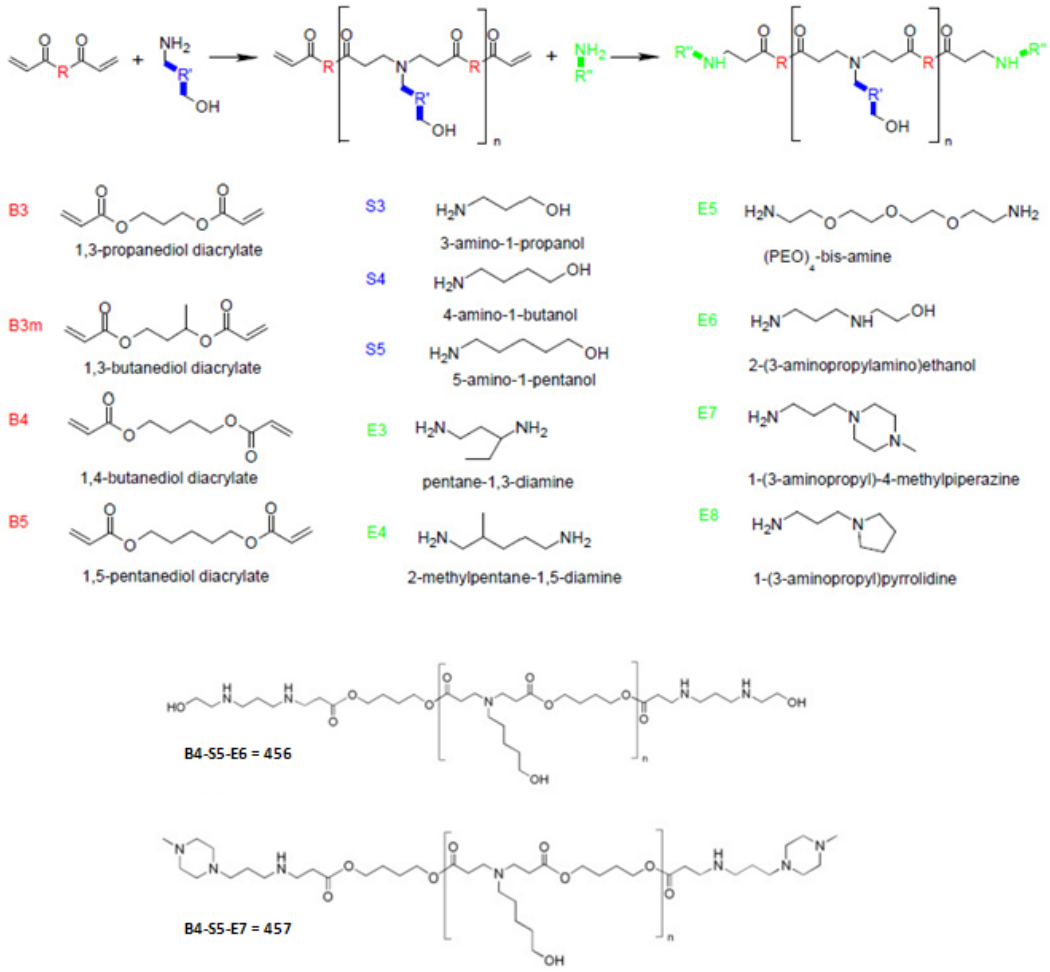

Figure 5.1. Poly(β-amino ester) synthesis scheme depicting the conjugate addition of amines to diacrylates in two steps. The three R groups allow modifications to the polymer backbone (R), side chain (R') and end-groups (R''). Each monomer comprises a backbone (B), a side chain (S) or an end-group (E).

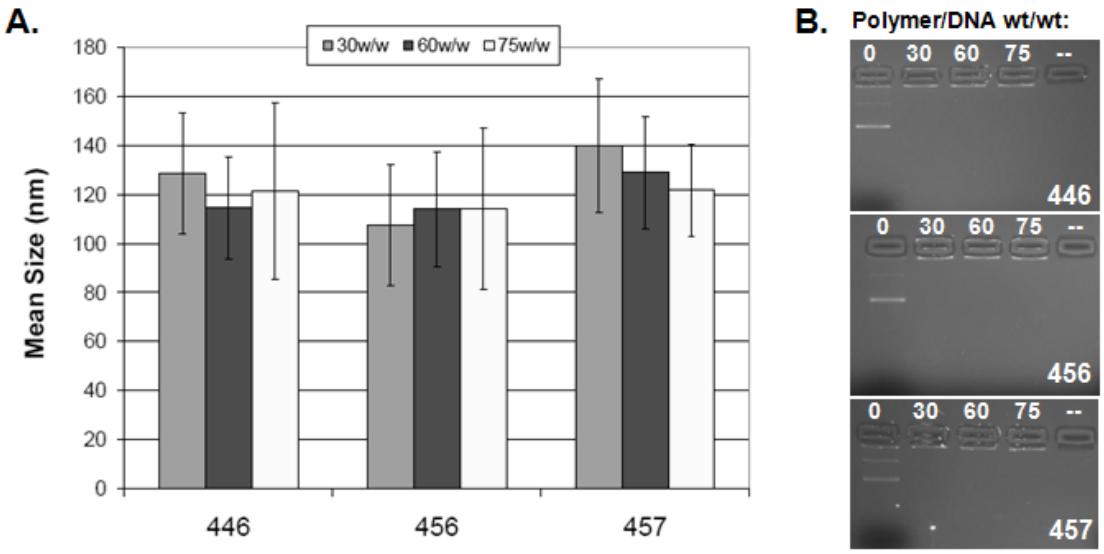

Figure 5.2. Nanoparticle characterization. The ability of the PBAEs to form nanoparticles was examined using NTA to determine the nanoparticle size. **(A)** and by gel electrophoresis. **(B)** Gel electrophoresis of the nanoparticles shows that at the proper PBAE:DNA weight:weight ratios, the DNA is completely complexed by the polymers. In general, the nanoparticle diameters range from 100 nm to 200 nm, with the range for the select polymers shown from 100 – 150 nm.

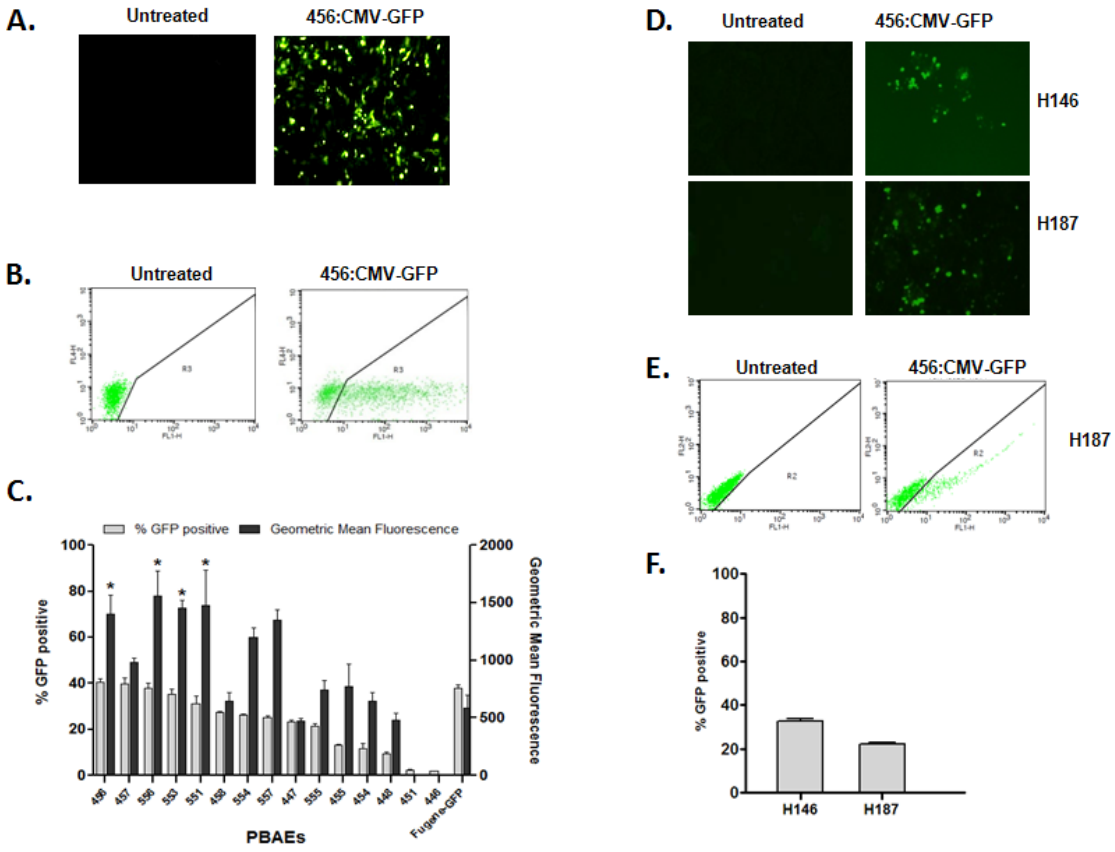

Figure 5.3. A GFP-based secondary screen identifies several PBAE polymers that can deliver genes to adherent and suspension SCLC cell lines at efficiencies comparable to commercially available reagents. **(A-B)** H446 cells were transfected with PBAEs complexed with CMV-GFP DNA then analyzed by microscopy and flow cytometry. **(C)** The transfection efficiency and geometric mean fluorescence of 15 PBAE polymers are shown; the PBAE polymers are indicated across the x-axis. Percent transfection is presented as the mean +/- SEM of triplicate runs and the geometric mean fluorescence is the geometric mean FL1 signal +/- SEM of triplicate runs. Fugene HD was used as a control. Statistical significance of geometric mean fluorescence was determined by one-way ANOVA comparing each group with Fugene-HD (*: $p \leq 0.01$). **(D-F)** Two SCLC suspension cell lines, H146 and H187 cells were transfected with 456:CMV-GFP and analyzed by fluorescence microscopy and flow cytometry.

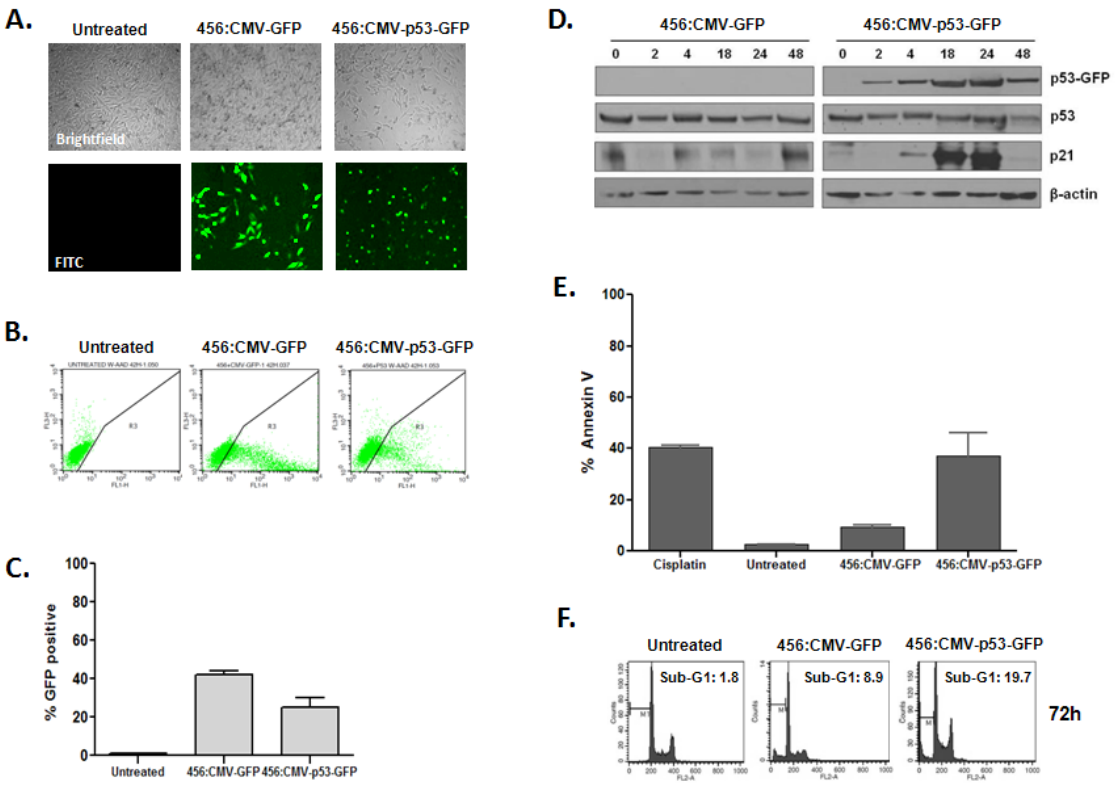

Figure 5.4. Delivery of p53-GFP by 456 polymers induces morphologic changes, p21 expression, apoptosis and sub-G1 accumulation in bulk transfected cells. **(A-B)** H446 cells were transfected with 456 polymers complexed with either CMV-GFP plasmid or a CMV-p53-GFP and visualized by microscopy **(A)** and flow cytometry **(B)**. **(C)** Percent transfection is presented as the mean +/- SEM of triplicate runs. **(D)** Cells were harvested at serial time points after transfection; lysates were examined for p53-GFP, p53 and p21 expression using anti-p53, anti-p21, anti-GFP (to visualize p53-GFP) antibodies. Actin was used as a loading control. **(E)** Annexin V staining was performed at 48 hours after transfection, cisplatin treated cells were used as a positive control for the assay. **(F)** Cell cycle analysis at 72 hours post-transfection.

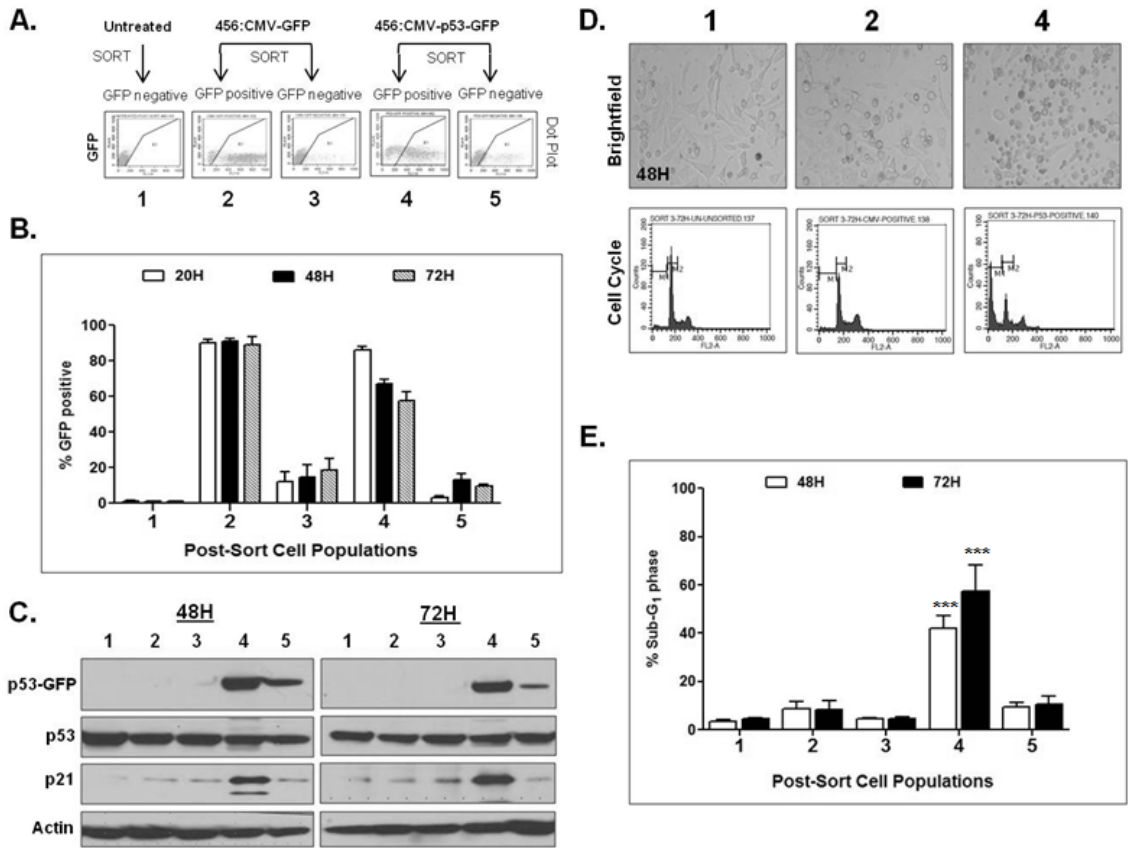

Figure 5.5. Cells sorted for p53-GFP expression exhibit marked morphologic changes, p21 induction and accumulation in sub-G1 consistent with functional p53 activity. **(A)** H446 cells were transfected with 456 polymers complexed with either CMV-GFP or CMV-p53-GFP and sorted for GFP positive and negative populations (populations 2-5) and plated in fresh media. Untreated, sorted cells were used as a control for changes due to the sorting procedure (population 1). **(B)** GFP expression was quantitated by flow cytometry immediately post-sort (20H), 48 and 72 hours post-transfection. **(C)** Western analysis confirmed p53-GFP expression and p21 induction primarily in the p53-GFP positive (4) population. **(D-E)** Morphologic changes were observed by brightfield microscopy and cell cycle analysis demonstrated accumulation of cells in sub-G1. Statistical significance was determined by one-way ANOVA comparing all groups at 48 and 72 hours (***: $p \leq 0.0001$ population 4 vs. 2 or 1)

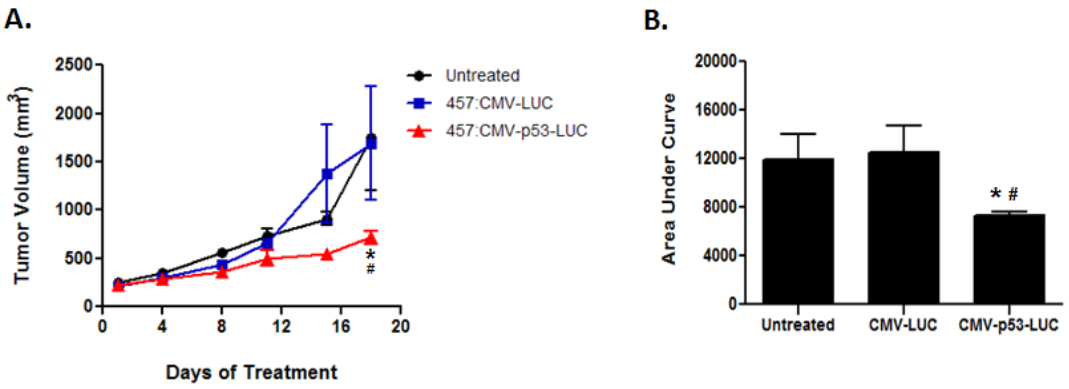

Figure 5.6. Intratumoral delivery of 457:CMV-p53-LUC causes tumor growth inhibition. Nude mice bearing H446 xenografts received twice weekly IT injections of 457:CMV-LUC nanoparticles (n=3), 457:CMV-p53-LUC nanoparticles (n=4), or neither agent (n=3). Tumors were measured twice weekly. Group means and SEM were calculated and are shown. **(A)** IT injection of 457:CMV-p53-LUC resulted in statistically significant tumor growth inhibition compared with controls. **(B)** Area under the tumor growth curve by day 18. Statistical significance was determined by two-way ANOVA at day 18 (**: $p \leq 0.001$ CMV-p53-LUC vs. CMV-LUC; $^{\#}$: $p \leq 0.01$ CMV-p53-LUC vs. untreated).

5.7 Supplementary Methods

5.7.1 Cell lines

All cell lines were obtained from American Type Culture Collection (ATCC). IMR-90 and WI38 cell lines were grown in complete EMEM supplemented with 10% fetal bovine serum, L-glutamine, pen/strep, sodium pyruvate, HEPES, and sodium bicarbonate.

5.7.2 High-throughput screening of PBAE polymer library

H446 cells were seeded at 15,000 cells/well in 96-well plates in 100 μL of complete RPMI one day prior to transfection. The nanoparticles were made as discussed in the *nanoparticle preparation* section, with luciferase (CMV-Luc) plasmid DNA at 30, 60, 75, 100, 125, or 150 w/w of PBAE. Twenty μL of the nanoparticle solution was then added per well to the complete RPMI. Untreated wells served as negative controls, while Lipofectamine 2000 and FuGene HD, leading commercially available non-viral reagents, were used as positive controls as per the manufacturer's instructions. After 4 hours, the transfection solution was removed and fresh media was added to the cells. Transfection efficacy was analyzed 2 days after transfection by measuring the luminescence using the BrightGlo luciferase assay as we have previously described using a BioTek Synergy 2 plate reader. Luminescence was averaged within groups of quadruplicates and normalized by the untreated group.

5.7.3 Transfection protocol

Adherent (DMS-114, WI-38, IMR-9) and suspension cells (H69, H82, H345, H1930) were transfected following the protocol described in the Material and Methods.

5.7.4 Fluorescence microscopy

GFP positive cells were analyzed using a Motic AE31 inverted microscope using a FITC 480nm filter. Cy5 labeled cells were visualized and analyzed using a Zeiss Axio Observer microscope fitted with a Cy5 specific filter (emission wavelength of 690nm).

5.7.5 Flow cytometry

GFP fluorescence was used to indicate successful transfection, propidium iodide (PI) was used for dead cell discrimination, and Cy5 fluorescence to indicate successful nanoparticle association using a FACSCalibur flow cytometer (BD Biosciences, Rockville, MD). Briefly, adherent cells were trypsinized, centrifuged and resuspended in 500 μL of fresh media and analyzed by flow cytometry. A total of 10,000 cells were acquired per analysis. All analyses were run with triplicate samples. Data analysis was performed using BD CellQuest Pro software (BD Biosciences).

5.8 Supplementary Figures

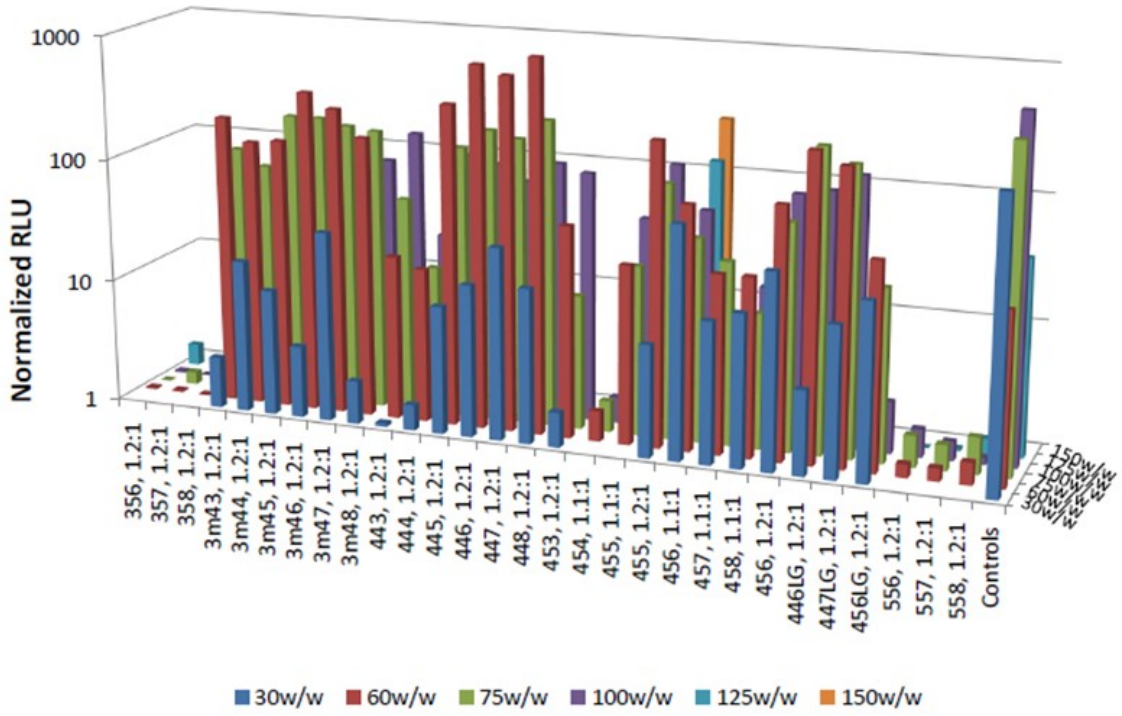

Figure 5.S1. High-throughput screen of a library of PBAE polymers. H446 cells were plated in 96-well plates and incubated with the indicated PBAE complexed with CMV-LUC plasmids at multiple w/w combinations. The control samples are Lipofectamine 2000, FuGene HD 3:1, FuGene HD 4:1, FuGene HD 5:1, and FuGene HD 6:1 formulations, respectively from front to back. Luminescence was measured with a multi-well plate reader and normalized to untreated cell. N = 4 wells per condition.

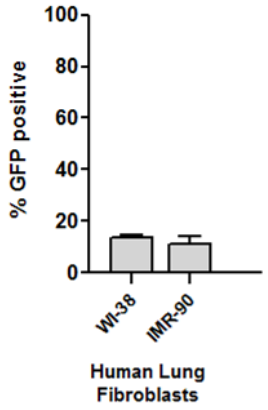

Figure 5.S2. The transfection efficiency of 456 polymers in two non-transformed human lung fibroblast cell lines. WI-38 and IMR-90 cell lines were transfected with 456 polymers complexed with CMV-GFP DNA and then analyzed by flow cytometry. Percent transfection (% GFP positive) is presented as the mean +/- SEM of triplicate runs.

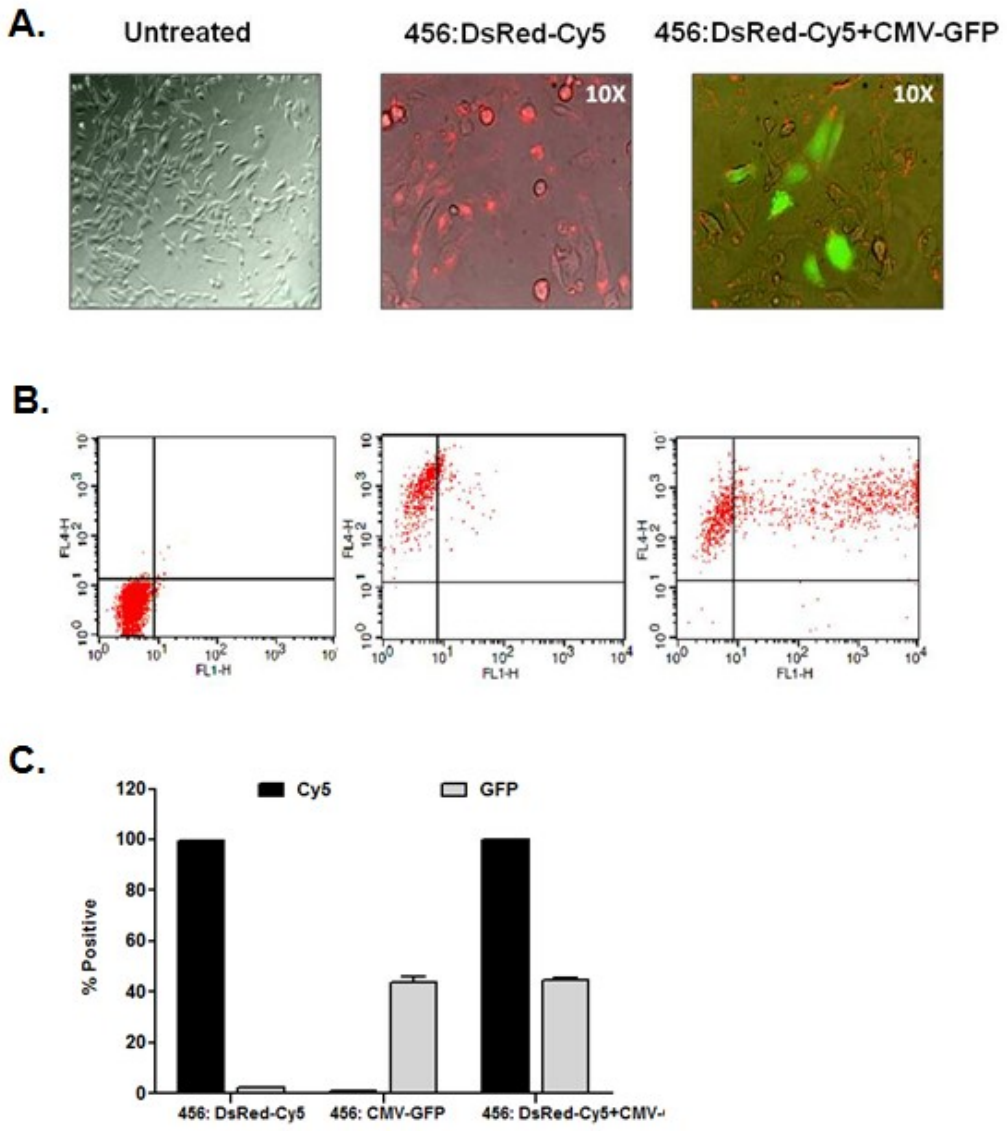

Figure 5.S3. The transfection efficiency of 456 polymers is limited by events downstream of binding and uptake. To address whether binding and uptake limit the transfection efficiency of 456 polymers, we transfected cells with Cy5-labeled DsRed DNA which allowed for visualization of cellular binding and uptake by flow cytometry without the requirement for downstream processing or protein expression. H446 cells were transfected with either 456:Cy5-DsRed or 456 polymers co-complexed with Cy5-DsRed and CMV-GFP plasmids and evaluated by microscopy and flow cytometry **(A-B)**. We observed that >99% cells transfected with 456:Cy5-DsRed were Cy5 positive while only 39% of cells transfected with 456:Cy5-DsRED + CMV-GFP were GFP positive **(C)**. Analyses using Cy5-labeled DsRed with suspension cells, H146 and H187, also showed similar results (data not shown).

5.9 References

1. Siegel R, Naishadham D, Jemal A. Cancer statistics. CA Cancer J Clin 2012 Jan-Feb;62(1):10-29.

2. Oze I, Hotta K, Kiura K, Ochi N, Takigawa N, Fujiwara Y, et al. Twenty-seven years of phase III trials for patients with extensive disease small-cell lung cancer: disappointing results. PloS one 2009;4(11):e7835.

3. Vogelstein B, Lane D, Levine AJ. Surfing the p53 network. Nature 2000 Nov 16;408(6810):307-310.

4. Junttila MR, Evan GI. p53--a Jack of all trades but master of none. Nat Rev Cancer 2009 Nov;9(11):821-829.

5. Hollstein M, Rice K, Greenblatt MS, Soussi T, Fuchs R, Sorlie T, et al. Database of p53 gene somatic mutations in human tumors and cell lines. Nucleic acids research 1994 Sep;22(17):3551-3555.

6. Olivier M, Eeles R, Hollstein M, Khan MA, Harris CC, Hainaut P. The IARC TP53 database: new online mutation analysis and recommendations to users. Human mutation 2002 Jun;19(6):607-614.

7. Li M, Brooks CL, Wu-Baer F, Chen D, Baer R, Gu W. Mono- versus polyubiquitination: differential control of p53 fate by Mdm2. Science 2003 Dec 12;302(5652):1972-1975.

8. Scheffner M, Werness BA, Huibregtse JM, Levine AJ, Howley PM. The E6 oncoprotein encoded by human papillomavirus types 16 and 18 promotes the degradation of p53. Cell 1990 Dec 21;63(6):1129-1136.

9. Yew PR, Liu X, Berk AJ. Adenovirus E1B oncoprotein tethers a transcriptional repression domain to p53. Genes Dev 1994 Jan;8(2):190-202.

10. Ventura A, Kirsch DG, McLaughlin ME, Tuveson DA, Grimm J, Lintault L, et al. Restoration of p53 function leads to tumour regression in vivo. Nature 2007 Feb 8;445(7128):661-665.

11. Xue W, Zender L, Miething C, Dickins RA, Hernando E, Krizhanovsky V, et al. Senescence and tumour clearance is triggered by p53 restoration in murine liver carcinomas. Nature 2007 Feb 8;445(7128):656-660.

12. COSMIC. Wellcome Trust Sanger Institute Cancer Genome Project web site.

13. Meuwissen R, Linn SC, Linnoila RI, Zevenhoven J, Mooi WJ, Berns A. Induction of small cell lung cancer by somatic inactivation of both Trp53 and Rb1 in a conditional mouse model. Cancer Cell 2003 Sep;4(3):181-189.

14. Sutherland KD, Proost N, Brouns I, Adriaensen D, Song JY, Berns A. Cell of origin of small cell lung cancer: inactivation of Trp53 and Rb1 in distinct cell types of adult mouse lung. Cancer Cell 2011 Jun 14;19(6):754-764.

15. Adachi J, Ookawa K, Shiseki M, Okazaki T, Tsuchida S, Morishita K, et al. Induction of apoptosis but not G1 arrest by expression of the wild-type p53 gene in small cell lung carcinoma. Cell Growth Differ 1996 Jul;7(7):879-886.

16. Nemunaitis J, Swisher SG, Timmons T, Connors D, Mack M, Doerksen L, et al. Adenovirus-mediated p53 gene transfer in sequence with cisplatin to tumors of patients with non-small-cell lung cancer. J Clin Oncol 2000 Feb;18(3):609-622.

17. Schuler M, Herrmann R, De Greve JL, Stewart AK, Gatzemeier U, Stewart DJ, et al. Adenovirus-mediated wild-type p53 gene transfer in patients receiving chemotherapy for advanced non-small-cell lung cancer: results of a multicenter phase II study. J Clin Oncol 2001 Mar 15;19(6):1750-1758.

18. Wang ZX, Lu BB, Yang JS, Wang KM, De W. Adenovirus-mediated siRNA targeting c-Met inhibits proliferation and invasion of small-cell lung cancer (SCLC) cells. The Journal of surgical research 2011 Nov;171(1):127-135.

19. Zandi R, Xu K, Poulsen HS, Roth JA, Ji L. The effect of adenovirus-mediated gene expression of FHIT in small cell lung cancer cells. Cancer Invest 2011 Dec;29(10):683-691.

20. Check E. Gene therapy put on hold as third child develops cancer. Nature 2005 FEB 10;433(7026):561-561.

21. Kay MA, Glorioso JC, Naldini L. Viral vectors for gene therapy: the art of turning infectious agents into vehicles of therapeutics. Nat Med 2001 Jan;7(1):33-40.

22. Putnam D. Polymers for gene delivery across length scales. Nature materials 2006 Jun;5(6):439-451.

23. Sunshine JC, Bishop CJ, Green JJ. Advances in polymeric and inorganic vectors for nonviral nucleic acid delivery. Therapeutic delivery 2011 Apr;2(4):493-521.

24. Partridge KA, Oreffo ROC. Gene delivery in bone tissue engineering: Progress and prospects using viral and nonviral strategies. Tissue engineering 2004 JAN-FEB;10(1-2):295-307.

25. Shmueli RB, Sunshine JC, Xu Z, Duh EJ, Green JJ. Gene delivery nanoparticles specific for human microvasculature and macrovasculature. Nanomedicine 2012 Feb 1.

26. Bhise NS, Gray RS, Sunshine JC, Htet S, Ewald AJ, Green JJ. The relationship between terminal functionalization and molecular weight of a gene delivery polymer and transfection efficacy in mammary epithelial 2-D cultures and 3-D organotypic cultures. Biomaterials 2010 Nov;31(31):8088-8096.

27. Tzeng SY, Hung BP, Grayson WL, Green JJ. Cystamine-terminated poly(beta-amino ester)s for siRNA delivery to human mesenchymal stem cells and enhancement of osteogenic differentiation. Biomaterials 2012 Nov;33(32):8142-8151.

28. Green JJ. 2011 Rita Schaffer lecture: nanoparticles for intracellular nucleic acid delivery. Annals of biomedical engineering 2012 Jul;40(7):1408-1418.

29. Green JJ, Langer R, Anderson DG. A combinatorial polymer library approach yields insight into nonviral gene delivery. Accounts of chemical research 2008 May 29;41(6):749-759.

30. Sonawane ND, Szoka FC, Jr., Verkman AS. Chloride accumulation and swelling in endosomes enhances DNA transfer by polyamine-DNA polyplexes. J Biol Chem 2003 Nov 7;278(45):44826-44831.

31. Sunshine J, Green JJ, Mahon K, Yang F, Eltoukhy A, Nguyen DN, et al. Small molecule end group of linear polymer determine cell-type gene delivery efficacy. Advanced Materials 2009;21(48):4947-4951.

32. Tzeng SY, Guerrero-Cazares H, Martinez EE, Sunshine JC, Quinones-Hinojosa A, Green JJ. Non-viral gene delivery nanoparticles based on Poly(beta-amino esters) for treatment of glioblastoma. Biomaterials 2011 Aug;32(23):5402-5410.

33. Showalter SL, Huang YH, Witkiewicz A, Costantino CL, Yeo CJ, Green JJ, et al. Nanoparticulate delivery of diphtheria toxin DNA effectively kills Mesothelin expressing pancreatic cancer cells. Cancer Biol Ther 2008 Oct;7(10):1584-1590.

34. Sunshine JC, Akanda MI, Li D, Kozielski KL, Green JJ. Effects of Base Polymer Hydrophobicity and End-Group Modification on Polymeric Gene Delivery. Biomacromolecules 2011 Sep 9.

35. Bhise NS, Shmueli RB, Gonzalez J, Green JJ. A novel assay for quantifying the number of plasmids encapsulated by polymer nanoparticles. Small 2012 Feb 6;8(3):367-373.

36. Schaffer BE, Park KS, Yiu G, Conklin JF, Lin C, Burkhart DL, et al. Loss of p130 accelerates tumor development in a mouse model for human small-cell lung carcinoma. Cancer Res 2010 May 15;70(10):3877-3883.

37. Martins CP, Brown-Swigart L, Evan GI. Modeling the therapeutic efficacy of p53 restoration in tumors. Cell 2006 Dec 29;127(7):1323-1334.

38. Sharma B, Ma W, Adjei IM, Panyam J, Dimitrijevic S, Labhasetwar V. Nanoparticle-mediated p53 gene therapy for tumor inhibition. Drug delivery and translational research 2011 Feb;1(1):43-52.

39. Wang Y, Suh YA, Fuller MY, Jackson JG, Xiong S, Terzian T, et al. Restoring expression of wild-type p53 suppresses tumor growth but does not cause tumor regression in mice with a p53 missense mutation. J Clin Invest 2011 Mar;121(3):893-904.

40. Zandi R, Selivanova G, Christensen CL, Gerds TA, Willumsen BM, Poulsen HS. PRIMA-1Met/APR-246 induces apoptosis and tumor growth delay in small cell lung cancer expressing mutant p53. Clin Cancer Res 2011 May 1;17(9):2830-2841.

41. Akinc A, Langer R. Measuring the pH environment of DNA delivered using nonviral vectors: implications for lysosomal trafficking. Biotechnology and bioengineering 2002 Jun 5;78(5):503-508.

42. Zhou J, Liu J, Cheng CJ, Patel TR, Weller CE, Piepmeier JM, et al. Biodegradable poly(amine-co-ester) terpolymers for targeted gene delivery. Nature materials 2012 Jan;11(1):82-90.

43. Cheng H, Hong B, Zhou L, Allen JE, Tai G, Humphreys R, et al. Mitomycin C potentiates TRAIL-induced apoptosis through p53-independent upregulation of death receptors: Evidence for the role of c-Jun N-terminal kinase activation. Cell Cycle 2012 Sep 1;11(17).

44. Vaculova A, Kaminskyy V, Jalalvand E, Surova O, Zhivotovsky B. Doxorubicin and etoposide sensitize small cell lung carcinoma cells expressing caspase-8 to TRAIL. Mol Cancer 2011;9:87.

45. Kaminskyy VO, Surova OV, Vaculova A, Zhivotovsky B. Combined inhibition of DNA methyltransferase and histone deacetylase restores caspase-8 expression and sensitizes SCLC cells to TRAIL. Carcinogenesis 2011 Oct;32(10):1450-1458.

46. Huang YH, Zugates GT, Peng W, Holtz D, Dunton C, Green JJ, et al. Nanoparticle-delivered suicide gene therapy effectively reduces ovarian tumor burden in mice. Cancer Res 2009 Aug 1;69(15):6184-6191.

47. Harris TJ, Green JJ, Fung PW, Langer R, Anderson DG, Bhatia SN. Tissue-specific gene delivery via nanoparticle coating. Biomaterials 2010 Feb;31(5):998-1006.

48. Shmueli RB, Anderson DG, Green JJ. Electrostatic surface modifications to improve gene delivery. Expert Opin Drug Deliv 2010 2010;7(4):535-550.

49. Aletsee-Ufrecht MC, Langley K, Rotsch M, Havemann K, Gratzl M. NCAM: a surface marker for human small cell lung cancer cells. FEBS letters 1990 Jul 16;267(2):295-300.

50. Fossella F, Woll P, Lorigan P, Tolcher A, O'Brien M, O'Keefe J. Clinical Experience of Imgn901 (Bb-10901) in patients with small cell lung carcinoma (SCLC). 13th World Conference on Lung Cancer; 2009; San Francisco; 2009.

Chapter 6

Gene Delivery Nanoparticles Specific for Human Microvasculature and Macrovasculature

6.1 Introduction

Endothelial cells play important roles in various ocular diseases, such as age-related macular degeneration, diabetic retinopathy, and retinoblastoma [1]. The dysregulation and subsequent angiogenic proliferation of these ocular microvascular endothelial cells represents the key step in most retinal causes of blindness. Regulation of this angiogenesis by anti-angiogenic drugs such as ranibizumab is now the first-line therapy and there is continued interest in more effective anti-angiogenic therapies [2]. Gene delivery is one such alternative method for delivery of anti-angiogenic factors to endothelial cells, such as endostatin, angiostatin, and vascular endothelial growth factor-binding protein [3, 4]. In addition, gene therapy can be used to correct specific genetic deficiencies within the endothelial cell population. In this strategy, therapeutic genes that can either add or block a function are delivered to a targeted cell population. Additionally, such gene delivery methods can also be very useful in the study of cellular biology and disease.

This chapter was originally published as Shmueli, RB, Sunshine JC, Xu Z, Duh EJ, Green JJ. "Gene delivery nanoparticles specific for human microvasculature and macrovasculature." Nanomedicine 2012 Oct; 8(7):1200-7.

Non-viral transfection of human retinal endothelial cells (HRECs) remains a challenge as does transfection of many other cell types. For example, one recent report using lipid coated magnetic nanoparticles achieved only ~5% transfection efficacy [5]. Leading commercial reagents, such as Lipofectamine 2000, can improve the transfection of HRECs. One study found that this approach could lead to 42%-67% knockdown of a target receptor's surface expression following plasmid transfection [6]. Macrovascular (human umbilical vein endothelial cells, HUVECs) are also generally difficult to transfect as a lead polymer (polyethylenimine) plus magnetofection yielded transfection efficacy of only 39% positive cells [7]. New nanomedicines are needed to further increase the effectiveness of non-viral gene delivery.

Certain poly(β-amino esters) (PBAEs) have recently shown good transfection efficacy to a variety of cell types, including hard to transfect cell types like human mammary epithelium in 2D and 3D [8], human brain cancer cells [9], and HUVECs [10]. Particular polymers formulations have shown selectivity in terms of transfecting brain cancer cells as compared to normal astrocytes [9]. In addition, polymer end-group modification has been suggested as a tool to tune transfection efficacy [10-12]. The objectives of this study were to investigate the endothelial and retinal cell-type specificities of PBAE-based nanoparticles and also to identify novel nanoparticles that can achieve high transfection of human endothelial cells with minimal toxicity. A new PBAE combinatorial polymer library was synthesized and evaluated to discover nanoparticles that can transfect either macrovascular (HUVECs) or microvascular (HRECs) human endothelial cells or both.

6.2 Materials and Methods

6.2.1 Materials

All chemicals and solutions were used as received unless otherwise indicated. Monomers and vendors used for synthesis are the following: from Acros Organics [1-(3-aminopropyl)pyrrolidine (E8)], Alfa Aesar [3-amino-1-propanol (S3), 4-amino-1-butanol (S4), 5-amino-1-pentanol (S5), 1,4-butanediol diacrylate (B4), 1,6-hexanediol diacrylate (B6), 1-(3-aminopropyl)-4-methylpiperazine (E7)], Fluka [2-(3-aminopropylamino)ethanol (E6)], Monomer-Polymer and Dajac Laboratories [1,3-propanediol diacrylate (B3), 1,5-pentanediol diacrylate (B5)], Sigma-Aldrich [1,3-diaminopropane (E1), 2,2-Dimethyl-1,3-propanediamine (E2), cystamine dihydrochloride (E10), 2-(1H-imidazol-4-yl)ethanamine (E12)], and TCI America [1,3-diaminopentane (E3), 2-methyl-1,5-diaminopentane (E4), (PEO)4-bis-amine (E5)]. Anhydrous DMSO and 3 M sodium acetate buffer were purchased from Sigma Aldrich. Sodium acetate buffer was diluted to 25 mM and filtered through 0.2 μm filter. pCMV-eGFP DNA was purchased from Aldevron. PBS, 0.25% trypsin-EDTA, Fu-Gene HD, and Lipofectamine 2000 were purchased from Invitrogen. CellTiter 96® AQ_{ueous} One MTS assay was purchased from Promega. 96-well TCP and non-TCP round-bottom plates were purchased from Sarstedt. Human Umbilical Vein Endothelial Cells (HUVECs) and EGM-2 Bullet Kit and Reagent Pack were purchased from Lonza. Human retinal endothelial cells (HRECs) were obtained from Cell Systems and cultured in EGM2-MV

(from Lonza), as previously described [13, 14]. The immortalized human RPE cell line, ARPE-19, was obtained from the Dr. James Handa [15].

6.2.2 Synthesis of Poly(beta-amino ester) (PBAE)

The structures of these polymers were chosen so that there are ester linkages to ensure degradability of the polymers and amine groups to ensure the ability to bind DNA and form nanoparticles. The base polymers were synthesized by mixing diacrylates, labeled as 'B#' in the text, and amino alcohols, 'S#', at a molar ratio of 1.2:1 in glass scintillating vials with teflon stir bars, forming 'B#-S#' base polymers. The reaction was run at 90^{o}C for 24 hours. The base polymer was then dissolved at 167mg/mL in DMSO. In the last step of the reaction, 480 μL containing 80 mg of the base polymer and 320 μL of 0.5 M end-capping amine, 'E#', were mixed in a 1.5 mL eppendorf tubes in a shaker for 1 hour. Completed polymers were aliquoted into smaller volumes and stored at 4^{o}C. The completed polymers are designated as 'B#-S#-E#'; for example, B3-S5-E1 is an end-modified PBAE formed from the B3-S5 base polymer which is then end-modified with the end-capping amine E1. Polymer molecular weights were typically ~10 kDa as we previously have reported and among these polymers we have found that molecular weight is not correlated to transfection efficacy.[16] We have recently published the polymer characterization of these synthetic biomaterials including ^{1}H-NMR and Gel Permeation Chromatography of each polymer [16].

6.2.3 Nanoparticle Sizing

DNA was diluted in 25 mM sodium acetate buffer to 0.01 mg/mL. Polymer was diluted in sodium acetate buffer to either 30 or 60 times that concentration (30 and 60

weight to weight, w/w, ratios), added to the DNA solution and incubated at room temperature for 10 minutes. Nanoparticles were then diluted 20 fold into PBS and loaded into NS500 nanosight tracking analysis (NTA) system. Nanosight videos were captured for 60 seconds and then analyzed used the NTA software, version 2.2.

6.2.4 Transmission Electron Microscopy (TEM) imaging

Nanoparticles were prepared the same way as for sizing by NTA. 10 uL of sample was dropped onto carbon coated copper grids and left to dry in chemical hood for 2 hours. Unstained TEM imaging was then performed using the Philips CM120 system. Nanoparticle sizing was performed using ImageJ software.

6.2.5 Green Fluorescent Protein (GFP) transfection

HUVECs and HRECs were seeded at 2,500-5,000 cells/well onto 96-well plates and allowed to adhere overnight, in 100 μL of the appropriate media per well (EGM-2 for HUVECs and EGM-2 MV for HRECs). Immediately before transfection, media in plates were replaced with 10% supplemented FBS HUVEC media, 100 μL per well. For RPE transfections, ARPE-19 cells were seeded at 15,000 cells/well and allowed to grow to confluence over 3 days, and then transfected in DMEM with 10% supplemented FBS. Polymers and pCMV-eGFP DNA were diluted in 25mM sodium acetate buffer. The final DNA concentration of the mixture was 0.03 mg/mL, with PBAEs at either at 0.9 or 1.8 mg/mL (30 w/w and 60 w/w ratios, respectively). Solution was mixed, incubated for 10 minutes at room temperature and then 20 μL were added per well. FuGene HD and Lipofectamine 2000 were screened to find best formulation by following the manufacturer's guidelines. FuGene HD-DNA ratio of 4-1 was used, with 10 μL added

per well, while Lipofectamine 2000-DNA ratio of 1.5-1 was used, with 10 μL added per well. Plates then incubated for 4 hours, after which nanoparticle loaded media was removed and fresh EGM-2 and EGM-2 MV media were added, 100 μL/well. Each experimental condition was evaluated in quadruplicate. Duplicate plates were made for each experimental group to use one each for cell viability and transfection efficiency measurements.

6.2.6 Cell metabolism/viability

Twenty-four hours after transfection, designated plates were used for the CellTiter 96® AQ_{ueous} One MTS assay. 10 μL of the aliquoted assay solution was added per well. Plates were incubated for 1-4 hours, after which absorbance at 490 nm was measured using the BioTek Synergy 2 Plate Reader. Absorbance measurements were corrected from background media signal and normalized by untreated groups. Each experimental condition was evaluated in quadruplicate.

6.2.7 Flow cytometry

Forty-eight hours after transfection, flow cytometry was performed using the Accuri C6 flow cytometer with IntelliCyt high-throughput attachment. Cells were washed with 1x PBS and trypsinized with 30 μL/well of 0.25% trypsin-EDTA. 170 μL FACS buffer (2% FBS, 1x PBS) was added to cells and 200 μL/well transferred to 96-well round-bottom plates. The plates were centrifuged at 1000 rpm for 5 minutes, after which 170 μL/well of the supernatant was removed. The pellets were re-suspended in the remaining 30μL of buffer. Plates were then placed onto the IntelliCyt high-throughput

attachment and HyperCyt software was to acquire and process data. FlowJo was used to analyze the flow cytometry data.

6.3 Results

6.3.1 Polymer and Nanoparticle Synthesis

A polymer library was synthesized for gene delivery, such that a large diversity of structures could be investigated, each with small differential structural changes from each other. The structures of these polymers were chosen so that there are ester linkages to ensure degradability of the polymers and amine groups to ensure the ability to bind DNA and form nanoparticles. These polymers were synthesized from a pool of 4 acrylate monomers, 3 side chain monomers, and 12 end-chain capping molecules as described in the methods. The synthetic polymers are referred to by a 'B' number, a 'S' number, and an 'E' number, each referring to their constituent monomers. The number following the 'B' or the 'S' corresponds to the number of carbons between functional groups in the diacrylate or amino-alcohol monomers; thus 'B4-S5' is a polymer formed from a base diacrylate with 4 carbons between each acrylate group, and an amino-alcohol with 5 carbons between the amine and the alcohol functional groups.

Nanoparticles are formed through electrostatic self-assembly, due to attractive interactions between cationic polymers and anionic DNA. We use relatively high polymer to DNA weight ratios (w/w) such that the polymers encapsulate 100% of the DNA as we have recently described [17]. Representative polymers of interest were

chosen for sizing measurements. Even though polymer structure varied, nanoparticle size was found to be similar with these different types of polymers (**Figure 6.2A**). Hydrodynamic diameter of the nanoparticles was approximately 150 nm, with a range of 110-190 nm in the particle distributions that was dependent on polymer to DNA weight-to-weight (w/w) formulation ratio. The average diameter of a nanoparticle formed from B3-S5-E1 at 60 w/w as measured by TEM was 147 nm (**Figure 6.2B**), which closely matches the results found from NTA. There was no correlation between the sizes of nanoparticles that transfected the cells well (B3-S5-E# and B4-S4-E# series) as compared to those that transfected the cells less well (B3-S4-E# series). Therefore, we hypothesize that chemical structure, not nanoparticle physical properties, is the driver of the differences seen in transfection efficacy.

6.3.2 Nanoparticle-mediated Gene Delivery

Leading polymeric nanoparticles were found to be very effective for gene delivery to human microvascular and macrovascular endothelial cells. Significantly, transfection efficiencies of up to 85% for HRECs and 65% for HUVECs were observed as opposed to 49% (HREC) and 32% (HUVEC) with a leading commercially available reagent, Lipofectamine 2000 (**Figures 6.3A-B**). Lipofectamine 2000 was also more toxic than the PBAE nanoparticles (**Figures 6.3C-D**). The polymeric nanoparticles were found to display a wide range of transfection efficacies with both HRECs and HUVECs, which was dependent on polymer structure. Both the choice of base polymer and end-capping groups had a large effect on the transfection efficacy. The B4, B5, and B6 diacrylates differ by one carbon, yet there are significant differences in toxicity and transfection

efficacy. A similar effect was observed when changing the side-chain amines. For example, B3-S4-based polymeric nanoparticles had very low transfection (< 10%), but a single carbon added to each of the side-chain monomers (B3-S5-based polymeric nanoparticles) resulted in highly effective gene delivery for both HRECs (up to 76%) and HUVECs (up to 64%). The end-group of the polymer made a big difference to endothelial cell gene delivery as well, where the best formulations usually contained E5, E6, and E7.

In order to better isolate the effects from changing each component of the polymer, the data were averaged together across two of the three polymer elements that compose each synthetic polymer. In general, B4 and B5 based polymers had the highest gene delivery efficacy (**Figure 6.4A**) and reveal an optimal base diacrylate length. On the other hand, we observe an increasing monotonic trend with increasing length for the various side-chain amines used in this experiment, with S5 based polymers performing best (**Figure 6.4B**). Unlike with the structure of the base polymers, a clear trend in the structure of the end-group with transfection efficacy is not observed (**Figure 6.4C**). However, there are some end-capping amines, such as E6, which dramatically improve delivery, and others, such as E12, that are much less effective. These results motivate further studies on how polymer structure affects endothelial cell gene delivery.

6.3.3 Endothelial Cell-specific Gene Delivery

Comparing the transfection efficiencies between the different cell types and tissues revealed interesting trends (**Figure 6.5**). In this study, the HREC and HUVEC transfection profiles were positively correlated (linear regression, R^2= 0.81), with greater

transfection efficiencies for HRECs overall. Similar viability profiles were also observed between HUVECs and HRECs. On the other hand, using the same set of nanoparticles, there is very little correlation between the transfection efficacies for gene delivery to HRECs as compared to retinal pigment epithelium (RPEs, linear regression, $R^2 = 0.21$), or HUVECs as compared to RPEs (linear regression, $R^2 = 0.23$). Polymers that performed better on the endothelial cell types as compared the regression line include B4-S4 and B3-S5, as well as some B4-S5-based polymers (upper left hand corner of Figures 5B and 5C). As a group, these polymers were synthesized by diacrylate monomers that were less hydrophobic and contained 3 or 4 carbons between diacrylate monomer groups. On the other hand, there are some polymers that work better on the epithelial cells, such as B6-S5 (lower right hand corner of Figures 5B and 5C). This polymer is more hydrophobic than the polymers that tend to be better at transfecting endothelial cells and this polymer contains 6 carbons between its diacrylate monomer groups. The polymers that work well on both endothelial and epithelial cell types include B5-S5 based-polymers (upper right hand corner of Figures 5B and 5C), which have an intermediate level of hydrophobicity and 5 carbons between its diacrylate monomer groups. Strikingly, these structural changes are quite subtle and they do not influence nanoparticle size (**Figure 6.2)**.

6.4 Discussion

Synthesis and testing of a PBAE library resulted in the identification of polymeric nanoparticles that can transfect human endothelial cells, HRECs and HUVECs, with high

efficiency as compared to current commercially available standards. The best polymers (both good transfection and viability), B3-S5-E# and B4-S4-E# series, are new PBAE structures that were able transfect at least as well as the commercially available reagents and in some cases with less toxicity. Additionally, Small molecular changes to polymer backbone, side chain or end-group structure dramatically changed transfection efficiency. The best polymers were ones that contained B4 and B5, and S4 and S5, with a few different E# groups. The most hydrophilic polymers, such as B3-S4, were not good at transfecting the cells, while their toxicity was also minimal. On the other hand, the most hydrophobic polymers, such as the B6-S5 series, were usually relatively toxic to the endothelial cells, subsequently also reducing the transfection efficiency. This trend is mirrored when looking at the effects of the different diacrylate monomers used (Figure 4A), where B4 and S5 performed best. While among certain structures, high hydrophobicity correlated to increased cytotoxicity and reduced transfection, overall, when all the data is evaluated together, there is not a strong correlation between transfection efficiency and viability (R^2 =0.06, data not shown).

Interestingly, the gene delivery efficacy across the entire polymer library was highly correlated between transfection of HREC and HUVEC cells – nanoparticle formulations that performed well for HRECs also performed well for HUVECs (R^2 = 0.81). This is dramatically different when compared to the performance of the same nanoparticles with retinal pigment epithelium, indicating that formulations could potentially be found which selectively transfect one ophthalmic cell type and not the other, as can be observed in Figures 5B and 5C. To our knowledge this phenomenon, that specific ocular cell types can be targeted directly by fine-tuning of the polymer structure

that composes nanoparticles, is striking and surprising. This finding also suggests that biomaterial-mediated targeting from this class of materials may be able to be combined with other methods of gene delivery targeting such as ligand or coating-mediated cell uptake [18-20] and transcriptional targeting [21, 22] to further improve specificity and efficacy to only one specific type of cell.

In particular, we show that the polymers in the middle of the hydrophobicity scale for this PBAE library worked very well for the endothelial cells, but much less so for the epithelial cells. On the other hand, those that were more hydrophobic, such as the B6-S5, worked well for the epithelial cells. Taken together, these correlations indicate that there may be natural cell type specificity for polymeric nanoparticles of this class.

Safe and effective gene delivery vehicles can have a large impact on biological studies and for the treatment of diseases. For example, researchers have developed a system for gene delivery of sFLT using adeno-associated virus (AAV) to bind VEGF in monkeys as a potential treatment for age-related macular degeneration [23]. However, viral gene therapy has limitations that may preclude many clinical applications due to carrying capacity constraints and safety concerns [24]. In contrast, our study reveals premiere non-viral nanoparticles that are enabling technologies for transfection of endothelial cells *in vitro* and are promising for use *in vivo* as delivery vehicles for genetic nanomedicines. We also show that polymer structure itself, may enable cell-specific non-viral gene delivery.

6.5 Acknowledgments

The authors thank the TEDCO MSCRF(2009-MSCRFE-0098-00), the NIH (R21CA152473), and MSTP (to JCS) for support in part of this work. EJD is supported by a Career Development Award from Research to Prevent Blindness. The authors also thank Corey Bishop for help with TEM imaging and Dr. James Handa's lab (JHMI-Wilmer Eye Institute) for ARPE-19 cells.

6.6 Figures

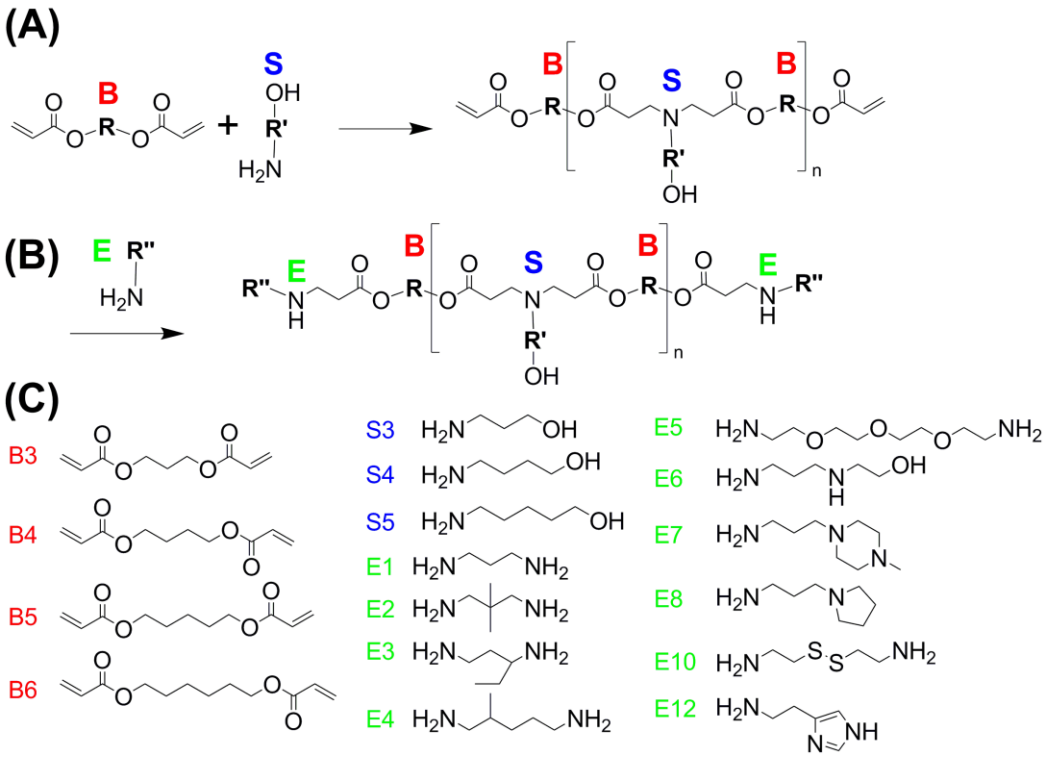

Figure 6.1. (A) Polymers were synthesized by reacting a diacrylate, 'B#', with an amino alcohol, 'S#'; **(B)** These were then reacted with an end-group, 'E#'; **(C)** Monomer structures.

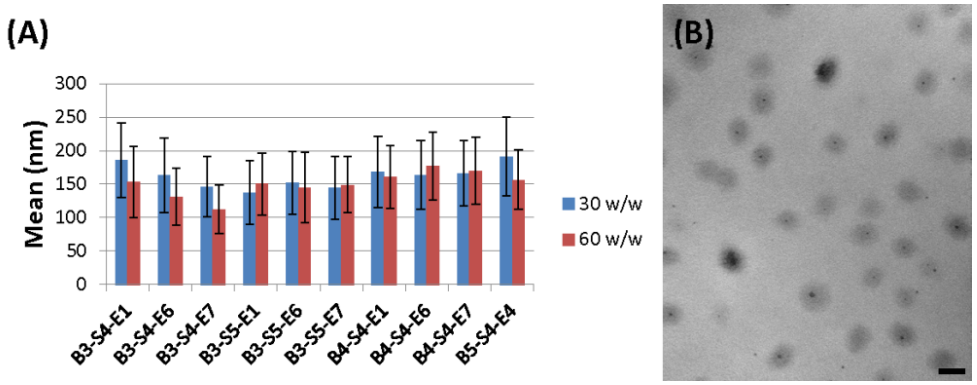

Figure 6.2. (A) Hydrodynamic diameter by nanoparticle tracking analysis. **(B)** Transmission Electron Microscopy of nanoparticles formed from B3-S5-E1 (60 w/w); scale bar is 200nm.

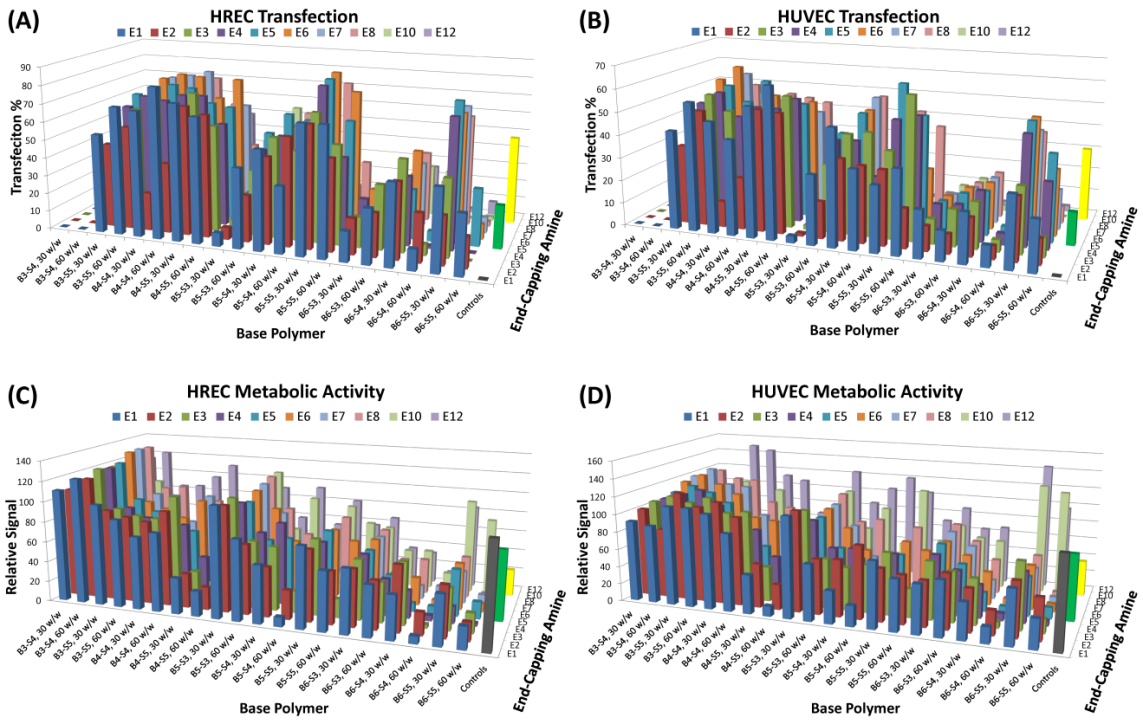

Figure 6.3. **(A)** HUVEC and **(B)** HREC transfection percentage. **(C)** HREC and **(D)** HUVEC metabolic activity relative to untreated control. Controls: Gray=untreated, Green=FuGene HD, Yellow=Lipofectamine 2000.

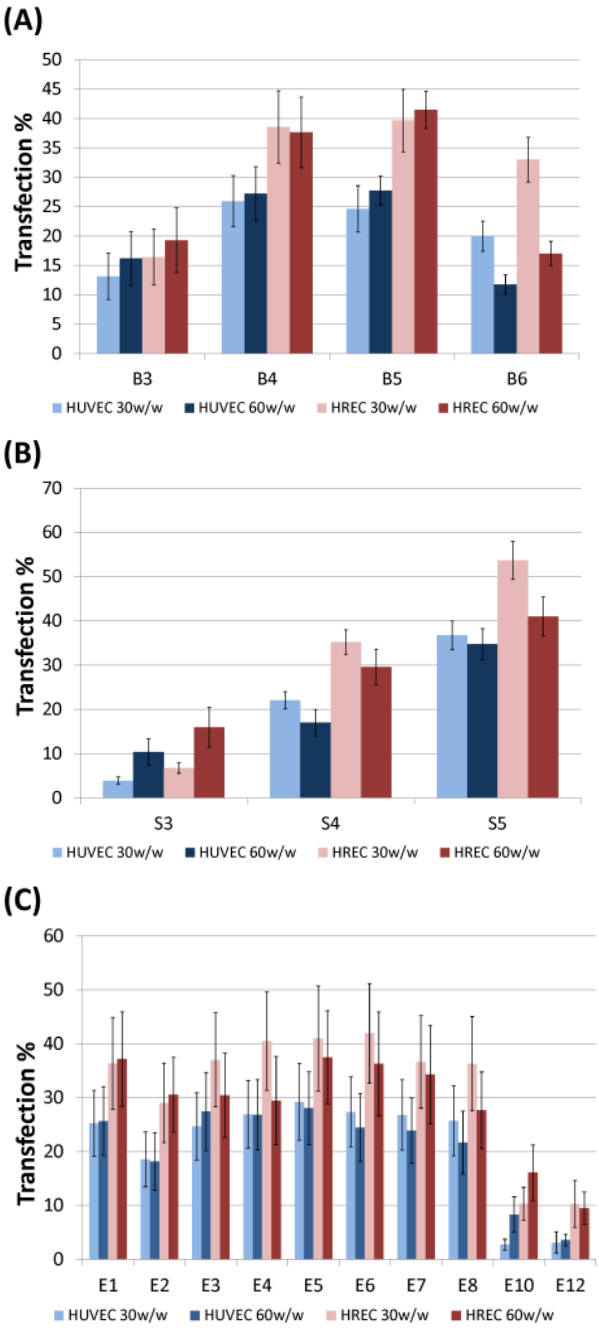

Figure 6.4. Panel of monomer effects on transfection %. Collapsing (averaging) two of three types of monomers attempt to isolate effects of each monomer change. **(A)** Diacrylate base, **(B)** Side-chain amine base, **(C)** End-group amine.

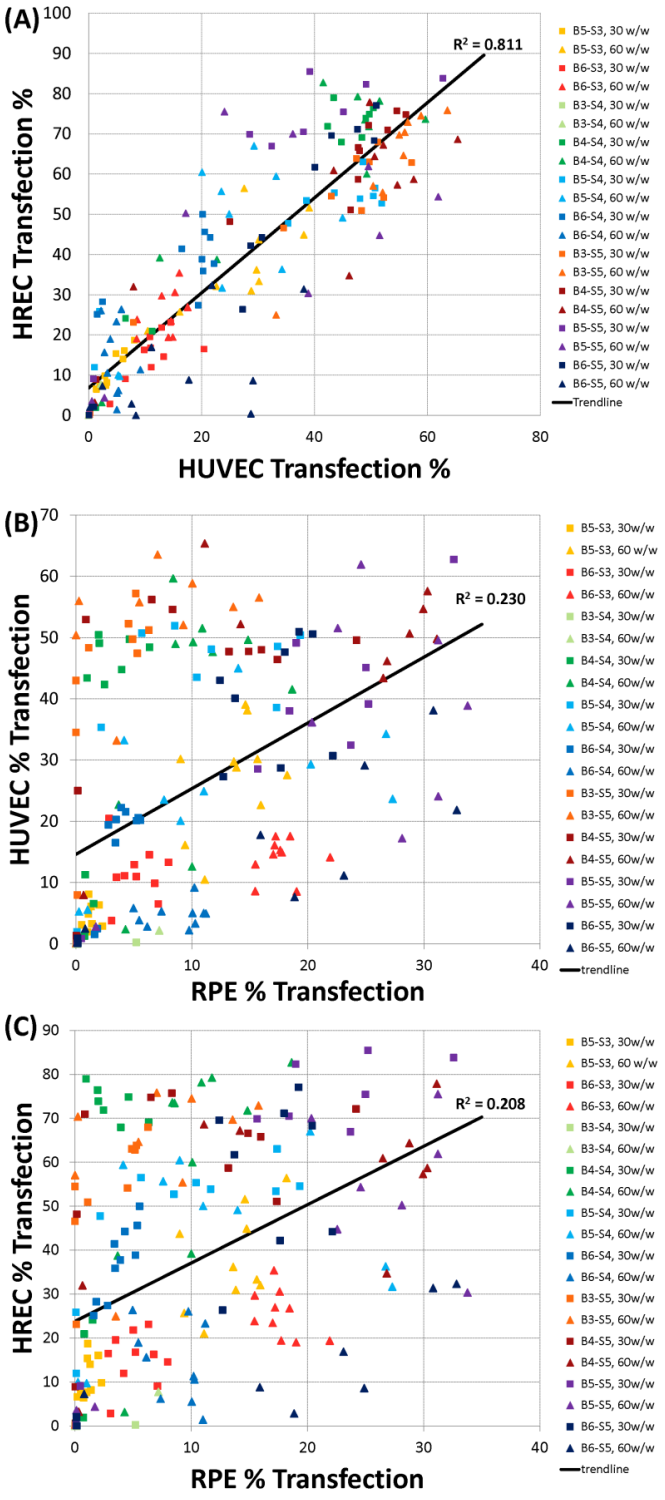

Figure 6.5. (A) There is a strong correlation between transfection of HUVEC and HRECs and **(B-C)** a much weaker correlation when compared to transfection of RPEs.

6.7 References

1. Jo DH, Kim JH, Kim JH. How to Overcome Retinal Neuropathy: The Fight against Angiogenesis-related Blindness. Archives of Pharmacal Research 2010 Oct;33(10):1557-1565.

2. Bhise NS, Shmueli RB, Sunshine JC, Tzeng SY, Green JJ. Drug delivery strategies for therapeutic angiogenesis and antiangiogenesis. Expert Opinion on Drug Delivery 2011 Apr;8(4):485-504.

3. Adhim Z, Lin X, Huang W, Morishita N, Nakamura T, Yasui H, et al. E10A, an adenovirus-carrying endostatin gene, dramatically increased the tumor drug concentration of metronomic chemotherapy with low-dose cisplatin in a xenograft mouse model for head and neck squamous-cell carcinoma. Cancer Gene Ther 2011 Nov 25.

4. Campochiaro PA. Gene transfer for ocular neovascularization and macular edema. Gene Ther 2011 Nov 10.

5. Prow T, Smith JN, Grebe R, Salazar JH, Wang N, Kotov N, et al. Construction, gene delivery, and expression of DNA tethered nanoparticles. Mol Vis 2006;12:606-615.

6. Spoerri PE, Afzal A, Li Calzi S, Shaw LC, Cai J, Pan H, et al. Effects of VEGFR-1, VEGFR-2, and IGF-IR hammerhead ribozymes on glucose-mediated tight junction expression in cultured human retinal endothelial cells. Mol Vis 2006;12:32-42.

7. Krotz F, Sohn HY, Gloe T, Plank C, Pohl U. Magnetofection potentiates gene delivery to cultured endothelial cells. J Vasc Res 2003 Sep-Oct;40(5):425-434.

8. Bhise NS, Gray RS, Sunshine JC, Htet S, Ewald AJ, Green JJ. The relationship between terminal functionalization and molecular weight of a gene delivery polymer and transfection efficacy in mammary epithelial 2-D cultures and 3-D organotypic cultures. Biomaterials 2010 Nov;31(31):8088-8096.

9. Tzeng SY, Guerrero-Cazares H, Martinez EE, Sunshine JC, Quinones-Hinojosa A, Green JJ. Non-viral gene delivery nanoparticles based on Poly(beta-amino esters) for treatment of glioblastoma. Biomaterials 2011 Aug;32(23):5402-5410.

10. Sunshine J, Green JJ, Mahon KP, Yang F, Eltoukhy AA, Nguyen DN, et al. Small-Molecule End-Groups of Linear Polymer Determine Cell-Type Gene-Delivery Efficacy. Advanced Materials 2009 Dec 28;21(48):4947-4951.

11. Green JJ, Shi J, Chiu E, Leshchiner ES, Langer R, Anderson DG. Biodegradable polymeric vectors for gene delivery to human endothelial cells. Bioconjugate Chem 2006 Sep 20;17(5):1162-1169.

12. Green JJ, Langer R, Anderson DG. A combinatorial polymer library approach yields insight into nonviral gene delivery. Acc Chem Res 2008 May 29;41(6):749-759.

13. Maiti D, Xu Z, Duh EJ. Vascular endothelial growth factor induces MEF2C and MEF2-dependent activity in endothelial cells. Invest Ophthalmol Vis Sci 2008 Aug;49(8):3640-3648.

14. Xu Z, Yu Y, Duh EJ. Vascular endothelial growth factor upregulates expression of ADAMTS1 in endothelial cells through protein kinase C signaling. Invest Ophthalmol Vis Sci 2006 Sep;47(9):4059-4066.

15. Handa JT, Reiser KM, Matsunaga H, Hjelmeland LM. The advanced glycation endproduct pentosidine induces the expression of PDGF-B in human retinal pigment epithelial cells. Exp Eye Res 1998 Apr;66(4):411-419.

16. Sunshine JC, Akanda MI, Li D, Kozielski KL, Green JJ. Effects of Base Polymer Hydrophobicity and End-Group Modification on Polymeric Gene Delivery. Biomacromolecules 2011 Sep 9.

17. Bhise NS, Shmueli RB, Gonzalez J, Green JJ. A Novel Assay for Quantifying the Number of Plasmids Encapsulated by Polymer Nanoparticles. Small 2011 Dec 5.

18. Green JJ, Chiu E, Leshchiner ES, Shi J, Langer R, Anderson DG. Electrostatic ligand coatings of nanoparticles enable ligand-specific gene delivery to human primary cells. Nano Lett 2007 Apr;7(4):874-879.

19. Harris TJ, Green JJ, Fung PW, Langer R, Anderson DG, Bhatia SN. Tissue-specific gene delivery via nanoparticle coating. Biomaterials 2010 Feb;31(5):998-1006.

20. Shmueli RB, Anderson DG, Green JJ. Electrostatic surface modifications to improve gene delivery. Expert Opin Drug Deliv 2010 2010;7(4):535-550.

21. Huang YH, Zugates GT, Peng W, Holtz D, Dunton C, Green JJ, et al. Nanoparticle-delivered suicide gene therapy effectively reduces ovarian tumor burden in mice. Cancer Res 2009 Aug 1;69(15):6184-6191.

22. Showalter SL, Huang YH, Witkiewicz A, Costantino CL, Yeo CJ, Green JJ, et al. Nanoparticulate delivery of diphtheria toxin DNA effectively kills Mesothelin expressing pancreatic cancer cells. Cancer biology & therapy 2008 Oct;7(10):1584-1590.

23. MacLachlan TK, Lukason M, Collins M, Munger R, Isenberger E, Rogers C, et al. Preclinical Safety Evaluation of AAV2-sFLT01-A Gene Therapy for Age-related Macular Degeneration. Mol Ther 2011 Feb;19(2):326-334.

24. Thomas CE, Ehrhardt A, Kay MA. Progress and problems with the use of viral vectors for gene therapy. Nature reviews Genetics 2003 May;4(5):346-358.

Chapter 7

Long-Term Suppression of Choroidal Neovascularization by Microparticle Peptide Delivery

7.1 Introduction

Pathologic angiogenesis plays an important role in several classes of diseases. In cancer, angiogenesis supports the growth of tumors [1]. In patients with neovascular age-related macular degeneration (NVAMD), angiogenesis leads to the loss of central vision [2]. There are several angiogenic factors that contribute to pathologic angiogenesis, such as vascular endothelial growth factor (VEGF-A), platelet-derived growth factor (PDGF-BB), and stromal derived factor (SDF-1) and neutralization of one or more of these can provide therapeutic benefits [3]. Patients with NVAMD have experienced improved visual outcomes from intraocular injections of various types of VEGF antagonists including ranibizumab (Lucentis®), an Fab; bevacizumab (Avastin®), a full-length antibody; and aflibercept (EYLEA®), a fusion protein consisting of the binding domains of VEGF receptors 1 and 2 and Fc fragment [4, 5], but frequent injections over a prolonged period are needed to maintain visual benefits. Failure to return for follow up which can occur for a variety of reasons such as illness, travel, or transportation difficulties can result in permanent loss of vision. More durable treatments are needed to

This chapter was originally published as Shmueli RB, Ohnaka M, Miki A, Pandey NB, Lima e Silva R, Koskimaki JE, Kim J, Popel AS, Campochiaro PA, Green JJ. "Long-term suppression of ocular neovascularization by intraocular injection of biodegradable polymeric particles containing a serpin-derived peptide." Biomaterials. 2013 Oct;34(30):7544-51.

mitigate these risks. Biomaterials for controlled drug delivery can potentially facilitate both protection of sensitive biological molecules from quick clearance and degradation as well as provide a mechanism for sustained and long-term release.

We have discovered classes of peptides with very strong anti-angiogenic properties, including collagen IV-derived, thrombospondins, CXC chemokines, somatotropins and serpins [6]. These peptides have been developed by combining experimental and computational approaches and several have been validated by inhibiting tumor growth in cancer models [7]. One class of these peptides, the serpin-derived peptides, are able to inhibit angiogenesis by both inducing endothelial cell apoptosis as well as decreasing their migration by increasing adhesion [8]. One of these serpin-derived peptides, which we refer to as SP6001, more specifically derived from DEAH box polypeptide 8 protein, was selected and evaluated unencapsulated, in nanoparticles, and in microparticles in the mouse model of laser-induced choroidal neovascularization.

Generally, small peptides possess many advantageous characteristics as therapeutic agents, such as high specificity and low toxicity [9]; the main disadvantage is their short half-life. Biomaterials, nanoparticles, and microparticles have the potential to significantly impact medicine as delivery systems for diverse biological molecules, including peptides. A long-term controlled release system can help overcome problems associated with current AMD treatments. A number of different polyester polymers, such as poly(lactic-co-glycolic acid) (PLGA), have been commonly used in long-term release systems. PLGA has been used in several FDA approved devices such as sutures and drug delivery devices. It is a material that is biodegradable in water and is generally

recognized as safe. PLGA nanoparticles have been used to increase the half-life of therapeutics, such as in the encapsulation of a peptide integrin antagonist in PLA/PLA-PEO nanoparticles [10], as well as encapsulation of the antibody bevacizumab [11]. In contrast to nanoparticles, which generally act short-term, larger implantable devices are a drug delivery strategy that has been investigated to enable controlled long-term delivery [12, 13]. By using polymers such as PLGA, implantable devices can be designed to be biodegradable so that they do not need to be surgically removed at a future time [14].

In order to protect the SP6001 peptide from degradation and to extend its delivery, the peptide can be complexed and/or encapsulated by biodegradable polymers. The SP6001 peptide is negatively charged due to a number of glutamic acid residues. Therefore, a cationic polymer, such as a poly(beta-amino ester), PBAE, can be used to self-assemble with the peptide. PBAEs are also hydrolytically degradable due to the ester bonds in the polymer backbone. As such, these polymers have been previously used to self-assemble with DNA and RNA to form effective gene delivery nanoparticles [15-17]. To further extend release, these polymer-peptide nanoparticles can be encapsulated into PLGA microparticles. These microparticles can degrade over time to release the nanoparticles and peptide into the eye and create a new treatment for NVAMD.

7.2 Materials and Methods

7.2.1 Chemicals

PLGA [Poly(D,L-lactide-co-glycolide); lactide:glycolide (65:35); Mw 40,000-75,000] and DCM [Dichloromethane] were purchased from Sigma (St. Louis, MO). We synthesized PBAE [Poly(beta-amino ester)], as previously described [18], from the following monomers: 3-amino-1-propanol (S3) purchased from Alfa Aesar (Ward Hill, MA), 1,3-propanediol diacrylate (B3) purchased from Dajac laboratories (Trevose, PA), and 2-(3-aminopropylamino)ethanol (E6) purchased from Fluka/Sigma. The PBAE polymer, 2-(3-aminopropylamino)ethanol end-capped 1,3-propanediol diacrylate-co-3-amino-1-propanol (abbreviated based on its constituent monomers as B3-S3-E6), was synthesized at a B3 to S3 molar ratio of 1.05:1. Polymer B3-S3-E6 was kept stored in anhydrous DMSO at 100 mg/mL with desiccant at -20°C. Peptides (SP6001 and FITC-SP6001) were purchased from American Peptide (Sunnyvale, CA). Sodium Acetate buffer (NaAc) (pH=5) was purchased from Invitrogen (Grand Island, NY). PVA [Poly(vinyl alcohol); Mw 25,000] was purchased from Polysciences (Warrington, PA).

7.2.2 Nanoparticle formation

For sizing with a Nanosight NS500: In an eppendorf tube, SP6001 peptide (20 μg/μL in DMSO) was diluted to 1.2 μg/μL in milli-Q water. In a second tube, 25 mM NaAc was added to the PBAE to obtain the desired PBAE concentration. For example, for 5:1 weight/weight (w/w) of PBAE to peptide, 125.3 μL NaAc was added to 8 μL (100 μg/μL) of B3-S3-E6. 100 μL of PBAE solution was added to 100 μL of peptide solution, vortexed, and incubated at room temperature for 10 min to allow for nanoparticle formation. To characterize nanoparticle size by nanoparticle tracking analysis, 100 μL of

nanoparticle solution was diluted into 400 µL milli-Q water and run on a Nanosight NS500.

For *in vivo* injections: In separate eppendorf tubes 1.25 µL (100 µg/µL) B3-S3-E6 + 8.75 µL NaAc was prepared as was 1.25 µL (20 µg/µL) SP6001 + 8.75 µL PBS. The solutions were mixed together and then an additional 5 µL PBS was added to bring the total peptide concentration to 1.0 µg/µL. For corresponding controls: Buffer only contained 2.5 µL DMSO + 13.75 µL PBS + 8.75 µL NaAc; Peptide only contained 1.25 µL (20 µg/µL) peptide + 13.75 µL PBS mixed with 1.25 µL DMSO + 8.75 µL NaAc; Polymer only contained 1.25 µL (100 µg/µL) PBAE + 8.75 µL NaAc mixed with 1.25 µL DMSO + 13.75 µL PBS. For all samples of nanoparticles containing peptide and corresponding peptide controls, 1 µL of 1 µg/µL peptide solutions were intravitreally injected into each mouse eye.

7.2.3 Microparticle formulation

One hundred mg of PLGA was first dissolved into 2.5 mL of DCM in a test tube and vortexed to fully dissolve. The aqueous phase was prepared by mixing peptide (SP6001 or FITC-SP6001), PBAE (B3-S3-E6), and milli-Q water in an eppendorf tube. First 12.5 µL (20 µg/µL) SP-6001 + 8.33 µL water were mixed, then 2.5 µL (100 µg/µL) B3-S3-E6 1.05:1 + 18.33 µL water was added, and then this was diluted with an additional 26.67 µL water. For blank microparticles, the aqueous phase was 41.67 µL water. The aqueous phase was micropipetted to the PLGA/DCM solution and vortexed on high. The mixture was sonicated with the test tube on ice to create the first w/o emulsion. Sonication was performed with an amplitude setting of ‘30’, which equals

approximately 10 W for 20 seconds. The primary emulsion was poured into 50 mL of 1% PVA solution and homogenized at 3.6-3.8 krpm for 1 minute to create the w/o/w secondary emulsion. The full volume was transferred into 100 mL of 0.5% PVA solution and stirred in a chemical hood for 3 hours. Three wash steps were then performed. For each wash step, the microparticle solution was centrifuged at 4^{o}C, 4 krpm, for 5 minutes, and then the supernatant was removed. Subsequently, 40 mL of refrigerated water was added, the microparticle pellet was resuspended and the washing steps were repeated. After the last centrifugation step, 5 mL of water was added. Samples were snap frozen in liquid nitrogen and immediately placed in a lyophilizer. Following lyophilization, all microparticles were stored at -20^{o}C. For release and *in vivo* studies, an appropriate amount of microparticles were weighed out and suspended in an appropriate amount of PBS to reach the desired concentration.

7.2.4 SEM imaging of microparticles and ImageJ quantification

Lyophilized particles were placed on carbon tape (Electron Microscopy Sciences, Hatfield, PA) placed on aluminum mounts. Samples were sputtered with gold-palladium, and SEM imaging was performed with a LEO/Zeiss FESEM at the JHU School of Medicine MicFac.

7.2.5 Microparticle loading and release profiles

Microparticles were prepared as described with 10% or 100% of the peptide labeled with FITC. Loading efficiency was quantified by dissolving the microparticles in DMSO and adding to PBS. The solution was centrifuged to separate out the PLGA precipitate and the supernatant was collected for fluorescence measurement. For release

studies, microparticles were diluted in PBS at 40 mg/mL in a 1.5 mL tube and incubated at 37^{o}C with light shaking. At the specified time points, samples were vortexed, spun down, supernatant was collected, and new PBS added to the microparticle pellet. DMSO was added to the supernatant so that the final solution for fluorescence measurements was constant 5% v/v DMSO/PBS. Fluorescence measurements were obtained using a BioTek Synergy 2 plate reader with an excitation filter of 485 +/- 20 nm and an emission filter of 528 +/- 20 nm. Peptide concentration was obtained by comparison to a standard curve for 6001-FITC in 5% v/v DMSO/PBS.

7.2.6 *In vitro* assays for determination of peptide effects

Human retinal endothelial cells (HRECs) (all cells used were P8-P12) were tested in three separate assays. SP6001's effect on HREC apoptosis was tested by the caspase-glo 3/7 assay purchased from Promega (Madison, WI). Cells were plated at 5,000 cells/well in opaque 96-well plates to minimize well-to-well cross-talk. After 24 h, complete endothelial cell media was replaced with serum free media. Next, media with 30/10 ng/mL (bFGF/VEGF) was added with or without peptide at 10 μM. After 48 h, caspase-glo luminescent reagent was added at 100 μL/well, and luminescence measured with a Victor V plate reader (Perkin Elmer). The experiment was repeated twice.

We used the ACEA cell migration assay to assess SP6001 effect on cell adhesion, SP6001 was added to complete endothelial cell medium at 12.5 μM, and cells allowed to adhere in special E-plate (Roche, IN), suitable for cell culture with sensing electrodes. Impedance, correlated to cell adhesion, was measured using a RT-CIM system (ACEA Biosciences, Inc., San Diego, CA). HRECs were trypsinized and plated at 25,000

cells/well. Cells settled for 30 minutes before being loaded into the ACEA machine. Values are scaled to percent increase above the negative control (complete endothelial cell media), at 10 h time point.

HREC migration was tested using the Platypus migration assay. Specialized plates with stoppers were purchased from Platypus Technologies (Madison, WI). HRECs were plated at 20,000 cells/well in the presence or absence of SP6001 at 10 μM in complete endothelial cell media for 2 h, then stoppers were removed and cells allowed to migrate. After 20 h cells were stained with calcein AM (Invitrogen, Carlsbad, CA) and read with a Victor V plate reader (Perkin Elmer, Waltham, MA). Digital micrographs were taken using a Nikon Inverted Scope Eclipse T-100 scope (Nikon Instruments, Inc., Melville, NY), and are representative of each image.

7.2.7 Mouse model of choroidal neovascularization

Choroidal NV was induced by laser photocoagulation-induced rupture of Bruch's membrane, as previously described [19]. Briefly, 5- to 6-wk-old female C57BL/6 mice were anesthetized with ketamine hydrochloride (100 mg/kg body weight) and pupils were dilated. Laser photocoagulation was performed in the 9, 12, and 3 o'clock positions of the posterior pole of each eye with the slit lamp delivery system of an OcuLight GL diode laser (Iridex, Mountain View, CA, USA) and a coverslip as a contact lens to view the retina. Production of a tissue bubble by the laser, which indicates rupture of Bruch's membrane, is an important factor in obtaining choroidal NV; therefore, only burns in which a bubble was produced were included in the study. After 14 days, the mice were perfused with 1 ml of PBS containing 50 mg/ml of fluorescein-labeled dextran (2×10^6 Da

average molecular mass; Sigma-Aldrich, St. Louis, MO, USA) and choroidal flat mounts were examined by fluorescence microscopy. Image analysis software (Image-Pro Plus; Media Cybernetics, Silver Spring, MD, USA) was used to measure the area of choroidal NV at each rupture site. To measure the long-term efficacy, Bruch's membrane was ruptured at various time points after intravitreous injection (of 1.0 μL of peptide, buffer without peptide, nanoparticles containing peptide, polymer without peptide, microparticles containing peptide, or empty microparticles). Intravitreous injections were done under a dissecting microscope with a Harvard Pump Microinjection System (Harvard Apparatus, Holliston, MA, USA) and pulled glass micropipettes, as previously described [20].

7.2.8 Mouse model statistical comparisons

Data are presented graphically as mean+s.e.m. Experiments were designed so that there were fellow-eye controls and comparisons were done using a two-way analysis of variance or paired *t* test. *P*-values are two-tailed, * indicates $p < 0.05$ and ** indicates $p < 0.01$.

7.3 Results

The serpin-derived peptide, SP6001 (sequence shown in **Figure 7.1**), has been previously shown to have anti-angiogenic properties in macrovascular endothelial cells and in a cancer model [8]. However, its potential inhibitory effect on retinal microvascular endothelial cells, its effects on ocular NV, and whether or not a sustained

delivery formulation could be achieved were unknown. SP6001 statistically significantly increases both apoptosis and adhesion in HRECs, as well as inhibits the migration of these cells (**Figure 7.2**). Biodegradable materials were used to construct a long-term peptide delivery system. In the first step, a peptide-polymer nanoparticle was formed with a PBAE, a biodegradable and cationic polymer. In the second step, these nanoparticles were encapsulated into larger PLGA microparticles that serve as a reservoir for long-term release. The polymer structures, peptide structure, and particle diagram are shown in **Figure 7.1**. The negatively charged peptide forms nanoparticles with the positively charged, biodegradable polymer through electrostatic self-assembly. Polymer B3-S3-E6 was chosen due to its biodegradability, positive charge, biocompatibility with cells, and for its ability to form self-assembled particles with SP6001. The size of the self-assembled peptide-polymer nanoparticles formed was determined by use of the Nanosight Nanoparticle Tracking Analysis instrument and software. The B3-S3-E6/SP6001 nanoparticles had a mode size of 119 nm as shown in **Figure 7.3A**.

In the next step, microparticles were formed using PLGA via a standard double emulsion method. The resulting microparticles were observed using SEM and sizes were quantified using imageJ (**Figure 7.3B**). The number fraction average size was approximately 6 μm and the volume fraction weighted size was approximately 12 μm. Addition of peptide-polymer nanoparticles did not affect microparticle size or morphology of the microparticles. The presence or absence of labeled peptide as compared to unlabeled peptide also did not affect particle size or morphology. The encapsulation efficiency of the labeled peptide was determined to be approximately 70% of the initially loaded peptide amount. The microparticle fabrication process was also

evaluated for endotoxin level to ensure that the particles were appropriate to use for subsequent *in vivo* experiments. According to the LAL endotoxin assay, all polymer and particle samples contained less than the 0.1 EU/mL of the lowest control sample (**Figure 7.3F**). The release of labeled peptide from the microparticles was quantified *in situ* under physiological conditions and observed to last for over 200 days, as seen in **Figure 7.4**. The release curve demonstrates that there is near linear release for approximately 140 days at ~0.008 μg peptide / mg particle released per day. This is followed by slightly slower release phase at additional 60 days. The full release extends over 7 months under physiological conditions *in situ*.

After developing the peptide release system, we sought to compare its effects with the naked peptide *in vivo*. Free SP6001 was injected at different concentrations on the same day as rupture of Bruch's membrane and after 2 weeks, there was significant suppression of choroidal NV in eyes that had been injected with 0.01 μg or 0.1 μg (**Figure 7.5A**). The 0.1 μg dose was chosen as the total peptide dose to use in all subsequent experiments. Next, the SP6001/B3-S3-E6 nanoparticles were tested for activity as compared to a scrambled control peptide. While none of the controls (buffer, scrambled peptide, PBAE polymer) had any anti-angiogenic effect, both the free peptide and nanoparticle-complexed peptides caused significant suppression (**Figure 7.5B**).

Next, we tested the effect of encapsulating the peptide-containing nanoparticles into microparticles. At short time points (2-4 weeks), both the free peptide and the peptide in nanoparticles and microparticles significantly suppresses choroidal NV; however, at time points longer than 1 month, there was good suppression by the

encapsulated peptide but not the free peptide (**Figure 7.6**). A single injection of the encapsulated peptide inhibited choroidal NV for at least 14 weeks. It is important to note that even though the microparticle groups contain the same total peptide dose as the free peptide dose, and only release a small fraction of peptide at a given time point, the microparticle group performed similarly to free peptide at the early time points (<1 month). This demonstrates both that the peptide is potent at low doses and that controlled constant release, rather than injection of a bolus, may be especially advantageous for treating NVAMD. Fundus photographs showed slow disappearance of the microparticles from mouse eyes that correlated well with the duration of bioactivity (**Figure 7.7**).

7.4 Discussion

The eye is a relatively isolated tissue compartment and local delivery can facilitate high drug levels within the eye and low systemic levels in other tissues. Systemic administration of VEGF antagonists in patients with cancer provides some benefits, but also has potential complications including hypertension, thromboembolic events, and renal damage [21, 22]. These problems have been largely circumvented in patients with NVAMD by intravitreous injections of VEGF antagonists, which neutralize VEGF in the eye for 1-2 months in most patients with little effect on systemic VEGF levels. However, a month after injection of ranibizumab and possibly as long as 2 months after an injection of aflibercept, VEGF is no longer neutralized causing recurrent leakage and collection of fluid in the macula that reduces vision. Timely reinjection of a VEGF antagonist can stop leakage allowing vision to be regained, but failure to re-inject allows

growth of the NV, recruitment of retinal pigmented epithelial cells and glia, and scarring that damages photoreceptors resulting in permanent reduction in vision. Attempts to reduce follow up and frequency of anti-VEGF injections have resulted in poorer visual outcomes than those achieved with monthly injections. Therefore, sustained suppression of choroidal NV is needed to achieve the best long-term outcomes in patients with NVAMD, and this is difficult to sustain with current treatments that require very frequent follow up and injections.

In this study, we have demonstrated sustained suppression of choroidal NV for at least 14 weeks after a single injection of an anti-angiogenic peptide encapsulated in nanoparticles and microparticles. Specifically, we report on the efficacy of an anti-angiogenic serpin-derived peptide, SP6001, to treat AMD and its improved long-term efficacy *in vivo* when released from a biodegradable drug delivery system composed of PBAE nanoparticles in PLGA microparticles. The peptide SP6001 shows anti-angiogenic efficacy comparable to a recently approved AMD therapeutic, aflibercept, using the same mouse model [23]. Statistically significant suppression of choroidal NV was caused by the microparticles encapsulating peptide compared to empty control microparticles for at least 14 weeks after a single intravitreal injection. The degradation rate of the particles *in vivo* was observed to be faster (approximately twice as fast) as what was observed *in situ*. This is not unexpected as the *in vivo* microenvironment in the eye contains additional degradative enzymes and clearance mechanisms that are not captured in an *in situ* degradation experiment. Biomaterial modification (i.e. PLGA copolymer composition) can be used to further slow degradation rate if needed.

PLGA, a biodegradable polymer that has been used in FDA approved devices, has been used to deliver a number of different drugs in the eye and has been shown to be generally well tolerated [11, 24, 25]. For example, Shelke et al. have observed safe and sustained release of an encapsulated hydrophilic drug *in vivo* [24]. Mordenti et al. delivered a humanized antibody encapsulated in PLGA to rabbit eyes and observed some initial immune response, but no resulting safety issues [26]. Pan et al. have shown long-term release of PLGA-encapsulated bevacizumab in a similar laser photocoagulation model in rats over the course of a few weeks [27]. In this study they observed a statistically significant decrease in CNV area at four weeks and at eight weeks post-injection, but not at six weeks post-injection. In another example, Xu et al. delivered dexamethasone acetone loaded PLGA nanoparticles using a rat laser photocoagulation model and observed inhibition of CNV [28]. However, here we show a peptide controlled release system that maintains anti-angiogenic activity in this laser-induced choroidal neovascularization model that lasts for at least 14 weeks following a single injection. In this manuscript, we report a potent anti-angiogenic peptide for NVAMD, SP6001, and a biodegradable polymeric particle delivery system able to maintain long-term peptide efficacy in the eye.

7.5 Conclusion

We have demonstrated that the combination of a novel serpin-derived peptide and its polymeric delivery system is promising as a potential therapeutic for NVAMD. The peptide is able to inhibit angiogenesis through multiple mechanisms including interfering

with proliferation, adhesion, and migration. The peptide has anti-angiogenic efficacy in mice with choroidal NV that peaks at ~50% inhibition at 2 weeks and persists for an additional two weeks. By complexing the serpin-derived peptide with a poly(beta-amino ester) to form nanoparticles and then encapsulating these nanoparticles within PLGA microparticles, inhibition of angiogenesis using the same peptide dose can be extended to at least 14 weeks following a single intravitreal injection. The particles are made of safe, hydrolytically degradable polymers and have low endotoxin. By delivering the peptide in a long-term release system, this treatment may potentially be able to improve patient outcomes, both by sustaining suppression of choroidal NV for long periods and through the action of a multimodal anti-angiogenic therapeutic.

7.6 Acknowledgements

The authors thank the Edward N. & Della L. Thome Memorial Foundation (Bank of America, Trustee) Awards Program in AMD Research, the NIH (1R21EY022986-01 and R01EY012609), and the Wallace H. Coulter Foundation for support of this work.

7.7 Disclosure

JJG and ASP are co-founders and officers of AsclepiX Therapeutics, LLC; Potential conflicts of interest are managed by the Johns Hopkins Medical Institutions Committee on Outside Interests.

7.8 Figures

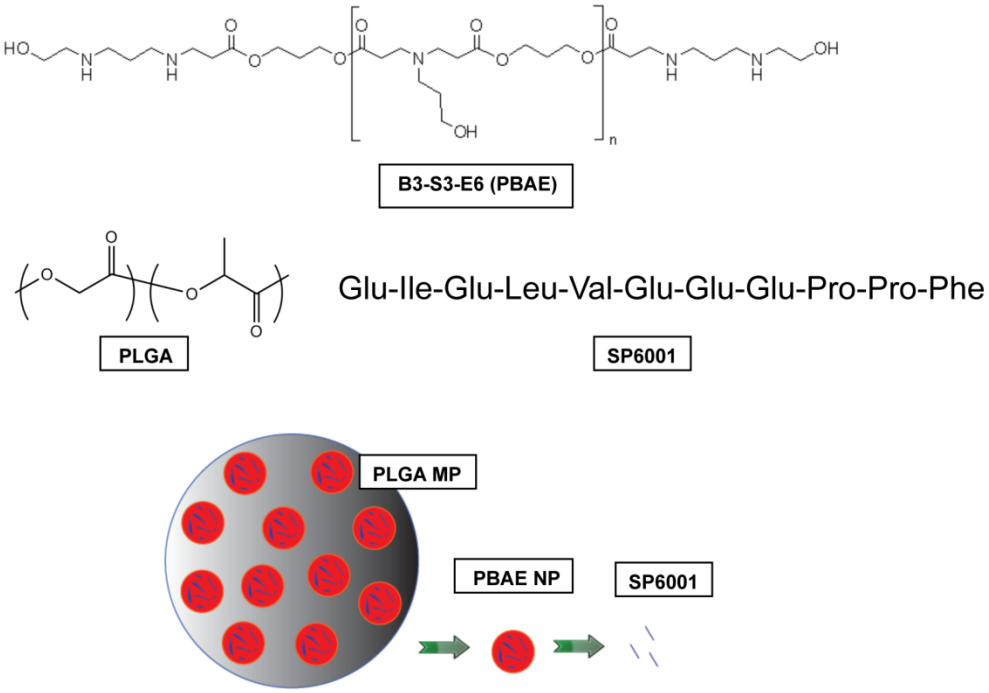

Figure 7.1. Polymer, peptide, and particle structures. Structure of PBAE (B3-S3-E6), structure of PLGA, SP6001 peptide sequence, and the peptide particle delivery system.

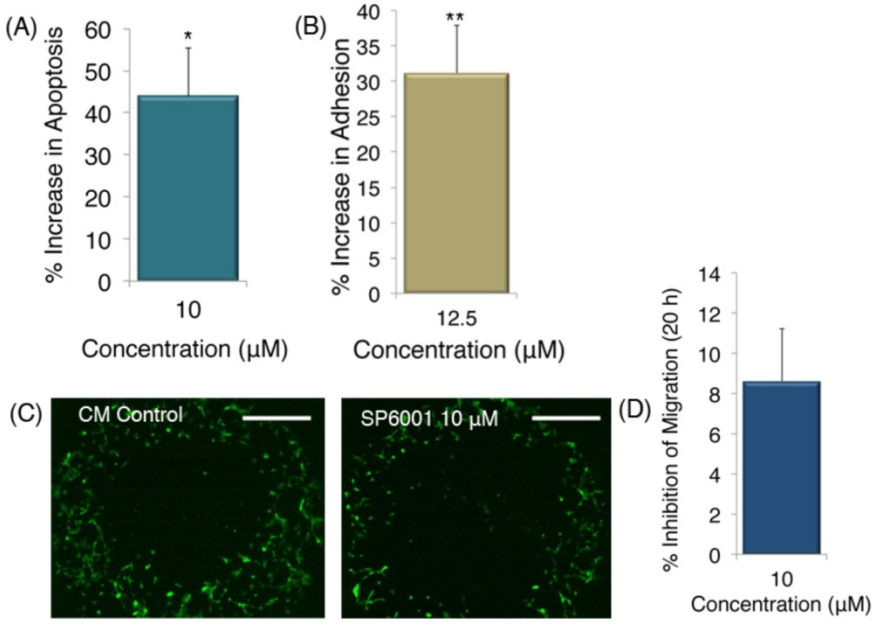

Figure 7.2. SP6001 effects on HRECs. **(A)** SP6001 evaluated in the caspase-glo 3/7 assay to measure apoptosis, normalized to the negative control. **(B)** ACEA cell migration

assay. Values are scaled to percent increase above the negative control (complete endothelial cell media), at the 10 hour time point, **(C)** Platypus cell migration assay. Digital micrographs are shown representative of each condition. Scale bars represent 500 μm. **(D)** Quantification from the cell migration assay. Values are significant for *p<0.05.

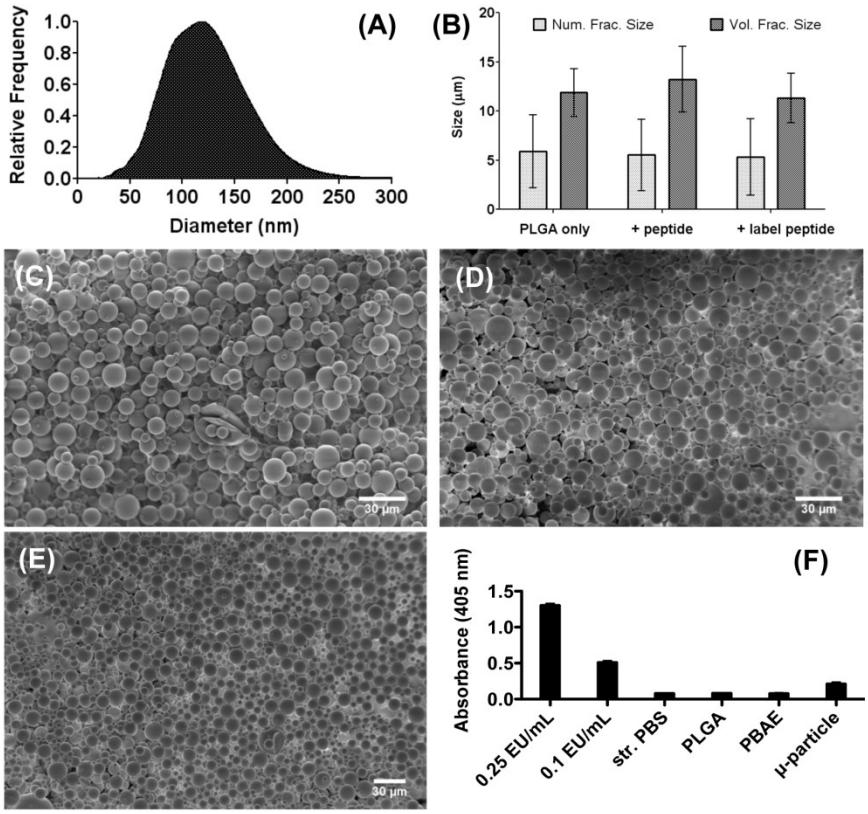

Figure 7.3. Peptide delivery system characterization. **(A)** Nanoparticle formation between the SP6001 peptide and PBAE B3-S3-E6, as measured by NanoSight NTA. The mode of the particle distribution is 119 nm. SEM of microparticles, **(B)** ImageJ size quantification. Error bars represent standard deviations of the mean of each sample, **(C)** Empty microparticles with aqueous phase only, **(D)** Microparticles encapsulating peptide SP6001/PBAE B3-S3-E6 nanoparticles, **(E)** Microparticles encapsulating peptide FITC-SP6001/PBAE B3-S3-E6 nanoparticles, **(F)** Limulus amebocyte lysate endotoxin assay test performed on LPS controls, as well as polymer and microparticle samples. All polymeric samples contained less than the 0.1 EU/mL control and are comparable to sterile PBS. Error bars represent standard deviation of the mean of each sample.

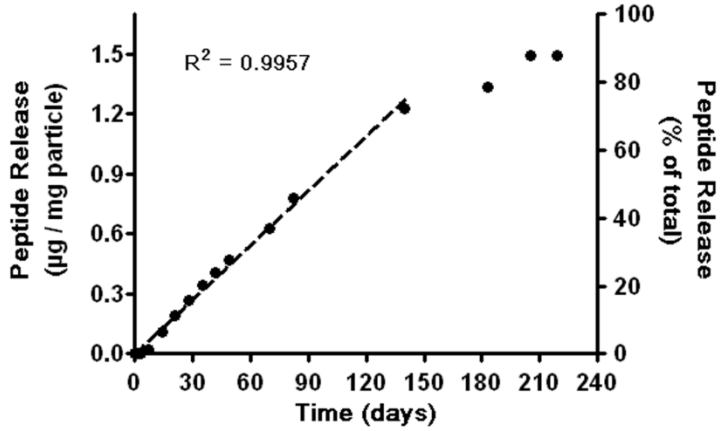

Figure 7.4. Microparticle release profile. Microparticles are loaded with FITC-SP6001/B3-S3-E6 nanoparticles and release experiments are performed in phosphate buffered saline at 37°C on a shaker.

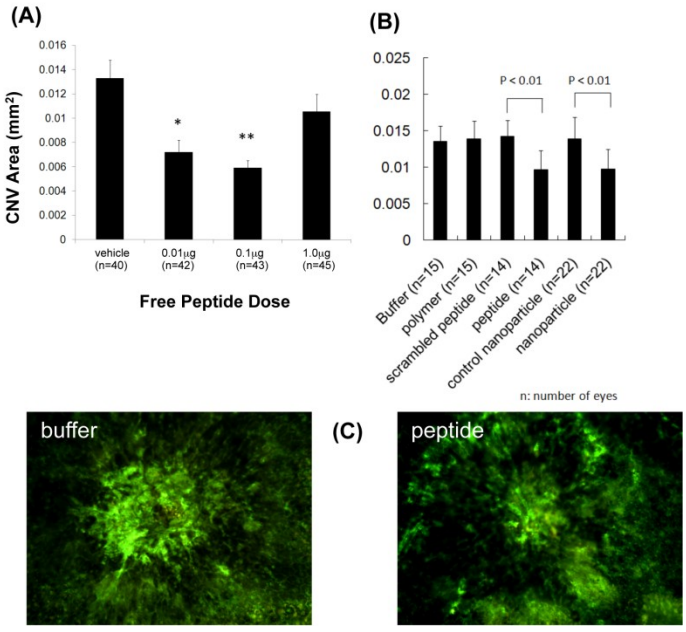

Figure 7.5. *In vivo* efficacy of peptide and nanoparticles. *In vivo* fluorescein isothiocyanate-dextran stained mouse eyes were analyzed in the laser-induced CNV model. **(A)** Free peptide injections, * = $p < 0.05$, ** = $p < 0.01$. **(B)** Polymer, peptide, and nanoparticle injections including polymer = B3-S3-E6, nanoparticle = B3-S3-E6 + SP6001, control nanoparticle = B3-S3-E6 + scrambled SP6001. **(C)** Representative fluorescence micrographs from buffer injected and peptide injected conditions.

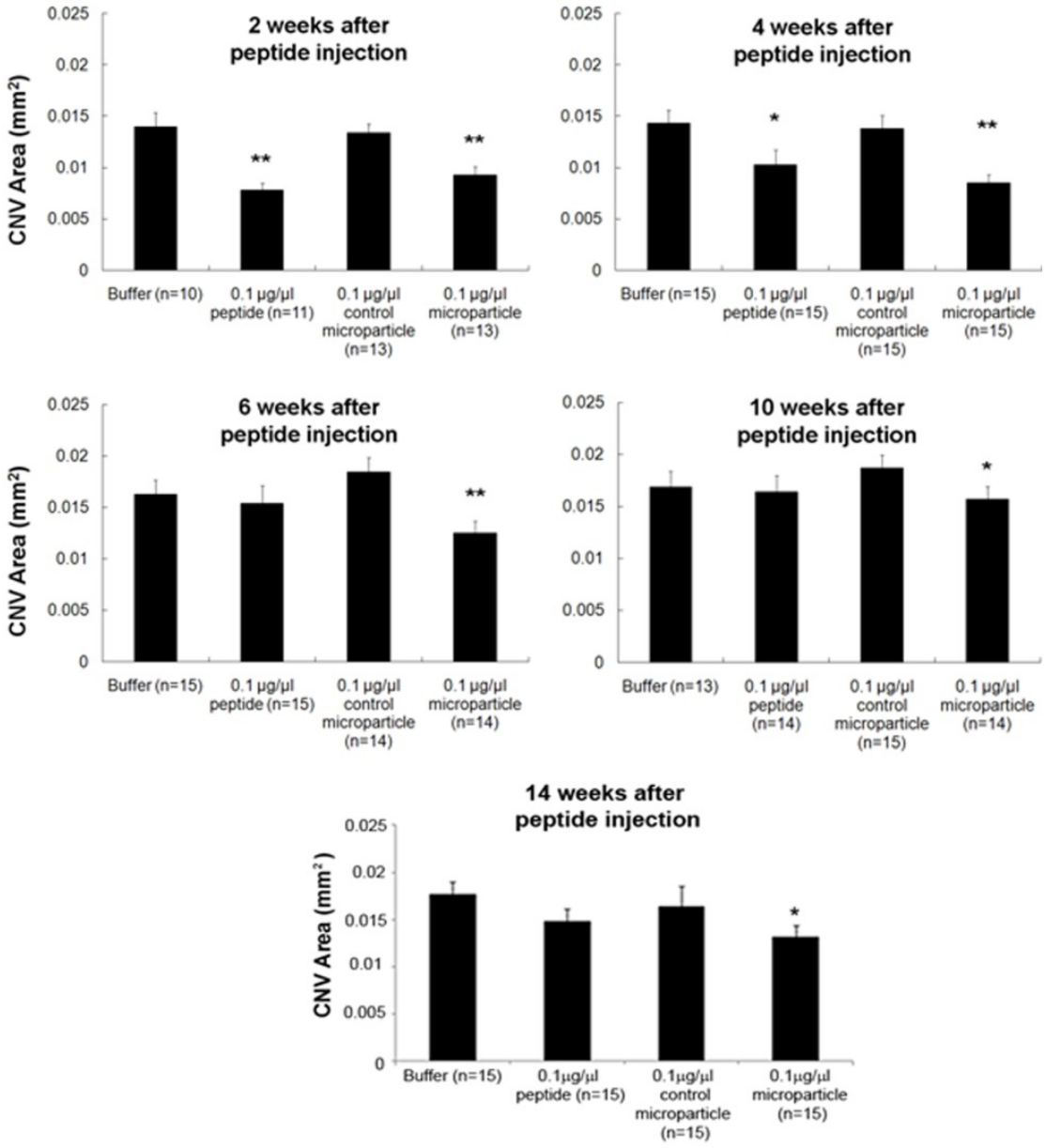

Figure 7.6. *In vivo* efficacy of microparticles. *In vivo* fluorescein isothiocyanate-dextran stained mouse eyes were analyzed in the laser-induced CNV model. "Control microparticles" do not contain peptide whereas "0.1 µg/µl microparticles" contain 0.1 µg of peptide per injection. * = $p < 0.05$, ** = $p < 0.01$.

Figure 7.7. Persistence of microparticles *in vivo*. Fundus photographs showed slow degradation of the microparticles in the mouse eyes over 18 weeks.

7.9 References

1. Folkman J. Tumor angiogenesis: therapeutic implications. N Engl J Med 1971;285(21):1182-1186.

2. Bressler SB. Introduction: Understanding the role of angiogenesis and antiangiogenic agents in age-related macular degeneration. Ophthalmology 2009;116(10 Suppl):S1-7.

3. Distler JH, Hirth A, Kurowska-Stolarska M, Gay RE, Gay S, Distler O. Angiogenic and angiostatic factors in the molecular control of angiogenesis. Q J Nucl Med 2003;47(3):149-161.

4. Holash J, Davis S, Papadopoulos N, Croll SD, Ho L, Russell M, et al. VEGF-Trap: a VEGF blocker with potent antitumor effects. Proc Natl Acad Sci U S A 2002;99(17):11393-11398.

5. Heier JS, Brown DM, Chong V, Korobelnik JF, Kaiser PK, Nguyen QD, et al. Intravitreal aflibercept (VEGF Trap-Eye) in wet age-related macular degeneration. Ophthalmology 2012;119:2537-2548.

6. Karagiannis ED, Popel AS. A systematic methodology for proteome-wide identification of peptides inhibiting the proliferation and migration of endothelial cells. Proc Natl Acad Sci U S A 2008;105(37):13775-13780.

7. Koskimaki JE, Karagiannis ED, Rosca EV, Vesuna F, Winnard PT, Jr., Raman V, et al. Peptides derived from type IV collagen, CXC chemokines, and thrombospondin-1 domain-containing proteins inhibit neovascularization and suppress tumor growth in MDA-MB-231 breast cancer xenografts. Neoplasia 2009;11(12):1285-1291.

8. Koskimaki JE, Rosca EV, Rivera CG, Lee E, Chen W, Pandey NB, et al. Serpin-derived peptides are antiangiogenic and suppress breast tumor xenograft growth. Transl Oncol 2012;5(2):92-97.

9. Saladin PM, Zhang BD, Reichert JM. Current trends in the clinical development of peptide therapeutics. IDrugs : the investigational drugs journal. 2009;12:779-84.

10. Kim H, Csaky KG. Nanoparticle-integrin antagonist C16Y peptide treatment of choroidal neovascularization in rats. J Control Release 2010;142(2):286-293.

11. Li F, Hurley B, Liu Y, Leonard B, Griffith M. Controlled release of bevacizumab through nanospheres for extended treatment of age-related macular degeneration. Open Ophthalmol J 2012;6:54-58.

12. Campochiaro PA, Hafiz G, Shah SM, Bloom S, Brown DM, Busquets M, et al. Sustained ocular delivery of fluocinolone acetonide by an intravitreal insert. Ophthalmology 2010;117(7):1393-1399 e1393.

13. Lee JH, Pidaparti RM, Atkinson GM, Moorthy RS. Design of an implantable device for ocular drug delivery. J Drug Deliv 2012;2012:527516.

14. Yasukawa T, Kimura H, Kunou N, Miyamoto H, Honda Y, Ogura Y, et al. Biodegradable scleral implant for intravitreal controlled release of ganciclovir. Graefes Arch Clin Exp Ophthalmol 2000;238(2):186-190.

15. Green JJ, Zugates GT, Tedford NC, Huang YH, Griffith LG, Lauffenburger DA, et al. Combinatorial modification of degradable polymers enables transfection of human cells comparable to adenovirus. Advanced Materials 2007;19(19):2836-2842.

16. Shmueli RB, Sunshine JC, Xu Z, Duh EJ, Green JJ. Gene delivery nanoparticles specific for human microvasculature and macrovasculature. Nanomedicine 2012;8(7):1200-1207.

17. Tzeng SY, Hung BP, Grayson WL, Green JJ. Cystamine-terminated poly(beta-amino ester)s for siRNA delivery to human mesenchymal stem cells and enhancement of osteogenic differentiation. Biomaterials 2012;33(32):8142-8151.

18. Green JJ, Langer R, Anderson DG. A combinatorial polymer library approach yields insight into nonviral gene delivery. Acc Chem Res 2008;41(6):749-759.

19. Tobe T, Ortega S, Luna JD, Ozaki H, Okamoto N, Derevjanik NL, et al. Targeted disruption of the FGF2 gene does not prevent choroidal neovascularization in a murine model. Am J Pathol 1998;153(5):1641-1646.

20. Mori K, Duh E, Gehlbach P, Ando A, Takahashi K, Pearlman J, et al. Pigment epithelium-derived factor inhibits retinal and choroidal neovascularization. J Cell Physiol 2001;188(2):253-263.

21. Miki K, Miki A, Matsuoka M, Muramatsu D, Hackett SF, Campochiaro PA. Effects of intraocular ranibizumab and bevacizumab in transgenic mice expressing human vascular endothelial growth factor. Ophthalmology 2009;116(9):1748-1754.

22. Escalante CP, Zalpour A. Vascular endothelial growth factor inhibitor-induced hypertension: basics for primary care providers. Cardiol Res Pract 2011;2011:816897.

23. Saishin Y, Takahashi K, Lima e Silva R, Hylton D, Rudge JS, Wiegand SJ, et al. VEGF-TRAP(R1R2) suppresses choroidal neovascularization and VEGF-induced breakdown of the blood-retinal barrier. J Cell Physiol 2003;195(2):241-248.

24. Shelke NB, Kadam R, Tyagi P, Rao VR, Kompella UB. Intravitreal poly(L-lactide) microparticles sustain retinal and choroidal delivery of TG-0054, a hydrophilic drug intended for neovascular diseases. Drug Deliv Transl Res 2011;1(1):76-90.

25. Short BG. Safety evaluation of ocular drug delivery formulations: techniques and practical considerations. Toxicol Pathol 2008;36(1):49-62.

26. Mordenti J, Thomsen K, Licko V, Berleau L, Kahn JW, Cuthbertson RA, et al. Intraocular pharmacokinetics and safety of a humanized monoclonal antibody in rabbits after intravitreal administration of a solution or a PLGA microsphere formulation. Toxicol Sci 1999;52(1):101-106.

27. Pan CK, Durairaj C, Kompella UB, Agwu O, Oliver SC, Quiroz-Mercado H, et al. Comparison of long-acting bevacizumab formulations in the treatment of choroidal neovascularization in a rat model. J Ocul Pharmacol Ther 2011;27(3):219-224.

28. Xu J, Wang Y, Li Y, Yang X, Zhang P, Hou H, et al. Inhibitory efficacy of intravitreal dexamethasone acetate-loaded PLGA nanoparticles on choroidal neovascularization in a laser-induced rat model. J Ocul Pharmacol Ther 2007;23(6):527-540.

Chapter 8

Biodegradable Particles Containing a Collagen IV-Derived Peptide for Treatment of Ocular Neovascularization and Macular Edema

8.1 Introduction

Aberrant angiogenesis plays an important role in a number of eye diseases, including neovascular age-related macular degeneration (NVAMD) and macular edema (ME). While a host of genetic and environmental factors may lead to the development of such diseases, much of the vision loss occurs during advanced phases when aberrant angiogenesis causes leakage and subsequent damage to the macula. Diabetic macular edema (DME) is the leading cause of vision loss and blindness in the working-age population [1]. In the case of DME, if left untreated, 25% to 30% of patients suffer at least moderate vision loss, with many eventually going blind [2]. NVAMD is the leading cause of severe vision loss in patients over the age of 60 [3]. In both cases, a number of molecular factors may be involved, with vascular endothelial growth factor (VEGF) playing a critical role [4]. Therefore, blocking the action of VEGF has been widely investigated to treat these diseases. Currently approved therapeutics for NVAMD and ME, such as ranibizumab (along with off-label use of bevazicumab), and aflibercept, all work through this mechanism. While these therapies can halt the progression of the disease,

they require monthly, or bi-monthly, intravitreal injections to prevent further loss of vision.

There are a number of endogenous anti-angiogenic proteins that balance the actions of VEGF, and other pro-angiogenic factors [4]. Using a combination of computational and experimental techniques, groups have discovered, and then further developed, anti-angiogenic proteins and peptides with these various anti-angiogenic properties [5, 6]. One class of these peptides, the serpin-derived peptides, have been shown to be effective for inhibiting choroidal neovascularization (CNV) in a clinically relevant laser-induced CNV-AMD mouse model [7-9]. In order to reduce the number of injections required for therapy, one of these serpin-derived peptides was encapsulated in a biodegradable polymeric microparticle system [9]. Long-term efficacy up to 14-weeks was demonstrated with a single injection. This long-term efficacy is important since frequent intravitreal injections can both reduce patient compliance and increase the probability of damage due to intravitreal injections [10].

Another class of peptides, the collagen-IV derived peptides, has been shown to have very strong anti-angiogenic effects both *in vitro* and *in vivo* in mouse cancer models [11]. These peptides have a few advantages over the previously published serpin-derived peptide work. The biological pathway by which the collagen-IV derived peptides work has been partly elucidated. This is important for translating a therapeutic to the clinic. In this case, these peptides are able to interact with both integrin and integrin-connected complexes that leads to altering of cellular proliferation, adhesion, and migration [5, 12-

14]. Here it will be shown that these peptides also show additional anti-angiogenic properties in the eye in a number of relevant and important animal models.

In order to incorporate these peptides in a long-term release system, they are encapsulated into biodegradable polymeric microparticles. As previously described, these peptides are encapsulated using poly(lactide-co-glycolide) (PLGA) [9], a generally regarded as safe (GRAS) substance as defined by the FDA. Different versions of PLGA are tested in order to extend the release window of the peptide. This long-term release strategy further enhances the clinical relevance of the system described here, allowing for fewer injections of a potentially more efficacious anti-angiogenic therapy.

8.2 Materials and Methods

8.2.1 Materials

PLGA [Poly(D,L-lactide-co-glycolide); lactide:glycolide (65:35), Mw 40k–75k; lactide:glycolide (75:25), Mw 76k-115k; lactide:glycolide (85:15), Mw 190k-240k], DMSO [Dimethylsulfoxide], DCM [Dichloromethane], and acriflavine were purchased from Sigma (St. Louis, MO). PVA [Poly(vinyl alcohol); Mw 25,000] was purchased from Polysciences (Warrington, PA). Peptide (SP2043) was purchased from New England Peptide (Gardner, MA).

8.2.2 Microparticle formation

PLGA was first dissolved into DCM, at 20 mg/mL in a test tube and vortexed to fully dissolve. Peptide stock in DMSO (20 mg/mL) was micropipetted to the PLGA/DCM solution. The initial mass ratio of peptide to PLGA can vary; common formulations are 1:50 and 1:20 peptide:PLGA. Similarly, for the test microparticles loaded with acriflavine, acriflavine in DMSO was added to the PLGA/DCM solution. For blank microparticle, equivalent volume of DMSO only was pipetted. The mixture was sonicated with the test tube on ice. Sonication (Misonix) was performed with an amplitude setting of '30', which equals approximately 5-10 W, for 20 seconds. This primary emulsion was immediately poured into 50 mL of 1% PVA solution and homogenized (Ika T25 digital Ultra-Turrax) at 3.6-3.8 krpm for 1 minute. The full volume was then transferred to 100 mL of 0.5% PVA solution and stirred in a chemical hood for about 3.5 hours. Three wash steps were then performed. For each wash step, the microparticle solution was centrifuged at 4°C, 4 krpm, for 5 minutes, and then the supernatant was removed. Subsequently, 40 mL of refrigerated Milli-Q water was added, the microparticle pellet was resuspended and the washing steps were repeated. After the last centrifugation step, 5 mL of water was added to resuspend the sample. Samples were snap frozen in liquid nitrogen and immediately placed in a lyophilizer. Following lyophilization, all microparticles were stored at -20°C.

8.2.3 Scanning electron microscopy (SEM) characterization

Lyophilized particles were placed on carbon tape (Electron Microscopy Sciences, Hatfield, PA) placed on aluminum mounts. Samples were sputtered with gold-palladium, and SEM imaging was performed with a LEO/Zeiss FESEM at the JHU School of

Medicine MicFac. Sizing of microparticle samples was performed with ImageJ analysis of SEM images.

8.2.4 Microparticle loading and release quantification

To measure loading, a known mass of microparticles was dissolved in DMSO. For acriflavine loaded microparticles, the fluorescence of the dissolved sample was measured using a BioTek Synergy 2 plate reader with an excitation filter of 485 +/- 20 nm and an emission filter of 528 +/- 20 nm. Quantification was performed by comparison with an acriflavine standard in DMSO. For peptide loaded microparticles, and corresponding blank microparticles, quantification was performed by running gel electrophoresis (Bio-Rad Mini-PROTEAN system) and silver stain analysis (Invitrogen). A 12-well 10-20% Mini-PROTEAN tris-tricine gel was used (Bio-Rad), along with 10x tris/tricine/SDS running buffer (Bio-Rad) diluted to 1x in Milli-Q water. Each gel contained a standard series of a known amount of peptide. The peptide standard series included 0, 62.5, 125, 250, and 500 ng of peptide per well. The remaining wells included a protein standard, and the microparticle samples, both peptide loaded and blanks as controls. The DMSO samples were mixed 1:1 by volume with sample buffer. Sample buffer was made of 24% glycerol in 1x PBS. Gel electrophoresis was run until the 2.5 kDa band of the protein standard traveled approximately two-thirds of the way down the gel. The silver stain protocol was followed for gel staining. For the development step, the stop solution was added once the lowest peptide standard (in this case 62.5ng) began to appear. Gel images were captured with a digital camera and analyzed with ImageJ using gel band intensity quantification functionality.

To measure release, a known mass of microparticles was suspended in 1x PBS, placed on a shaker in a 37 ºC oven. At various time points, samples were centrifuged for 5 min at ~2.5 krcf. Supernatant was collected and stored at -80 ºC, and fresh PBS was added to samples. For acriflavine loaded microparticles, released acriflavine was quantified by measuring fluorescence as described above. For peptide loaded microparticles, released peptide was quantified using gel electrophoresis and silver staining, as described above. For peptide loaded microparticles, two different release experiments were performed. The first release experiment contained only 65/35 PLGA, and microparticles were suspended in PBS at 100 mg/mL. In the second release experiment, with both 65/35 and 85/15 PLGA, microparticles were suspended at 20 mg/mL in 1x PBS with 0.01% sodium azide and 0.01% polysorbate 20 (w/v %).

8.2.5 Laser-induced choroidal neovascularization mouse model

Choroidal NV was induced by laser photocoagulation-induced rupture of Bruch's membrane, as previously described [9, 15]. Briefly, 5- to 6-wk-old female C57BL/6 mice were anesthetized with ketamine hydrochloride and pupils were dilated. Laser photocoagulation was performed in the 9, 12, and 3 o'clock positions of the posterior pole of each eye. Only burns in which a bubble was produced, indicating a ruptured Bruch's membrane, were included in the study. Laser photocoagulation was performed at various time points after intravitreous injection (of 1.0 μL of peptide, alfibercept, buffer without peptide/aflibercept, microparticles containing peptide, or empty microparticles; for peptide groups at 1 μg/μL, for aflibercept at standard concentration), 14 days before the final end-point. After 14 days, at the final end-point time, the mice were perfused with 1

mL of PBS containing 50 mg/mL of fluorescein-labeled dextran (2×10^6 Da average molecular mass; Sigma–Aldrich, St. Louis, MO, USA) and choroidal flat mounts were examined by fluorescence microscopy. Image analysis software (Image-Pro Plus; Media Cybernetics, Silver Spring, MD, USA) was used to measure the area of choroidal NV at each rupture site. Intravitreous injections were done under a dissecting microscope with a Harvard Pump Microinjection System (Harvard Apparatus, Holliston, MA, USA) and pulled glass micropipettes, as previously described [16].

8.2.6 Macular edema mouse model

See reference [17] for full details on both development of the transgenic mouse model, as well as mouse disease model induction. Briefly, 1 μL of either peptide, aflibercept, buffer without peptide/aflibercept, microparticles containing peptide, or empty microparticles, was injected into transgenic mice. Three days before final assay time point, mice were given drinking water containing doxycycline. At final time points, eyes were evaluated by fundus photography, ocular coherence tomography (OCT), and histological analysis.

8.3 Results

Collagen-IV derived peptides have previously been shown to have potent anti-angiogenic effects *in vitro* and *in vivo* in mouse cancer models [11, 14]. Here, the specific biomimetic peptide SP2043 was first tested for its anti-angiogenic efficacy in various eye disease models. Further, the efficacy over time of both peptide and a slow-release

formulation of the peptide were tested. Long-term release was achieved by encapsulating the peptide into PLGA microparticles. These microparticles were made by a double emulsion technique commonly employed. Initially, 65/35 PLGA was used to make microparticles. **Figure 8.1A-C** shows SEM images of these microparticles made with an initial peptide:PLGA mass ratio of 0, 1:50, and 1:20. Loading quantification indicated a loading efficiency of about 20%. The number average diameter of all of these microparticles was about 5 μm as quantified by ImageJ analysis (**Figure 8.1D**).

Release of the peptide in an *in vitro* system was measured and found to last around 10 months (**Figure 8.2**). The release experiment was performed in microcentrifuge tubes with PBS, placed in a 37ºC oven on a shaker. The release profile showed a relatively linear portion over the first few months, followed by a slow-down of release, and ending with a final burst. This profile is not uncommon for PLGA-based release systems [18].

Peptide, peptide encapsulated in microparticles, and aflibercept were then tested for their ability to inhibit CNV in a laser-induced CNV mouse model (**Figure 8.3**). Samples were intravitreally injected on day 0, with laser-induction performed two weeks before the final assay time point. Representative images, as well as quantification of corresponding CNV, are shown in **Figure 8.3A**. These results show that after two weeks, SP2043 inhibits CNV better than aflibercept at a standard dose. Additionally, the amount of peptide released has a statistically significant effect compared to blank microparticles and seems to have a comparable effect to aflibercept at this time point. In **figure 8.3B-D**, free and encapsulated peptide were injected and CNV was quantified at various time

points. As expected, free peptide efficacy decreases over time, while peptide released from microparticle maintains its efficacy over time. However, by 12 weeks, the efficacy disappears. Fundus images (not shown here) seem to indicate that microparticles are no longer around in the eye, matching this activity result.

In order to increase the residence time of the microparticle samples in the eye, PLGA with different lactide:glycolide ratios were investigated. PLGA with L/G ratios of 65/35, 75/25, and 85/15 were used to make microparticles encapsulating the fluorescent molecule acriflavine. Release was quantified over time (**Figure 8.4**). Release over the first few months was similar across groups, after which a separation can be observed between the groups, with the 85/15 microparticles released acriflavine most slowly, as expected.

85/15 PLGA was then used in order to encapsulate SP2043 for further experiments. SEM imaging was performed to confirm microparticle formation (**Figure 8.5**). These microparticles, along with free peptide and aflibercept, were again tested in the laser-induced CNV mouse model. As expected, efficacy of free peptide and aflibercept decreased over time. On the other hand, the efficacy of the microparticle sample maintains efficacy over time, and some efficacy lasts until 16 weeks. Note that the total initial dose of the peptide in the free and encapsulated case is the same. In order to test the ability of the free and encapsulated peptide to treat macular edema, a doxocyclin-induced, tet/VEGF/opsin genetic mouse model was used. This is a particularly aggressive model where induction of VEGF causes complete retinal detachment in the mice. Free peptide strongly inhibits retinal detachment (data to be

shown in future publication). Encapsulated peptide also can inhibit retinal detachment at the two week, and to some extent also the two month time point (**Figure 8.7**).

For larger animal testing, a functional rabbit assay was developed by Dr. Campochiaro's lab. Data in a future publication will show that the peptide inhibits this NV at least as well as aflibercept. In the next step, blank 85/15 PLGA microparticles were injected into the rabbit eye in order to see how these microparticles might distribute throughout the eye, as well as to track these particles over time. The goal was to inject the microparticles inferiorly so that they form a depot out of the visual axis so as not to prevent vision. **Figure 8.8** shows that this is possible, with a microparticle mass observed in the inferior region, while none in the visual axis of the rabbit eye. In one of two rabbits tested, the microparticle mass can be observed one month after injection in the same place. The rabbits are allowed to move freely during this time. The rabbits were sacrificed after one month, with various parts of the eye, including the microparticle mass collected. The microparticle mass was taken in order to visualize with SEM (**Figure 8.9**) One can still observe the microparticles intact and comparable to pre-injected microparticles. As can be seen in **Figure 8.9**, the sizes of the microparticle groups are similar.

8.4 Discussion

The ability to translate a therapeutic to the clinic is dependent on a number of factors. Efficacy must be validated on multiple scales, from *in vitro* cell cultures, to *in*

vivo pre-clinical models, and finally in clinical trials. The biological pathway of activity should also be elucidated. Additionally, the therapeutic needs to be active at a level where there is minimal toxicity. Ideally, the therapy is also one that is easy for patients to comply with and reduces any side-effects of the therapy itself or the route by which it is administered. In this chapter, a delivery system is described that was developed in a collaborative effort with the labs of Dr. Popel and Dr. Campochiaro, one that attempts to address all of these important criteria.

The peptide, SP2043, was previously shown to have potent anti-angiogenic effects in a number of *in vitro* assays [14]. SP2043 was shown to decrease human umbilical vein endothelial cell (HUVEC) viability, inhibit HUVEC migration, as well as inhibit tube formation of HUVECs, microvascular endothelial cells (MECs), and lymphatic endothelial cells (LECs). The study also revealed some of the biological pathways that this peptide affects. In MECs, SP2043 blocks both HGF- and IGF-induced receptor tyrosine kinase activities, pathways involved in various angiogenic effects. The peptide does this by interfering with the various protein complexes required to form for the activation of these receptor tyrosine kinases. One such partner in these complexes is integrin β1, previously also shown to be a target of an earlier version of this peptide [19]. In relation to the earlier collagen-IV peptide, SP2043 was designed to be easier to manufacture, while retaining its biological properties.

The activity of SP2043 is shown here to extend to *in vivo* models. Importantly, the mouse models used are clinically relevant ones. For example, the laser-induced CNV model was used to accurately predict efficacy of the most recently approved therapy

aflibercept [8]. Here it is shown that SP2043 has efficacy at least as potent as aflibercept (**Figure 8.3**). In addition to inhibiting CNV, these peptides show the ability to prevent retinal detachment in a particularly aggressive model of macular edema [17].

In order to further improve the therapy, SP2043 was encapsulated into PLGA microparticles. Currently approved therapeutics need to be injected intravitreally monthly or bi-monthly. Such a procedure reduces patient compliance, which is a problem since repeated dosing is required to prevent further vision loss [4]. Further, repeated injections can potentially cause adverse events to the patients [10]. Peptide therapeutics are known to have shorter half-lives, and, as can be seen in **Figure 8.3**, efficacy of free peptide decreases over time. Therefore, a long-term releasing peptide system can be an important advance in the treatment of ocular diseases such as AMD and ME.

PLGA is used in a many biomedical applications, has a long track record of being safe in humans, and is therefore a GRAS substance as classified by the FDA for various applications. Previous work has shown that PLGA can be well tolerated in the eye with *in vivo* models [20]. Other research has shown that there can be an initial inflammation response to particles and this response dissipates over a few weeks [21]. It is likely the case that the amount and extent of inflammation will depend on the amount of PLGA in the eye, the way it is injected, the version of PLGA used, and the type of particle that is made. Therefore, while PLGA has been shown to be safe in the eye in some cases, toxicity tests are of course still necessary. While no overall signs of toxicity were noticed in the described experiments, further safety studies are required. One other issue is that the injected particle system should not remain in the visual axis so that vision would not

be blocked. While there have been some observed cloudiness in nanoparticle injections, this can be avoided in microparticle injections [22]. Here, in a more physiologically relevant rabbit model [23], the microparticles are injected inferiorly in the eye (**Figure 8.8**). Although the rabbits are free to move around, the microparticle bolus remains in the same position as where it was injected, and, most importantly, out of the visual axis. The microparticles retain their approximate shape and size over the course of one month in the rabbit (**Figure 8.9**), indicating the potential for long-term release in the rabbit, and then possibly also in human patients.

The microparticle delivery system showed release of the peptide *in vitro* over the course of many months (**Figure 8.2**). However, i*n vitro* release systems might not always recapitulate the *in vivo* environment well enough. While efficacy of both free peptide and aflibercept decrease over time in the laser-induced CNV model (**Figure 8.3**, and **Figure 8.6**), a single injection of microparticle encapsulated peptides retains efficacy over time (**Figure 8.3** and **Figure 8.6**). The extent of efficacy can be modulated by altering the structure of PLGA used to make the microparticles. Increasing the L:G ratio extended the efficacy over time as seen in **Figure 8.6**. Efficacy was also observed at the two month time point in the aggressive macular edema mouse model (**Figure 8.7**). Future experiments will include testing the long-term improvements in efficacy in rabbit models.

An important point is that in all of these experiments, the total injected dose of peptide in the microparticle case was the same as for the free peptide groups. Therefore, for the controlled release formulations, there is less peptide available to the eye at any given time compared to bolus injection. Future experiments will investigate higher

loading and the effect of dosage. Peptide releasing microparticles may be a viable treatment strategy for NVAMD and ME.

8.5 Conclusion

A collagen-IV derived peptide, SP2043, was shown to have potent anti-angiogenic effects in various relevant animal models. In a CNV mouse model, SP2043 significantly inhibits NV, while also showing an ability to regress already formed NV. In a VEGF-inducible model, an aggressive macular edema model, SP2043 is able to prevent retinal detachment. Additionally, this peptide efficacy was shown to be at least as good as that of the leading approved therapeutic, aflibercept. The peptide was also successfully encapsulated in PLGA microparticles. These microparticles were able to release the peptide over many months *in vitro*. Optimization of the biomaterial was performed with the purpose of extending long-term release of the peptide. The peptide release *in vivo* was also evaluated in the multiple animal models described and showed efficacy over long time points. Therefore, this therapy shows promise for the treatment of NVAMD as well as ME.

8.6 Acknowledgements

The work described above is a result of collaboration between the labs of Dr. Jordan Green, Dr. Aleksander Popel, and Dr. Peter Campochario. Dr. Jordan Green, Dr.

Aleksander Popel, Dr. Peter Campochario, and Dr. Niranjan Pandey developed the ideas, and designed the experiments, of this project. Dr. Raquel Formica and Rishi Chadha performed the animal experiments described above. Ron Shmueli and Jayoung Kim assisted with the rabbit work. Ron Shmueli and Jayoung Kim performed experiments of synthesis and characterization of the various PLGA microparticle systems. The authors thank the NIH (R21EY022986), the Coulter Foundation, and MD TEDCO for support of this work.

8.7 Figures

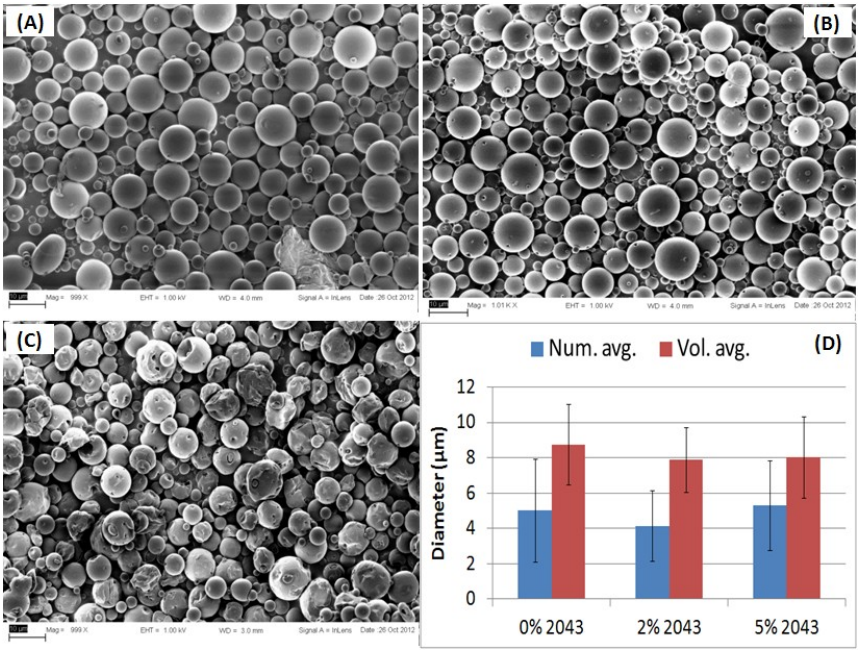

Figure 8.1. 65/35 PLGA MPs encapsulating SP2043. **(A)** 0% SP2043, **(B)** Initial 1:50 SP2043:PLGA, **(C)** Initial 1:20 SP2043:PLGA. **(D)** ImageJ based size quantification, error bars represent sample standard deviation.

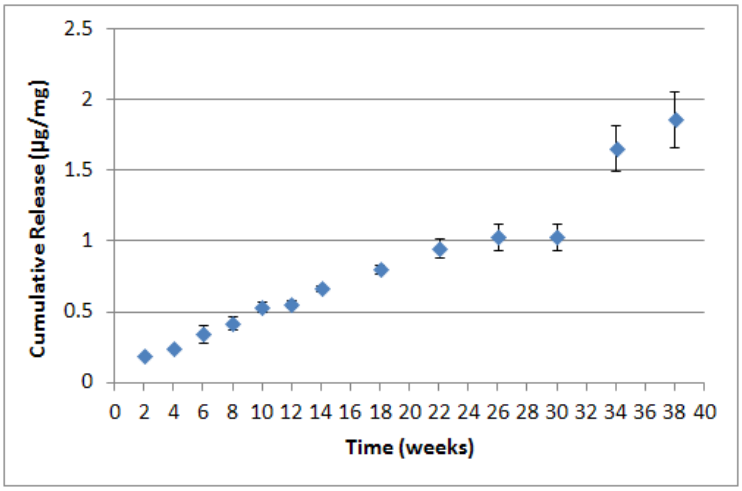

Figure 8.2. SP2043 release from 65/35 PLGA microparticles suspended in PBS at ~100mg/mL on shaker in 37ºC oven. At indicated time points, supernatant collected and

peptide quantified. Error bars represent standard deviation of sample (n = 3 at each time point).

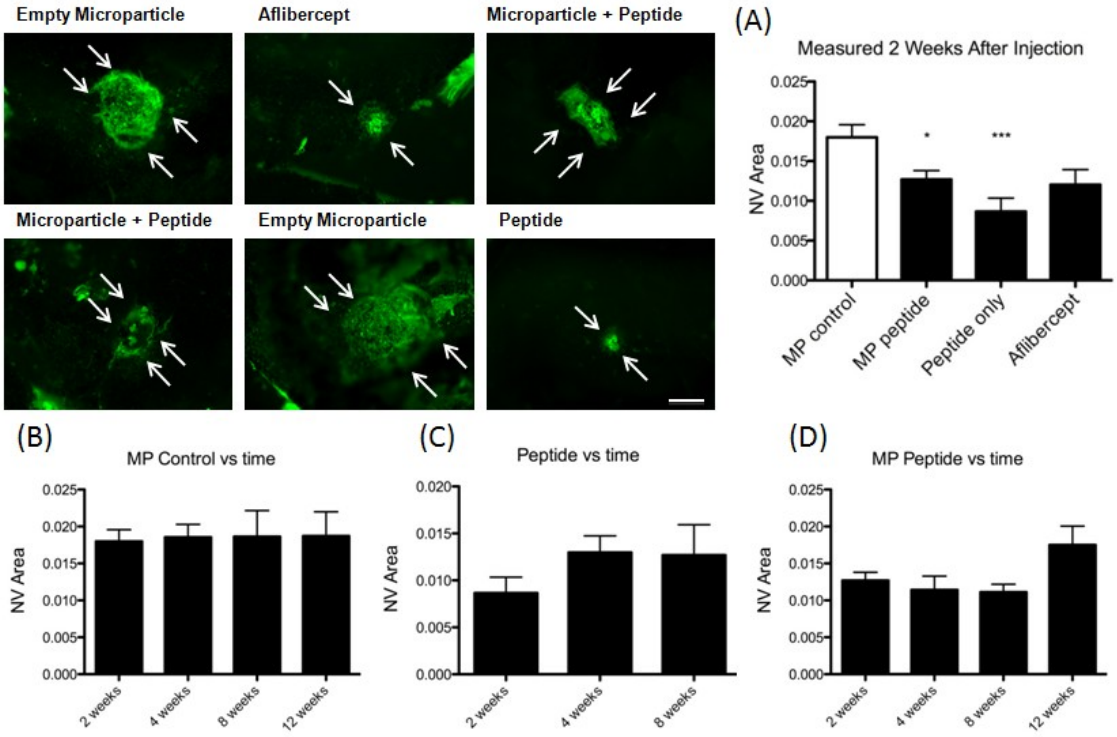

Figure 8.3. Microparticle effects in a laser-induced CNV mouse model. CNV induction was performed at different times in order to test long-term release and efficacy of the peptide in inhibiting angiogenesis. CNV inhibition is quantified by measuring area of FITC-dextran in back of the eye. Groups include MP control, MP loaded with peptide, peptide only and aflibercept. **(A)** Two week time point representative images and corresponding quantification. **(B-D)** Long-term time points in CNV mouse model.

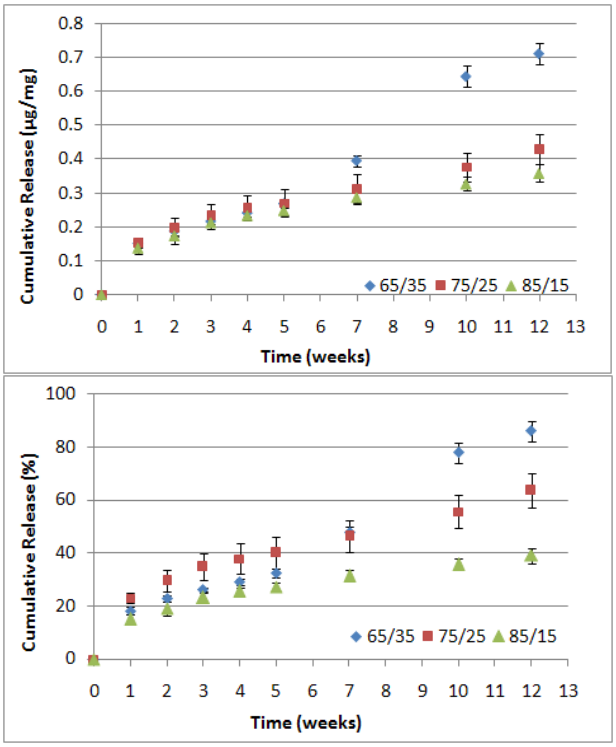

Figure 8.4. Microparticles loaded with acriflavine using 65/35, 75/25, and 85/15 L/G PLGA. Release quantified by measuring fluorescence of collected supernatant over time from MPs suspended in PBS at 37ºC on shaker. Error bars represent standard deviation at each time point (n = 3).

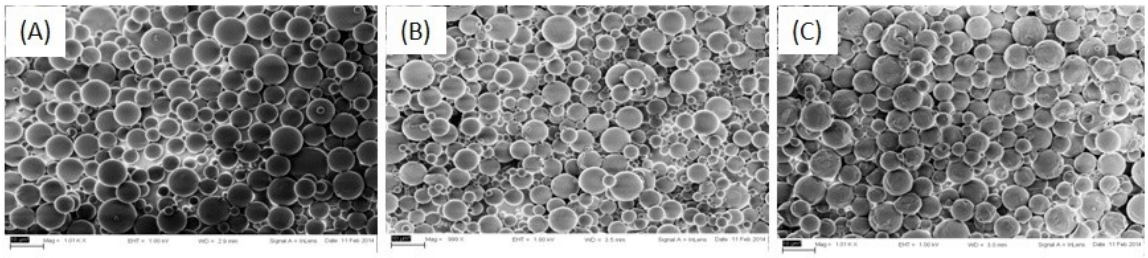

Figure 8.5. MPs made with 85/15 PLGA and 2043, using same double emulsion technique as described previously. Lyophilized samples then imaged with SEM. **(A)** 0% loading; **(B)** 0.6% final peptide loading by weight; **(C)** 1% final loading.

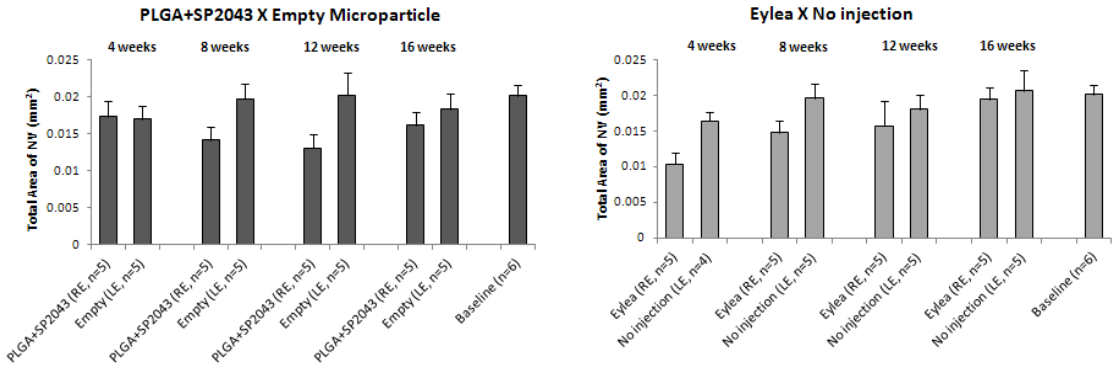

Figure 8.6. 85/15 PLGA microparticle effects in a laser-induced CNV mouse model. **(Left)** Peptide loaded microparticles; **(Right)** Aflibercept.

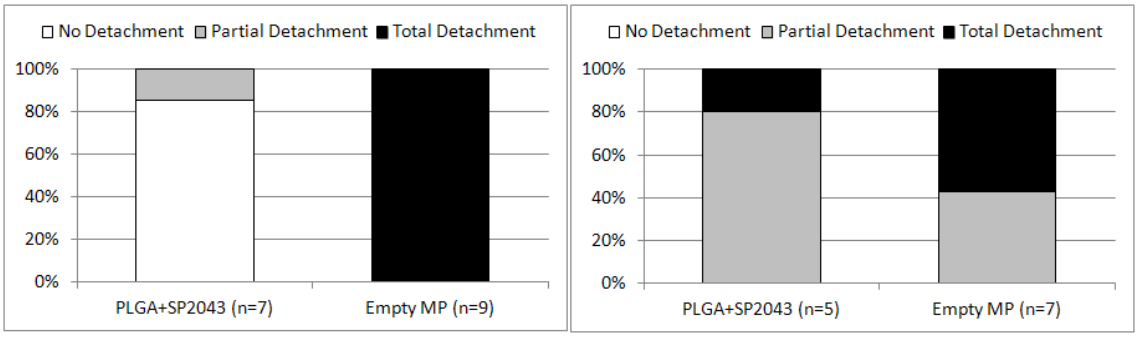

Figure 8.7. Leakage, retinal detachment model of ME. **(Left)** Retinal detachment after two weeks; **(Right)** Retinal detachment of two months.

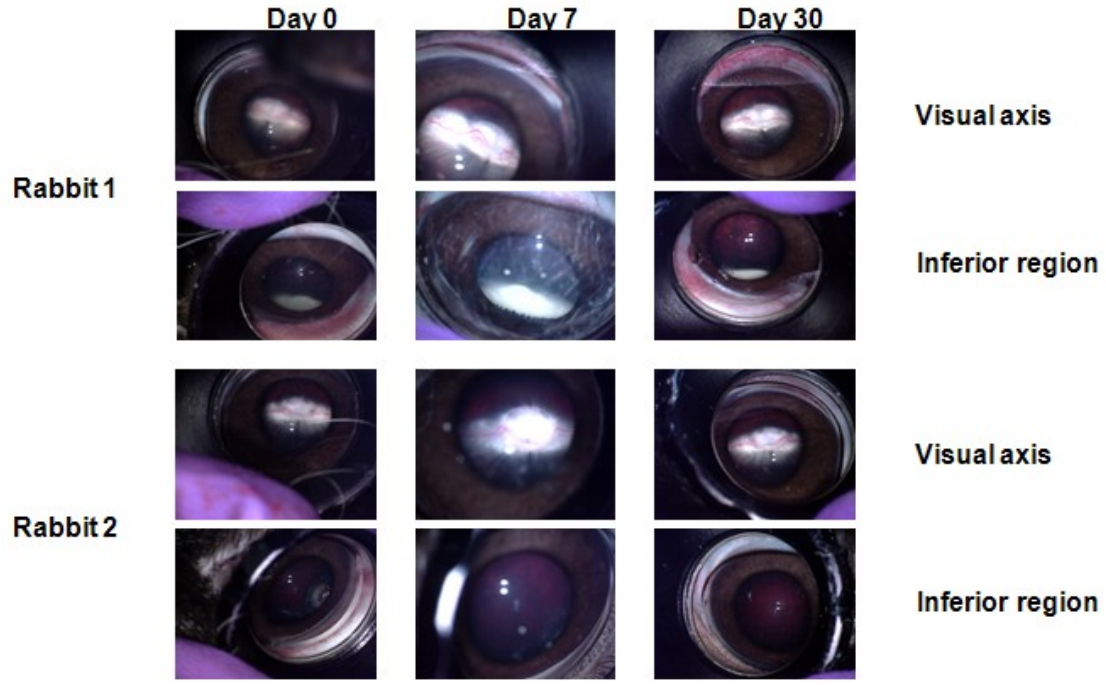

Figure 8.8. Persistence of 85/15 MPs intravitreally injected inferiorly in rabbit eye. Use fundus imaging to track the injected MP mass over time. Visual axis remains clear, with MP mass remaining in bottom of eye for one of two rabbit.

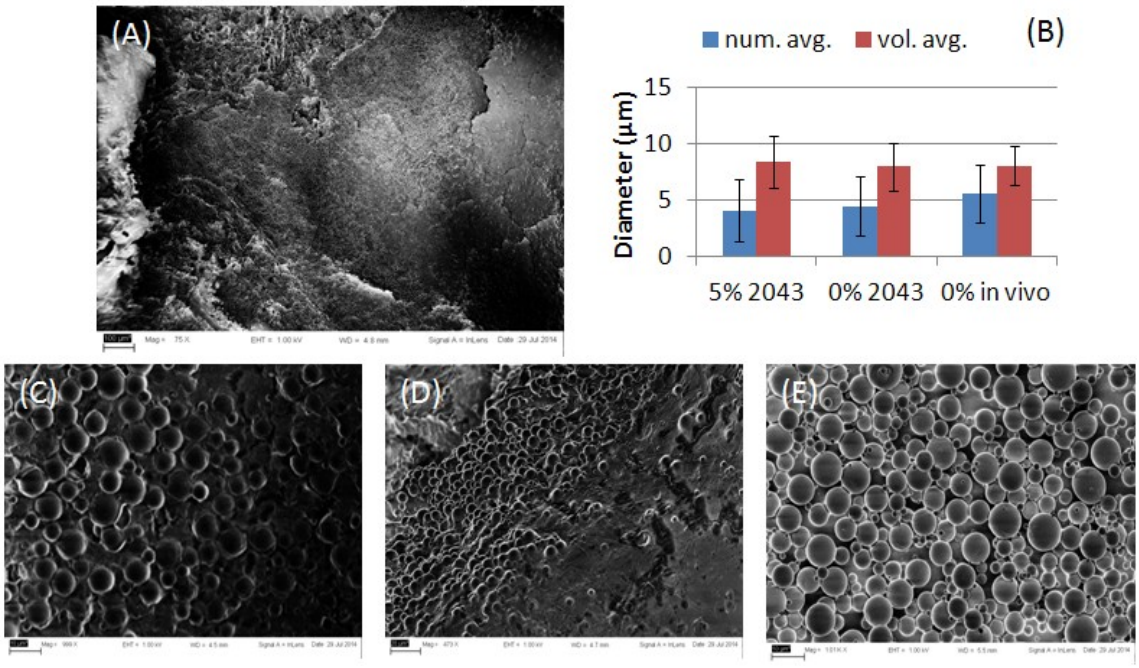

Figure 8.9. SEM analysis of persistence of 85/15 MPs intravitreally injected inferiorly in rabbit eye. **(A)** Zoomed out image of MPs from rabbit eye. **(C)** and **(D)** Zoomed in images of that sample. **(E)** SEM image of pre-injected MPs. **(B)** Quantification of size for MP samples with and without peptide and pre- and post-injected (after one month) into rabbit eye. Quantification performed with ImageJ. Error bars represent sample standard deviations.

8.8 References

1. Romero-Aroca P. Managing diabetic macular edema: The leading cause of diabetes blindness. World J Diabetes Jun 15;2(6):98-104.

2. Morello CM. Etiology and natural history of diabetic retinopathy: an overview. Am J Health Syst Pharm 2007 Sep 1;64(17 Suppl 12):S3-7.

3. Klein R, Klein BE, Linton KL. Prevalence of age-related maculopathy. The Beaver Dam Eye Study. Ophthalmology 1992 Jun;99(6):933-943.

4. Campochiaro PA. Gene transfer for ocular neovascularization and macular edema. Gene Ther 2012 Feb;19(2):121-126.

5. Karagiannis ED, Popel AS. A systematic methodology for proteome-wide identification of peptides inhibiting the proliferation and migration of endothelial cells. Proc Natl Acad Sci U S A 2008 Sep 16;105(37):13775-13780.

6. Koskimaki JE, Karagiannis ED, Rosca EV, Vesuna F, Winnard PT, Jr., Raman V, et al. Peptides derived from type IV collagen, CXC chemokines, and thrombospondin-1 domain-containing proteins inhibit neovascularization and suppress tumor growth in MDA-MB-231 breast cancer xenografts. Neoplasia 2009 Dec;11(12):1285-1291.

7. Kwak N, Okamoto N, Wood JM, Campochiaro PA. VEGF is major stimulator in model of choroidal neovascularization. Invest Ophthalmol Vis Sci 2000 Sep;41(10):3158-3164.

8. Saishin Y, Takahashi K, Lima e Silva R, Hylton D, Rudge JS, Wiegand SJ, et al. VEGF-TRAP(R1R2) suppresses choroidal neovascularization and VEGF-induced breakdown of the blood-retinal barrier. J Cell Physiol 2003 May;195(2):241-248.

9. Shmueli RB, Ohnaka M, Miki A, Pandey NB, Lima e Silva R, Koskimaki JE, et al. Long-term suppression of ocular neovascularization by intraocular injection of biodegradable polymeric particles containing a serpin-derived peptide. Biomaterials 2013 Oct;34(30):7544-7551.

10. Shikari H, Silva PS, Sun JK. Complications of intravitreal injections in patients with diabetes. Semin Ophthalmol 2014 Sep-Nov;29(5-6):276-289.

11. Koskimaki JE, Karagiannis ED, Tang BC, Hammers H, Watkins DN, Pili R, et al. Pentastatin-1, a collagen IV derived 20-mer peptide, suppresses tumor growth in a small cell lung cancer xenograft model. BMC Cancer 2010;10:29.

12. Rosca EV, Koskimaki JE, Pandey NB, Tamiz AP, Popel AS. Structure-activity relationship study of collagen-derived anti-angiogenic biomimetic peptides. Chem Biol Drug Des 2012 Jul;80(1):27-37.

13. Rosca EV, Penet MF, Mori N, Koskimaki JE, Lee E, Pandey NB, et al. A biomimetic collagen derived peptide exhibits anti-angiogenic activity in triple negative breast cancer. PLoS One 2014;9(11):e111901.

14. Lee E, Lee SJ, Koskimaki JE, Han Z, Pandey NB, Popel AS. Inhibition of breast cancer growth and metastasis by a biomimetic peptide. Sci Rep 2014;4:7139.

15. Tobe T, Ortega S, Luna JD, Ozaki H, Okamoto N, Derevjanik NL, et al. Targeted disruption of the FGF2 gene does not prevent choroidal neovascularization in a murine model. Am J Pathol 1998 Nov;153(5):1641-1646.

16. Mori K, Duh E, Gehlbach P, Ando A, Takahashi K, Pearlman J, et al. Pigment epithelium-derived factor inhibits retinal and choroidal neovascularization. J Cell Physiol 2001 Aug;188(2):253-263.

17. Ohno-Matsui K, Hirose A, Yamamoto S, Saikia J, Okamoto N, Gehlbach P, et al. Inducible expression of vascular endothelial growth factor in adult mice causes severe proliferative retinopathy and retinal detachment. Am J Pathol 2002 Feb;160(2):711-719.

18. Faisant N, Akiki J, Siepmann F, Benoit JP, Siepmann J. Effects of the type of release medium on drug release from PLGA-based microparticles: experiment and theory. Int J Pharm 2006 May 18;314(2):189-197.

19. Rosca EV, Koskimaki JE, Pandey NB, Wolff AC, Popel AS. Development of a biomimetic peptide derived from collagen IV with anti-angiogenic activity in breast cancer. Cancer Biol Ther 2011 Nov 1;12(9):808-817.

20. Amrite AC, Ayalasomayajula SP, Cheruvu NP, Kompella UB. Single periocular injection of celecoxib-PLGA microparticles inhibits diabetes-induced elevations in retinal PGE2, VEGF, and vascular leakage. Invest Ophthalmol Vis Sci 2006 Mar;47(3):1149-1160.

21. Short BG. Safety evaluation of ocular drug delivery formulations: techniques and practical considerations. Toxicol Pathol 2008;36(1):49-62.

22. Anderson OA, Bainbridge JW, Shima DT. Delivery of anti-angiogenic molecular therapies for retinal disease. Drug Discov Today 2010 Apr;15(7-8):272-282.

23. Myers AC, Lovestam Adrian M, Bruun A, Ghosh F, Andreasson S, Ponjavic V. Retinal function and morphology in rabbit after intravitreal injection of VEGF inhibitors. Curr Eye Res 2012 May;37(5):399-407.

Chapter 9

Nanoparticle Formulations for the Targeting and Treatment of Tumor Vasculature

9.1 Introduction

Tumors depend on angiogenesis in order to grow beyond a certain size and spread throughout the body [1, 2]. Inhibiting tumor angiogenesis can help prevent tumor growth [3]. A number of therapeutics, such as bevacizumab and sunitinib, have been developed to inhibit tumor angiogenesis that are now clinically approved. These therapeutics usually are active against vascular endothelial growth factor (VEGF) or its receptor. However, while these therapies have been shown to extend survival in many types of cancers, very often the tumors grow back and clinical benefit is reduced [4]. The limitations of such therapies might be due to a few factors. At least some of these angiogenic inhibitors, such as sunitinib, have been shown to have biphasic dose-response curves [5, 6]. It is also hypothesized that tumors can develop or take advantage of alternate pathways to VEGF in order to recruit and develop tumor angiogenesis. This might be either in response to anti-VEGF or anti-VEGFR therapy or even as a base case in some patients [7]. In order to further anti-angiogenic cancer therapy, the development of alternative anti-angiogenic agents, controlling the delivery profile of such agents, and combining these agents into combination therapies are being pursued [8].

Dr. Popel's lab has discovered and developed a number of classes of anti-angiogenic peptides [9]. These peptides have been shown to have potent anti-angiogenic activity *in vitro* and *in vivo* in cancer animal models [10, 11]. One such class is the collagen-IV derived peptides, which have shown to be able to inhibit tumor growth in a number of models, including a metastatic tumor model by inhibiting both angiogenesis and lymphangiogenesis [12, 13]. The collagen-IV derived peptides have been shown to bind to and disrupt integrin and integrin-dependent protein signaling pathways [9, 13, 14]. Therefore, not only have these peptides shown very promising pre-clinical data, but they also target pathways alternative to VEGF, thereby expanding the arsenal of anti-cancer therapies.

In general, peptides have certain ideal properties as therapeutics, such as high specificity [15]. However, peptides can also be difficult to translate to the clinic, for example due to short half-lives [16]. One way this can be overcome is by the use of nanoparticle (NP) formulations. Nanoparticle formulations have been used to deliver a number of therapeutics in various cancer models [17]. Nanoparticle formulations can allow for extended half-life by avoiding certain clearance mechanisms, such as enzymatic or renal removal. Nanoparticles can also increase biodistribution to the tumor by taking advantage of the enhanced permeation and retention (EPR) effect [18]. Enhanced permeation is due to the fact that the vasculature recruited by tumors is often irregular and poorly formed, with larger pores than normal vasculature. Similarly, the enhanced retention is due to irregularly formed lymph vessels that don't drain fluid as well as normal lymph vessels do.

There are various nanoparticle parameters that can be altered to affect their efficacy. Altering the size and shape can alter how cells interact with the particles [19, 20]. Particles can be made of different materials, which can affect how particles degrade and release their cargo, how they distribute in the body, and play a role in a number of other ways [8]. One other strategy is coating of nanoparticles in an attempt to improve targeting to specific tissues or cell types [21]. Nanoparticles can be coated with elements that can target specific receptors on cancer cells, or endothelial cells lining tumor vasculature.

In this chapter, various nanoparticle systems are investigated as possible delivery vehicles for the collagen-IV derived peptides. The biomaterials used include poly(beta-amino esters) (PBAEs), poly(lactide-co-glycolide) (PLGA), and poly(lactide-co-glycolide)-poly(ethylene glycol) (PLGA-PEG) block copolymers in order to encapsulate the peptides. Preliminary evidence to be discussed includes the possibility of the peptides used in a dual role as both therapeutic and targeting ligand.

9.2 Materials and Methods

9.2.1 Materials

PLGA [Poly(D,L-lactide-co-glycolide); lactide:glycolide (65:35)], DMSO [Dimethylsulfoxide], DCM [Dichloromethane], 3M NaAc [Sodium acetate] buffer, sucrose, and Sephadex G75 superfine beads were purchased from Sigma (St. Louis, MO). PVA [Poly(vinyl alcohol); Mw 25,000] was purchased from Polysciences (Warrington,

PA). Peptides (SP2012, SP2024, SP2024-TAMRA, SP2043, and SP2043-IRD800) were purchased from New England Peptide (Gardner, MA). The monomers for the PBAEs [Poly(β-amino esters)] were purchased as follows: from Acros Organics [1-(3-aminopropyl)pyrrolidine (E8)], Alfa Aesar [3-amino-1-propanol (S3), 4-amino-1-butanol (S4), 5-amino-1-pentanol (S5), 1,4-butanediol diacrylate (B4), 1-(3-aminopropyl)-4-methylpiperazine (E7)], Fluka [2-(3-aminopropylamino)ethanol (E6)], Monomer-Polymer and Dajac Laboratories [1,3-propanediol diacrylate (B3), 1,5-pentanediol diacrylate (B5), 2-(benzoyloxymethyl)-2-ethylpropane-1,3-diyl diacrylate (BL1), ethoxylated bisphenol A diacrylate (BL2), glycerol 1,3-diglycerolate diacrylate (BH1)], Sigma-Aldrich [1,3-diaminopropane (E1), 2,2-Dimethyl-1,3-propanediamine (E2)], and TCI America [1,3-diaminopentane (E3), 2-methyl-1,5-diaminopentane (E4), (PEO)4-bis-amine (E5)]. PBAEs were synthesized and characterized as previously described [22].

9.2.2 PBAE-peptide complexes

Each type of PBAE and peptide (SP2043) was diluted in NaAc buffer at varying concentrations depending on desired PBAE:SP2043 mass ratios (from 1:1 to 100:1). The PBAE solution was pipetted to the SP2043 solution and incubated at room temperature for 5 minutes.

9.2.3 Solid PLGA nanoparticles

PLGA was first dissolved into DCM, at desired concentration (usually 20 mg/mL or 40 mg/mL), in a test tube and vortexed to fully dissolve. Peptide stock in DMSO (usually 20 mg/mL) was micropipetted to the PLGA/DCM solution. The mass ratio of peptide to PLGA can vary; a common formulation is 1:50 peptide:PLGA. For blank

nanoparticle, an equivalent volume of DMSO only was pipetted. The mixture was sonicated with the test tube on ice. Sonication (Misonix) was performed with an amplitude setting of '30', which equals approximately 5-10 W, for 20 seconds. This primary emulsion was immediately poured into 50 mL of 1% PVA solution and sonicated at an amplitude setting of anywhere from '30' to '100' for 2 minutes on ice. The full volume was then transferred to 100 mL of 0.5% PVA solution and stirred in a chemical hood for ~3.5 hours. Three wash steps were then performed. For each wash step, the microparticle solution was centrifuged at 4°C, 17 krpm, for 10 minutes, and then the supernatant was removed. Subsequently, 30 mL of refrigerated Milli-Q water was added, the microparticle pellet was resuspended and the washing steps were repeated. After the last centrifugation step, 5 mL of water was added to resuspend the sample. Samples were snap frozen in liquid nitrogen and immediately placed in a lyophilizer. Following lyophilization, all microparticles were stored at -20°C.

Solid PLGA nanoparticles were also stretched, as previously described [20]. Briefly, lyophilized nanoparticle mass was weighed out and suspended in water, which was then added to a PVA/glycerol solution and mixed thoroughly. The solution was added to a mold and allowed to dry into a film. The film was then stretched via a custom made stretching device, after which the film is dissolved and the nanoparticles are collected and stored for future use.

9.2.4 PLGA-PEG nanoparticles

PLGA-PEG-methoxy was first dissolved in DMF at 10 mg/mL (or other desired concentration). Then peptide (SP2043 or SP2043-IRD800; stocks at 20 mg/mL in

DMSO) were added to the polymer/DMF solution for initial peptide w/w% of 2% (or other desired ratio). For blank nanoparticles, an equivalent volume of DMSO only was added to polymer solution. The polymer/peptide/DMF solution was added dropwise to Milli-Q water spinning on stir plate for final volume ratio of organic:aqueous at 1:10. The mixture was spun in the chemical hood for about 4 hours. Particles were washed twice using Amicon Ultra-15 centrifuge tubes (Millipore) at 4°C, for 10 min each spin. Concentrated particles were stored either in water at 4°C, or lyophilized with different amounts of sucrose.

9.2.5 NP characterization – Sizing and Loading

For sizing, nanoparticles were first diluted to 1 mg/mL in water or PBS and then sized by Nanoparticle Tracking Analysis (NTA, Nanosight NS500), and Dynamic Light Scattering (DLS, Malvern Zetasizer Nano ZS90), or transmission electron microscopy (TEM). For TEM, 10 uL of sample was dropped onto carbon coated copper grids and left to dry in chemical hood for 2 hours. Unstained TEM imaging was then performed using the Philips CM120 system.

For loading quantification, particles were first dissolved in DMSO. For labeled peptide, a Biotek Synergy 2 plate reader was used to measure fluorescence of the samples and of a labeled peptide only standard. For non-labeled SP2043 samples, quantification was performed by running gel electrophoresis (Bio-Rad Mini-PROTEAN system) and silver stain analysis (Invitrogen). A 12-well 10-20% Mini-PROTEAN tris-tricine gel was used (Bio-Rad), along with 10x tris/tricine/SDS running buffer (Bio-Rad) diluted to 1x in Milli-Q water. Each gel contained a standard series of a known amount of peptide. The

peptide standard series included 0, 62.5, 125, 250, and 500 ng of peptide per well. The remaining wells included a protein standard, and the nanoparticle samples, both peptide loaded and blanks as controls. The DMSO samples were mixed 1:1 by volume with sample buffer. Sample buffer was made of 24% glycerol in 1x PBS. Gel electrophoresis was run until the 2.5 kDa band of the protein standard traveled about two-thirds of the way down the gel. The silver stain protocol was followed for gel staining. For the development step, the stop solution was added once the lowest peptide standard (in this case 62.5ng) just began to appear. Gel images were captured with a digital camera and analyzed with ImageJ using gel band intensity quantification functionality.

9.2.6 *In vitro* assays

Human umbilical vein endothelial cells (HUVECs) and EGM-2 Bullet Kit and Reagent Pack were purchased from Lonza, and cultured as recommended. Cells were grown on a 96-well plate. Proliferation assay was performed using CellTiter 96® AQ_{ueous} One MTS assay, one day after adding either peptide only, polymer only, or peptide plus polymer. 10 μL of the aliquoted assay solution was added per well. Plates were incubated for 1-4 hours, after which absorbance at 490 nm was measured using the BioTek Synergy 2 Plate Reader. Absorbance measurements were corrected from background media signal and normalized by untreated groups. Each experimental condition was evaluated in quadruplicate.

9.2.7 Biodistribution experiment

MDA-MB-231 cells were orthotopically injected into the mammary fat pads of athymic nude mice, as previously described [23]. Once tumors reached the appropriate

size, samples were injected intravenously. The total peptide (SP2043-IRD800) injected was 20 μg per mouse and was kept constant across the different groups that contained peptide. The groups included PBS only, free peptide, solid spherical PLGA NPs loaded with peptide, solid ellipsoidal PLGA NPs loaded with peptide, and PLGA-PEG NPs loaded with peptide. The total injected peptide amount was determined according the ability to load the peptide into solid PLGA nanoparticles. In order to collect blood from the mice, retro-orbital bleeding was performed at the pre-specified time points and blood was collected into heparinized capillaries. After 24 hours, the mice were sacrificed and the organs were collected. Fluorescence imaging was performed on all blood and organ samples using a Xenogen imager.

Quantification of the images was performed using ImageJ analysis on the "luminescent" Xenogen images. Comparisons were made after normalizing the fluorescence signal within each mouse. First, the organ background fluorescence, as measured from the PBS only injected group, was subtracted from the fluorescence signal obtained in the other groups. Second, for the "Per organ area" plots, the fluorescence of each organ per mouse was divided by the total fluorescent signal summed from all the collected organs within each mouse, while for the "Total signal" plots, the all fluorescence values were multiplied by the area of that organ, as measured by ImageJ. For the blood clearance quantification, the Xenogen "luminescent" images were also quantified by ImageJ analysis.

Note, injections for experiment were performed on different days, with one mouse per group injected each day. There were, however, some differences between the

protocols used on different days. The mice used on days 1 and 2 were originally injected with cancer cells in media, while the mice used on days 3 and 4 were injected with cancer cells mixed with matrigel. The PLGA-PEG NPs were prepared all injections of day 2, whereas they were prepared right before the specific mouse injection on days 3 and 4. Statistical analysis was performed using Graphpad's Two-way ANOVA test with a Bonferroni post-test.

9.3 Results

Various nanoparticle systems were developed and explored with the eventual purpose of improved delivery of collagen-IV derived anti-angiogenic peptides. It has previously been shown that a serpin derived peptide, SP6001, can be complexed by certain PBAEs [24]. However, that peptide was negatively charged due to glutamic acid residues, allowing for the potential to complex with a positively charged polymer. The collagen-IV derived peptides are more hydrophobic and much less charged, with some in this class with a slight positive charge, such as SP2012, and some that are neutral, such as SP2043.

In order to see if these peptides can self-assemble with PBAEs, they were mixed together in solution and sized with DLS and NTA in order to check for NP formation. **Figure 9.1A** seems to indicate that SP2012 does not readily, or obviously, form NPs when mixed with some PBAEs. For the less hydrophobic PBAEs, those without the "L" designation, the size is found to be similar to the SP2012 only in solution. In the case of

the more hydrophobic "L" PBAEs, the size was similar to the PBAE only sizes. This is to say that the NPs observed in each case were similar to the peptide or polymer only cases, and so it is difficult to tell if anything new is happening when mixing the two together. However, a further *in vitro* efficacy test was performed in order to see if any changes could be observed there when mixing SP2012 and PBAE, **Figure 9.1B**. Peptide only, polymer only, and peptide-polymer mixes were added to HUVECs in a 96-well plate. A metabolic assay was used to determine the relative effects on the cells. The signal from the peptide-polymer samples were normalized by the polymer only and peptide only effects. While there were no statistically significant effects, there were some conditions where there might be some increased effect (decreased cellular activity) as compared to peptide only, for example with some of the B3S5 polymers. However, this could be due to independent effects of the polymer and peptide on the cells, for example, if the presence of the (free) PBAEs allowed for better interaction of the peptide with the cells.

Next, SP2043 was tested to see if it can form NPs with PBAEs, with data for two such PBAEs shown in **Figure 9.2**. Both the mean and mode of the NP distributions increased when comparing the PBAEs mixed with peptide as compared to PBAEs only. This difference seemed to decrease as the mass ratio of PBAE to peptide increased. The relative concentration of NPs, as well as the relative maximum brightness of the NPs, also seemed to increase when adding in the peptides. This seems to suggest that there is some interaction between some PBAEs and SP2043. However, another PBAE tested, B3S5E1, didn't show these changes upon addition of the peptide (data not shown). It should also be noted that the light scattering observed through the Nanosight seemed to

flicker to some extent, possibly indicating non-spherical complexes. Further experiments, such as TEM imaging, might reveal more about any possible NP formation.

Other, more developed, NP systems were then explored. PLGA NPs were made using a commonly employed double emulsion protocol. The sonication settings and surfactant concentration were varied in an attempt to modulate the size of the PLGA NPs, **Figure 9.3**. If the sonication setting was too low, such as at 30A, the particles formed in the few micron range (data not shown). Increasing the sonication setting to 60A produced NPs in the 200-300nm range, with only moderate reductions in size when increasing the sonication power past 60A. Increasing the PVA concentration a few fold also did not reduce the NP size much. SEM images of the NPs can be seen in the inset of **Figure 9.3**. The shape of NPs has been previously shown to have effects on the biological response to these particles. Using previously developed methods, these PLGA NPs were also stretched to create ellipsoidal PLGA NPs, as seen in TEMs in **Figure 9.4**. Loading efficiency of the peptide into these PLGA NPs was generally found to be in the 20%-30% range.

Further, PLGA-PEG NPs were also made to provide yet another option for the encapsulation and delivery of these peptides. These NPs were made with a nanoprecipitation/emulsion technique that is commonly used with PLGA-PEG block co-polymers. Here, NPs with sub-100nm size were made, **Figure 9.5**. Loading SP2024-TAMRA into the NPs increased their size to an extent, and in all cases, these NPs are stable in water at 4ºC for up to a week, **Figure 9.5A**. These NPs could also be formulated with SP2043-IRD800, as seen in **Figure 9.2B**. These NPs were stable in both water, as

well as to an extent in PBS and FBS, but the polydispersity index increaseds as stability did begin to decrease over time, especially in 100% FBS. It was observed that the concentration at which these NPs were lyophilized, as well as the addition of a lyoprotectant, in this case sucrose, could affect the stability of the NPs during lyophilization, **Figure 9.6**. When no sucrose was added, NPs aggregated into larger particles after lyophilization. Increasing the amount of sucrose maintained a particle size closer to the original pre-lyophilization size. However, it appears that when loaded with the peptide it is more difficult to maintain the exact original size. Similarly, increasing the NP concentration before lyophilization can also result in aggregation, especially when no lyoprotectant is added.

A biodistribution experiment was then performed using a number of these NP systems. An orthotopic xenograft breast cancer mouse model was used for this experiment, using a near infrared fluorescent tagged peptide, SP2043-IRD800. The injected groups were PBS only, free peptide, spherical PLGA NPs with peptide, ellipsoidal PLGA NPs with peptide, and PLGA-PEG NPs with peptide. In all peptide groups, the total amount of peptide injected was the same, at 20µg per mouse. There were two groups of mice that were injected. The first group was inoculated with MDA-MB-231 cells in media, whereas the second group was inoculated with same cells mixed with matrigel. Due to potential differences, the plots in **Figure 9.7** show data from the cell/matrigel inoculated mice.

In **Figure 9.7A**, the relative distribution of the fluorescence across the different organs within each mouse is shown. While the free peptide was more likely to be end up

in the kidneys, the NPs were more likely to end up in the liver. There were no statistically significant differences between the groups in terms of accumulation in the tumor after 24 hours. However, it is interesting that the free peptide was able to match the NP accumulation of 10%. Another interesting point is that the ellipsoidal NPs might have some extra preference to go to the spleen. The blood clearance was more difficult to determine due to weaker signals over background (**Figure 9.7B**), however, an attempt was made to quantify the half-lives using a simple, single exponential decay fitting function with GraphPad. The half-lives were each estimated to be approximately 10 minutes. Further experiments are need to increase the sample size to determine the half-lives with greater precision.

9.4 Discussion and Future Directions

Many promising therapeutics have been discovered that have various limitations when attempting to translate to the clinic. For example, while peptides have very good specificity, they usually have short half-lives and poor bioavailability [25]. The use of nanoparticles to improve delivery has therefore been investigated. Encapsulating therapeutics in NPs helps protect the cargo while altering the biodistribution profile in a way that can enhance the delivery of the cargo to the appropriate physiological space. In the case of treating cancer, in addition to cargo protection, NPs can help targeting to tumors in two general ways. NPs can passively target tumors due to the EPR effect. The pore size in the leaky tumor vasculature can range from 200 nm – 2,000 nm, depending on the tumor type and its particular environment [21]. NPs that are in the range of 10 nm

– 200 nm might be optimal since they can take advantage of the EPR effect, while reducing renal and reticulo-endothelial system (RES) clearance [26]. NPs can also provide active targeting either due specifically to the biomaterial that is encapsulating the cargo, or by coating the NP surface with a targeting ligand.

Here, a number of NP systems are discussed with the purpose of delivery a potent anti-angiogenic class of peptide. PBAEs have displayed some innate cellular targeting *in vitro*, both in the case of cancer and endothelial cell specificity [27, 28]. Initial attempts were made to see if some PBAEs could then self-assemble with some of the collagen-IV derived peptides. The SP2043 peptide seems to be able to self-assemble with PBAEs, **Figure 9.2**. However, further characterization is required to explore these as potential therapeutic NPs. Additionally, a larger library of PBAEs can be tested for the ability to form NPs.

PLGA is a commonly used biomaterial, and one that is recognized as generally regarded as safe (GRAS) by the FDA for certain applications. The peptides were successfully encapsulated in a number of PLGA NPs, including solid spherical NPs, solid ellipsoidal NPs, and PEG coated NPs. These formulations allow for the exploration of both shape and surface properties on the ability of the NPs to deliver to the tumor. Some research indicates that increasing the aspect ratio of the NPs could increase tumor targeting [21]. It has also been shown that PEGylation can increase the half-life of a number of particles [21], which can increase the likelihood that the NPs can be passively targeted to the tumor. A biodistribution experiment was then performed with these various systems and with free peptide (SP2043 tagged with a near infrared dye was used

in all cases). The largest observed difference in the organ distribution after 24 hours was that, as expected, the free peptide is more likely to end up in the kidney, while the NPs are more likely to end up in the liver. It was interesting to see that there was at least some signal in the kidneys of mice injected with the NPs, however, it is not currently clear if this is released peptide, or NPs of a certain size that got stuck in the kidney.

In all cases, including the free peptide, around 5% - 10% of the measured signal ended up in the tumors, **Figure 9.7**. This is comparable to other reports in the field [29]. Another interesting finding is that the free peptide appears to have active targeting to the tumor. This suggests that the peptide can be used not only as the active therapeutic, but also as a targeting element for the NP system. It would be of interest to perform efficacy studies with these various NP systems.

9.5 Acknowledgements

The work described above is the result of a collaboration between the labs of Dr. Aleksander Popel and Dr. Jordan Green. Dr. Aleksander Popel, Dr. Jordan Green, Dr. Niranjan Pandey, and Ron Shmueli helped develop the ideas for the experiments. Ron Shmueli made and characterized the various NP systems described. Esak Lee performed the biodistribution experiment, with help from Ron Shmueli and Jayoung Kim. The authors would like to thank the NIH for funding (R01EB016721, R21CA152473).

9.6 Figures

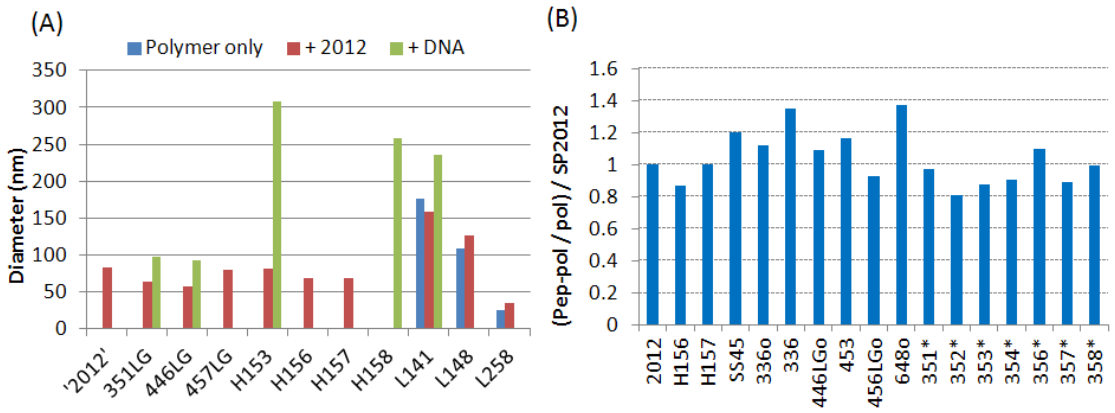

Figure 9.1. (A) Malvern sizing of polymer only, polymer with SP2012, or polymer with plasmid DNA. For polymer only, if no bar, no particles detected. For polymer + DNA, if no bars, no sample was measured. **(B)** Place mixtures of polymer and SP2012 onto HUVECs in cell culture and measure effects with use of cell titer metabolic assay. Y-axis represents the signal of polymer + peptide after normalizing to both polymer only and peptide only effects.

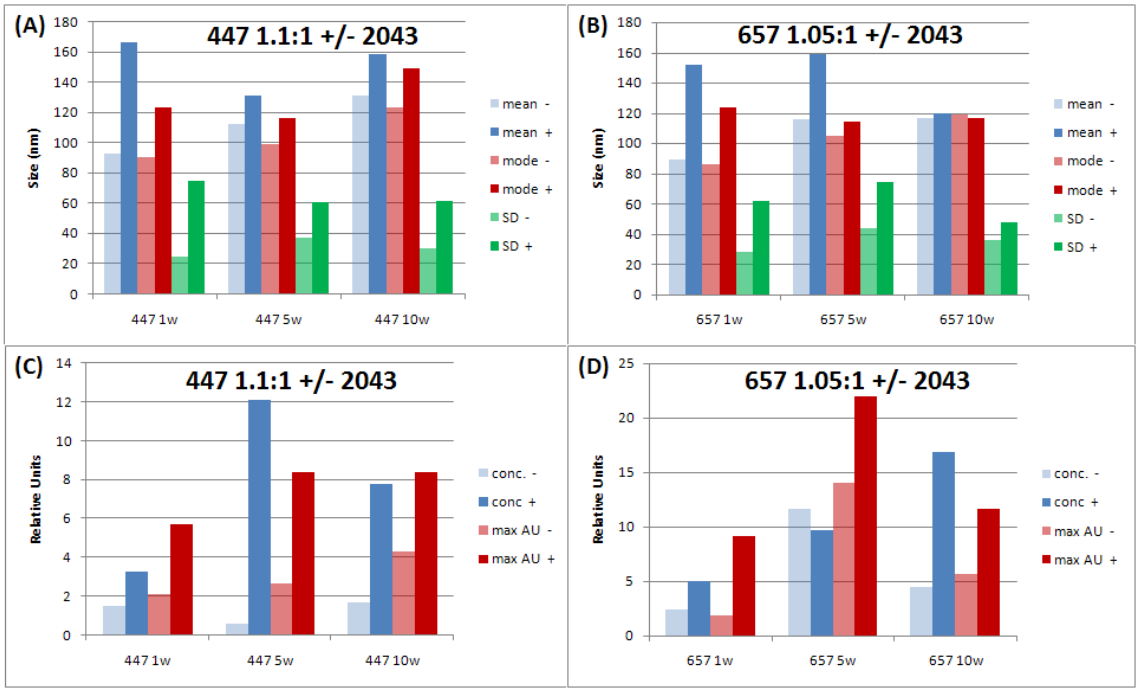

Figure 9.2. PBAE-SP2043 conjugation attempts, as measured with Nanosight NTA. **(A)** and **(C)** Using PBAE B4S4E7; **(B)** and **(D)** Using PBAE B6S5E7. **(A)** and **(B)** Measures of mean, mode, and standard deviation of complexes with and without SP2043; **(C)** and **(D)** Measures of relative concentration and maximum brightness of complexes with and without peptide.

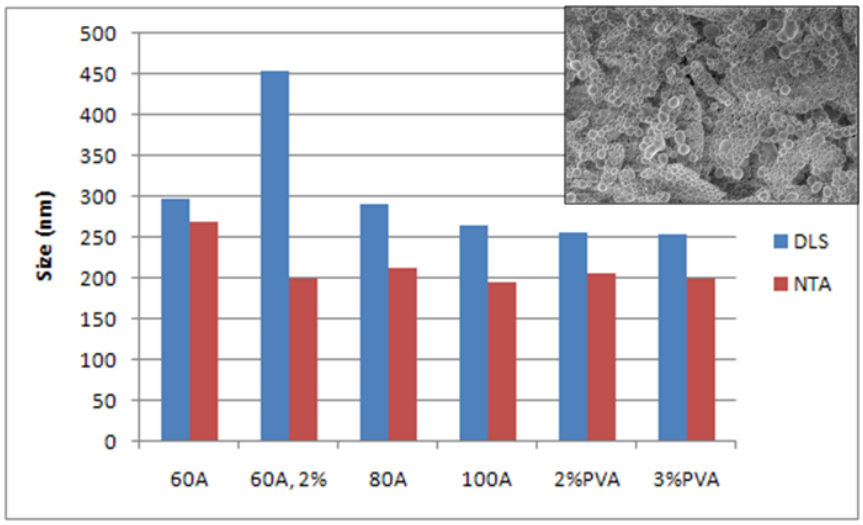

Figure 9.3. PLGA nanoparticles made with varying sonication settings and PVA concentrations. Sizing measured with DLS and NTA. Inset shows SEM of PLGA NPs made at 60A loaded with initial 2% by mass SP2024-TAMRA.

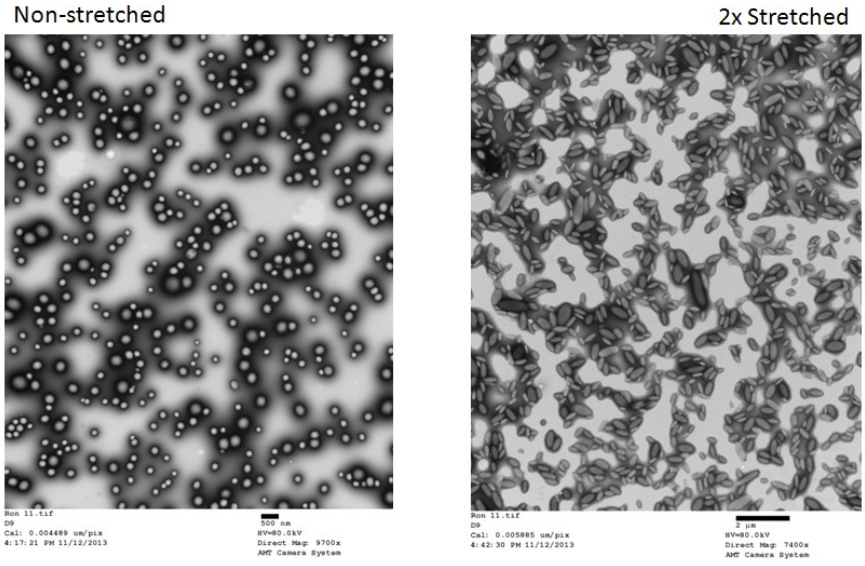

Figure 9.4. TEM images of PLGA NPs nonstretched **(left)** or 2x stretched **(right)**.

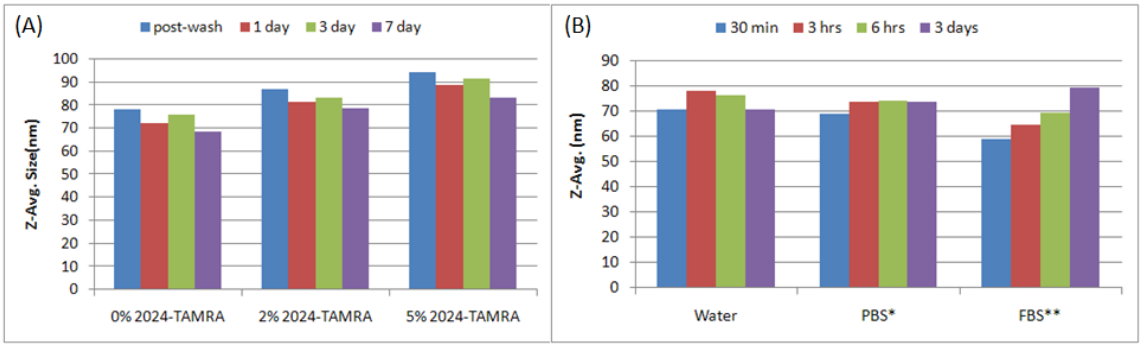

Figure 9.5. PLGA-PEG NPs sizing with Malvern Zetasizer. **(A)** Varying the initial loading w/w% of SP2024-TAMRA, and tracking NPs stored over a few days at 4ºC. **(B)** Varying media in which NPs are stored. These NPs loaded with SP2043-IRD800, initially 2% by mass.

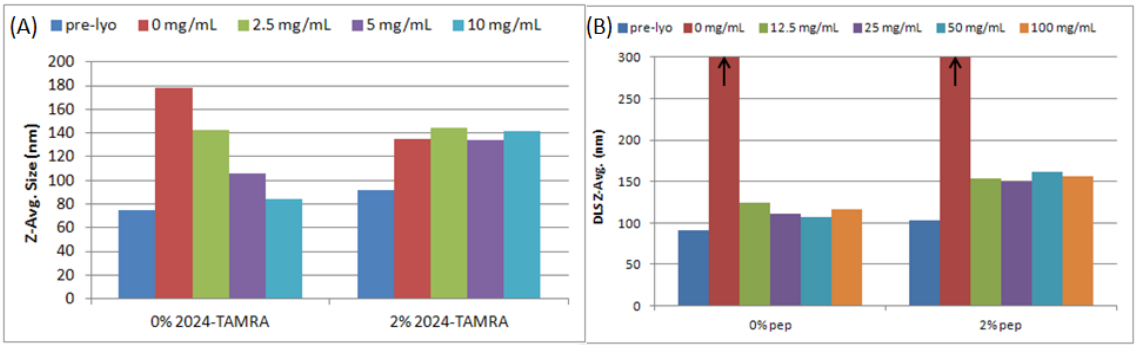

Figure 9.6. PLGA-PEG stability after lyophilization depends on NP concentration before lyophilization and on lyoprotectant concentration. **(A)** Pre-lyophilization NP concentration at 2.5 mg/mL, varying sucrose concentration. **(B)** Pre-lyophilization NP concentration at 6 mg/mL, varying sucrose concentration. For both 0 mg/mL sucrose samples, NP size in the micron range.

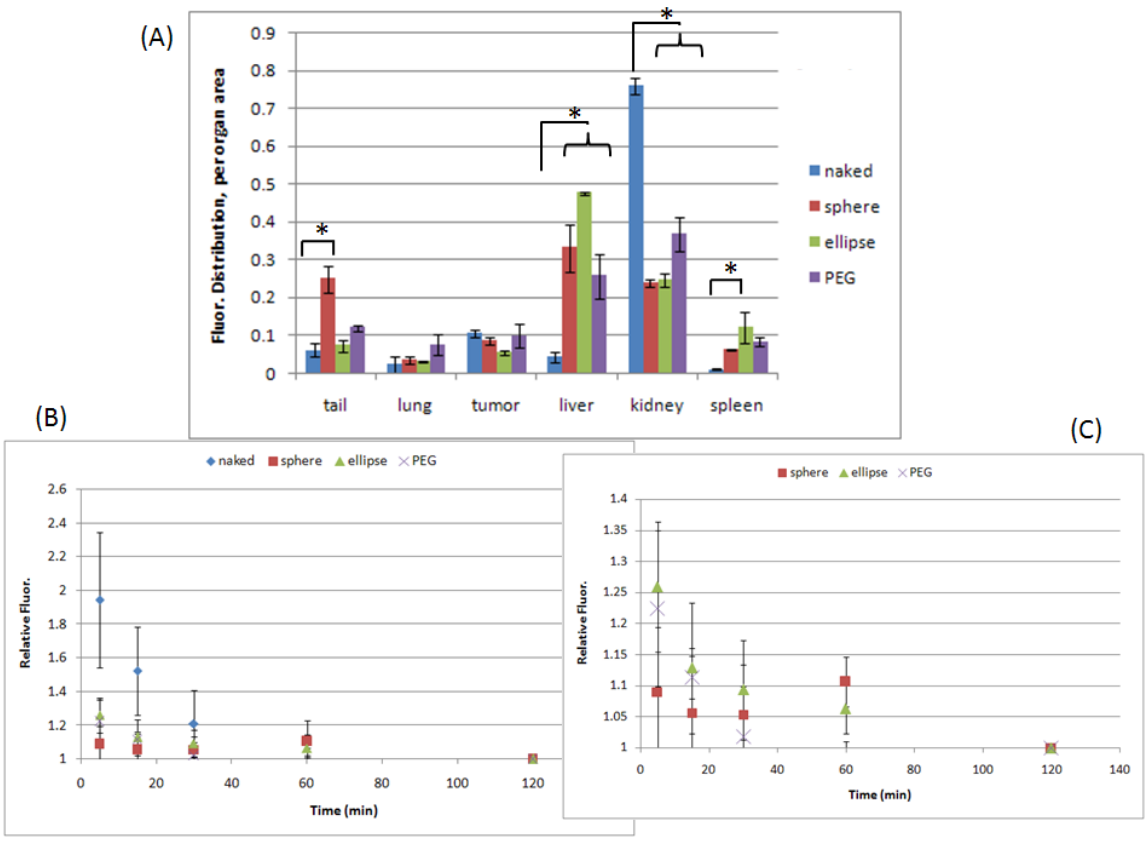

Figure 9.7. Biodistribution experiment; naked = free peptide, sphere = solid spherical PLGA NP, ellipse = solid ellipsoidal PLGA NP, PEG = PLGA-PEG NPs. NPs all loaded with SP2043-IRD800. **(A)** Sample organ biodistribution normalized by organ background fluorescence and normalized to total signal within each mouse. Two-way ANOVA with Bonferroni posttest, * < 0.05. **(B)** Blood clearance plot and **(C)** zoomed in for three of the groups listed in legend.

9.7 References

1. Folkman J. Tumor angiogenesis: therapeutic implications. N Engl J Med 1971 Nov 18;285(21):1182-1186.

2. Hanahan D, Weinberg RA. The hallmarks of cancer. Cell 2000 Jan 7;100(1):57-70.

3. Folkman J. Angiogenesis: an organizing principle for drug discovery? Nat Rev Drug Discov 2007 Apr;6(4):273-286.

4. Miller KD, Sweeney CJ, Sledge GW, Jr. Can tumor angiogenesis be inhibited without resistance? EXS 2005(94):95-112.

5. Folkman J. Angiogenesis. Annu Rev Med 2006;57:1-18.

6. Ebos JM, Lee CR, Christensen JG, Mutsaers AJ, Kerbel RS. Multiple circulating proangiogenic factors induced by sunitinib malate are tumor-independent and correlate with antitumor efficacy. Proc Natl Acad Sci U S A 2007 Oct 23;104(43):17069-17074.

7. Bergers G, Hanahan D. Modes of resistance to anti-angiogenic therapy. Nat Rev Cancer 2008 Aug;8(8):592-603.

8. Bhise NS, Shmueli RB, Sunshine JC, Tzeng SY, Green JJ. Drug delivery strategies for therapeutic angiogenesis and antiangiogenesis. Expert Opin Drug Deliv 2011 Apr;8(4):485-504.

9. Karagiannis ED, Popel AS. A systematic methodology for proteome-wide identification of peptides inhibiting the proliferation and migration of endothelial cells. Proc Natl Acad Sci U S A 2008 Sep 16;105(37):13775-13780.

10. Koskimaki JE, Karagiannis ED, Rosca EV, Vesuna F, Winnard PT, Jr., Raman V, et al. Peptides derived from type IV collagen, CXC chemokines, and thrombospondin-1 domain-containing proteins inhibit neovascularization and suppress tumor growth in MDA-MB-231 breast cancer xenografts. Neoplasia 2009 Dec;11(12):1285-1291.

11. Koskimaki JE, Rosca EV, Rivera CG, Lee E, Chen W, Pandey NB, et al. Serpin-derived peptides are antiangiogenic and suppress breast tumor xenograft growth. Transl Oncol 2012 Apr;5(2):92-97.

12. Rosca EV, Penet MF, Mori N, Koskimaki JE, Lee E, Pandey NB, et al. A biomimetic collagen derived peptide exhibits anti-angiogenic activity in triple negative breast cancer. PLoS One 2014;9(11):e111901.

13. Lee E, Lee SJ, Koskimaki JE, Han Z, Pandey NB, Popel AS. Inhibition of breast cancer growth and metastasis by a biomimetic peptide. Sci Rep 2014;4:7139.

14. Rosca EV, Koskimaki JE, Pandey NB, Tamiz AP, Popel AS. Structure-activity relationship study of collagen-derived anti-angiogenic biomimetic peptides. Chem Biol Drug Des 2012 Jul;80(1):27-37.

15. Saladin PM, Zhang BD, Reichert JM. Current trends in the clinical development of peptide therapeutics. IDrugs 2009 Dec;12(12):779-784.

16. Vlieghe P, Lisowski V, Martinez J, Khrestchatisky M. Synthetic therapeutic peptides: science and market. Drug Discov Today 2010 Jan;15(1-2):40-56.

17. Brigger I, Dubernet C, Couvreur P. Nanoparticles in cancer therapy and diagnosis. Adv Drug Deliv Rev 2002 Sep 13;54(5):631-651.

18. Prabhakar U, Maeda H, Jain RK, Sevick-Muraca EM, Zamboni W, Farokhzad OC, et al. Challenges and key considerations of the enhanced permeability and retention effect for nanomedicine drug delivery in oncology. Cancer Res 2013 Apr 15;73(8):2412-2417.

19. Sunshine JC, Perica K, Schneck JP, Green JJ. Particle shape dependence of CD8+ T cell activation by artificial antigen presenting cells. Biomaterials 2014 Jan;35(1):269-277.

20. Meyer RA, Sunshine JC, Perica K, Kosmides AK, Aje K, Schneck JP, et al. Biodegradable Nanoellipsoidal Artificial Antigen Presenting Cells for Antigen Specific T-Cell Activation. Small 2015 Jan 12.

21. Bertrand N, Wu J, Xu X, Kamaly N, Farokhzad OC. Cancer nanotechnology: the impact of passive and active targeting in the era of modern cancer biology. Adv Drug Deliv Rev 2013 Feb;66:2-25.

22. Sunshine JC, Akanda MI, Li D, Kozielski KL, Green JJ. Effects of base polymer hydrophobicity and end-group modification on polymeric gene delivery. Biomacromolecules 2011 Oct 10;12(10):3592-3600.

23. Lee E, Koskimaki JE, Pandey NB, Popel AS. Inhibition of lymphangiogenesis and angiogenesis in breast tumor xenografts and lymph nodes by a peptide derived from transmembrane protein 45A. Neoplasia 2013 Feb;15(2):112-124.

24. Shmueli RB, Ohnaka M, Miki A, Pandey NB, Lima e Silva R, Koskimaki JE, et al. Long-term suppression of ocular neovascularization by intraocular injection of biodegradable polymeric particles containing a serpin-derived peptide. Biomaterials 2013 Oct;34(30):7544-7551.

25. Witt KA, Gillespie TJ, Huber JD, Egleton RD, Davis TP. Peptide drug modifications to enhance bioavailability and blood-brain barrier permeability. Peptides 2001 Dec;22(12):2329-2343.

26. Kobayashi H, Watanabe R, Choyke PL. Improving conventional enhanced permeability and retention (EPR) effects; what is the appropriate target? Theranostics 2014;4(1):81-89.

27. Tzeng SY, Guerrero-Cazares H, Martinez EE, Sunshine JC, Quinones-Hinojosa A, Green JJ. Non-viral gene delivery nanoparticles based on poly(beta-amino esters) for treatment of glioblastoma. Biomaterials 2011 Aug;32(23):5402-5410.

28. Shmueli RB, Sunshine JC, Xu Z, Duh EJ, Green JJ. Gene delivery nanoparticles specific for human microvasculature and macrovasculature. Nanomedicine 2012 Feb 1.

29. Bartlett DW, Su H, Hildebrandt IJ, Weber WA, Davis ME. Impact of tumor-specific targeting on the biodistribution and efficacy of siRNA nanoparticles measured by

multimodality in vivo imaging. Proc Natl Acad Sci U S A 2007 Sep 25;104(39):15549-15554.

Vita

Ron Boris Shmueli was born in New York City, New York on April 15th 1986, son of Zvi and Frieda Shmueli, and eventual elder brother of Dan Shmueli. He has had the good fortune of attending many great schools over his academic career. This began at his elementary school the Early Childhood Center, where he first developed a love of learning all about the natural world, continuing through his middle school, the NYC Lab School for Collaborative Studies, and high school, Stuyvesant High School, where he was surrounded with exceptional classmates. He then went on to Columbia University Fu Foundation School of Engineering, where he graduated with a Bachelor of Science in Chemical Engineering and a minor in Biomedical Engineering. There he was first exposed to cutting-edge research, including in the field of biomaterials.

In order to further pursue his interests in the field of biomaterials, he joined the Ph.D. program at Johns Hopkins School of Medicine Department of Biomedical Engineering. There he has been exposed to, and participated in, many exciting research projects under the mentorship of Dr. Jordan Green, together with collaborations with researchers throughout the School of Medicine. He has worked on the development of polymers for non-viral gene delivery, as well as polymeric long-term release systems in order to treat ocular diseases. This work has resulted in a number of publications, and hopefully will contribute to clinically relevant therapies in the future.